25/1106

NUREG/CR-1106
TC-486

Tsunami Atlas for the Coasts of the United States

NEWARK PUBLIC LIBRARY

DEC 5 1979

U. S. GOVT. PUBS.
DEPOSITORY 376

Prepared by M. Brandsma, D. Divoky, L. Hwang

Tetra Tech, Inc.

Prepared for
U. S. Nuclear Regulatory
Commission

READEX
FICHE

Y 3.N88:

NOTICE

This report was prepared as an account of work sponsored by an agency of the United States Government. Neither the United States Government nor any agency thereof, or any of their employees, makes any warranty, expressed or implied, or assumes any legal liability or responsibility for any third party's use, or the results of such use, of any information, apparatus product or process disclosed in this report, or represents that its use by such third party would not infringe privately owned rights.

Available from

GPO Sales Program
Division of Technical Information and Document Control
U.S. Nuclear Regulatory Commission
Washington, D.C. 20555

and

National Technical Information Service
Springfield, Virginia 22161

NUREG/CR-1106
TC-486
RD

Tsunami Atlas for the Coasts of the United States

Manuscript Completed: June 1978
Date Published: November 1979

Prepared by
M. Brandsma, D. Divoky, L. Hwang

Tetra Tech, Inc.
630 North Rosemead Boulevard
Pasadena, CA 91107

Prepared for
Division of Reactor Safety Research
Office of Nuclear Regulatory Research
U.S. Nuclear Regulatory Commission
Washington, D.C. 20555
NRC FIN No. B-3016

NOTICE

Conclusions and methodology contained herein reflect the contractor's (Tectra Tech) opinion based upon numerical simulation models of seismically generated water waves.

The staff of the U.S. Nuclear Regulatory Commission will assess the work contained herein for application to the licensing of sites for reactors and other material utilization facilities. The conclusions obtained herein, therefore, should not be considered directly applicable to any regulatory action at this time.

PREFACE

This report describes a study of tsunami hazard on the Pacific, Atlantic and Gulf coasts of the United States. The work was performed under Contract AT (49-24) - 0203 between Tetra Tech, Inc. and the United States Nuclear Regulatory Commission.

The study was performed and the report written by Mr. Maynard Brandsma with the assistance and supervision of Mr. David Divoky. Dr. Li-San Hwang provided overall direction and assistance in project planning.

The authors wish to thank Dr. Jerry Harbour, Mr. L. G. Hulman, and Dr. Myron Fliegel of the Nuclear Regulatory Commission for discussions which were very helpful in guiding the course of this study.

EXECUTIVE SUMMARY

Coastal power plant siting and safety analysis requires consideration of wave action and extreme water levels, both high and low. The run-up of large amplitude long waves, such as tsunamis, may pose a hazard to a coastal facility through direct dynamic effects on plant structures, through destruction of protective breakwaters and beaches, and the like. Extreme low water levels are of concern in design of coolant intake structures.

The importance of tsunamis in these analyses, especially along Pacific coasts, makes specification of potential tsunami histories necessary. The present report addresses this problem. A large hypothetical earthquake is defined by appeal to history and tectonic theory. This canonical source serves as input to a numerical hydrodynamic model which computes the resulting wave history anywhere within the ocean basin. This procedure is repeated for a number of potential source locations, chosen according to degree and type of seismic activity. In this way, hypothetical coastal histories of great tsunamis emanating from any potential source area are simulated.

The results of this study are offshore incident wave systems and do not include the complex, site-dependent, nearshore transformations. Users must account for such local effects in any specific application.

TABLE OF CONTENTS

Page No.

1. INTRODUCTION 1

2. TECTONICS 4
   - 2.1 Outline of Plate Tectonics 4
   - 2.2 Tsunamigenic Zones 8
   - 2.3 Earthquake Prediction in Subduction Zones . . 15
   - 2.4 Canonical Earthquake and Bottom Displacement. 19

3. TSUNAMI GENERATION 31
   - 3.1 Influence of Source Characteristics 31
   - 3.2 Selection of Source Locations. 33

4. TSUNAMI PROPAGATION 39
   - 4.1 Equations of Motion 39
   - 4.2 Computational Scheme. 41
   - 4.3 Boundary Conditions. 44
   - 4.4 Calculation. 45
   - 4.5 Standardization of Depths 47
   - 4.6 Verification of the Method 50

5. RESULTS 54

6. INTERPRETATION AND USE OF RESULTS. 60

7. SENSITIVITY 63

8. SUMMARY 65

Table of Contents (Continued)

Page No.

REFERENCES. 67

APPENDIX A RESULTS FOR THE PACIFIC COAST . . . A-1

APPENDIX B RESULTS FOR THE ATLANTIC COAST . . B-1

APPENDIX C LISTING OF PROGRAM SEAWAVE C-1

APPENDIX D USER'S MANUAL FOR PROGRAM SEAWAVES . . D-1

LIST OF TABLES

1 Values of Constants for Subduction Zones of the Pacific Seismic Belt . . . 20

2 Parameters for Locating Canonical Bottom Displacements in the Pacific Ocean . . . 35

3 Parameters for Locating Canonical Bottom Displacements in the Atlantic Ocean . . . 37

4 Pacific Coastal Stations . . . 56

5 Atlantic Coastal Stations . . . 59

6 Sensitivity of Calculations for Pacific Stations . . . 70

7 Sensitivity of Calculations to Reduction in Grid Size from 1 Degree to 0.5 Degree . . . 75

A-1 Tsunamis Arriving at Station 1 Ranked by Maximum Wave Displacement . . . A-1

A-2 Tsunamis Arriving at Station 2 Ranked by Maximum Wave Displacement . . . A-4

A-3 Tsunamis Arriving at Station 3 Ranked by Maximum Wave Displacement . . . A-7

A-4 Tsunamis Arriving at Station 4 Ranked by Maximum Wave Displacement . . . A-10

A-5 Tsunamis Arriving at Station 5 Ranked by Maximum Wave Displacement . . . A-13

A-6 Tsunamis Arriving at Station 6 Ranked by Maximum Wave Displacement . . . A-16

A-7 Tsunamis Arriving at Station 7 Ranked by Maximum Wave Displacement . . . A-19

A-8 Tsunamis Arriving at Station 8 Ranked by Maximum Wave Displacement . . . A-22

A-9 Tsunamis Arriving at Station 9 Ranked by Maximum Wave Displacement . . . A-25

A-10 Tsunamis Arriving at Station 10 Ranked by Maximum Wave Displacement . . . A-28

A-11 Tsunamis Arriving at Station 11 Ranked by Maximum Wave Displacement A-31

A-12 Tsunamis Arriving at Station 12 Ranked by Maximum Wave Displacement A-34

A-13 Tsunamis Arriving at Station 13 Ranked by Maximum Wave Displacement A-37

A-14 Tsunamis Arriving at Station 14 Ranked by Maximum Wave Displacement A-40

A-15 Tsunamis Arriving at Station 15 Ranked by Maximum Wave Displacement A-43

A-16 Tsunamis Arriving at Station 16 Ranked by Maximum Wave Displacement A-46

A-17 Tsunamis Arriving at Station 17 Ranked by Maximum Wave Displacement A-49

A-18 Tsunamis Arriving at Station 18 Ranked by Maximum Wave Displacement A-52

A-19 Tsunamis Arriving at Station 19 Ranked by Maximum Wave Displacement A-55

B-1 Tsunamis Arriving at Staiton 1 Ranked by Maximum Wave Displacement B-1

B-2 Tsunamis Arriving at Station 2 Ranked by Maximum Wave Displacement B-3

A-3 Tsunamis Arriving at Station 3 Ranked by Maximum Wave Displacement B-5

A-4 Tsunamis Arriving at Station 4 Ranked by Maximum Wave Displacement B-7

B-5 Tsunamis Arriving at Station 5 Ranked by Maximum Wave Displacement B-9

B-6 Tsunamis Arriving at Station 6 Ranked by Maximum Wave Displacement B-11

B-7 Tsunamis Arriving at Station 7 Ranked by Maximum Wave Displacement B-13

B-8 Tsunamis Arriving at Station 8 Ranked by Maximum Wave Displacement B-15

B-9 Tsunamis Arriving at Station 9 Ranked by Maximum Wave Displacement B-17

B-10 Tsunamis Arriving at Station 10 Ranked by Maximum Wave Displacement B-19

B-11 Tsunamis Arriving at Station 11 Ranked by Maximum Wave Displacement B-21

B-12 Tsunamis Arriving at Station 12 Ranked by Maximum Wave Displacement B-23

B-13 Tsunamis Arriving at Station 13 Ranked by Maximum Wave Displacement B-25

B-14 Tsunamis Arriving at Station 14 Ranked by Maximum Wave Displacement B-27

B-15 Tsunamis Arriving at Station 15 Ranked by Maximum Wave Displacement B-29

B-16 Tsunamis Arriving at Station 16 Ranked by Maximum Wave Displacement B-31

B-17 Tsunamis Arriving at Station 17 Ranked by Maximum Wave Displacement B-33

B-18 Tsunamis Arriving at Station 18 Ranked by Maximum Wave Displacement B-35

B-19 Tsunamis Arriving at Station 19 Ranked by Maximum Wave Displacement B-37

B-20 Tsunamis Arriving at Station 20 Ranked by Maximum Wave Displacement B-39

B-21 Tsunamis Arriving at Station 21 Ranked by Maximum Wave Displacement B-41

B-22 Tsunamis Arriving at Station 22 Ranked by Maximum Wave Displacement B-43

B-23 Tsunamis Arriving at Station 23 Ranked by Maximum Wave Displacement B-45

B-24 Tsunamis Arriving at Station 24 Ranked by Maximum Wave Displacement B-47

B-25 Tsunamis Arriving at Station 25 Ranked by Maximum Wave Displacement B-49

B-26 Tsunamis Arriving at Station 26 Ranked by Maximum Wave Displacement B-51

B-27 Tsunamis Arriving at Station 27 Ranked by Maximum Wave Displacement B-53

LIST OF FIGURES

1. Schematic Representation of the Three Major Boundary Types For Crustal Plates 5

2. Schematic Illustration of Relationships Between Tectonic Plates 7

3. Distribution of World Earthquakes of 1961-1967 at Depths Less Than 100 Kilometers, (Barazangi and Dorman, 1969) . . . 9

4. Distribution of World Earthquakes of 1961-1967 With Focal Depths Between 100 KM and 700 KM (Barazangi and Dorman, 1969) . . 10

5. Summary Map of Slip Vectors Derived from Studies of Earthquake Mechanisms, (Isacks et al, 1968) 11

6. Pacific Ocean Areas With Tectonic Structure Capable of Generating a Large Tsunami Are Shown With Hatched Lines . . . 13

7. Atlantic Ocean Areas Capable of Generating a Large Tsunami Are Shown Within Hatched Lines 14

8. Bottom Displacements (in feet) for the Chilean Earthquake of 1960 (inferred from Plafker and Savage, 1970) . . . 22

9. Bottom Displacements (in feet) for the Alaskan Earthquake of 1964 (inferred from Plafker, 1969) 23

10. Simple Model of Dipolar Displacement 24

11. Profile Along Major Axis of Bottom Displacement. 25

12. Contours of Canonical Bottom Displacement (only positive side is shown) 28

13. Perspective View of Canonical Bottom Displacement . . . 29

14. Distribution of Canonical Earthquakes in Pacific Basin (Numbers Correspond to Those in Table 2) 36

15. Distribution of Cannonical Earthquakes in Atlantic Basin (Numbers Correspond to Those in Table 3) 38

16. Staggered Grid 43

17. Wake Island Record of the Alaska 1964 Tsunami (Van Dorn, 1969) and the History Computed by the Present Numerical Model (Dashed Curve) 52

18. Computed and Observed Results at Sitka, Alaska (Earthquake Occurred at 3:36 GMT) 54

19. Pacific Coast Station and Maximum Absolute Wave Displacement from Still Water Level for Any Tsunami 57

20. Atlantic Coast Stations and Maximum Absolute Wave Displacement from Still Water Level for Any Tsunami 60

21. Waves Computed With Coarse (1° x 1°) Grid and Fine (0.5° x 0.5°) Grid and Observed (Van Dorn, 1970) Wave at Wake Island for 1964 Gulf of Alaska Tsunami 73

22. Waves Computed With Coarse (1° x 1°) Grid and Fine (0.5° x 0.5°) Grid and Observed (Van Dorn, 1970) Wave at Sitka, Alaska for 1964 Gulf of Alaska Tsunami 74

A-1 Largest Tsunami Arriving at Station 1 Offshore of Cape Flattery, WA A-2

A-2 Second and Third Largest Tsunamis Arriving at Station 1 . . . A-3

A-3 Largest Tsunami Arriving at Station 2 Offshore of Grays Harbor, WA A-5

A-4 Second and Third Largest Tsunamis Arriving at Station 2 . . . A-6

A-5 Largest Tsunami Arriving at Station 3 Offshore of Tillamook Head, OR . A-8

A-6 Second and Third Largest Tsunamis Arriving at Station 3 . . . A-9

A-7 Largest Tsunami Arriving at Station 4 Offshore of Cascade Head, OR A-11

A-8 Second and Third Largest Tsunamis Arriving at Station 4 . . . . A-12

A-9 Largest Tsunami Arriving at Station 5 Offshore of Hecata Head, OR . A-14

A-10 Second and Third Largest Tsunamis Arriving at Station 5 . . . . A-15

A-11 Largest Tsunami Arriving at Station 6 Offshore of Cape Blanco, OR A-17

A-12 Second and Third Largest Tsunamis Arriving at Station 6 . . . . A-18

A-13 Largest Tsunami Arriving at Station 7 Offshore of Crescent City, CA A-20

A-14 Second and Third Largest Tsunamis Arriving at Station 7 . . . . A-21

A-15 Largest Tsunami Arriving at Station 8 Offshore of Eureka, CA . . A-23

A-16 Second and Third Largest Tsunamis Arriving at Station 8 . . . A-24

A-17 Largest Tsunami Arriving at Station 9 Offshore of Cape Mendocino . . A-26

A-18 Second and Third Largest Tsunamis Arriving at Station 9 . . . A-27

A-19 Largest Tsunami Arriving at Station 10 Offshore of Point Arena, CA . A-29

A-20 Second and Third Largest Tsunamis Arriving at Station 10 . . . A-30

A-21 Largest Tsunami Arriving at Station 11 Offshore of Point Reyes, CA . A-32

A-22 Second and Third Largest Tsunamis Arriving at Station 11 . . . A-33

A-23 Largest Tsunami Arriving at Station 12 Offshore of Monterey Bay, CA . A-35

A-24 Second and Third Largest Tsunamis Arriving at Station 12 . . . A-36

A-25 Largest Tsunami Arriving at Station 13 Offshore of Point Sur, CA . . A-38

A-26 Second and Third Largest Tsunamis Arriving at Station 13 . . A-39

A-27 Largest Tsunami Arriving at Station 14 Offshore of Point Buchon, CA . A-41

A-28 Second and Third Largest Tsunamis Arriving at Station 14 . . . . A-42

A-29 Largest Tsunami Arriving at Station 15 Offshore of Santa Rosa Island, CA A-44

A-30 Second and Third Largest Tsunamis Arriving at Station 15 . . . A-45

A-31 Largest Tsunami Arriving at Station 16 Offshore of Santa Catalina Island, CA A-47

A-32 Second and Third Largest Tsunamis Arriving at Station 16 . . . A-48

A-33 Largest Tsunami Arriving at Station 17 Offshore of San Onofre, CA . A-50

A-34 Second and Third Largest Tsunamis Arriving at Station 17 . . . A-51

A-35 Largest Tsunami Arriving at Station 18 Offshore of Punta San Miguel, B. C., Mexico A-53

A-36 Second and Third Largest Tsunamis Arriving at Station 18 . . . A-54

A-37 Largest Tsunami Arriving at Station 19 Offshore of Punta Colnett, B. C., Mexico A-56

A-38 Second and Third Largest Tsunamis Arriving at Station 19 . . . A-57

B-1 Largest Tsunami Arriving at Station 1 Offshore of Mouth of Bay of Fundy B-2

B-2 Largest Tsunami Arriving at Station 2 Offshore of Mt. Desert Rock, ME . B-4

B-3 Largest Tsunami Arriving at Station 3 Offshore of Owls Head, ME . . B-6
B-4 Largest Tsunami Arriving at Station 4 Offshore of Walkers Point, ME . B-8
B-5 Largest Tsunami Arriving at Station 5 Offshore of Cape Code, MA . . B-10
B-6 Largest Tsunami Arriving at Station 6 Offshore of Nantucket Island, MA . B-12
B-7 Largest Tsunami Arriving at Station 7 Offshore of Newport, RI . . B-14
B-8 Largest Tsunami Arriving at Station 8 Offshore of Montauk Point, NY . B-16
B-9 Largest Tsunami Arriving at Station 9 Offshore of New York, NY . . B-18
B-10 Largest Tsunami Arriving at Station 10 Offshore of Point Pleasant, NY . B-20
B-11 Largest Tsunami Arriving at Station 11 Offshore of Atlantic City, NY . B-22
B-12 Largest Tsunami Arriving at Station 12 Offshore of Assateague Island, MD B-24
B-13 Largest Tsunami Arriving at Station 13 Offshore of Newport News, VA . B-26
B-14 Largest Tsunami Arriving at Station 14 Offshore of Albemarle Sound, NC B-28
B-15 Largest Tsunami Arriving at Station 15 Offshore of Pamlico Sound, NC . B-30
B-16 Largest Tsunami Arriving at Station 16 Offshore of Onslow Bay, NC. . B-32
B-17 Largest Tsunami Arriving at Station 17 Offshore of Myrtle Beach, SC . B-34
B-18 Largest Tsunami Arriving at Station 18 Offshore of Cape Romain, SC . B-36
B-19 Largest Tsunami Arriving at Station 19 Offshore of Parris Island, SC . B-38
B-20 Largest Tsunami Arriving at Station 20 Offshore of St. Andrew Sound, GA B-40
B-21 Largest Tsunami Arriving at Station 21 Offshore of St. Augustine, FL . B-42
B-22 Largest Tsunami Arriving at Station 22 Offshore of Merritt Island, FL . B-44
B-23 Largest Tsunami Arriving at Station 23 Offshore of Vero Beach, FL . . B-46
B-24 Largest Tsunami Arriving at Station 24 Offshore of Jupiter, FL . . B-48
B-25 Largest Tsunami Arriving at Station 25 Offshore of Hollywood, FL . . B-50
B-26 Largest Tsunami Arriving at Station 26 Offshore of Key Largo, FL . . B-52
B-27 Largest Tsunami Arriving at Station 27 Offshore of Cape Sable, FL. . B-54

1. INTRODUCTION

This report presents the results of a study to determine the distribution of offshore wave heights and time histories for coastal segments of the United Stated due to distantly generated tsunamis. The hypothetical tsunamis considered here are generated by vertical displacement of the sea floor associated with very large earthquakes. With the exception of southern Alaska, the Aleutians, Puerto Rico and the Virgin Islands, these major events occur at great distances from the coastal segments of interest. Only the grosser features of sea floor displacement are of importance to the characteristics of a tsunami after traveling over a large distance, Hammack (1972). Since these features are now known in an approximate way, they are adopted as initial conditions for a numerical model of tsunami propagation.

This study does not consider the effects of locally generated major tsunamis since the local bathymetry and the small scale features of bottom displacement are very important in these cases. Nor does the study consider minor tsunamis of only local effect caused, for example, by movements on strike-slip faults or by submarine landslides. Horizontal displacements in the above cases may be of importance locally but they do not influence far field effects.

The first portion of the report is devoted to establishing the likely areas at which large scale tsunamis could be generated. For engineering purposes it is desired to predict the following by rational means:

1) areas in which great earthquakes are likely to occur
2) frequencies of occurrence
3) earthquake magnitudes
4) tsunamigenic character of the ground motion.

Reliable prediction of these parameters is only just coming over the scientific horizon. There are two approaches.

The first uses statistical methods based on historical earthquakes. Statistical methods can be used when dealing with a large number of earthquakes of about the same intensity (such as those occurring in Japan where historical data extends back hundreds of years). This method is not valid for the infrequently occurring great earthquakes. In such cases, methods based on seismology and plate tectonics are available.

The second method is based on geologic principles. The manner of earthquake occurrence in the area of interest is examined in the light of the theory of plate tectonics and the local geologic structure. Earthquake frequency is estimated from the relative movements of the crustal blocks bordering the fault zone. For this purpose the size of the block, the depth of the surfaces comprising its boundaries, its geological age and its rate of movement are investigated. These parameters all influence the amount of strain energy that can be stored up before the interface between blocks ruptures. From this information, the rate of accumulation of strain energy can be estimated. If some seismic history is available, the size and recurrence rate of strain relieving earthquakes can, perhaps, be estimated.

Because of the scarcity of data on large magnitude earthquakes and because the local geologic mechanisms are often not clear, geophysicists are forced to rely on the second method. Estimates produced thereby may not be reliable.

In order that the reader will have an appreciation for the factors involved in selecting canonical sources for use in the calculations, Chapter 2 includes an outline of the theory of plate tectonics, and a qualitative discussion of earthquake prediction as they apply to this study.

Chapter 3 contains a discussion of tsunami generation and lists the sources used for this study. Chapter 4 presents the method of calculation of tsunami propagation.

Chapter 5 gives an overview of the results of the computations. Data is presented for each coastal segment giving maximum water surface displacements from tidal level for any distant source. The results show that a small portion of the set of canonical sources is responsible for most of the tsunami hazard in coastal areas. The locations of the significant sources are discussed. The appendices contain detailed results for each coastal segment.

Chapters 6 and 7 discuss the interpretation of the results and sensitivity. The final chapter summarizes these results and presents recommendations for their use and future improvement.

2. TECTONICS

2.1 Outline of Plate Tectonics

The current- and generally accepted - model of the earth's surface has been formulated over the past fifteen years. It depicts the surface as being divided into a small number of distinct, rigid plates floating on a hot plastic mantle. These plates are composed of a strong outer crust overlying a weaker layer, and the composite is termed the lithosphere. The thickness of the lithosphere averages 110 km at the continents and 75 km in the oceans. (The thickness of the outer crust varies from an oceanic average of 9 km to a continental average of 40 km). Relative motion occurs between plates, with rates as high as several centimeters per year. The driving force for such motion may be convection currents in the earth's mantle.

The drifting of crustal plates over the spheroidal earth is accommodated by three types of boundary interactions: spreading zones, transform fault zones, and subduction zones. Figure 1 is a schematic representation of the way in which combinations of the three boundary types allow separate motion of the plates.

Spreading zones are regions of locally thinner crust with ridge-like topography incorporating a central rift into which mantle material (lava) intrudes to form new plate boundaries. The major spreading zones comprise the system of midocean ridges of which examples are the East Pacific Rise and the Mid-Atlantic ridge. Spreading zones are characterized by tensional normal faulting, magnetic anomalies, high heat flow and moderate seismicity. These zones are the regions where new sea floor is created.

Transform fault zones are regions where crustal plates slip horizontally past one another. The major transform fault zones form the connecting link between spreading zones and subduction zones. Transform faults are also integral parts of the midocean ridges, being the mechanism by which the ridges change direction. Transform fault

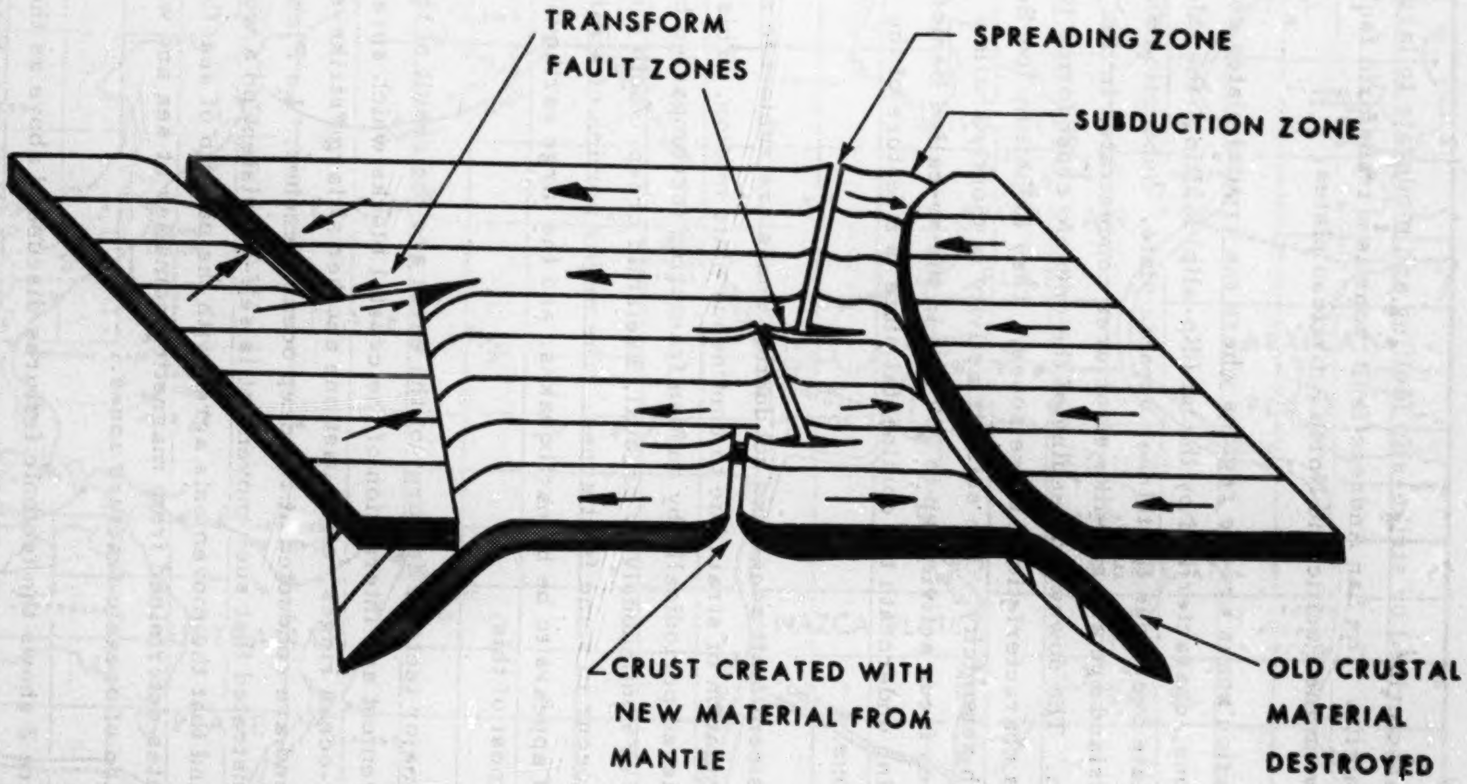
TRANSFORM FAULT ZONES
SPREADING ZONE
SUBDUCTION ZONE
CRUST CREATED WITH NEW MATERIAL FROM MANTLE
OLD CRUSTAL MATERIAL DESTROYED

Figure 1. Schematic representation of the three major boundary types for crustal plates. Arrows represent relative crustal movement. The South Pacific has this type of tectonic structure; the Tonga-Kermadec Trench on the left, the East Pacific rise in the center and the Peru-Chile trench on the right.

zones are characterized by strike-slip faulting and moderate to large shallow seismicity. The San Andreas fault zone is a transform fault boundary between the Pacific and North American plates.

Subduction zones are the regions where the crustal plates collide. In these regions, characterized by thrust (dip-slip) faulting, the thicker continental plate overrides the thinner oceanic plate. Subduction zones occur at the island arc and arc-like structures concentrated in the Pacific Ocean. The downward bending of the oceanic crust forms the deep trenches characteristic of these zones. They exhibit by low heat flow, and high seismicity. The seismic activity is mostly shallow focus, but deep focus activity (up to 700 km) in the so-called Beniof zones extending underneath the continental plate is a feature of the subduction zone.

Transform fault zones and subduction zones are subject to a steady accumulation of strain due to continuous plate motion. This strain is relieved periodically by sudden fracturing (accompanied by earthquakes) or continuously by gradual, aseismic creep. Both mechanisms may occur in some fault zones. The major portion of strain energy relief appears to be by earthquakes, and the large earthquakes account for most of this.

The major tectonic features of the earth are the result of the relative movement and interaction of the crustal blocks which spread apart at mid-ocean ridges, slide past one another at large strike-slip fault zones and are subducted at the deep ocean trenches. Le Pichon (1968) demonstrated that such movement is self-consistent on a worldwide scale and that the movements agree with the pattern of sea-floor spreading rates determined from magnetic anomalies at sea and with the orientation of oceanic fracture zones.

Figure 2 shows the tectonic features discussed above as they occur in the world oceans. The following section will discuss those tectonic features associated with tsunami generation.

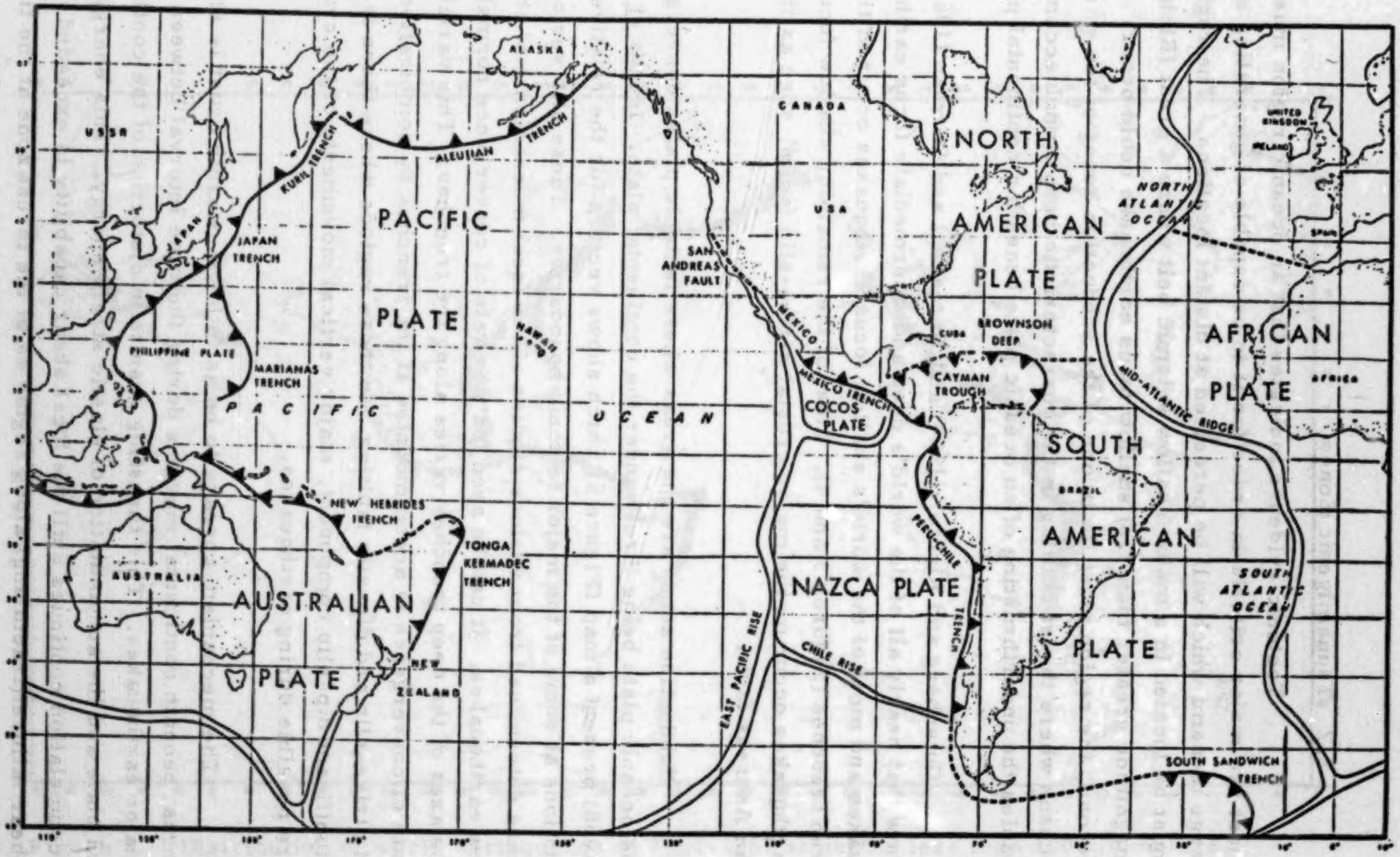
USSR
ALASKA
KURIL TRENCH
ALEUTIAN TRENCH
JAPAN
JAPAN TRENCH
PACIFIC PLATE
PHILIPPINE PLATE
MARIANAS TRENCH
HAWAII
P A C I F I C O C E A N
NEW HEBRIDES TRENCH
TONGA KERMADEC TRENCH
AUSTRALIA
AUSTRALIAN PLATE
NEW ZEALAND
CANADA
USA
SAN ANDREAS FAULT
MEXICO
MEXICO TRENCH
COCOS PLATE
EAST PACIFIC RISE
CHILE RISE
NAZCA PLATE
PERU-CHILE TRENCH
NORTH AMERICAN PLATE
CUBA
BROWNSON DEEP
CAYMAN TROUGH
SOUTH AMERICAN PLATE
BRAZIL
NORTH ATLANTIC OCEAN
UNITED KINGDOM
IRELAND
SPAIN
AFRICAN PLATE
AFRICA
MID-ATLANTIC RIDGE
SOUTH ATLANTIC OCEAN
SOUTH SANDWICH TRENCH

Figure 2. Schematic illustration of relationships between tectonic plates.

2.2 Tsunamigenic Zones

Tectonic evidence indicates that an oceanic region must meet two major criteria in order for it to be capable of generating a large tsunami which will be perceived at distant locations. The region must be located in a major shallow seismic belt where a great (Richter magnitude greater than 7.8) shallow focus earthquake could occur. Second, the region must lie in one of the subduction zones of the world oceans where thrust faulting in the characteristic deep trench accompanies the underthrusting of an oceanic plate beneath a continental plate.

Gutenberg and Richter (1954) and Barazangi and Dorman (1969) show that nearly all of the world's deep and intermediate focus earthquakes and most of the world's shallow focus earthquakes occur at the deep trenches (Figures 3 and 4). Most of the remaining shallow focus earthquakes occur on the major crustal strike-slip faults, such as the San Andreas fault.

Subduction zones are the areas where tectonic plates converge, the oceanic plate being thrust under the continental plate. Isacks et al (1968) present a map (Figure 5) which shows vectors for the relative motions at some of the major tectonic boundaries. These slip vectors were determined from various studies of the focal mechanisms of shallow earthquakes. It can be seen that the rate of convergence normal to the axes of the deep trenches varies along the trenches. This variable rate of convergence is accommodated at the trenches by combinations of strike-slip and dip-slip faulting. In those regions where there is a significant dip-slip component, major vertical movements of the crust are possible during earthquakes.

The mechanism appears to be as follows: oceanic crust is slowly thrust beneath continental margins during the time interval between major earthquakes. This thrusting results in distortion of the continental plate and the accumulation of elastic strain energy. This energy accumulation continues until the local shear capability is exceeded. Shear failure (fracturing) along segments of the thrust zone at the time

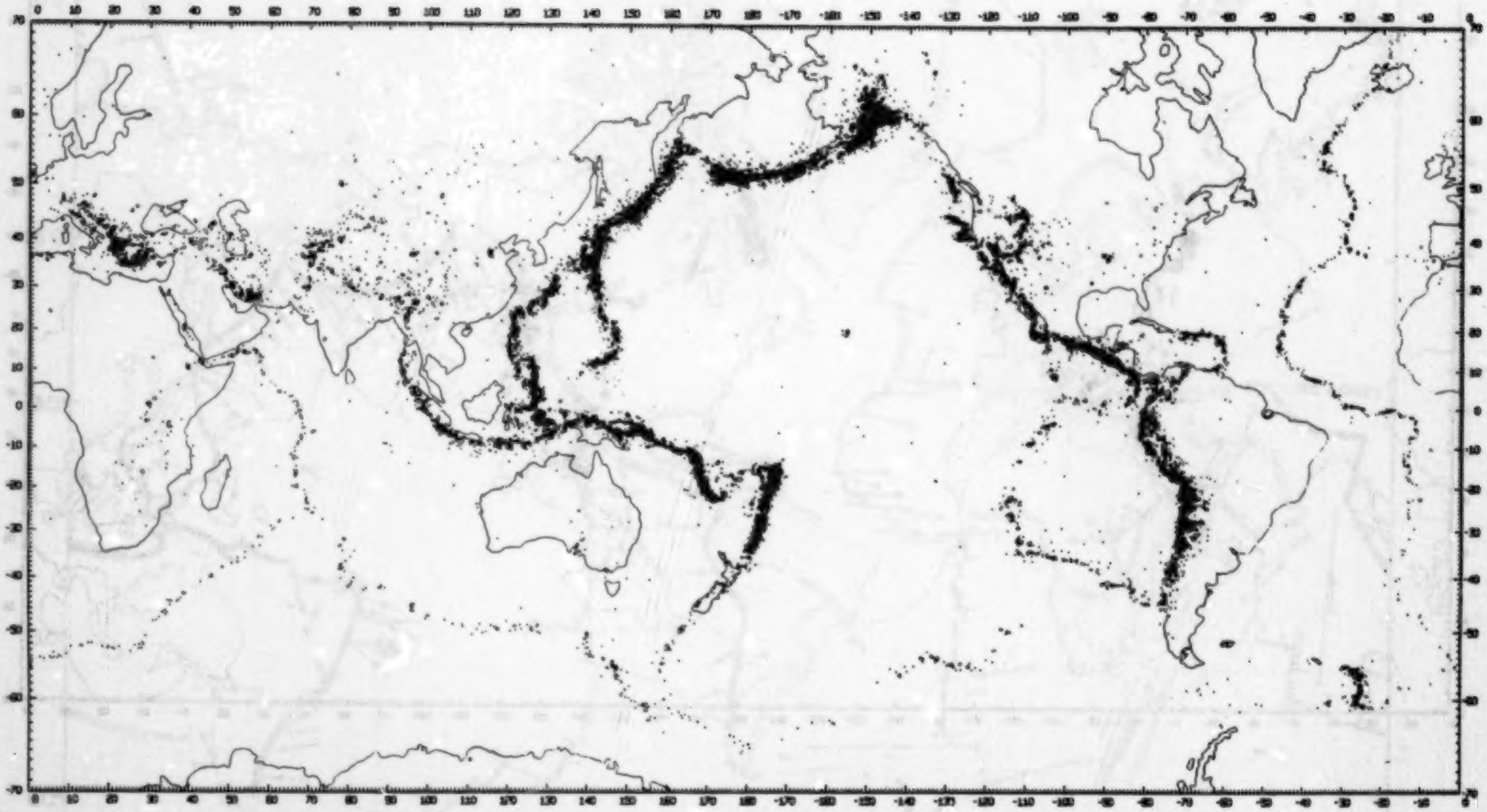

Figure 3. Distribution of world earthquakes of 1961-1967 at depths less than 100 kilometers, (Barazangi and Dorman, 1969).

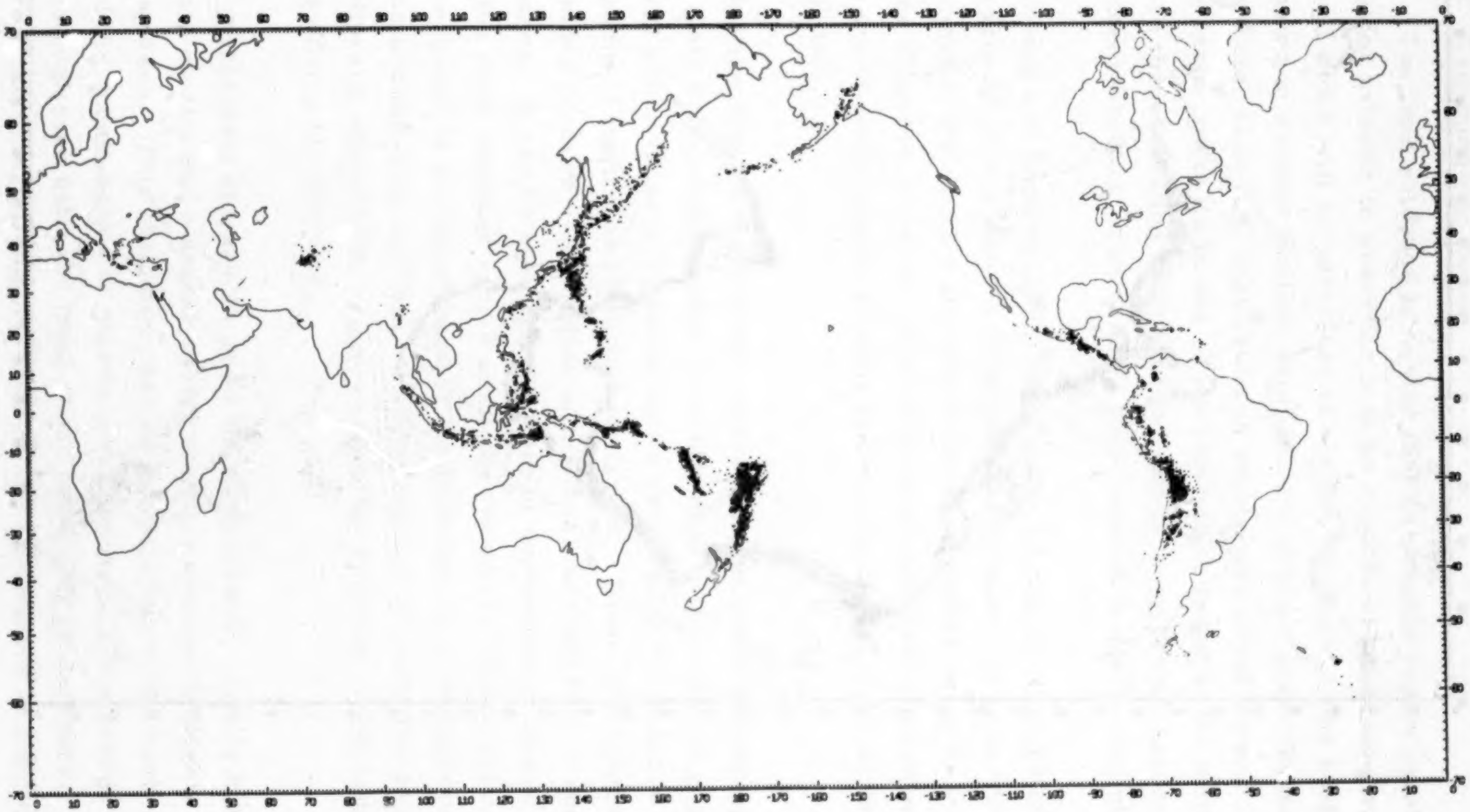
0
10
20
30
40
50
60
70
80
90
100
110
120
130
140
150
160
170
180
-170
-160
-150
-140
-130
-120
-110
-100
-90
-80
-70
-60
-50
-40
-30
-20
-10
0
70
60
50
40
30
20
10
0
-10
-20
-30
-40
-50
-60
-70

Figure 4. Distribution of world earthquakes of 1961-1967 with focal depths between 100 km and 700 km (Barazangi and Dorman, 1969).

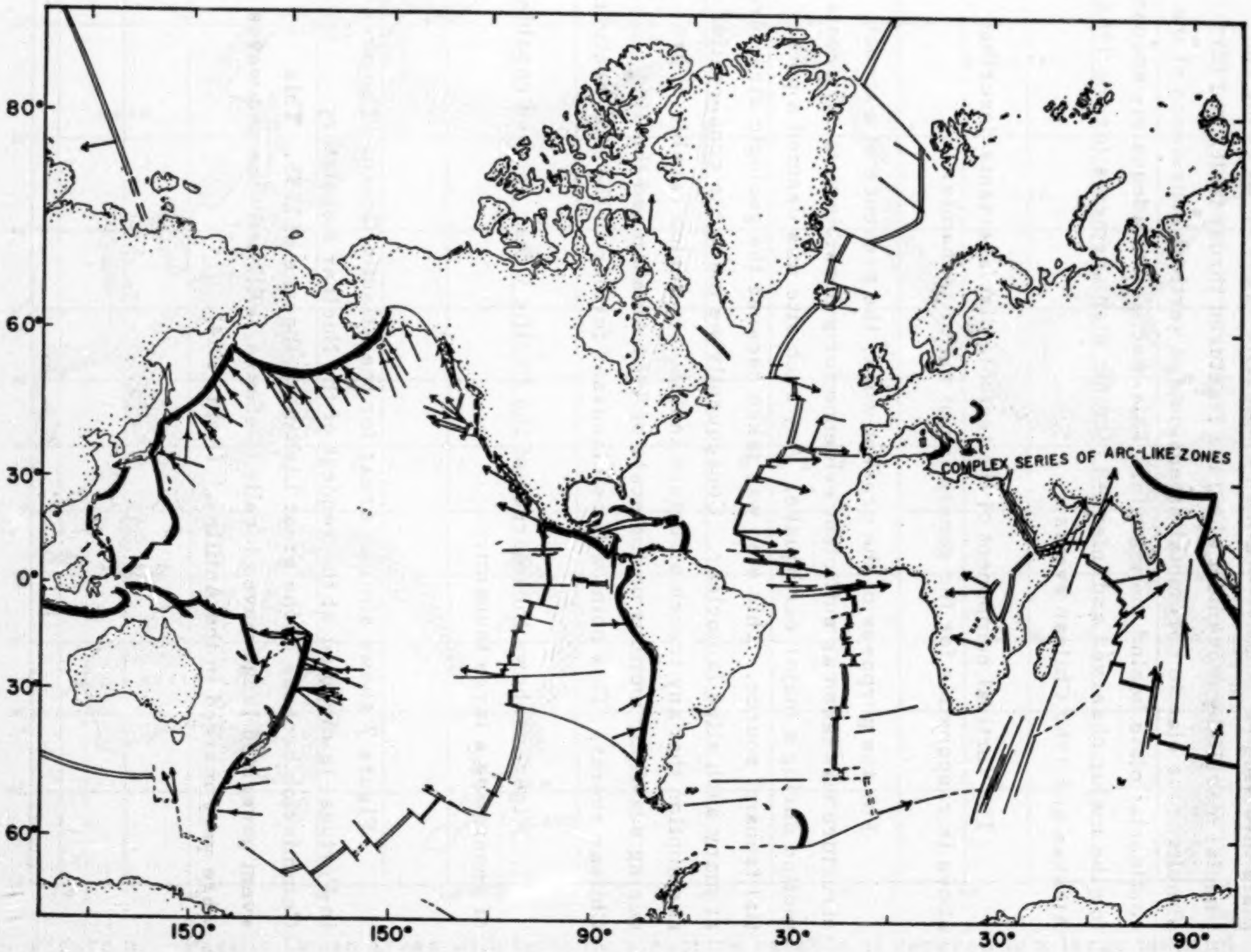
80°
60°
30°
0°
30°
60°
150°
150°
90°
30°
30°
90°
COMPLEX SERIES OF ARC-LIKE ZONES

Figure 5. Summary map of slip vectors derived from studies of earthquake mechanisms, (Isacks et al, 1968).

of great earthquakes is accompanied by elastic rebound in the continental plate involving (1) relative seaward displacement and uplift of the continental margin by movement along the fractured thrust fault, and (2) simultaneous elastic horizontal extension and vertical subsidence of the continental plate behind the margin. This mechanism adequately accounts for the major observed and inferred tectonic displacements for the 1964 Alaskan and 1960 Chilean events.

The vertical component of the tectonic displacements described above is responsible for the generation of major tsunamis.

For the purposes of the present work, the presence of a trench structure was taken as sufficient evidence for a possible vertical crustal motion during a major earthquake. Any such site was deemed a potential tsunami source. This step was taken because the geologic structure at many such sites is unclear. Consequently we make the conservative assumption that any trench structure indicates a region capable of producing sea-floor motions on the scale of 1964 Alaskan and the 1960 Chilean events. This point will be discussed further in the next section.

Figure 6 shows those areas of the Pacific Ocean deemed capable of generating a large tsunami.

Figure 7 shows similar areas for the Atlantic Ocean. The area in Portugal is included at the request of the Nuclear Regulatory Commission because of the great Lisbon earthquake of 1755. This event generated large waves locally (DeSousa, 1911) and "the sea waves were very marked in the Antilles." (Reid, 1914).

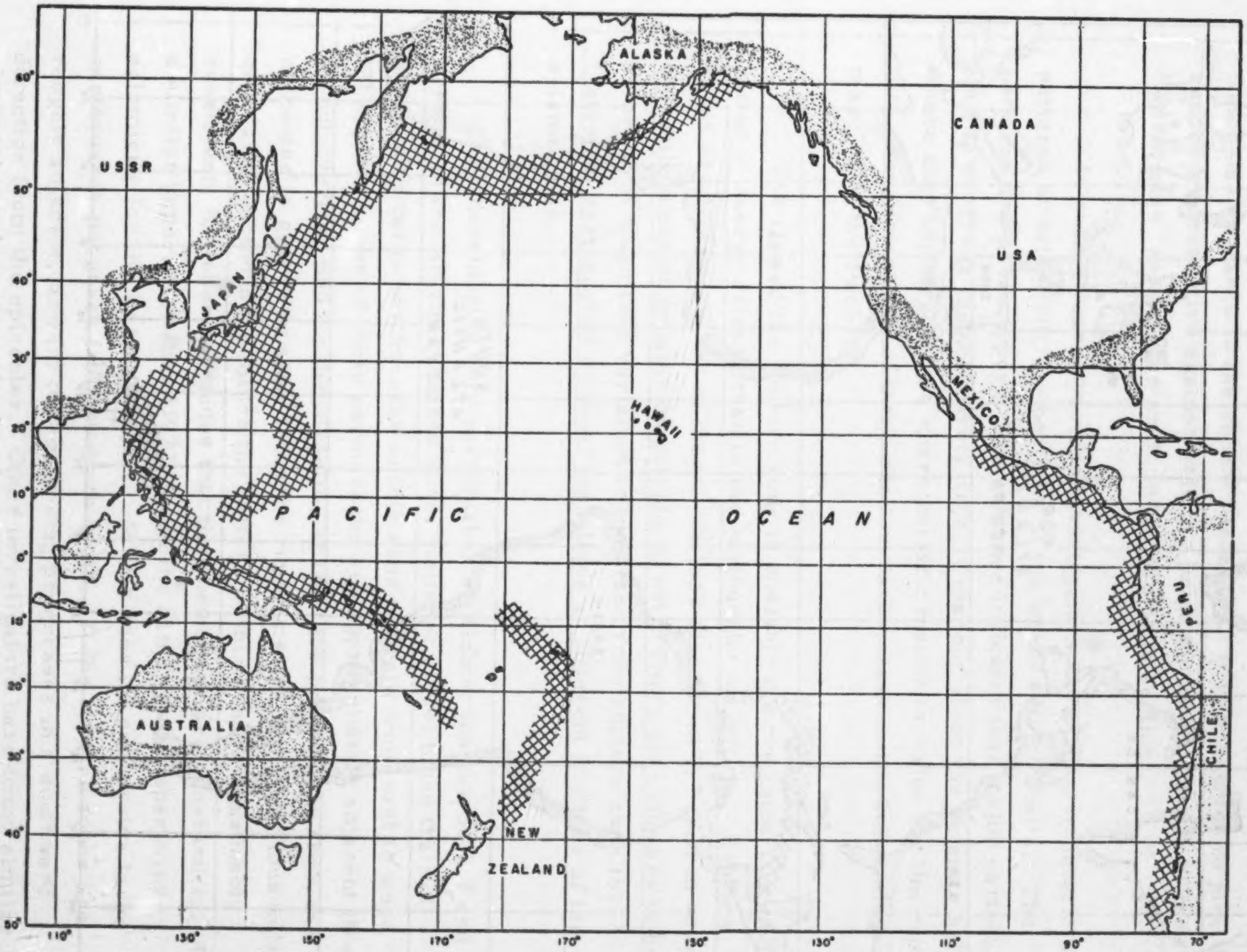
USSR
ALASKA
CANADA
USA
JAPAN
MEXICO
HAWAII
PACIFIC
OCEAN
PERU
CHILE
AUSTRALIA
NEW ZEALAND
60°
50°
40°
30°
20°
10°
0°
10°
20°
30°
40°
50°
110°
130°
150°
170°
170°
150°
130°
110°
90°
70°

Figure 6. Pacific Ocean areas with tectonic structure capable of generating a large tsunami are shown with hatched lines.

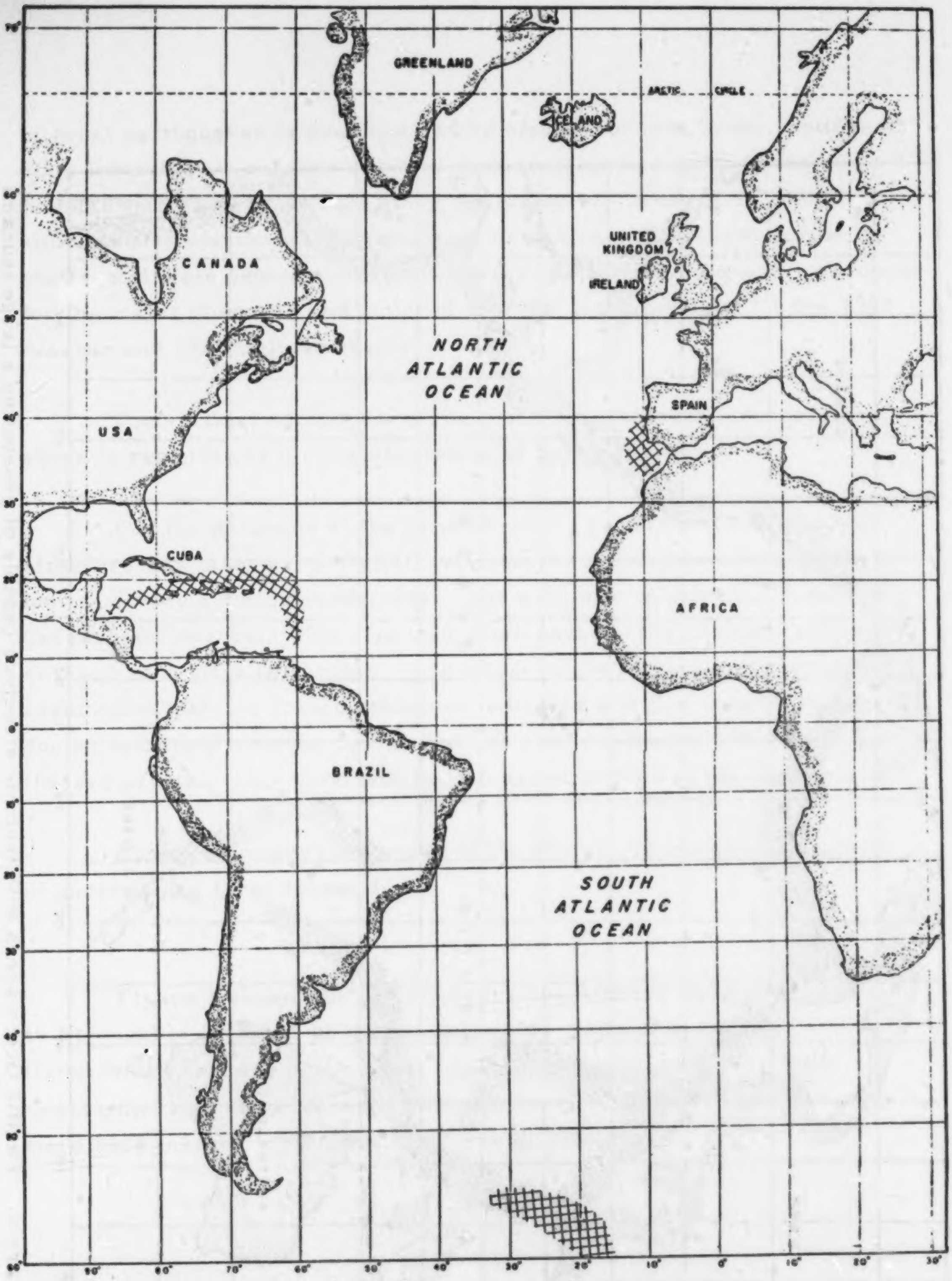
GREENLAND
ARCTIC CIRCLE
ICELAND
UNITED KINGDOM
IRELAND
CANADA
NORTH ATLANTIC OCEAN
USA
SPAIN
CUBA
AFRICA
BRAZIL
SOUTH ATLANTIC OCEAN
70°
60°
50°
40°
30°
20°
10°
0°
10°
20°
30°
40°
50°
60°
90°
80°
70°
60°
50°
40°
30°
20°
10°
0°
10°
20°
30°

Figure 7. Atlantic Ocean areas capable of generating a large tsunami are shown within hatched lines

2.3 Earthquake Prediction in Tsunamigenic Zones

This section summarizes work on earthquake prediction which has appeared in the recent literature. It is presented to give the reader a perspective against which to judge the conservatism of the "worst case" assumption made in the previous section.

In recent years, various investigators have begun to determine patterns of seismicity for portions of the world seismic belts. The patterns are of two types. The evidence indicates that major earthquakes tend to progress in a relatively orderly manner along the seismic belts. There also appears to be a characteristic maximum value for the rupture zone dimensions of large shallow earthquakes in the subducting margins of the Pacific.

The size of the rupture zone is possibly a more important indication of energy release than is the earthquake magnitude. Rupture zones of adjacent quakes of magnitude less than about 7.7 tend to overlap while those of greater magnitude do not. There also appears to be an order of magnitude variation in the size of the rupture zone for historical earthquakes of equal magnitude at different portions of the seismic belt.

By considering only earthquakes of Richter magnitude 7.7 and greater in the Aleutian-Alaska zone, Kelleher (1970) found that; (1) successive large earthquakes in this zone migrate from east to west, (2) rupture zones of these earthquakes are approximately adjacent (they do not overlap, and (3) the direction of fracture propagation from the epicenter is generally away from the rupture zone of the previous adjacent large earthquake. Since the pattern in this area is reasonably consistent, Kelleher concludes that the phenomena are non-random. In a similar paper, Kelleher (1972) found the same type of space-time seismicity for the Peru-Chile arc. In this zone (1) successive large earthquakes progress from north to south, (2) the rupture zones are roughly adjacent, and (3) the fracturing progresses in a southward direction from the epicenter. Other investigators have found similar patterns for the Japan and Kurile-Kamchatka arcs.

In a separate study, Kelleher et al (1974) found that the characteristic maximum dimensions for a particular segment of a subduction zone are strongly influenced by the tectonic geometry of the zone, in particular the width of the interface between the continental and oceanic slabs of lithosphere. This width is the downdip dimension of the zone of contact between slabs. Geometry dictates that the zone of contact will widen as the downdip angle of the oceanic slab decreases. As the width and contortion of such an interface increase, larger amounts of tectonic strain may be stored; hence larger amounts of energy are available for release when the zone fractures, as it ultimately must. Kelleher et al conclude that detailed knowledge of interface geometries may provide a technique for estimating the extent of the greatest shallow earthquake likely to occur in a given area.

Using the relative motions at plate boundaries together with the conclusions of the above studies, it is possible to roughly locate areas where the risk of a large earthquake is high with respect to that in surrounding areas. The technique has not advanced to the point where it is possible to assign a hard probability to such an event.

The theory of plate tectonics allows the estimation of the rate of strain energy accumulation at subduction zones due to the motion of the adjoining plates. Vulcanism, earthquakes and aseismic creep are the mechanisms by which this accumulated energy is released. In those areas where creep is not important, the infrequent, great earthquake ($M \geq 7.8$) accounts for nearly all of the seismic energy release (Sykes, 1971). The manner of energy release along the convergent margin of a plate will depend in rough fashion upon the structure of the interface. Near a short segment of the plate boundary with a narrow interface, plate motion may be accomodated by moderate and relatively frequent events, whereas along a nearby segment with a wider interface, plate motion may be accomodated by larger but less frequent events.

The presence of a segment along a subduction zone where seismic activity has been low for 10's or 100's of years leads generally to two possible conclusions. Either strain energy is being released by tectonic creep, or energy is accumulating for a large earthquake. The record of historical earthquakes in the area may help to decide between the alternatives. Recent investigations suggest that seismic gaps are more likely to be locations for large earthquakes in the near future than are those segments of a plate boundary that have ruptured recently as a result of large earthquakes (Kelleher et al, 1973). If large earthquakes occurred in such an area at 10's of years intervals, then this activity is expected to continue. If no historic earthquakes have occurred then the historic record may be only a fraction of the recurrence interval in an area. In this case, seismologists generally take the conservative view that in such areas strain is building for an earthquake of unknown recurrence interval.

In summary, tectonic strain along subduction zones appears to be relieved mostly by periodic large earthquakes, regardless of the presence of fault creep and small-magnitude earthquakes. Kelleher et al (1973) argue that fault segments characterized by aseismic creep should still be considered potential sites for large earthquakes unless persuasive evidence to the contrary is available.

As an aside to this study, we outline below those areas picked by Kelleher as having above average potential for a large magnitude earthquake within approximately the next decade. Note that the sites listed below are only those located in tsunami producing subduction zones. Kelleher (1970) suggests that a major earthquake may occur in the Alaska-Aleutian arc with epicenter near 56°N - 158°W before about 1980 with a rupture zone extending southwest. The northern Kurile Islands and the Commander Islands also are listed as likely locations for future large earthquakes. We note that the strike component of any fault slip at the Commander Islands may account for most of the motion and hence the possible vertical component may not be as large as for major fault slips in the rest of the Aleutian arc. This means that the Commander Islands area may have less potential for tsunami generation than other subduction zone areas. Kelleher (1972) concludes that southern Peru (12.5°S - 14°S) and northern Chile (17°S - 25°S) are the regions of the South American subduction zone with above average seismic potential.

2.4 Canonical Earthquake and Bottom Displacement

In this section, we will present some of the deterministic results for earthquake magnitude, energy, length of fault slip and maximum displacement. The limitations of these results will be discussed and then the rationale for our choice of canonical earthquake and its associated ground motion will be presented.

The common measure of the size of an earthquake is its Richter magnitude, M, defined as the logarithm to base 10 of the maximum displacement (in microns) traced on a seismograph of standard type (Weed-Anderson, static magnification 2800) at a distance of 100 km from the epicenter. The number thus defined has no physical significance, it merely is a convenient indicator of size. There appears to be a close relationship between energy released as seismic waves and earthquake magnitude. The Richter magnitude is empirically related to the energy released in seismic waves by the expression of Gutenberg and Richter (1956)

$$\log_{10} E_s = 11.8 + 1.5\,M \qquad (1)$$

where E_s is in ergs. Other investigators have determined expressions with similar form and differing numerical constants. It has been estimated that the greatest earthquake possible would release 5×10^{25} ergs of seismic energy (Okamoto, 1973, p. 40). This corresponds to a Richter magnitude of 9.27 by equation (1). Some investigators feel that the size of the rupture zone is a more important indication of energy release for great earthquakes than is the magnitude (Kelleher, 1970). This upper limit should be viewed with skepticism.

Frequency-magnitude relationships have been empirically derived for various regions of the Pacific seismic belt. These equations take the form

$$\log_{10} N = a + b\,(8 - M) \qquad (2)$$

where N is the mean annual number of occurrences, and a and b are constants which vary for different regions. Table 1 gives values of these constants for some subduction zones of the Pacific Seismic belt.

TABLE 1

Region	Coefficients of Equation (2)		Earthquake Magnitude for N=0.1 (Once/10 yrs.)	Time Interval (1/N yrs.) for M=8 Earthquake	Reference
	a	b			
Alaska	-1.02	0.98	8.0	10	Berg, E., 1964
Japan	-1.08	0.72	7.9	12	Tsuboi, 1957
	-0.90	0.80	8.1	8	Gutenberg and Richter, 1954
South America	-1.10	0.45	7.8	13	Gutenberg and Richter, 1954
Southwest Pacific	-1.23	1.01	7.8	17	Gutenberg and Richter, 1954

Unfortunately for the present study, the data upon which equation (2) and Table 1 are based is statistically valid only for moderate to large earthquakes ($M \leq 7$). Relations of the form of equation (2) become unreliable for very large magnitudes due to the scarcity of data.

Recent investigators have made estimates of recurrence intervals for great earthquakes based on tectonic theory. Estimates for the Gulf of Alaska region have ranged from 30 to 850 years for an earthquake of the size of the 1964 event (Sykes, 1971). If the recurrence interval is truly 850 years then such an event is of minor significance for common engineering design. On the other hand, this event recurring at 30-year intervals would be of critical importance to a design with a projected life of 50 years. Faced with this uncertainty, the conservative design engineer may have to specify the maximum possible (reasonable?) event.

It has been found that great earthquakes ($M > 7.8$) show a marked tendency for elongation of their rupture zones. A number of investigators have found empirical relations between the length of slipped fault and earthquake magnitude (Wilson, 1969). However, data on which these relations are based comes primarily from earthquakes on strike-slip faults and consequently are not strictly applicable to this study.

The best indications of the dimensions of the area of permanent vertical displacement due to great earthquakes are those found by Plafker and Savage (1970) for the May, 1960 Chilean event of magnitude 8.5 and by Plafker (1972, 1971) for the 1964 Gulf of Alaska event of magnitude 8.4. These displacements are shown in Figures 8 and 9. The Chilean event had vertical displacement over an area of approximate dimensions 1,050 km long by 300 km wide. The Alaskan event had vertical displacements over an area of approximate dimensions 950 km long by 500 km wide.

There are relations obtained by several investigators for the maximum amount of fault displacement (magnitude of horizontal and vertical displacement). Wilson (1969) gives the following conservative relation for magnitude M greater than 7.5:

$$\log_{10} \Delta = .45M - 2.72 \qquad (3)$$

where Δ is the magnitude of the displacement (in meters). The size of the vertical component of Δ which is of the most importance to this study will depend upon the nature of the faulting. The Chilean event had a maximum vertical displacement of 5.7 meters and the Alaskan event had a maximum vertical displacement of 11.3 meters (Plafker, 1972).

The displacement profile across a continental margin (subduction zone) for a very large earthquake appears to be typically dipolar in nature; uplift of the sea floor and subsidence of the adjacent land. This can be explained by the simple model shown in Figure 10. Figure 10a shows a schematic of a subduction zone where a continental plate is overriding an oceanic plate, but no elastic stress has accumulated. Over a period of many years (perhaps centuries) the underthrusting oceanic

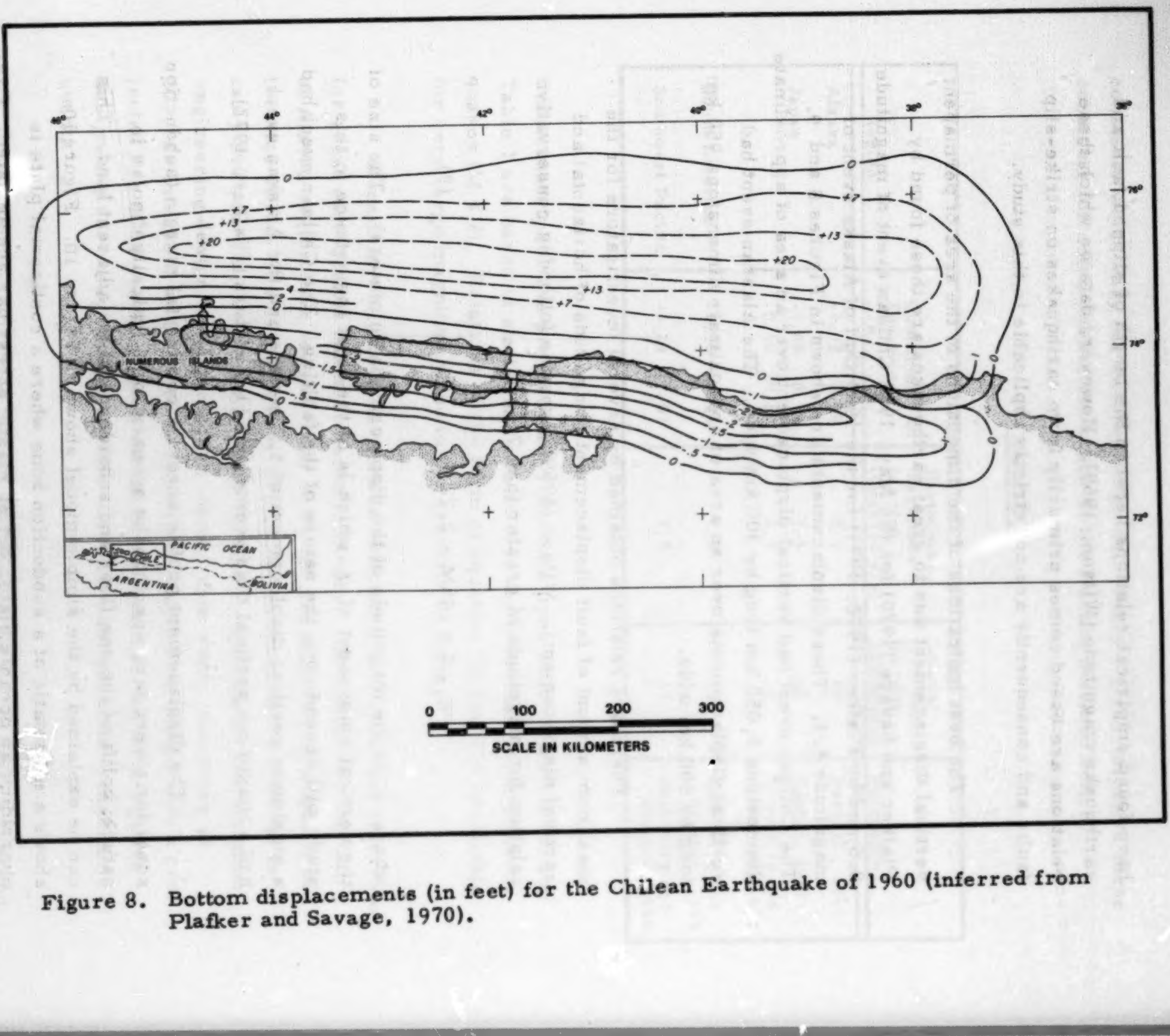
46°
44°
42°
40°
38°
36°
76°
74°
72°
0
+7
+13
+20
4
2
0
-.5
-1
-1.5
-2
NUMEROUS ISLANDS
PACIFIC OCEAN
CHILE
ARGENTINA
BOLIVIA
0
100
200
300
SCALE IN KILOMETERS

Figure 8. Bottom displacements (in feet) for the Chilean Earthquake of 1960 (inferred from Plafker and Savage, 1970).

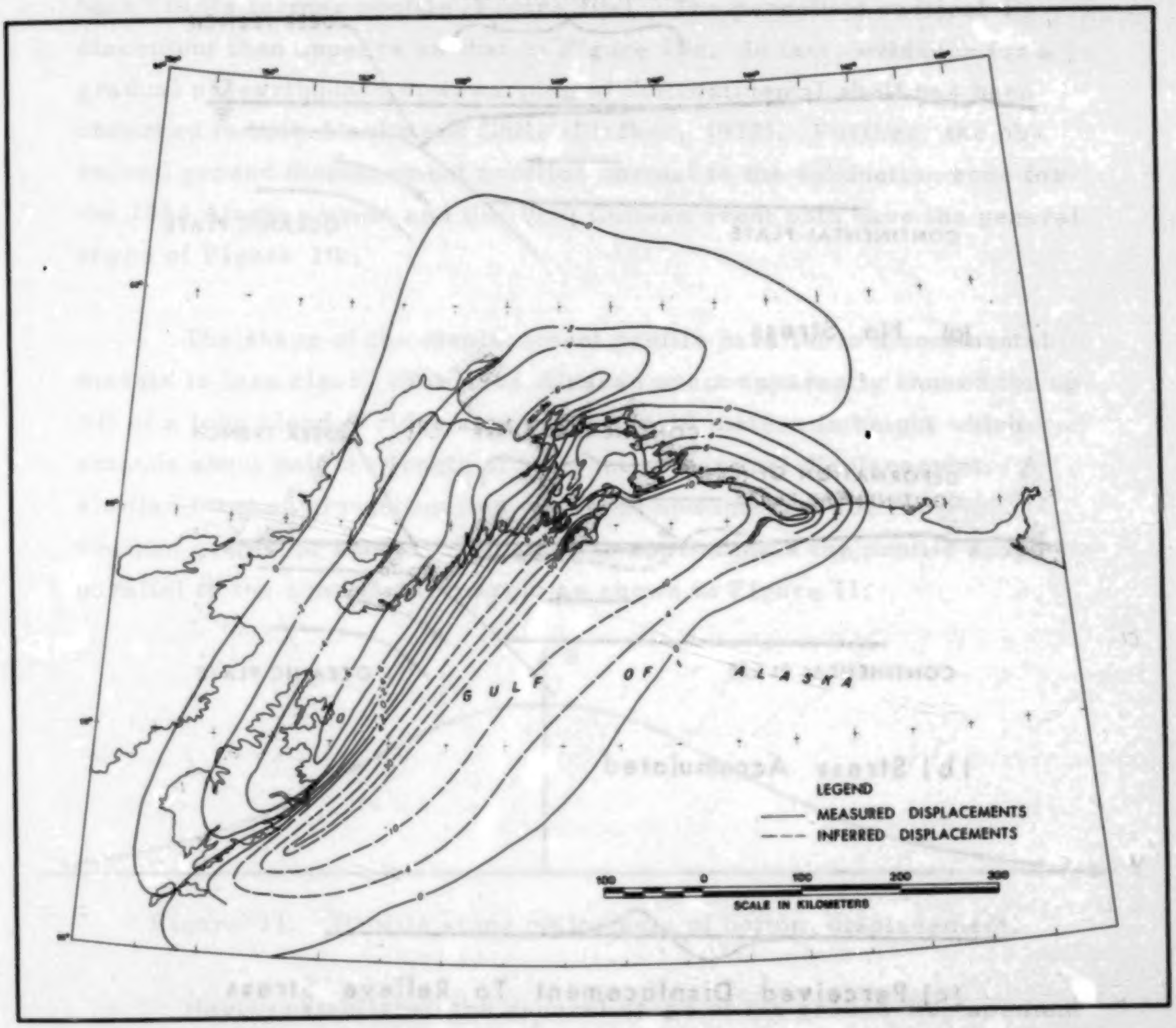
GULF OF ALASKA
LEGEND
MEASURED DISPLACEMENTS
INFERRED DISPLACEMENTS
100 0 100 200 300
SCALE IN KILOMETERS

Figure 9. **Bottom displacements (in feet) for the Alaskan Earthquake of 1964 (inferred from Plafker, 1969).**

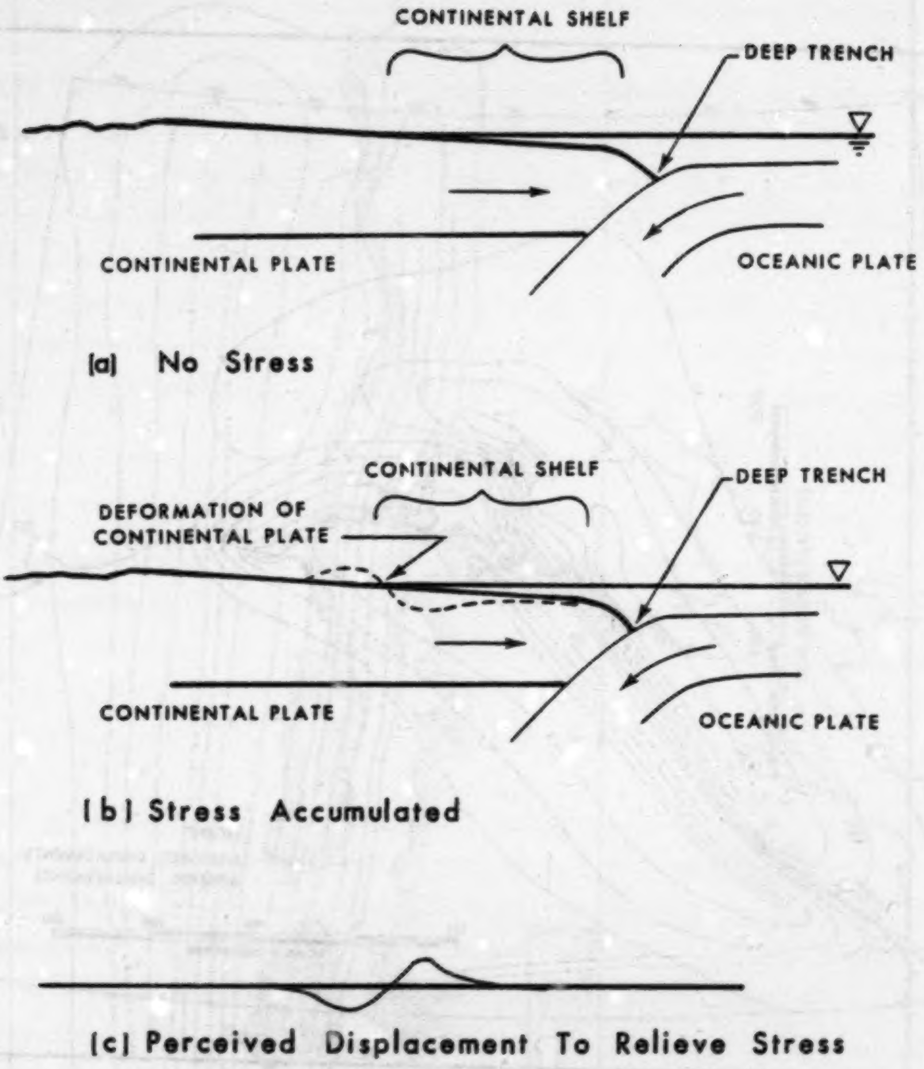
CONTINENTAL SHELF
DEEP TRENCH
CONTINENTAL PLATE
OCEANIC PLATE
(a) No Stress
CONTINENTAL SHELF
DEEP TRENCH
DEFORMATION OF CONTINENTAL PLATE
CONTINENTAL PLATE
OCEANIC PLATE
(b) Stress Accumulated
(c) Perceived Displacement To Relieve Stress

Figure 10. Simple model of dipolar displacement.

plate causes the continental plate to become warped in the manner shown in Figure 10b with consequent storage of elastic energy. When the thrust fault eventually fractures, the continental plate is allowed to "spring back" to its former profile (Figure 10a). The perceived vertical displacement then appears as that in Figure 10c. In fact, evidence for a gradual preearthquake downwarping of the continental shelf has been observed in both Alaska and Chile (Plafker, 1972). Further, the observed ground displacement profiles normal to the subduction zone for the 1964 Alaskan event and the 1960 Chilean event both have the general shape of Figure 10c.

The shape of the displacement profile parallel to a continental margin is less clear. The 1964 Alaskan event apparently caused the uplift of a long slender ridge approximately 10 meters in height which extends about half the length of the zone of vertical displacement. A similar marked elongation was observed and inferred for the 1960 Chilean event. It seems reasonable to approximate the profile shape parallel to the continental margin as shown in Figure 11.

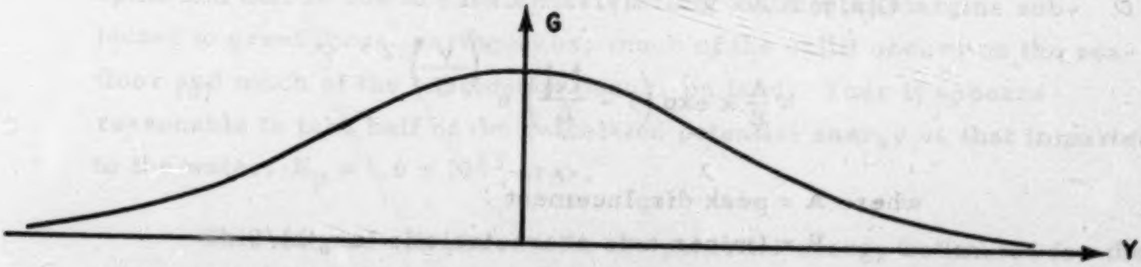

Figure 11. Profile along major axis of bottom displacement.

Having established the general shape of the ground displacement profiles normal and parallel to the subduction zone, the approximate horizontal dimensions of the zone of vertical motion and an approximate peak value, we can now postulate a canonical ground displacement which is reasonable for use in the numerical calculations of this study. In order that application of this ground displacement to subduction zones of various latitudes and orientations be convenient, an analytical form was desired.

The profile parallel to the subduction zone axis was chosen to be of Gaussian form

$$f(y) = e^{-\left(\frac{y}{c}\right)^2} \qquad (4)$$

where y is measured from the center of the elongated displacement region parallel to the major axis of the region (Figure 13), and c is an empirical constant. Note that $f(y) = 1$ when $y = 0$.

The profile normal to the subduction zone axis was chosen to be the exponential form

$$g(x) = \frac{1}{B}\, x \exp\left(1 - \frac{|x|}{B}\right) \qquad (5)$$

where x is measured from the center of the displacement region normal to the axis of the subduction zone and B is an empirical constant. Note that $g(x) = \pm 1$ when $x = \pm B$.

The expression for the displacement at any point within the displacement region is then the product of an amplitude A, f(y) and g(x):

$$G(x, y) = A \cdot g(x) \cdot f(y)$$

$$= \frac{A}{B}\, x \exp\left(1 - \frac{|x|}{B}\right) e^{-\left(\frac{y}{C}\right)^2} \qquad (6)$$

where A = peak displacement
B = (minor axis characteristic length)/9
C = (major axis characteristic length)/2.2

The characteristic lengths are defined with reference to contour values of the displacement. The major axis characteristic length is defined as twice the distance from the minor axis to the furthest point of the displacement contour with a value 3 percent of the peak value. The minor axis characteristic length is defined as twice the distance from the major axis to the furthest point of the displacement contour with a value of 8 percent of the peak displacement. The factors used in defining B and C were determined empirically.

The peak displacement was chosen to be 9.15 meters (30 feet). The minor axis length was chosen to be 480 km (260 nautical miles). The major axis length was chosen to be 1,066 km (575 nautical miles). These dimensions describe a composite of the 1960 Chilean and 1964 Alaskan displacements. This source is somewhat larger than either of two of the largest tsunamigenic earthquakes ever recorded. The family of contours defined by equation (6) are shown in Figure 12. A perspective view of the surface is shown in Figure 13.

The potential energy imparted to a packet of water with surface area S uplifted distance h is given by

$$E_p = \frac{1}{2}\rho g \, S \, h^2 \qquad (7)$$

This expression may be integrated over the region of ground motion with $h = G(x, y)$ to find the potential energy imparted by the canonical ground motion. If this is done for the ground motion described by equation (6) centered at the approximate latitude of the 1964 Gulf of Alaska earthquake (58°N), a potential energy of approximately 3.3×10^{23} ergs is obtained. Of this potential energy, half is due to uplift and half is due to subsidence. Along continental margins subjected to great thrust earthquakes, much of the uplift occurs on the seafloor and much of the subsidence occurs on land. Thus it appears reasonable to take half of the calculated potential energy as that imparted to the water, $E_p \approx 1.6 \times 10^{23}$ ergs.

This may be compared with the potential energy estimated for the 1964 Gulf of Alaska tsunami. According to Berg et al (1972) this is 2.2×10^{22} ergs. The energy released as seismic waves by the Gulf of Alaska event ($M \approx 8.4$) may be estimated using the Gutenberg-Richter formula as 2.5×10^{24} ergs. For this event the tsunami energy is 0.88 percent of the seismic energy. We note in passing that tsunami magnitude is extremely sensitive to the efficiency of the generator. Iida (1963) has presented empirical relations between tsunami magnitude and earthquake magnitude which suggest that the efficiency may range much higher than the value given above; however, the relations are based primarily upon data taken near Japan, and hence are not generally applicable.

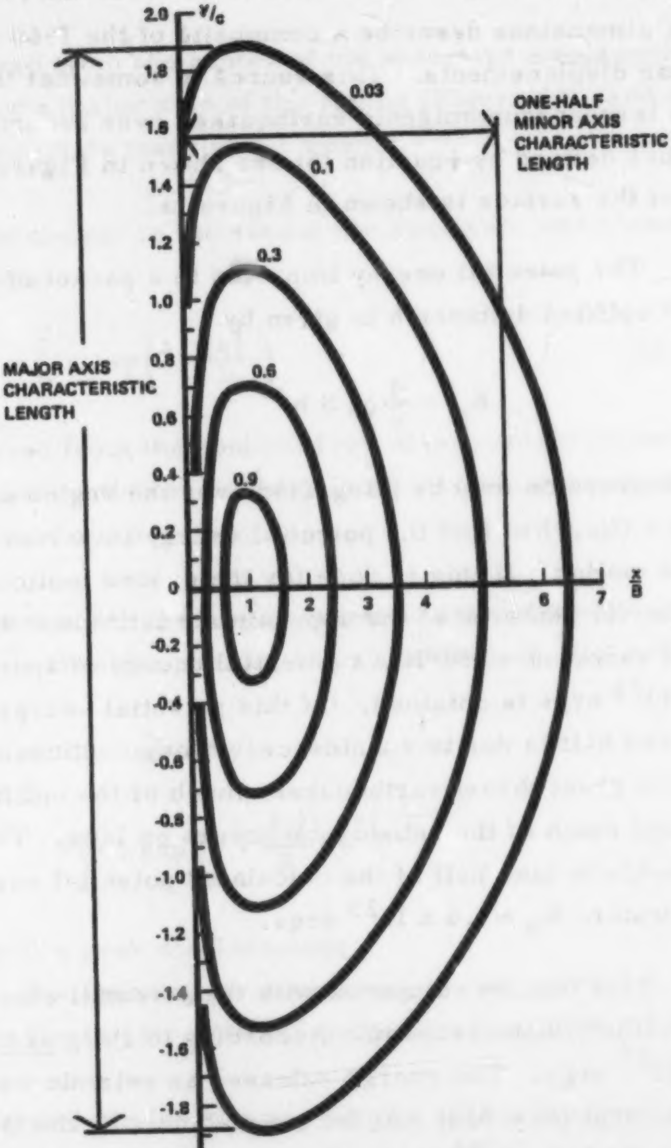

Figure 12. Contours of canonical bottom displacement (only positive side is shown).

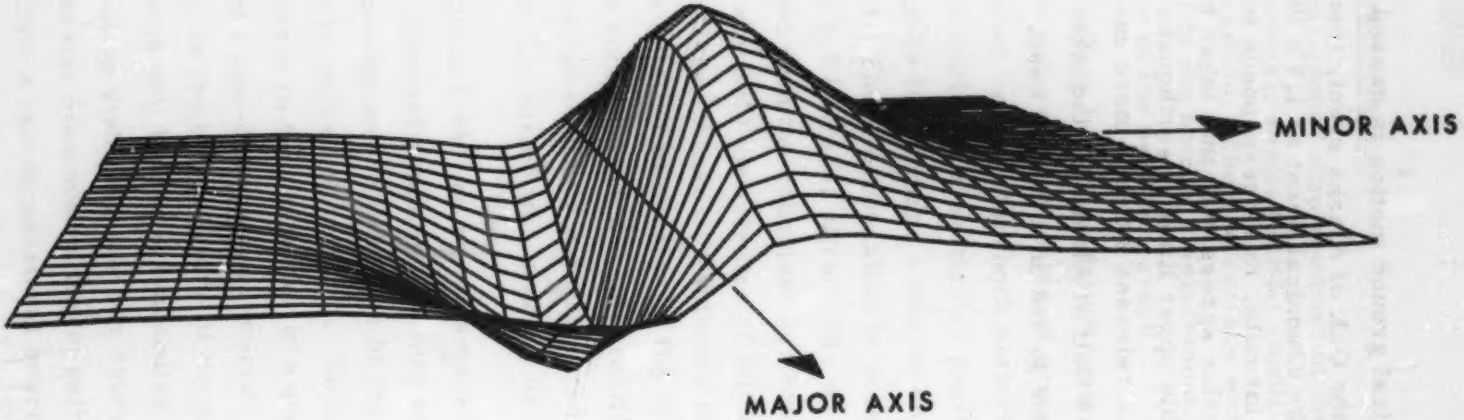
MINOR AXIS
MAJOR AXIS

Figure 13. Perspective view of canonical bottom displacement.

If the canonical ground motion is caused by a mechanism as efficient as that of the Gulf of Alaska event, then we can estimate the energy release of the canonical event as 1.9×10^{25} ergs. From the Gutenberg-Richter formula, this corresponds to an earthquake magnitude of 9.0. This value agrees with that taken by King and Knopoff (1968) as a reasonable upper limit to earthquake magnitude. The canonical earthquake releases 8 times more energy than the extraordinarily large 1964 Gulf of Alaska earthquake. Thus, the canonical event is probably safe to use as a "worst case."

3. TSUNAMI GENERATION

3.1 Source Characteristics

The canonical ground displacement of the previous section was used as an instantaneously applied initial condition for the calculations of tsunami propagation. The sea surface was assumed to have a displacement identical to the bottom displacement. The validity of this assumption is shown in the next paragraph.

An earthquake rupture begins at the epicenter and propagates as a shock wave radially out over the region of ground displacement which is roughly delineated by the aftershock pattern. This shock is thought to set off ground motion at a particular point as it passes that point; this motion continues for perhaps a minute and results in some permanent displacement. Shock propagation in rock occurs at a velocity on the order of 3.5 km/sec. From this we conclude that ground motion associated with the canonical earthquake will be entirely completed within approximately six minutes of initiation. If the water depth is taken as 500 meters, it takes 114 minutes for a long water wave to propagate across the smaller dimension of the displaced region. Thus the uplift which is completed in a small fraction of the characteristic wave travel time is conveniently approximated by an instantaneous uplift. The same conclusion was reached by Hammack (1972).

The work of Kajiura (1963) on an instantaneously generated tsunami in an ocean of constant depth and infinite extent allows us to make some general remarks on the influence of the source shape on the character of the distantly perceived tsunami. Kajiura shows that there is a fundamental difference in the character of waves from a one-dimensional source and a two-dimensional source. The leading wave from a line source will be the highest wave of the train while that from a two-dimensional source will be some succeeding wave, arriving later in the train with increasing distance from the source. These relative characteristics will persist even over a travel path with variable depth. The height of a wave from a two-dimensional source of any shape will be proportional to the total volume of deformation of the bottom.

Kajiura's results are obtained for the case where the distance from the source is very much greater than the source dimension. For source dimensions a and b and distance r, Kajiura requires

$$\frac{\sqrt{a^2 + b^2}}{r} << 1 \qquad (8)$$

It may be that the world oceans are simply not large enough to allow observation of the predicted effects. For a point offshore of the U. S. west coast (40°N, 125°W) and a source in the Western Pacific (2.5°S, 139.5°E) with the characteristic dimensions established in the previous section, Equation (8) gives a ratio of 0.11. For the same source located in the Gulf of Alaska (58°N, 152°W) the ratio is 0.92. Neither of these cases convincingly satisfies Equation (8).

How do these results relate to the present study? The canonical ground displacement may be expected to generate a wave train such that its maximum displacement from still water will occur at some wave after the leading wave. However, cases where this does not occur will not be surprising, since the effects of coastal boundaries and refraction are not accounted for by Kajiura and since the source dimension and source-receptor distance differ by less than a factor of 10. In any case, the magnitude of the peak displacement in the arriving wave train is expected to be directly proportional to the peak value of the canonical ground displacement.

3.2 Source Selection

The canonical ground displacement described in section 2.4 was successively fitted in an approximately contiguous manner into the subduction zones shown in Figure 6 for the Pacific Ocean and Figure 7 for the Atlantic Ocean. This procedure resulted in a set of 34 tsunamigenic bottom displacements in the Pacific and 5 in the Atlantic. Our choice of sources is conservative in the sense that any region with even a remote chance of generating a tsunami was considered a possible source. As future work improves our understanding of the undersea faulting, some of the sources used here may be found to be unrealistic.

Each bottom displacement is described by the latitude and longitude of its center; the bearing with respect to true North of a line directed from its center to the positive peak; a characteristic length describing the major axis; a characteristic length describing the minor axis; a peak displacement; and a shape parameter. The shape parameter allows specification of a negative monopole, a positive monopole or a dipole for the source. Dipolar sources were used exclusively in this study.

The parameters used for the Pacific sources are listed in Table 2, and the source locations are illustrated in Figure 14. The parameters used for the Atlantic sources are listed in Table 3, and the source locations are illustrated in Figure 15.

All of the sources listed were placed so that their major axes were parallel to the trench axes. The horizontal positions of the source centers place them on the continental side (the overthrusting side for oceanic trenches) of the trench. Note that by this placement, some of the ground displacement pattern will usually fall on land areas, with consequent reduction of tsunami energy. This is an important effect, but since the same thing will happen in prototype displacements, we have not tried to normalize the sources to have similar energies.

All of the sources were placed at known or suspected subduction zones with a single exception. In the Atlantic Ocean, displacement number 4 is located on the coast of Portugal at the request of the Nuclear Regulatory Commission based on the great earthquake which occurred there in 1755.

TABLE 2

Parameters for Locating Canonical Bottom Displacements in Pacific Ocean

The following characteristics are the same for all bottom displacements: Major axis characteristic length - 1,066 km (575 n.m.), Minor axis characteristic length - 480 km (260 n.m.), dipolar shape, peak displacement 9.15 meters (30 feet).

No.	Latitude	Longitude	Bearing	Identification
1	30°S	178°W	108°	Kermadec Islands
2	20°S	174°W	110°	Tonga Islands
3	13.5°S	175°W	40°	Samoan Islands
4	21°S	168°E	55°	Loyalty Islands
5	13°S	165°E	61°	Santa Cruz Islands
6	8°S	157°E	31°	Solomon Islands
7	4°S	148°E	8°	Bismarck Sea
8	2.5°S	139.5°E	16°	New Guinea
9	1.5°N	131°E	36°	Moluccan Islands
10	9°N	127°E	81°	Mindanao, Philippines
11	18°N	123.5°E	67°	Luzon, Philippines
12	25.5°N	126°E	145°	Okinawa
13	32.5°N	134°E	143°	Kyusku, Japan
14	8°N	136°E	146°	Palau
15	13°N	144.5°E	147°	Marianas-South
16	19.5°N	146.5°E	69°	Marianas-North
17	25°N	144.5°E	66°	Iwo Jima
18	31°N	141.5°E	79°	Japan Trench-South
19	39.5°N	143°E	108°	Japan Trench-North
20	45.5°N	150°E	143°	Kuril Islands
21	52°N	159°E	121°	Kamchatka Peninsula
22	54°N	169°E	212°	Near Islands
23	51.75°N	177.5°W	179°	Andreanof Islands
24	54°N	164°W	151°	Fox Islands
25	58°N	152°W	138°	Gulf of Alaska
26	17°N	100.5°W	202°	Mexico
27	13.5°N	91°W	205°	Guatemala
28	9°N	84°W	213°	Costa Rica
29	1°N	79.5°W	300°	Columbia-Equador
30	9°S	79°W	239°	Peru-North
31	16.5°S	73°W	220°	Peru-South
32	24°S	70.5°W	274°	Chile-North
33	33.5°S	72.5°W	280°	Chile-Central
34	43.5°S	74°W	280°	Chile-South

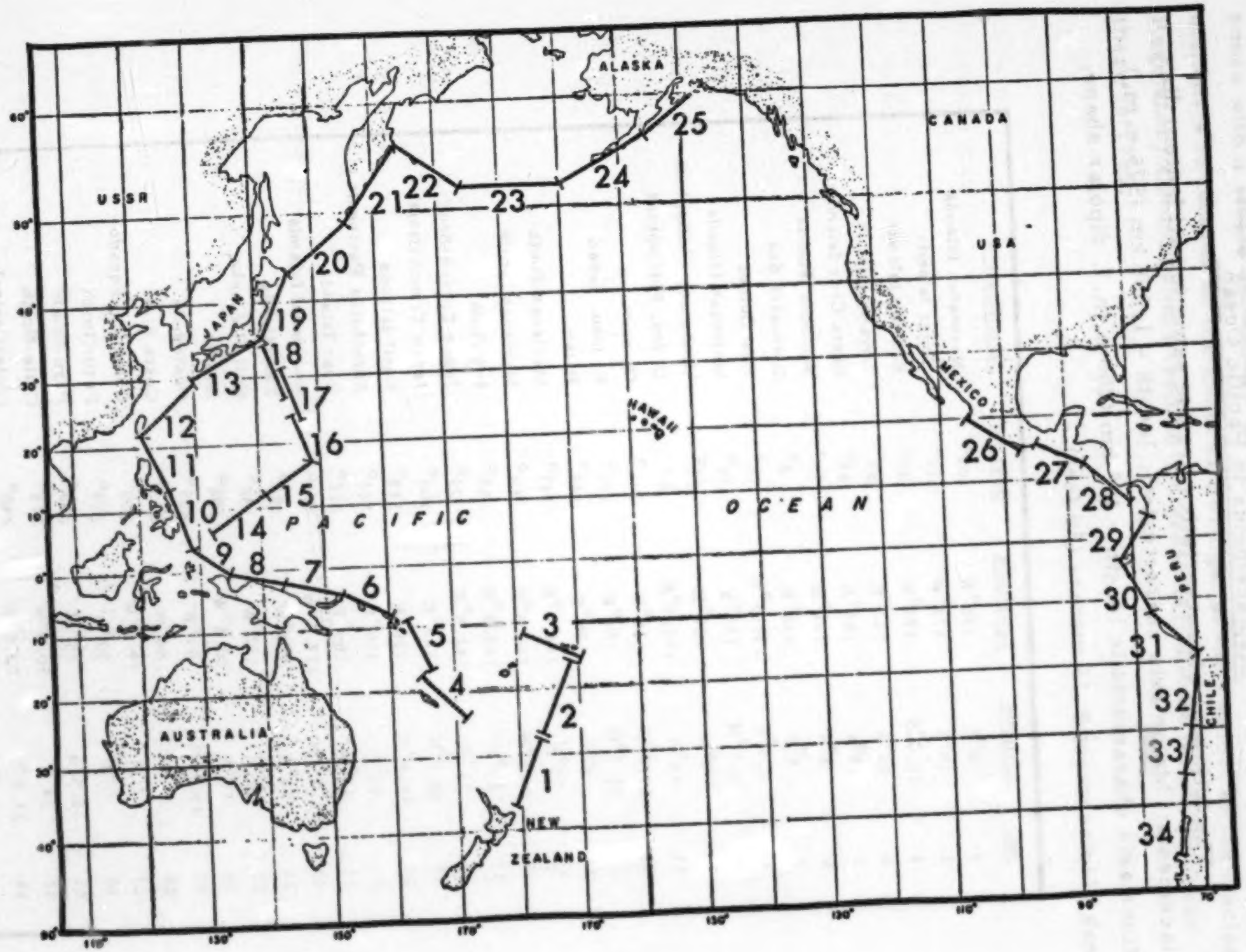
USSR
ALASKA
CANADA
USA
MEXICO
JAPAN
HAWAII
PACIFIC
OCEAN
PERU
CHILE
AUSTRALIA
NEW ZEALAND
1
2
3
4
5
6
7
8
9
10
11
12
13
14
15
16
17
18
19
20
21
22
23
24
25
26
27
28
29
30
31
32
33
34
60°
50°
40°
30°
20°
10°
0°
10°
20°
30°
40°
50°
110°
130°
150°
170°
170°
150°
130°
110°
90°
70°

Figure 14. Distribution of Canonical Earthquakes in Pacific Basin. Numbers correspond to those in Table 2.

TABLE 3

Parameters for Locating Canonical Bottom Displacements in Atlantic Ocean

The following characteristics are the same for all bottom displacements: Major axis characteristic length - 1,066 km (575 n.m.), Minor axis characteristic length - 480 km (260 n.m.), dipolar shape, peak displacement 9.15 meters (30 feet).

No.	Latitude	Longitude	Bearing	Identification
1	19°N	80°W	340°	Cuba
2	19°N	67°W	0°	Haiti
3	16°N	62°W	70°	Leeward Islands
4	38°N	10°W	255°	Lisbon, Portugal
5	56°S	27°W	10°	South Sandwich Islands

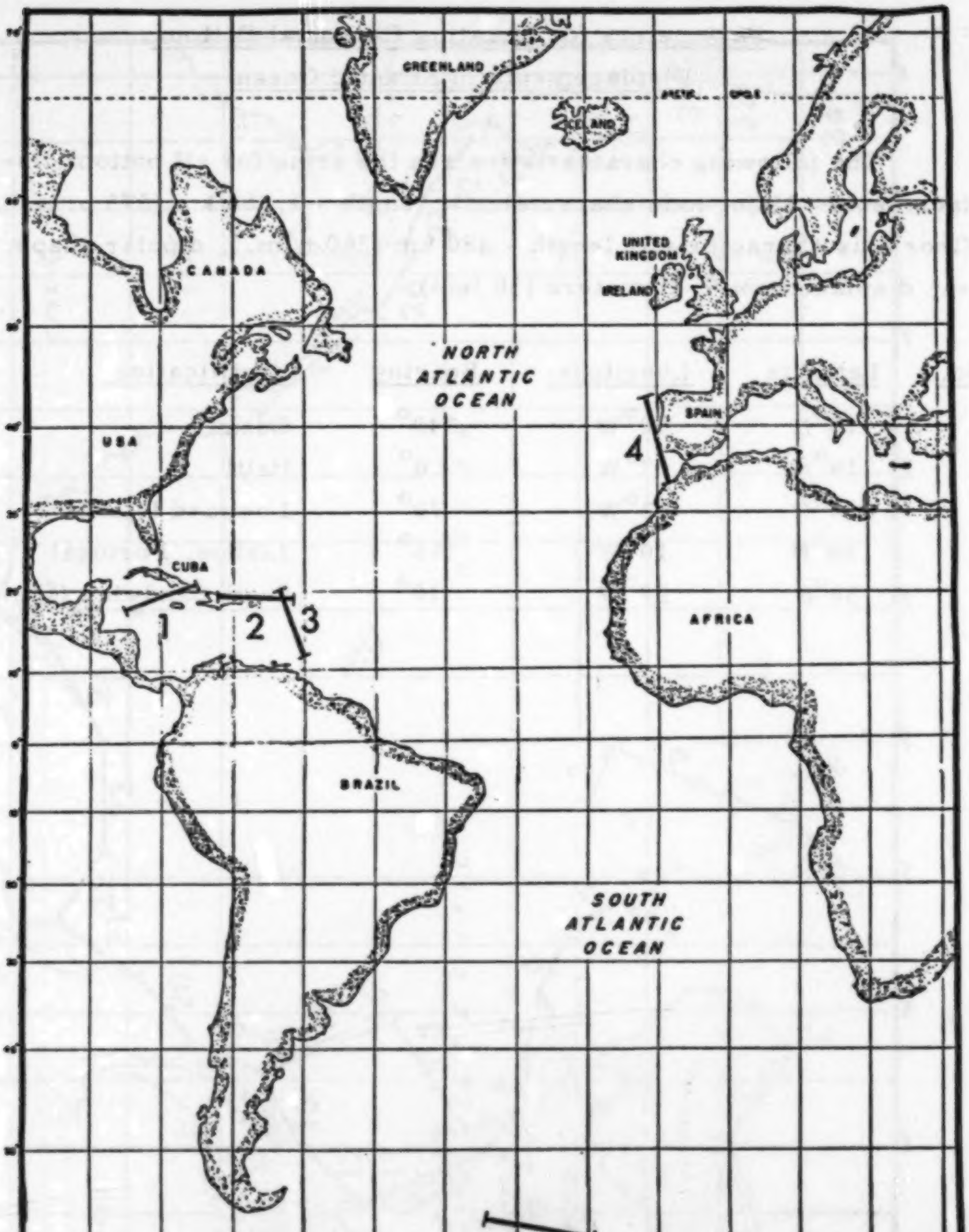
GREENLAND
ICELAND
UNITED KINGDOM
IRELAND
CANADA
NORTH ATLANTIC OCEAN
SPAIN
4
USA
CUBA
1
2
3
AFRICA
BRAZIL
SOUTH ATLANTIC OCEAN
5

Figure 15. Distribution of Canonical Earthquakes in Atlantic Basin. Numbers correspond to those in Table 3.

4. TSUNAMI PROPAGATION

4.1 Equations of Motion

The linearized equations of motion for long water waves propagating in a thin layer over a rotating sphere are:

$$u_t = -\frac{g}{R}\frac{\partial\eta}{\partial\theta} + fv \qquad (9)$$

$$v_t = -\frac{g}{R\sin\theta}\frac{\partial\eta}{\partial\varphi} - fu \qquad (10)$$

$$\frac{1}{R\sin\theta}\left\{\frac{\partial}{\partial\theta}\left((h)u\sin\theta\right) + \frac{\partial}{\partial\varphi}\left((h)v\right)\right\} = -\frac{\partial}{\partial t}(\eta) \qquad (11)$$

where subscripts denote partial differentiation and

η = displacement of the water surface from the still water level
u = velocity component in the θ-direction
v = velocity component in the φ-direction
θ = latitude measured from zero at the North Pole
φ = longitude measured east from Greenwich
t = time
g = acceleration of gravity
h = water depth
R = Earth radius
f = Coriolis parameter ($2\Omega\cos\theta$)
Ω = Earth's rotation rate

These equations are derived from the Navier-Stokes equations in spherical coordinates by assuming vertical accelerations to be small. This implies that pressures may be assumed hydrostatic and that higher order terms may be neglected. The interested reader is referred to Batchelor (1967).

A few words are in order regarding the validity of the numerical model. Granting that tsunamis are shallow water waves, there are three sets of differential equations that have been successfully used for describing long water waves. These are the finite-amplitude equations, the Boussinesq equations, and the linearized long-wave equations (which are adopted in this study). The selection of the most appropriate of these sets of equations is dictated by two parameters, σ^2 and ϵ. σ is the ratio of water depth to wavelength, and ϵ is the ratio of wave amplitude to water depth. Mathematically, ϵ and σ are parameters in power series expansions of the inviscid, incompressible versions of the Navier-Stokes equations and the appropriate boundary conditions. The sizes of the parameters dictate which terms are to be kept in deriving simplified equations. Further, the parameters indicate the time scales within which a simplified equation set applies. Physically, ϵ is a measure of amplitude dispersion and σ^2 is a measure of frequency dispersion. The ratio of these, ϵ/σ^2, is called the Ursell parameter. In what follows, we make use of order notation, viz., O(1) means "of order unity."

Peregrine (1972a) develops each of the three sets of equations and we now summarize his results. The finite amplitude equations are valid for small values of ϵ as long as σ is sufficiently small, that is, $U >> 1$. The Boussinesq equations are applicable if ϵ is small and if σ^2 is of the same order as ϵ, that is $U \sim O(1)$. The linearized long-wave equations are valid for small σ as long as ϵ is sufficiently small, that is $U << 1$.

In this study, we are interested primarily in the longest period components (say 1 hour). We may take the average ocean depth h 5500 meters; surface displacement, $y \sim 0.2$ meter and wavelength $L \sim T\sqrt{gh} = (3600)(9.8 \text{ m/sec}^2 \times 5500 \text{ m})^{\frac{1}{2}} \sim 8.4 \times 10^5$. Then $\epsilon \sim 10^{-5}$ and $\sigma^2 \sim 10^{-5}$. In this case $U \sim O(1)$ and use of the Boussinesq equations is indicated.

The prospect of having to solve the Boussinesq equations in a region of variable depth is unsettling since such a solution in finite difference form is complex and there are numerous computational difficulties. Fortunately, solution of the Boussinesq equations is not necessary. Peregrine (1972b) has shown that the neglect of non-linear terms (as contained in the Boussinesq equations) causes a cumulative error on the solution to the linear equations which becomes appreciable after a dimensionless time $t \sim \epsilon^{-1}$. Thus, solutions to the linearized long-wave equations remain valid for small ϵ and σ as long as $t < \epsilon^{-1}$. To obtain time in dimensional units, the dimensionless time ϵ^{-1} must be multiplied by the scale factor $\sqrt{h_o/g}$, where h_o is a characteristic depth. Since tsunami travel time is spent almost entirely in the deep ocean ($\epsilon \sim 10^{-5}$), we obtain a maximum time of $(10^{-5})^{-1}$ $(5500/9.8)^{\frac{1}{2}}$ or $\sim 10^6$ seconds. On the other hand, the characteristic time of propagation of a tsunami across the oceans is $\sim 10^4$ seconds (maximum calculation time was 7×10^4 seconds). In short, the world oceans are simply not big enough to allow the errors caused by a linear treatment to grow to significant size. We conclude that the linear model used in the study is valid in this application.

Near the region of generation, non-linear effects become important and should be accounted for in calculating wave histories at near source points. However as the wave system traverses the open ocean the shorter waves (which require the non-linear treatment near the source) dissipate, leaving only the long components, and these are amenable to linear treatment. In fact the principle of superposition says that the long components can be treated linearly at any distance from the source.

It is also required, but often not stated, that derivatives of the depth (d_x, d_{xx}, etc.) be of order ϵ. This is a very restrictive condition in the context of steep island slopes or continental margins. However, as is often the case, it will appear that the theory can be pushed beyond these limits to quite a degree with good success (one thinks, for example, of the simplest sinusoidal deepwater wave theory which is strictly valid only for waves of zero height but which is remarkably accurate for waves of near limit steepness).

4.2 Computational Scheme

The finite difference scheme for the solution of equations (9), (10), and (11) is staggered in both space and time. The staggered spatial grid is shown in Figure 16. Water surface displacements are staggered in time with respect to velocities. Flow quantities are calculated on this grid at successive time steps, explicitly.

Let

$$u(x,y,t) = u\Big\{(j-\tfrac{1}{2})\,\Delta x,\ k(\Delta y),\ (n-\tfrac{1}{2})\,\Delta t\Big\} = u^{n}_{k,j}$$

$$v(x,y,t) = v\Big\{(j)\,\Delta x,\ (k-\tfrac{1}{2})\,\Delta y,\ (n-\tfrac{1}{2})\,\Delta t\Big\} = v^{n}_{k,j}$$

$$\eta(x,y,t) = \eta\Big\{(j)\,\Delta x,\ (k)\,\Delta y,\ (n)\,\Delta t\Big\} = \eta^{n}_{k,j}$$

Equations (8), (9), and (10) are written in finite difference form as:

$$u^{n+\frac{1}{2}}_{k,j} = u^{n-\frac{1}{2}}_{k,j} - \frac{g\Delta t}{R\cdot\Delta\theta}\,(\eta^{n}_{k,j} - \eta^{n}_{k,j-1}) + 2\cdot\Omega\cdot\cos\theta\cdot v^{n-\frac{1}{2}}_{k,j} \qquad (12)$$

$$v^{n+\frac{1}{2}}_{k,j} = v^{n-\frac{1}{2}}_{k,j} - \frac{g\cdot\Delta t}{R\cdot\Delta\phi\cdot\sin\theta_{j}}\,(\eta^{n}_{k,j} - \eta^{n}_{k-1,j}) - 2\cdot\Omega\cdot\cos\theta\cdot u^{n-\frac{1}{2}}_{k,j} \qquad (13)$$

$$\begin{aligned}\eta^{n+1}_{k,j} = \eta^{n}_{k,j} &- \frac{\Delta t}{2R\,\Delta\theta\sin\theta_{j}}\Big\{u^{n+\frac{1}{2}}_{k,j+1}\Big(d^{n}_{k,j+1} + d^{n}_{k,j}\Big)\sin\theta_{j+\frac{1}{2}} \\ &\qquad - u^{n+\frac{1}{2}}_{k,j}\Big(d^{n}_{k,j} + d^{n}_{k,j-1}\Big)\sin\theta_{j-\frac{1}{2}}\Big\} \\ &- \frac{\Delta t}{2R\,\Delta\phi\sin\theta_{j}}\Big\{v^{n+\frac{1}{2}}_{k+1,j}\Big(d^{n}_{k,j} + d^{n}_{k,j}\Big) \\ &\qquad - v^{n+\frac{1}{2}}_{k,j}\Big(d^{n}_{k,j} + d^{n}_{k-1,j}\Big)\Big\}\end{aligned} \qquad (14)$$

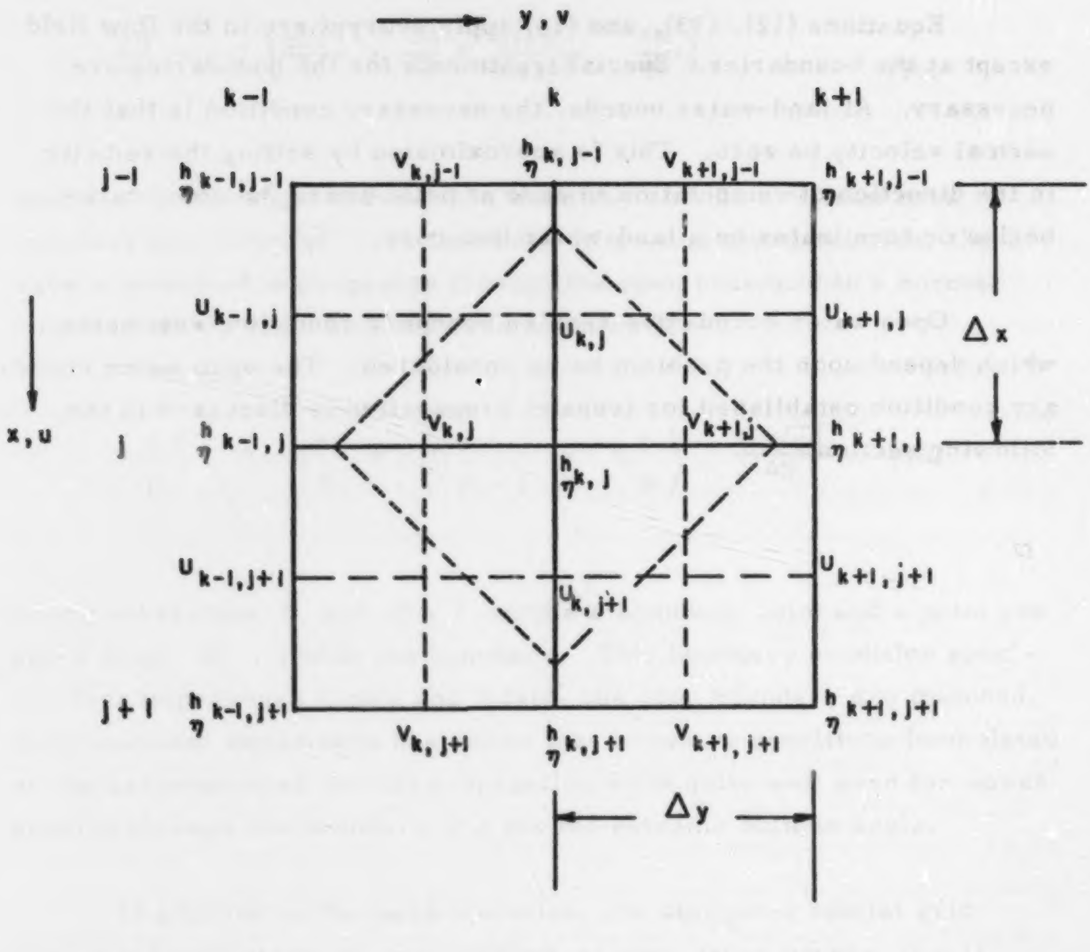
y, v
k−1
k
k+1
j−1
$\overset{h}{\eta}_{k-1,j-1}$
$V_{k,j-1}$
$\overset{h}{\eta}_{k,j-1}$
$V_{k+1,j-1}$
$\overset{h}{\eta}_{k+1,j-1}$
$U_{k-1,j}$
$U_{k,j}$
$U_{k+1,j}$
Δx
x, u
j
$\overset{h}{\eta}_{k-1,j}$
$V_{k,j}$
$V_{k+1,j}$
$\overset{h}{\eta}_{k+1,j}$
$\overset{h}{\eta}_{k,j}$
$U_{k-1,j+1}$
$U_{k,j+1}$
$U_{k+1,j+1}$
j+1
$\overset{h}{\eta}_{k-1,j+1}$
$V_{k,j+1}$
$\overset{h}{\eta}_{k,j+1}$
$V_{k+1,j+1}$
$\overset{h}{\eta}_{k+1,j+1}$
Δy

Figure 16. Staggered Grid

Superscripts denote time indices. Calculations for one time step are executed by computing velocities at time index $n + \frac{1}{2}$ using velocities at time index $n - \frac{1}{2}$ and η's at time index n, and then using the new set of velocities and η's at index n to compute the new set of wave elevations, η^{n+1}.

Equations (12), (13), and (14) apply everywhere in the flow field except at the boundaries. Special treatments for the boundaries are necessary. At land-water bounds, the necessary condition is that the normal velocity be zero. This is approximated by setting the velocity in the direction of computation to zero at point where the computation begins or terminates on a land-water boundary.

Open water boundaries require boundary condition treatments which depend upon the problem being considered. The open water boundary condition established for tsunami propagation is discussed in the following section.

4.3 Open Boundary Condition

At grid boundaries in open water, an outgoing tsunami should be totally transmitted through the boundary. The boundary condition should be:

$$\frac{\partial\eta}{\partial t} = -C \left[\frac{\cos\delta}{R} \cdot \frac{\partial\eta}{\partial\theta} + \frac{\sin\delta}{R\sin\theta} \quad \frac{\partial\eta}{\partial\varphi} \right] \qquad (15)$$

where δ is the angle between the wave ray and the artificial open boundary and $C \approx \sqrt{gd}$. In the finite difference approximation, the wave is assumed to propagate through the open boundary in a normal direction with a rigid profile. The equation is:

$$\eta_{B}^{n+1} = \eta_{B}^{n} + \left(\eta_{B-1}^{n} - \eta_{B}^{n} \right) \frac{\Delta t \sqrt{gd}}{\Delta S} \qquad (16)$$

where subscripts B and $B - 1$ denote a boundary point and a point one space step, ΔS , inside the boundary. This boundary condition specifies that impedances inside and outside the open boundary are matched. Computational experience has shown that boundary conditions formulated on the assumption of normal propagation work quite well even for waves passing through the boundary at a not too extreme oblique angle.

In addition to the wave elevation, the staggered spatial grid requires specification of u-velocities at open upper bounds $(j = 1)$ and of v-velocities at open left-side bounds $(k = 1)$. These are computed from the water surface slope.

4.4 Calculation

This section contains a description of the data used as input to the tsunami computations. The general comments here apply equally to calculations in both the Pacific and Atlantic Oceans.

The first step was the establishment of the finite difference grid upon which calculations were made. The choice of a grid involves a compromise balancing considerations of region size and accuracy of calculation against computer core size and execution time. In the present model, execution time varies inversely as the cube of the spatial step size. Previous computational experience has shown that a minimum of 7 grid points per wavelength are required for reasonable accuracy. On the other hand, using many more than this number for this study is not desirable because of the uncertainties of ground displacements and bathymetry detailed in previous sections. For convenience and ease of comparison of results, it was desired to have all sources within the Pacific and Atlantic basins lie within a single grid for each basin. Based on the above considerations, the spatial step size on the spherical coordinate grid was chosen as 1 degree in both latitudinal and longitudinal directions.

This step size allowed the use of a 178 x 118 grid in the Pacific extending from 62°N to 55°S and from 113°E to 70°W. The grid used in the Atlantic was 119 x 130 extending from 70°N to 60°S and from 98°W to 21°E. The numerical code measures longitude, φ , positive east from Greenwich. Latitude, θ , is measured positive south from the pole. The water depths used to describe the ocean bathymetry on these grids were taken from standard nautical charts. The depth grids thus obtained were modified by requiring that the minimum water depth be 600 feet. This minimum depth reduces the range of depths and hence computational difficulties inherent in finite difference models.

Computations made on these grids describe the water surface displacements at successive time steps. The time step DT must observe the Courant condition very strictly. In spherical coordinates, DT must everywhere satisfy:

$$DT \leq \frac{R \cdot \Delta\theta \cdot \Delta\varphi \cdot \sin\theta}{C\sqrt{(\Delta\theta)^2 + (\Delta\varphi \; \sin\theta)^2}} \qquad (17)$$

where $\Delta\theta$ and $\Delta\varphi$ are the latitudinal and longitudinal stepsizes in radians, and C is the wave celerity. Calculations were continued out to a time sufficient for the arrival of the first few waves of a wave train. In most cases, the upper time limit was 70,000 seconds.

Wave histories were recorded at selected points of interest for each canonical source. The primary points of interest for this study were offshore from the United States East, West, and Gulf coasts. In addition, the computed waves were recorded at selected island stations and at stations of the World Data Center Tsunami Network.

The calculations were made using the version of Tetra Tech's program SEAWAVE which is listed in Appendix C. This program was executed on a Control Data 7600 computer. Appendix D is a User's Manual for the program. Each routine is described and input requirements are listed.

4.5 Standardization of Depths at Coastal Points

The numerical code propagates waves to a point which is one grid step away from land. Depths at these points vary greatly. The calculated waves arriving at coastal points should be in uniform depths so as to facilitate comparison. This section presents a simple method for normalizing the computed results at coastal points to a standard depth.

Wave transformation due to varying depths at a coastal segment is approximated by considering wave transformation in a canal of constant width and variable depth. Following Lamb (1932), the one-dimensional equations of momentum and continuity may be combined (in rectangular coordinates) to give

$$\frac{\partial \eta^2}{\partial t^2} = g \frac{\partial}{\partial x} \left(d \frac{\partial \eta}{\partial x} \right) \qquad (18)$$

where η is surface displacement, t is time, x is position, d is depth and g is the acceleration of gravity. Assume that the depth in the canal varies from zero at the closed end ($x = 0$) to d_a at the open end ($x = a$). Consider a sinusoidal wave incident at the open end of the canal

$$\eta = A_o \cos (\sigma t + \delta) \qquad (19)$$

where σ is the angular frequency and δ is some phase factor. Substitution of equation (19) into equation (18) removes the time dependence, yielding

$$\frac{\partial}{\partial x} \left(d \frac{\partial \eta}{\partial x} \right) + \frac{\sigma^2}{g} \eta = 0 \qquad (20)$$

Make the substitutions

$$d = \frac{d_a x}{a} \quad \text{and} \quad k = \frac{\sigma^2 a}{g d_a} \tag{21}$$

and obtain

$$\frac{\partial}{\partial x}\left(x \frac{\partial \eta}{\partial x}\right) + k\eta = 0 \tag{22}$$

A solution of this equation is the power series

$$\eta = C_1 \left(1 - \frac{kx}{1^2} + \frac{k^2 x^2}{1^2 \cdot 2^2} - \ldots.\right) = C_1 J_o \left(2(kx)^{\frac{1}{2}}\right) \tag{23}$$

The Bessel function J_o may be viewed as the product of its modulus and phase factor

$$J_o (z) = M_o (z) \cos\theta_o (z) \tag{24}$$

where

$$M_o (z) = \left(J_o^{\,2} (z) + Y_o^{\,2} (z)\right)^{\frac{1}{2}} \tag{25}$$

Then

$$\eta = C_1 M_o \left(2(kx)^{\frac{1}{2}}\right) \cos\theta_o \left(2(kx)^{\frac{1}{2}}\right) \tag{26}$$

Thus the amplitude of η at some x is

$$A(x) = C_1 M_o \left(2(kx)^{\frac{1}{2}}\right) \tag{27}$$

The constant C_1 is determined by the fact that at $x = a$ the amplitude is $A(a)$, yielding

$$A(x) = \frac{M_o\left(2(kx)^{\frac{1}{2}}\right)}{M_o\left(2(ka)^{\frac{1}{2}}\right)} A(a) \tag{28}$$

The ratio of the moduli is the amplification factor for a sinusoidal wave in a canal whose depth varies to zero at its closed end $(x = 0)$. Note that equation (28) is singular at $x = 0$. Since the point of interest is never at $x = 0$ this behavior is not expected to harm the results. Since $\sigma = 2\pi/T$ where T is the wave period,

$$k = \frac{4\pi^2 a}{gT^2 d_a} . \tag{29}$$

The distance from the shore to the point of standard depth d_b is $b = ad_b/d_a$. Finally

$$A(b) = \frac{M_o\left(2(kb)^{\frac{1}{2}}\right)}{M_o\left(2(ka)^{\frac{1}{2}}\right)} A(a) \tag{30}$$

Equation (30) is the equation used to transform a computed wave displacement at a grid point adjacent to a coastline to the displacement at a point where the depth is the standard depth. For the present work the standard depth d_b was taken as 600 feet (183 meters). On the West coast the results presented apply to the 100 fathom (600 foot) contour. On the East coast the offshore points were set to the minimum depth of 600 feet and no transformation was necessary.

4.6 Verification of the Method

The numerical model used for this work was checked by calculating the tsunami generated by the 1964 Gulf of Alaska earthquake. Bottom displacements indicated by Plafker (1971) were used as the initial condition for the calculation. The calculated waves were compared with observed waves at two sites.

Van Dorn (1969) obtained a record of the 1964 tsunami from a pressure gauge located in 800 feet of water to the southwest of Wake Island. Measurements at this site are expected, a priori, to be somewhat better indicators of midocean tsunami character than those obtained at harbor tide gauges because of the relative absence of perturbing effects (very shallow water, large island, complicated bay-harbor resonance system, etc.). The computed and observed records are shown in Figure 17. The two records agree in general shape and in peak displacement. The greater length of the computed wave is probably due to the coarseness of the grid and the consequent inaccuracies in the initial water surface displacement and in the resolution of the ocean bathymetry, particularly near the source region. Despite these inaccuracies, the general character of the wave is preserved at transoceanic distances, and this strongly validates this application of the numerical method.

A second comparison was made for computed and observed results at Sitka, Alaska. The computed results were obtained at 57°N, 137°W in 7,620 feet of water. In order that the computed result could be compared with the tide gauge record, it was necessary to account in an approximate manner for differences in depth and distance between the points of computation and observation. Sitka is located at approximately 57°N, $135^\circ 20'$W. The water depth is taken as 60 feet at the gauge. The observed record shows a fundamental wave period of 1.8 hours. By the technique of section 4.5 the amplification factor is calculated as 1.6. The average depth over the path from the computation point to observation point is taken as 1,000 feet. Then the indicated time interval by

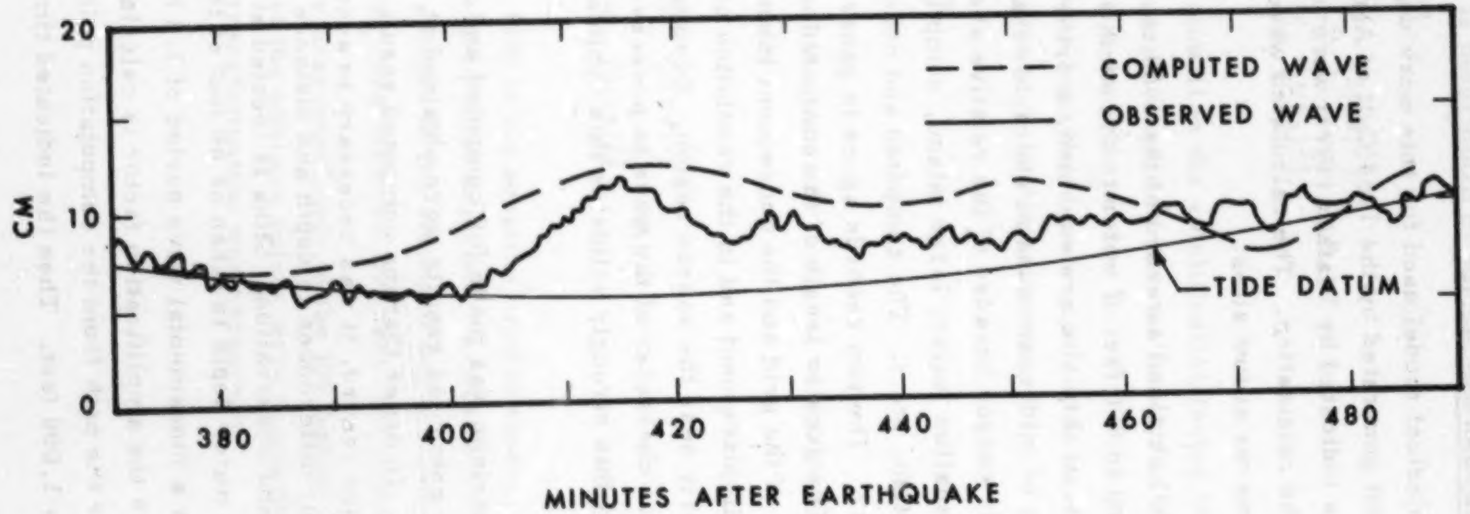

Figure 17. Wake Island record of the Alaska 1964 tsunami (Van Dorn, 1969) and the history computed by the present numerical model (dashed curve).

which to retard the calculated wave is approximately 1,800 seconds. The computed wave thus modified and the tide gauge observation are shown in Figure 18. The first two waves show a remarkable agreement, after which the records diverge. This is naturally expected due to the complicated local bathymetry which is not accounted for in the model.

The model appears to give reasonably good agreement with the best records obtainable of the deep water character of the tsunami. The reader is cautioned that the quality of the results deteriorates after the first few waves because of the perfectly reflecting numerical boundary condition and detailed local bathymetry. The observed and computed waves are in sufficient agreement both quantitatively and qualitatively, to conclude that the numerical model is a valid one.

To complete this verification, it was necessary to ensure that the differences between the computed and observed waves were due solely to resolution effects and not to numerical effects. The computation was repeated on a grid with 0.5 degree spacing interpolated from the 1.0 degree grid. The results (see Chapter 7) were substantially the same, indicating that the 1 degree grid size caused no numerical difficulties.

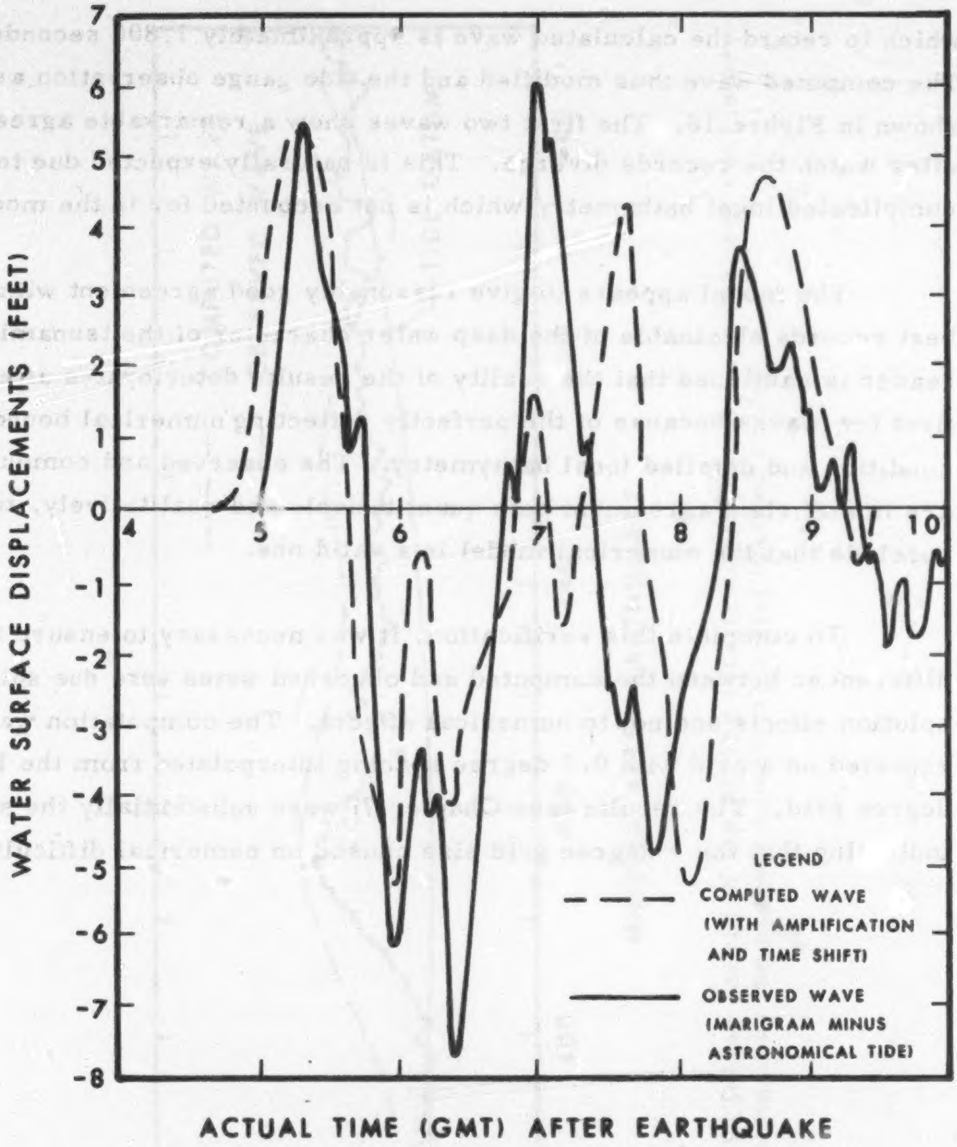

Figure 18. Computed and observed results at Sitka, Alaska. (Earthquake occurred at 3:36 GMT.)

5. RESULTS

This chapter presents the results of the calculated tsunamis arriving at selected stations offshore from the coasts of the United States. In order to facilitate comparisons of results at different stations, the depths at these stations were required to be the same (600 feet). Depths of offshore points on the East coast were increased to the minimum depth of 600 feet, while on the West coast the results were transformed from deeper water to the 600 foot contour. The results presented here show histories of water surface displacement from the levels which would have occurred in the absence of any tsunami ("still water"). The effects of astronomical and storm tides and wind waves should be added to the wave histories shown here to determine "worst case" wave histories.

The Pacific coastal stations for which wave histories are presented are listed in Table 4. Figure 19 shows the locations of these points, together with the highest displacement, at that station, of the canonical set of 34 tsunamis. Detailed results for each Pacific coastal station are presented in Appendix A. For each station, the following information is given: a table showing the displacements, source number, and region ranked by descending magnitude of displacement; a plot of the first 30,000 seconds of the largest tsunami arriving at that station and a similar plot of the next two highest tsunamis. Ignoring displacement and arrival times, one is struck by the similarity of wave shape for the three highest tsunamis arriving at any station and by similiarity of wave shape between stations. This similarity is due to the fixed shape of the canonical source. Note also that the position of the maximum displacement in a wave train occurs later in the train as the associated source becomes more distant from the observing station. This feature was anticipated by Kajiura (1963).

One of the following four sources was responsible for the greatest wave displacement at each of the 19 West coast stations: No. 24 - Fox Islands; No. 25 - Gulf of Alaska; No. 3 - Samoan Islands; and No. 8 - New Guinea. Of these greatest displacements, source 24 accounted for 10, source 25 accounted for 6, source 3 accounted for 2, and source 8 accounted for 1. The South Pacific sources, 3 and 8, accounted for

TABLE 4

PACIFIC COAST STATIONS

Station No.	Latitude	Longitude	Name
1	48°N	125°19'W	Cape Flattery, WA
2	47°N	124°58'W	Grays Harbor, WA
3	46°N	124°401W	Tillamook Head, OR
4	45°N	124°20'W	Cascade Head, OR
5	43°55'N	124°33'W	Hecata Head, OR
6	43°N	124°50'W	Cape Blanco, OR
7	42°03'N	124°35'W	Crescent City, CA
8	41°N	124°22'W	Eureka, CA
9	40°15'N	124°30'W	Cape Mendocino
10	39°N	123°55'W	Point Arena, CA
11	38°10'N	123°20'W	Point Reyes, CA
12	37°08'N	122°41'W	Monterey Bay, CA
13	36°12'N	121°50'W	Point Sur, CA
14	35°10'N	120°50'W	Point Buchon, CA
15	34°20'N	119°55'W	Santa Rosa Island, CA
16	33°401N	118°30'W	Santa Catalina Island, CA
17	33°N	117°19'W	San Onofre, CA
18	32°20'N	117°10'W	Punta San Miguel, B.C. Mexico
19	31°N	116°35'W	Punta Colnett, B.C., Mexico

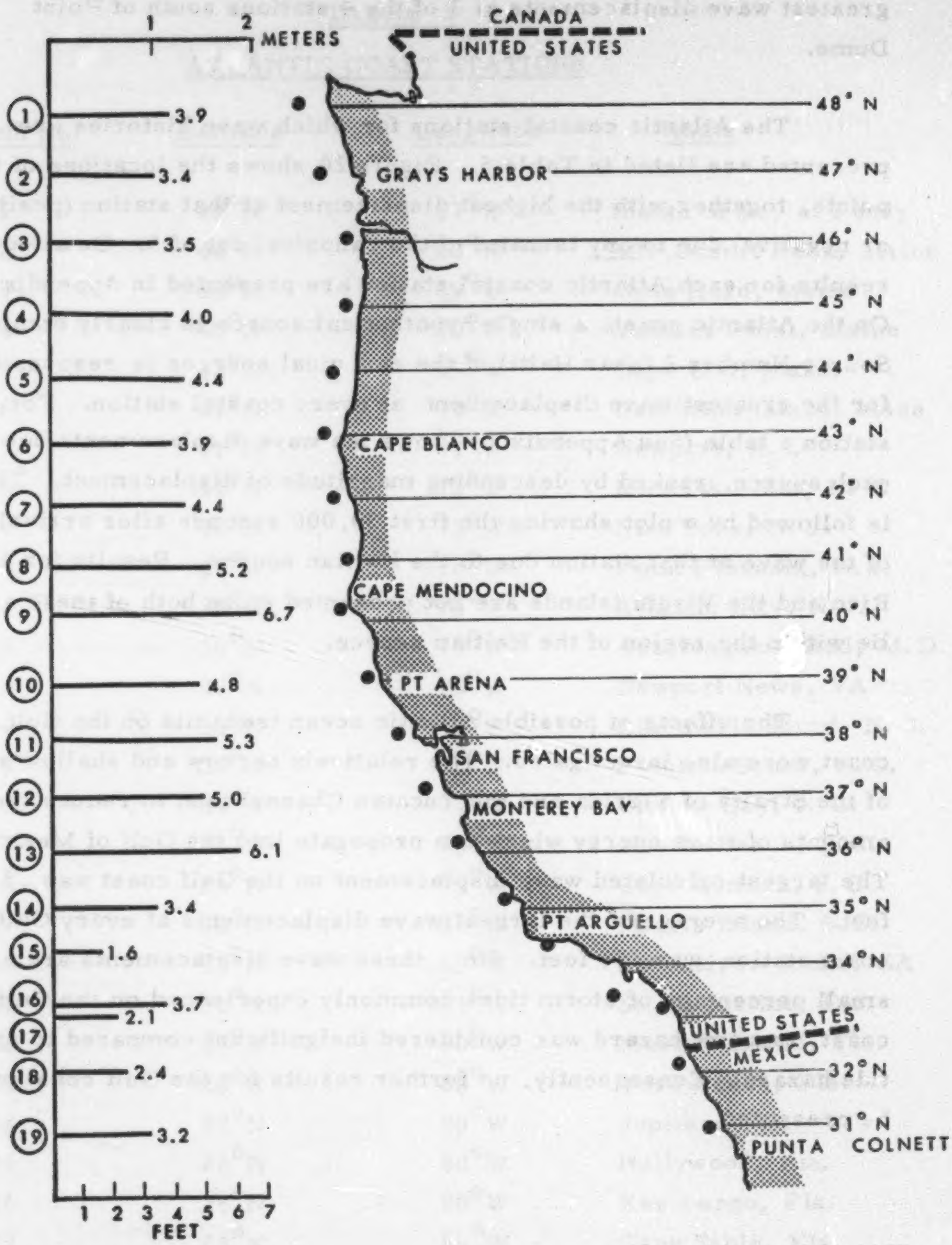

Figure 19. Pacific Coast station and maximum absolute wave displacement from still water level for any tsunami

greatest wave displacements at 3 of the 4 stations south of Point Dume.

The Atlantic coastal stations for which wave histories are presented are listed in Table 5. Figure 20 shows the locations of these points, together with the highest displacement at that station (positive or negative) due to any tsunami of the canonical set of 5. Detailed results for each Atlantic coastal station are presented in Appendix B. On the Atlantic coast, a single hypothetical source is clearly dominant. Source Number 2 (near Haiti) of the canonical sources is responsible for the greatest wave displacement at every coastal station. For each station a table (See Appendix B) shows the wave displacements due to each source, ranked by descending magnitude of displacement. This is followed by a plot showing the first 30,000 seconds after arrival time of the wave at that station due to the Haitian source. Results for Puerto Rico and the Virgin Islands are not presented since both of these areas lie within the region of the Haitian source.

The effects of possible Atlantic ocean tsunamis on the Gulf coast were also investigated. The relatively narrow and shallow areas of the Straits of Florida and the Yucatan Channel tend to reduce the amounts of wave energy which can propogate into the Gulf of Mexico. The largest calculated wave displacement on the Gulf coast was .81 feet. The average of the largest wave displacements at every Gulf coast station was .58 feet. Since these wave displacements are a small percentage of storm tides commonly experienced on the Gulf coast, tsunami hazard was considered insignificant compared to storm tide hazard. Consequently, no further results for the Gulf coast will be presented.

TABLE 5

ATLANTIC COAST STATIONS

Station No.	Latitude	Longitude	Name
1	44°N	67°W	Mouth of Bay of Fundy
2	44°N	68°W	Mt. Desert Rock, Maine
3	44°N	69°W	Owls Head, Maine
4	43°N	70°W	Walkers Point, Maine
5	42°N	69°W	Cape Cod, Mass.
6	41°N	70°W	Nantucket Island, Mass
7	41°N	71°W	Newport, R. I.
8	41°N	72°W	Montauk Point, N. Y.
9	40°N	73°W	New York, N. Y.
10	40°N	74°W	Point Pleasant, N. J.
11	39°N	74°W	Atlantic City, N. J.
12	38°N	75°W	Assateague Island, M. D.
13	37°N	75°W	Newport News, VA
14	36°N	75°W	Albemarle Sound, N. C.
15	35°N	76°W	Pamlico Sound, N. C.
16	34°N	77°W	Onslow Bay, N. C.
17	33°N	78°W	Myrtle Beach, S. C.
18	33°N	79°W	Cape Romain, S. C.
19	32°N	80°W	Parris Island, S. C.
20	31°N	81°W	St. Andrew Sound, GA
21	30°N	81°W	St. Augustine, Fla.
22	29°N	80°W	Merritt Island, Fla.
23	28°N	80°W	Vero Beach, Fla.
24	27°N	80°W	Jupiter, Fla.
25	26°N	80°W	Hollywood, Fla.
26	25°N	80°W	Key Largo, Fla.
27	25°N	81°W	Cape Sable, Fla.

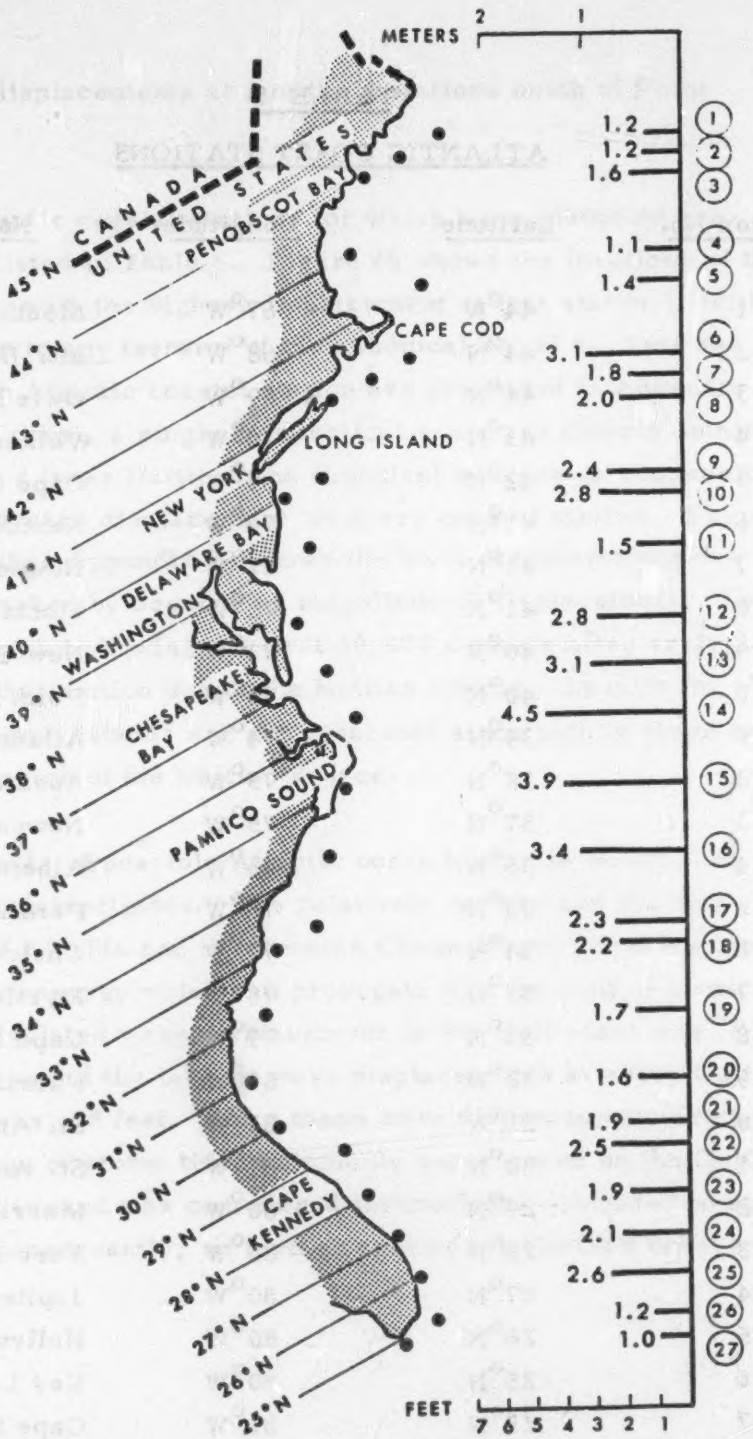
METERS
2
1
CANADA
UNITED STATES
PENOBSCOT BAY
CAPE COD
LONG ISLAND
NEW YORK
DELAWARE BAY
WASHINGTON
CHESAPEAKE BAY
PAMLICO SOUND
CAPE KENNEDY
45° N
44° N
43° N
42° N
41° N
40° N
39° N
38° N
37° N
36° N
35° N
34° N
33° N
32° N
31° N
30° N
29° N
28° N
27° N
26° N
25° N
1.2 ①
1.2 ②
1.6 ③
1.1 ④
1.4 ⑤
3.1 ⑥
1.8 ⑦
2.0 ⑧
2.4 ⑨
2.8 ⑩
1.5 ⑪
2.8 ⑫
3.1 ⑬
4.5 ⑭
3.9 ⑮
3.4 ⑯
2.3 ⑰
2.2 ⑱
1.7 ⑲
1.6 ⑳
1.9 ㉑
2.5 ㉒
1.9 ㉓
2.1 ㉔
2.6 ㉕
1.2 ㉖
1.0 ㉗
FEET
7 6 5 4 3 2 1

Figure 20. Atlantic Coast stations and maximum absolute wave displacement from still water level for any tsunami

6. INTERPRETATION AND USE OF RESULTS

The objective of this study is the determination of the probable highest tsunami which may strike a coastal area of the continental United States after propagating from a distant generator. The results described in the previous chapter can be used in this determination, subject to a certain amount of interpretation. The word interpretation is used because there is no rigid rule for extracting an incident wave train from a wave system of superimposed incident waves and reflections from a coastline of arbitrary shape in water of variable depth. Our intent here is to give some guidelines for interpretation and to suggest methods of handling the nearshore calculations.

There is some question as to the wave forms to be expected at the offshore site. The results of Kajiura (1963) for a wave propagating over an infinite sea indicate that the highest wave in a train appears later in the train with increasing distance from a two-dimensional source. Computational experience has shown that we have more confidence in the results of the numerical model for the first wave than for succeeding waves. This conflict can be resolved by remembering that we wish only a representation of a hypothetical tsunami, and not a hindcast of a historical event.

Hindcasts of actual events show general agreement in amplitudes of computed and observed waves and increasing phase differences after the first wave. These phase differences arise from the perfectly reflecting boundary condition of the numerical model and from the discrete nature of the resolution of the bathymetry.

Thus, the representation of a hypothetical event is expected to show the correct amplitude for the given displacement and a phase increasingly in error. Since a representation is all that is desired, this is probably acceptable. The user should be aware of this problem though.

The results presented in the previous chapter show wave histories computed at offshore stations in water of moderate depth (600 feet). In regions of simple bathymetry this depth corresponds to the edge of the continental shelf. In order that the results be properly implemented, the user must realize that the results include the influence of perfectly reflecting coastlines. Consequently, all wave elevations computed at offshore stations are the sums of incident and reflected components, and approximate what would be recorded by a gauge at that station.

The extraction of an incident wave from a wave system in an irregular geometry is a difficult problem. Yet some form of extraction must be done. The calculated wave system cannot be used directly as input for nearshore calculations because that would result in a double accounting for reflection at the shoreline, once by the large scale calculation and once by the nearfield calculation. One way that has been proposed to deal with this problem is the application of a matched impedance boundary condition (i.e., complete transmission) at the continental boundaries. This is not satisfactory because, physically, the incident wave at one section of coastline may be the direct result of reflection at another. We feel that a better scheme is to divide the computed wave history by some "reflection coefficient" which is a function of the angle of incidence to the section of coastline. The rationale for this procedure is described below.

The results given in this report show wave systems which account for reflection from all continental boundaries. Consider a tsunami normally on a straight coastline segment. Owing to the great wavelengths of tsunamis and the comparatively short distances from shore to the point of computation, it is reasonable to ignore any phase differences between the incident and reflected components of the resulting wave system. The system can then be considered a standing wave system of varying amplitude. Since the point of computation is near an antinode, it is expected that the amplitude of the standing wave is, on average, twice that of the incident wave. Evidently, a representative incident wave train for a normal direction of incidence to a relatively straight coastline segment can be obtained by dividing the wave histories calculated in this study by a factor 2.

Consider now a tsunami propagating parallel to a straight coastline segment. Neglecting the effects of refraction and friction, such a wave train will propagate with little change of form. In this case, the factor by which the computed wave system should be divided to obtain the incident wave system is unity.

So far we have said nothing of oblique reflection. Such work as has been done considers reflection from a plane wall in water of constant depth, and reflection of periodic and transient waves from a depth discontinuity. Weigel (1964) cites an unpublished study by Perroud of the reflection of solitary waves from a plane wall. When α, the angle between the incident wave ray and the wall exceeds 45 degrees, the wave is completely reflected. When the angle of incidence, α, was less than 20 degrees, a negligible reflected wave was observed. When the angle of incidence was between 20 degrees and 45 degrees Mach-stem reflection was observed. The wave height observed at the wall for α ranging from 0 degrees to 90 degrees, taking in all three reflection modes, can be conveniently approximated by:

$$\frac{H_w}{H_i} = \begin{cases} 2 & 45^\circ \leq \alpha \leq 90^\circ \\ (1 + \frac{\alpha}{45}) & 0^\circ \leq \alpha < 45^\circ \end{cases} \tag{31}$$

where H_w is the height at the wall and H_i is the height of the incident wave.

Pierson (1972) studied the reflection of monochromatic waves from a depth discontinuity (he uses the term caustic). He concludes that the wave pattern may be described approximately by two systems of crossing long crested waves, one incident and one reflected, forming a "waffle" pattern. The antinodes of this system propagate parallel to the reflective boundary and one set of antinodes is located at the reflective boundary.

These two studies lead us to suggest the following procedure for establishing an incident wave for use in nearshore calculations. To convert a calculated time history given on this report to an incident wave history, determine the angle of incidence, find the corresponding factor H_w/H_i (Equation 31) and divide the calculated history by this factor. A method for estimating the angle of incidence will be given later.

This artifice should give perfectly satisfactory estimates of design incident waves at computational points for the coastlines of the continental U.S. Of course, it is possible to visualize a coastal geometry for which no reflected waves would arrive at the offshore position and the artifice would not apply. For instance, a point of land with incident wave crests normal to the bisector of the point would direct reflected waves to either side of a position offshore from the point. In order for this to occur, however, the length scale of the point of land must be at least as large as the incident wave length. This will not be the case on the coasts of the U.S. for the very long waves considered in this study, and, consequently, our simple artifice can still be used.

Since our computations do not follow individual crests or rays, we do not have the necessary angles directly available. Instead, it is necessary to adopt another artifice sufficient for nearshore use.

Consider two adjacent nearshore stations at which we present tsunami histories. Call the line connecting them the baseline. A long wave front arriving normal to the baseline would be observed simultaneously at the two points. On the other hand, a wave front advancing parallel to the baseline would be observed first at one point and only after some interval at the second point. The interval will depend on point spacing, δ, and average wave speed, $\bar{C}$. If $\Delta\tau$ is the difference in arrival time at the two points for a given tsunami the approximate angle of incidence for intermediate points is given by:

$$\alpha \approx \cos^{-1}\left(\frac{c\Delta\tau}{\delta}\right) \qquad (32)$$

in which α is measured from the baseline. Note that $\Delta\tau$ can be defined as difference in arrival time of the first discernible disturbance, of the first crest, or of any other convenient and recognizable phase point. It is suggested that both first disturbances and first crest be computed and the results compared.

Application of a design incident wave to engineering analysis of a particular site requires consideration of a number of local factors which serve to transform the incident waves in a complex way. Users of these results must recognize that local modifications can be crucial in any shoreline behavior assessment. Two nearby areas - subjected to what is essentially the same incident wave - may respond in totally different fashions (consider, for example, the notoriously sensitive Crescent City, California and Hilo, Hawaii).

The manner in which the present results are used will depend upon particular local conditions and the engineering judgement of the user. However, an outline of what may be typically required is in order.

The user must account for the diverse effects of shallow and irregular bottom depth. Traditional engineering practice reduces this task to the separate analysis of refraction, diffraction, shoaling, breaking, reflection, and run-up (see, e.g. Wiegel, 1964 or USCERC, 1973). Additional features to be accounted for include Mach-stem formation and resonant interactions. We would suggest that while such methods may be useful, the extreme lengths of tsunamis place them outside the range of usual empirical formulas; consequently, caution is indicated.

It may be more acceptable to take results given here as input to a numerical simulation of nearshore transformation on a fine grid system. A model based upon the nonlinear long wave equations would directly account for coastal modifications other than breaking. Breaking would have to be treated separately, probably semi-empirically.

The adequate treatment of nearshore tsunami transformation in the general case must still be considered a research problem. There is no single numerical model for treating all of the flow phenomena possible in a nearshore calculation. Rather, a blend of methods will be necessary to produce a satisfying analysis. We suggest below a few of the available models and some additional references.

Probably the most elaborate prediction of tsunami inundation is that developed by Adams (1975) for the Hawaiian Islands. His paper outlines the various considerations necessary in a nearshore analysis.

A number of numerical realizations of the traditional ray tracing techniques have been developed. The method plots the positions of a wave front at successive times. Wave rays which are orthogonal to the wave front are also plotted, and the amplitude of a wave is approximately proportional to the inverse square-root of the distance between rays. Such a scheme requires care in interpretation and there are some limitations. Most of these models are based on an algorithm developed by Munk and Arthur (1951). Some additional references are Chao (1970), Coudert and Raichlen (1970), Hardy (1968), and Dobson (1967).

Computer programs for time-stepping on a rectangular grid have been used to model the behavior of tsunamis on the nearshore region. Representative linear models are those of Brandsma et. al., (1975) and Loomis (1972). A nonlinear model (which does not account for wave breaking) is that of Leendertse (1967). All of these models are based on the vertically integrated equations of motion and continuity.

Reid and Bodine (1968) have developed a numerical model for flooding problems which couples a finite difference solution of the linearized long wave equations with nonlinear, empirical formulas for flow in the regions that are normally shallow or dry. The empirical formulas are those for flow over broad crested weirs. The finite difference model includes quadratic friction terms, and, since it was developed for storm surge problems, wind stress and rainfall terms. A modification of this model could be productively applied to the problem of tsunami run-up.

In coastal regions where extensive investigations of tsunami run-up are deemed necessary, the Marker and Cell model developed by Welch et. al., (1966) will be useful for those cases where run-up over irregular terrain with obstacles must be determined.

The MAC method solves the full Navier-Stokes equations. While three dimensional applications have been made (Roache, 1972), the more practical use will be made in two dimensional cross-sectional models.

Of course, such models require a reasonable uniformity of cross-section in a direction normal to the cross-sectional plane. This type of model will show flow phenomena such as breaking and bore formation which are important in the run-up problem. Street et al, (1970) describes a version modified specifically for water wave problems in two dimensions, SUMMAC.

We have described some of the techniques and numerical models which can be applied to the problem of nearshore transformation and run-up of tsunamis. These models and the information supplied in this report should be sufficient to produce good estimates of the effects of tsunamis of maximum size likely to strike particular coastal areas. The key factors to a successful analysis will be the experience and judgement of the engineer.

7. SENSITIVITY

This chapter discusses the sensitivity of the computed results to changes in the characteristics of the canonical source. The important characteristics are: peak value of bottom displacement, length of the displacement region, width of the displacement region, and the azimuthal orientation of the source.

The sensitivity of the computed wave histories to changes in the peak source displacement is the simplest case to treat. Since the numerical model is linear, this dependence is linear. Cutting the peak source displacement by a factor of 2 cuts the displacements of the computed waves by half.

Canonical source number 24 (Fox Islands, Alaska) was used as a base against which to test the sensitivity of the Pacific coast stations to changes in the other three parameters.

Four runs were made with the basic parameters changed as follows: (1) major axis 200 percent of original; (2) major axis 150 percent of original; (3) minor axis 200 percent of original and (4) bearing 10 degrees less than original (anti-clockwise rotation). The peak displacements obtained at the Pacific coast stations from these four runs are expressed in Table 6 as percentages of the original displacement. The results indicate that for the three parameters the computed results are most sensitive to changes in the major axis length and least sensitive to changes in the orientation of the bottom displacement.

The computations for this study were made on a relatively coarse grid of 1 degree by 1 degree spacing. The behavior of the computational model under a finer grid spacing was investigated. Changes in the size of the grid spacing should not grossly alter the shape or amplitude of the leading wave. For coastal points however, succeeding waves will be altered more and more as they occur later in the wave train. This feature arises as a consequence of the more complicated bathymetry which is resolved by the finer grid. Figures 17 and 18 have shown the verification

TABLE 6

Sensitivity of Calculations for Pacific Stations*

Change in Original Displacement No. 24

Station	200% Major Axis	150% Major Axis	200% Minor Axis	10 % Decrease In Bearing
1	153	132	140	93
2	133	120	128	89
3	138	124	139	97
4	129	114	122	105
5	133	121	132	96
6	145	127	143	97
7	145	127	140	105
8	137	123	140	94
9	119	110	121	86
10	124	111	122	81
11	132	120	145	82
12	116	102	108	83
13	126	115	109	77
14	207	158	170	92
15	211	164	182	112
16	104	94	136	78
17	194	150	178	109
18	145	121	128	106
19	137	125	105	85

*** Changes in maximum wave displacements at Pacific Stations due to variations in parameters describing canonical source 24. Values are percentages of original calculated wave displacements.**

results computed on the 1.0 degree by 1.0 degree grid for the 1964 Gulf of Alaska tsunami at Wake Island and Sitka, Alaska respectively. Figures 21 and 22 for Wake Island and Sitka show the results of a similar computation using a 0.5 degree by 0.5 degree grid (dotted line) superimposed upon the original figures. Figure 21 shows good agreement of the two computations at Wake Island, as expected. The second crest computed on the fine grid is due to the increased resolution of the bathymetry in the source region. Figure 22 shows good agreement of the two computations at Sitka. As expected, the leading waves agree fairly closely while succeeding waves are increasingly divergent.

Table 7 is presented as a summary of the sensitivities of the results at various Pacific Ocean points to the halving of the grid size used in computing the 1964 Alaskan tsunami. The results are expressed as displacement of the first crest for each grid and the percentage change from the original 1 degree by 1 degree computation. After examination of the last two figures and Table 7, we conclude that the calculations presented in this report are not very sensitive to the numerical effects of a change in the grid size.

It has been noted by the reviewers of the draft of this report that the 1964 Gulf of Alaska tsunami calculated by program SEAWAVE (used in this study) for Wake Island (Figure 21) does not agree as well with the observed wave as does the result calculated by the earlier Tetra Tech program LONGWAV (Hwang et al., 1971 and Tetra Tech, 1974) using a 1/3 degree by 1/5 degree grid. The reason for this is discussed below. The two codes solve similar sets of equations by different computational techniques. SEAWAVE considers Coriolis accelerations while LONGWAV does not. Computational experience has shown that the presence or absence of Coriolis accelerations in the equations makes little difference in a calculation of this type. SEAWAVE neglects the contribution of wave height to total depths, while LONGWAV does not. SEAWAVE makes much more efficient use of computer resources, and so it was chosen for use in this study. The computations were made on a 1 degree by 1 degree grid, which gives sufficient resolution of the canonical source. The verification with the 1964 event was run on this grid and later on a 0.5 degree by 0.5 degree grid interpolated from the coarse grid. Since the second computation was a test of numerical effects only, no corrections of the interpolated grid were made to show the smaller scale features that could be resolved in the source region bathymetry, the bottom displacement, and the bathymetry around Wake Island. The close agreement of the leading waves shown in the two calculations confirmed the adequacy of the coarser grid. The calculation with program LONGWAV was performed with a yet finer grid. The fine grid used in this calculation was justified because it was a hindcast of a historical event for which the source displacement was fairly well known, and the received wave was precisely known.

The fine grid resolved the bathymetry in the source and receptor regions and the bottom displacement much more precisely. It is this more detailed representation of the bathymetry rather than any difference in the models which accounts for the difference in results. Indeed, the fact that SEAWAVE on a 1 by 1 degree grid produced a useable representation of the 1964 tsunami at Wake Island for a fraction (1/33) of the cost of the more elaborate earlier calculation is a remarkable confirmation of the utility of the model.

In conclusion, the use of a very fine grid, with the associated practical difficulties, is not justifiable for a study of tsunamis generated by hypothetical bottom motions.

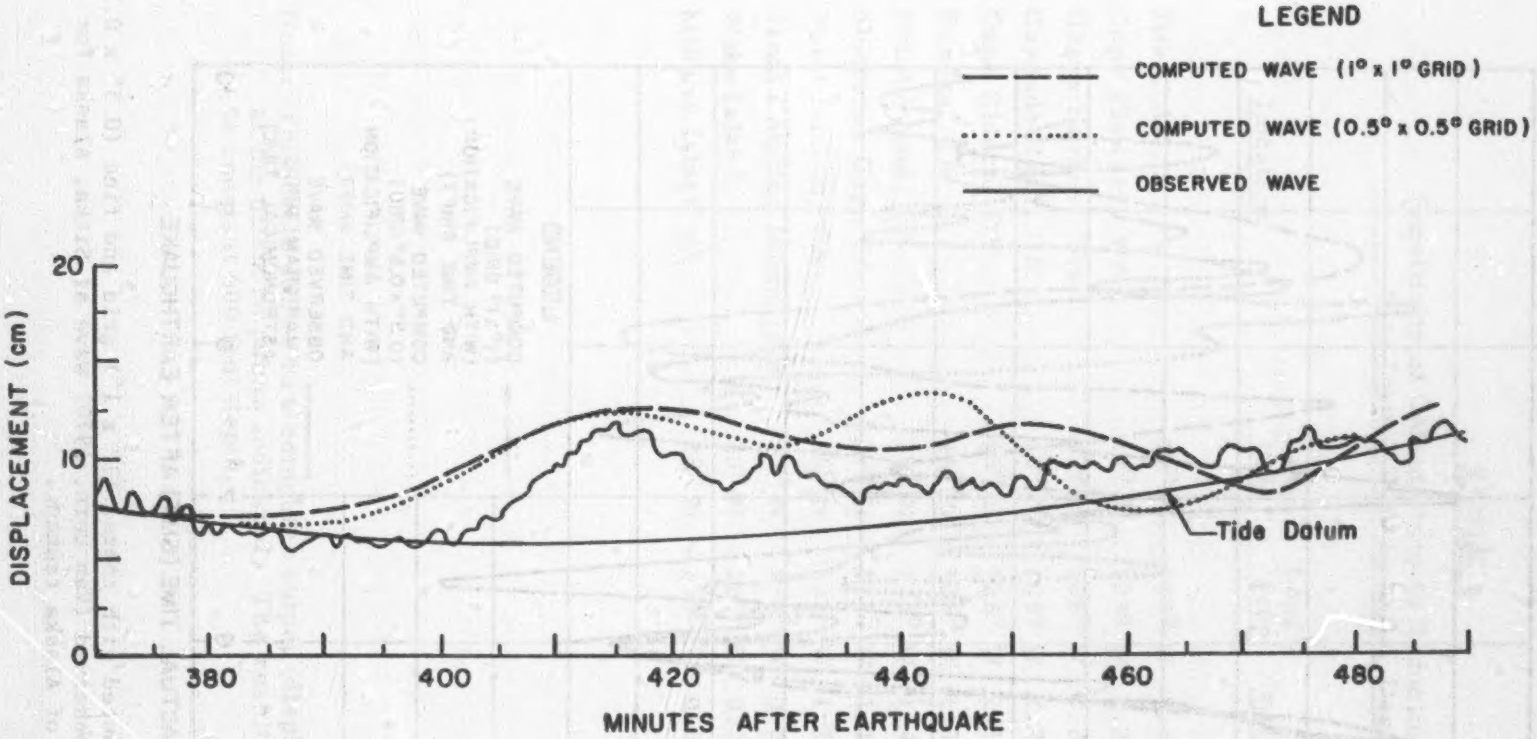

Figure 21. Waves computed with coarse (1° x 1°) grid and fine (0.5° x 0.5°) grid and observed (Van Dorn, 1970) wave at Wake Island for 1964 Gulf of Alaska tsunami.

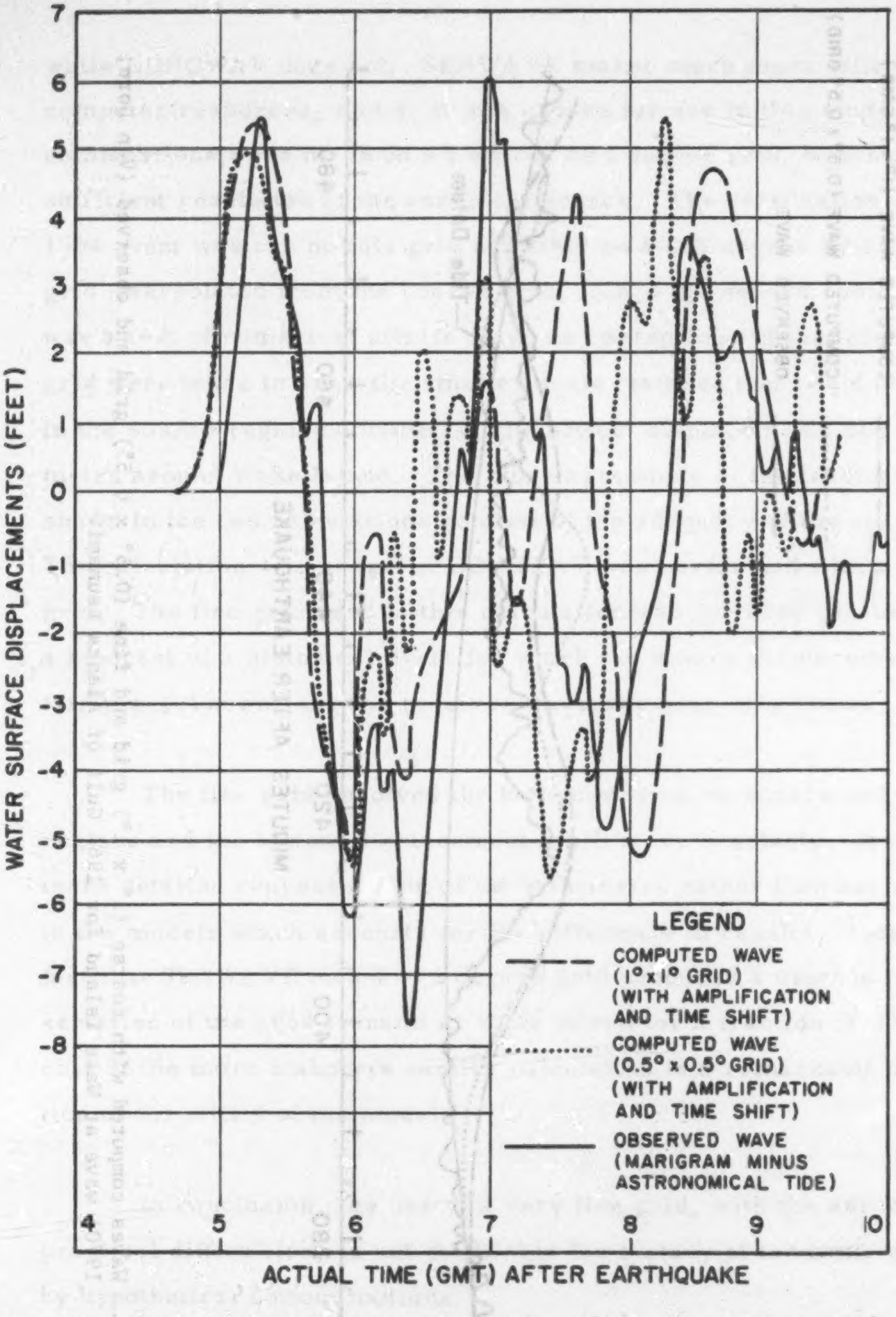

Figure 22. Waves computed with coarse (1° x 1°) grid and fine (0.5° x 0.5°) grid and observed (Van Dorn, 1970) wave at Sitka, Alaska for 1964 Gulf of Alaska tsunami.

TABLE 7

Sensitivity of Calculations to Reduction in Grid Size from 1 Degree to 0.5 Degree

Location	Latitude	Longitude	$\eta(1^\circ)$	$\eta(0.5^\circ)$	Percent Change
Sitka, AK	57° N	137° W	3.33	3.05	-8.4
Cape Flattery, WA	48° N	125° W	2.21	2.37	+7.3
Grays Harbor, WA	47° N	125° W	2.27	2.31	+1.6
Cascade Head, OR	45° N	125° W	2.20	2.38	+8.2
Cape Blanco, OR	43° N	125° W	2.14	2.19	+2.3
Eureka, CA	41° N	125° W	1.73	1.69	-2.4
Point Arena, CA	39° N	124° W	1.41	1.47	+4.3
Monterey Bay, CA	37° N	123° W	1.12	1.08	-3.9
Point Buchon, CA	35° N	121° W	1.17	1.27	+8.7
Santa Catalina Island, CA	33° N	119° W	0.56	0.63	+12.5
Wake Island	20° N	167° E	0.2288	0.2154	-5.8
Midway Island	28° N	177° W	0.3311	0.3065	-7.4

Note: This table shows raw computer output (displacements η in feet) at the offshore points indicated. The results are not normalized to constant 600 foot depth.

8. SUMMARY

In this report, we have demonstrated the effects on U. S. coasts of tsunamis generated by the canonical bottom displacement associated with a great earthquake occurring at selected points in the Pacific and Atlantic oceans. The results, which consist primarily of wave traces at offshore stations in 600 feet of water, show that significant tsunami hazard exists along the U. S. Pacific coast and Atlantic coast. Tsunami hazard along the Gulf coast, even allowing for its dynamic nature, appears to be insignificant compared to storm tide hazard.

The results presented here are intended as the first step of design calculations made for coastal installations at particular sites. As such, the results may be used as input to the analyses mentioned in Chapter 6 to find the nearshore tsunami wave history at a particular site. Once this is done, the astronomical tides and storm tides established for the site may be superimposed to obtain the maximum elevation and drawdown of the water surface which may be expected at the site. (The change in "still water level" due to astronomical and storm tides has little influence on the behavior of the tsunami and hence may be neglected).

The computations used a canonical tsunami source somewhat larger than any known to have occurred. It is expected that the results give the reasonable upper limit to tsunami waves which may be observed at offshore locations. In the event that an even larger source displacement is desired in a particular case, the discussion in Chapter 7 of the sensitivity of the results to changes in the source dimensions may be used to adjust the amplitude of the originally computed offshore wave.

The Pacific coast results indicate that tsunamis generated by four canonical bottom displacements form the controlling set. The most important sources for the whole coast are the Gulf of Alaska (source 25) and the Fox Island region of southwest Alaska (source 24). The sources

located near New Guinea (source 8) and Samoa (source 3) are the controlling sources south of Point Arguello in southern California.

On the Atlantic coast the controlling source at every station is that near Haiti (source 2).

Finally, we should like to emphasize that the wave histories presented in this report are the results of "worst case" computations. The canonical bottom displacement which generated these waves was based on two extraordinarily large earthquakes occuring in notoriously active portions of the Pacific seismic belt. The canonical displacement was used at every source location in order to give upper bounds on waves to be expected from any source, and to allow comparison of sources. The fact that this canonical displacement was used at a location such as Haiti does not in any way imply that the required 1,000 kilometer length of fault slip will occur there. Future seismological research may be able to determine maximum possible lengths of fault slip for various tsunamigenic zones. Such information would allow new and substantially more accurate computations for the controlling sources determined by this study.

REFERENCES

Adams, W. M. (1975), "Conditional Expected Tsunami Inundation for Hawaii," J. ASCE, Vol. 101, No. WW4, pp 319-329.

Barazangi, M. and Dorman, J. (1969), "World Seismicity Map of ESSA Coast and Geodetic Survey Epicenter Data for 1961-1967," Bull. Seism. Soc. Am., Vol. 59, p. 369.

Batchelor, G. K. (1967), An Introduction to Fluid Dynamics, Cambridge University Press, England, p. 615.

Berg, E. (1964), "The Alaskan Earthquake: Its Location and Seismic Setting," Proc. 15th Alaskan Sci. Conf., AAAS College, Alaska, September 1964, pp. 218-232.

Berg, E., et al., (1972), "Source of the Major Tsunami," in The Great Alaska Earthquake of 1964: Oceanography and Coastal Engineering, National Academy of Sciences, Washington, D.C., p. 122.

Brandsma, M., Divoky, D. and Hwang, L., (1975), "SEAWAVE" - A Revised Model for Tsunami Applications, "Report No. TC-354, Tetra Tech, Inc., Pasadena, California.

Chao, Y. Y. (1970), "The Theory of Wave Refraction in Shoaling Water," TR-70-7, Dept. Meteorology and Oceanography, New York University, New York.

Coudert, J. F. and Raichlen, F. (1970), "Wave Refraction Near San Pedro Bay, California," J. ASCE, Vol. 96, No. WW3, pp. 737-747.

De Sousa, F. L. (1911), "The Seismic Sea Wave of the Great Lisbon Earthquake," Comptes Rendus, French Academy of Science, Vol. 152, pp. 1129-1131.

Dobson, R. S. (1967), "Some Applications of Digital Computers to Hydraulic Engineering Problems," TR-80, Dept. Civil Engineering, Stanford University, California.

Gutenberg, B. and Richter, C. F., (1954), Seismicity of the Earth and Associated Phenomena, Princeton University Press, Princeton, N. J., p. 310.

Gutenberg, B. and Richter, C. F., (1956), "Earthquake Magnitude, Intensity, Energy and Acceleration," Bull. Seism. Soc. Am. Vol. 46, p. 105.

Hammack, J. L. (1972), "Tsunamis - A Model of Their Generation and Propagation," Report No. KH-R-28, Keck Laboratory of Hydraulics and Water Resources, California Institute of Technology, Pasadena, California, p. 261.

Hardy, J. R. (1968), "Some Grid and Projection Problems in the Numerical Calculation of Wave Refraction," J. Geophys. Res., Vol. 73, No. 22.

Hwang, L. S., Butler, H. L. and Divoky, D. J. (1971), "Rat Islands Tsunami Model: Generation and Open Sea Characteristics," Report prepared under AEC Contract No. AT(26-1)-289(M008), Tetra Tech, Pasadena, California.

Iida, K. (1963), "Magnitude, Energy and Generation Mechanisms of Tsunamis and a Catalog of Earthquakes Associated with Tsunamis," Proc. Tenth Pac. Sci. Cong., UIGG Monograph No. 24, p. 7-18.

Isacks, B., Oliver, J. and Sykes, L. R., (1968), "Seismology and the New Global Tectonics," J. Geophys. Res., Vol. 73, No. 18, p. 5855.

Kajiura, K. (1963), "The Leading Wave of a Tsunami," Bull. Earthquake Research Institute, University of Tokyo, Vol. 41, pp. 535-571.

Kelleher, J. A., (1970), "Space-Time Seismicity of the Alaska-Aleutian Seismic Zone," J. Geophys. Res., Vol. 75, No. 29, p. 5745.

Kelleher, J. A., (1972), "Rupture Zones of Large South American Earthquakes and Some Predictions," J. Geophys. Res., Vol. 77, No. 11, p. 2087.

Kelleher, J. A., Sykes, L. R. and Oliver, J., (1973), "Possible Criteria for Predicting Earthquake Locations and Their Application to Major Plate Boundaries of the Pacific and the Carribean," J. Geophys. Res., Vol. 78, No. 14, p. 2547.

Kelleher, J. A., et al., (1974), "Why and Where Great Thrust Earthquakes Occur Along Island Arcs," J. Geophys. Res., Vol. 79, No. 32 (Red), p. 4889.

King, C. Y. and Knopoff, L., (1968), "Stress Drop in Earthquakes," Bull. Seism. Soc. of Am., Vol. 58, No. 1, pp. 249-257.

Lamb, H., (1932), Hydrodynamics, 6th Ed., Cambridge University Press, London, England, p. 738.

Leendertse, J. J. (1967), "Aspects of a Computation Model for Long-Period Water-Wave Propagation," Memorandum RM-5294-PR, The Rand Corporation, New York.

LePichon, X., (1968), "Sea Floor Spreading and Continental Drift," J. Geophys. Res., Vol. 73, No. 12, p. 3661.

Loomis, H. G. (1972), "A Package Program for Time-Stepping Long Waves into Coastal Regions with Application to Haleiwa Harbor, Oahu," Hawaii Institute of Geophysics, Report No. HIG-72-71, University of Hawaii, Honolulu.

Munk, W. H. and Arthur, R. S. (1951), "Wave Intensity Along a Refracted Ray," Symposium on Gravity Waves, Circ. 521, Nat. Bureau of Standards, Washington, D.C.

Okamoto, S., (1973), Introduction to Earthquake Engineering, John Wiley and Sons, New York, p. 571.

Peregrine, D. H., (1972a), "Equations for Water Waves and the Approximation behind Them," in Waves on Beaches, R. E. Meyer, Ed., Academic Press, pp. 95-121.

Peregrine, D. H. (1972b), "Long Waves in Two and Three Dimensions," Proceedings of the Symposium on Long Waves, University of Delaware, Newark, Delaware.

Plafker, G., (1972), "Alaskan Earthquake of 1964 and Chilean Earthquake of 1960: Implications for Arc Tectonics," J. Geophys. Res., Vol. 77, No. 5, pp. 901-925.

Plafker, G., (1971), "Tectonics of the March 27, 1964, Alaska Earthquake, in The Great Alaska Earthquake of 1964: Geology, National Academy of Sciences, p. 47-122.

Plafker, G. and Savage, J. C., (1970), "Mechanism of the Chilean Earthquakes of May 21 and 22, 1960," Geological Society of America Bulletin, Vol. 81, pp. 1001-1030, April.

Reid, H. F., (1914), "The Lisbon Earthquake of November 1, 1755," Bull. Seis. Soc. Am., Vol. 4, No. 2, pp. 53-80.

Reid, R. O. and Bodine, B. R., (1968), "Numerical Model for Storm Surges in Galveston Bay," J. ASCE, Vol. 94, WW1, pp. 33-57.

Roache, P., (1972), Computational Fluid Dynamics, Hermosa Publishers, Albuquerque, New Mexico, p. 434.

Street, R. L., Chan, R.K.C. and Fromm, J. E., (1970), "The Numerical Simulation of Long Water Waves: Progress on Two Fronts," Tsunamis in the Pacific Ocean, W. M. Adams, ed. East-West Center Press, Honolulu, Hawaii.

Sykes, L. R., (1971), "Aftershock Zones of Great Earthquakes, Seismicity Gaps, and Earthquake Prediction for Alaska and the Aleutians," J. Geophys. Res., Vol. 76, No. 22, p. 8021.

Tetra Tech, (1974), "Numerical Modeling of Behavior of Long Waves," Report prepared for the Energy Research and Development Administration.

Tsuboi, C., (1957), "Energy Accounts of Earthquakes in and Near Japan," J. Phys. of the Earth, Vol. 5, No. 1, Japan, p. 7.

U. S. Army Coastal Engineering Research Center (1973), "Shore Protection Manual," U. S. Government Printing Office, Washington, D. C.

Van Dorn, W. G., (1969), "A Model Experiment on the Generation of the Tsunami of March 28, 1967 in Alaska," Int. Symposium of Tsunami and Tsunami Research.

Welch, J. E., Harlow, F. H., Shannon, J. P., and Daly, B. J., (1966), "The MAC Method: A Computing Technique for Solving Viscous, Incompressible, Transient Fluid-Flow Problems Involving Free Surfaces," Report LA-3425, Los Alamos Scientific Laboratory, Los Alamos, New Mexico, p. 146.

Wiegel, R. L. (1964), Oceanographical Engineering, Prentice Hall, Inc., Englewood Cliffs, New Jersey, p. 532.

Wilson, B. W., (1969), "Earthquake Occurrence and Effects in Ocean Areas, "U. S. Naval Civil Engineering Laboratory, Port Hueneme, California, p. 141 and app.

READEX FICHE

Street, R. L., Chan, R. K. C., and Fromm, J. E. (1970), "The Numerical Simulation of Long Water Waves: Progress on Two Fronts," Tsunamis in the Pacific Ocean, W. M. Adams, ed., East-West Center Press, Honolulu, Hawaii.

Sykes, L. R. (1971), "Aftershock Zones of Great Earthquakes, Seismicity Gaps, and Earthquake Prediction for Alaska and the Aleutians," J. Geophys. Res., Vol. 76, No. 32, p. 8021.

Tetra Tech, (1975), "Numerical Simulation of Generation of Long Waves," Report prepared for the Energy Research and Development Administration.

[illegible] [illegible], (19[illegible]), "Energy [illegible] of [illegible] of the [illegible] [illegible] [illegible]," [illegible]

U. S. Army Coastal Engineering Research Center (1973), "Shore Protection Manual," U. S. Government Printing Office, Washington, D. C.

Van Dorn, W. G. (1970), "A Model Experiment on the Generation of the Tsunami of March 28, 1964 in Alaska," Int. Symposium of Tsunami and Tsunami Research.

Welch, J. E., Harlow, F. H., Shannon, J. P., and Daly, B. J. (1966), "The MAC Method: A Computing Technique for Solving Viscous, Incompressible, Transient Fluid Flow Problems Involving Free Surfaces," Report LA-3425, Los Alamos Scientific Laboratory, Los Alamos, New Mexico, p. 146.

APPENDIX A

RESULTS FOR THE PACIFIC COAST

Table A-1

Tsunamis Arriving at Station 1
Ranked by Maximum Wave Displacement

RANK	DISP(FT)	ARRIVAL(SEC)	SOURCE	REGION
*1	3.65	10435.	25	GULF OF ALASKA
*2	2.14	12545.	24	FOX ISLANDS
*3	1.14	46870.	7	BISMARCK SEA
4	1.12	48559.	8	NEW GUINEA
5	.92	24293.	26	MEXICO
6	.90	17571.	23	ANDREANOF ISLANDS
7	.89	31219.	19	JAPAN TRENCH NORTH
8	.86	36634.	16	MARIANA ISLANDS NORTH
9	.84	38191.	3	SAMOAN ISLANDS
10	.83	55749.	33	CHILE CENTRAL
11	.82	52044.	32	CHILE NORTH
12	.74	41351.	29	COLUMBIA-EQUADOR
13	.73	47364.	6	SOLOMON ISLANDS
14	.70	35547.	28	COSTA RICA
15	.68	59292.	34	CHILE SOUTH
16	.66	34294.	18	JAPAN TRENCH SOUTH
17	.66	35308.	17	IWO JIMA
18	.63	44642.	5	SANTA CRUZ ISLANDS
19	.55	43629.	12	OKINAWA
20	.53	49889.	9	MOLUCCAN ISLANDS
21	.51	46074.	1	KERMADEC ISLANDS
22	.46	27743.	20	KURIL ISLANDS
23	.44	22056.	22	NEAR ISLANDS
24	.42	44993.	30	PERU NORTH
25	.41	24864.	21	KAMCHATKA PENINSULA
26	.40	30853.	27	GUATEMALA
27	.38	47714.	4	LOYALTY ISLANDS
28	.33	47435.	10	MINDINAU-PHILIPPINES
29	.33	41061.	2	TONGA ISLANDS
30	.31	46229.	11	LUZON-PHILIPPINES
31	.31	43056.	15	MARIANA ISLANDS SOUTH
32	.28	49790.	31	PERU SOUTH
33	.23	38060.	13	KYUSHU ISLAND-JAPAN
34	.23	45977.	14	PALAU ISLAND

* WAVES SHOWN IN FOLLOWING 2 FIGURES

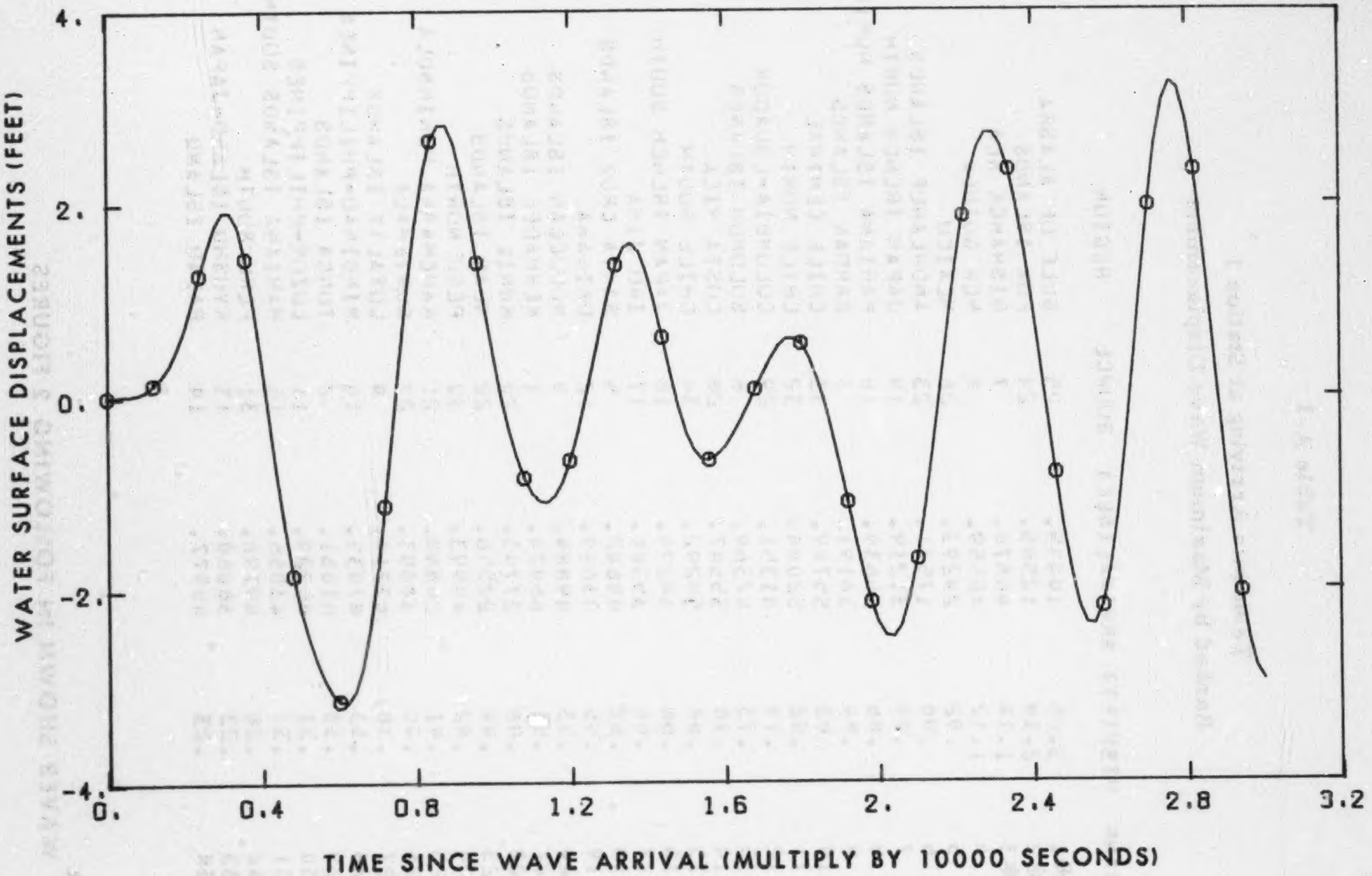

Figure A- 1: Largest Tsunami Arriving at Station 1 Offshore of Cape Flattery, WA

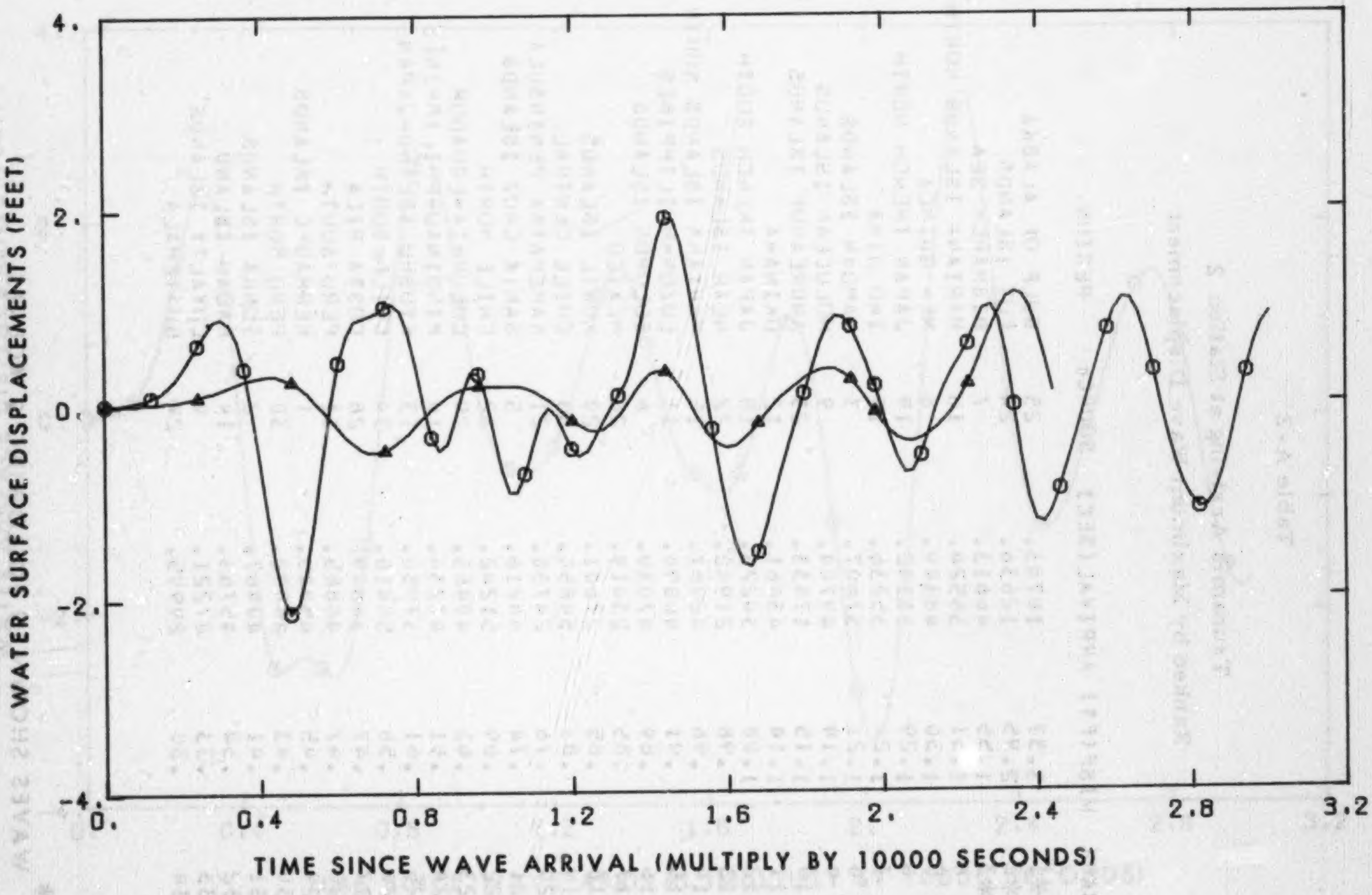

Figure A-2: Second and Third Largest Tsunamis Arriving at Station 1

Table A-2

Tsunamis Arriving at Station 2

Ranked by Maximum Wave Displacement

RANK	DISP(FT)	ARRIVAL(SEC)	SOURCE	REGION
*1	3.37	10743.	25	GULF OF ALASKA
*2	2.95	12636.	24	FOX ISLANDS
*3	1.55	46613.	7	BISMARCK SEA
4	1.51	36524.	16	MARIANA ISLANDS NORTH
5	1.30	48349.	8	NEW GUINEA
6	1.29	31142.	19	JAPAN TRENCH NORTH
7	1.24	35236.	17	IWO JIMA
8	1.21	37607.	3	SAMOAN ISLANDS
9	1.19	49744.	9	MOLUCCAN ISLANDS
10	1.15	17433.	23	ANDREANOF ISLANDS
11	1.14	43461.	12	OKINAWA
12	1.08	34223.	18	JAPAN TRENCH SOUTH
13	.98	21942.	22	NEAR ISLANDS
14	.96	42987.	15	MARIANA ISLANDS SOUTH
15	.91	46090.	11	LUZON-PHILIPPINES
16	.89	47039.	6	SOLOMON ISLANDS
17	.85	23419.	26	MEXICO
18	.85	27601.	20	KURIL ISLANDS
19	.81	54850.	33	CHILE CENTRAL
20	.76	24730.	21	KAMCHATKA PENINSULA
21	.74	44216.	5	SANTA CRUZ ISLANDS
22	.69	51242.	32	CHILE NORTH
23	.63	40463.	29	COLUMBIA-EQUADOR
24	.61	47234.	10	MINDINAO-PHILIPPINES
25	.61	37950.	13	KYUSHU ISLAND-JAPAN
26	.56	58416.	34	CHILE SOUTH
27	.47	34649.	28	COSTA RICA
28	.47	48885.	31	PERU SOUTH
29	.45	45445.	1	KERMADEC ISLANDS
30	.43	44092.	30	PERU NORTH
31	.41	40467.	2	TONGA ISLANDS
32	.34	45763.	14	PALAU ISLAND
33	.33	47221.	4	LOYALTY ISLANDS
34	.30	29995.	27	GUATEMALA

* WAVES SHOWN IN FOLLOWING 2 FIGURES

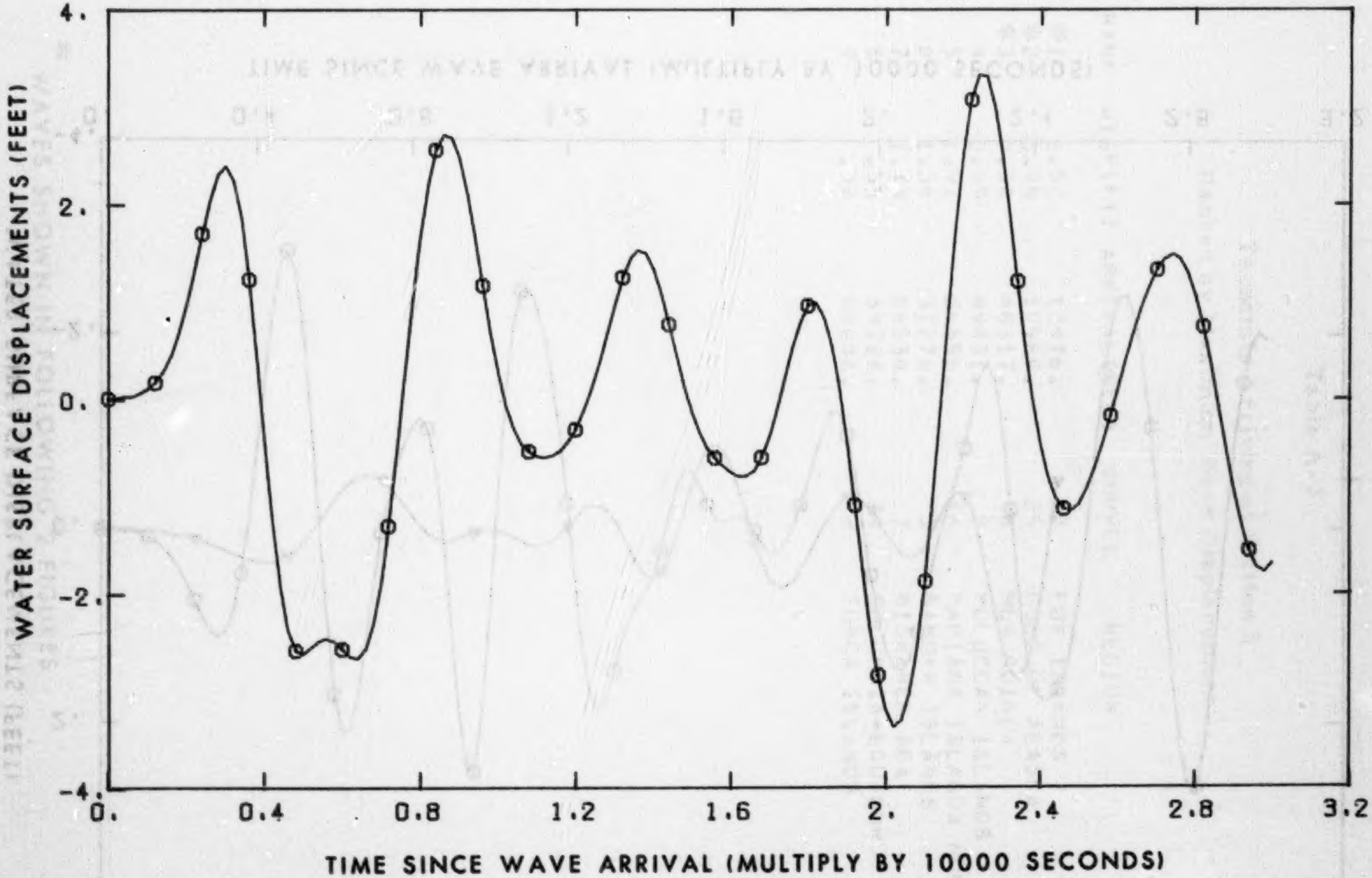

Figure A-3: Largest Tsunami Arriving at Station 2 Offshore of Grays Harbor, WA

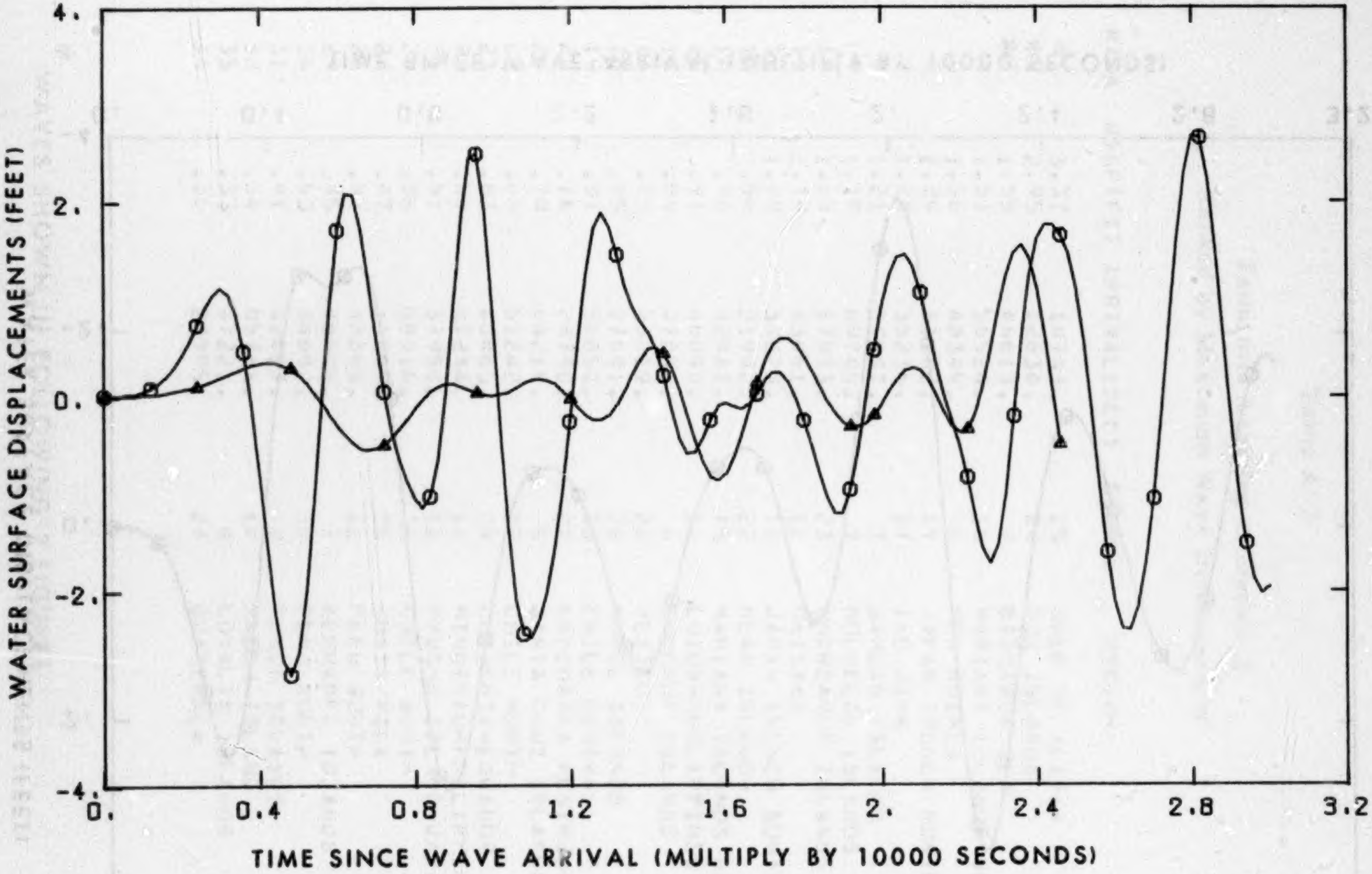

Figure A-4: Second and Third Largest Tsunamis Arriving at Station 2

Table A-3

Tsunamis Arriving at Station 3
Ranked by Maximum Wave Displacement

RANK	DISP(FT)	ARRIVAL(SEC)	SOURCE	REGION
*1	3.52	12976.	24	FOX ISLANDS
*2	3.45	10989.	25	GULF OF ALASKA
*3	2.30	48317.	8	NEW GUINEA
4	2.09	49831.	9	MOLUCCAN ISLANDS
5	1.97	36656.	16	MARIANA ISLANDS NORTH
6	1.36	37276.	3	SAMOAN ISLANDS
7	1.14	46534.	7	BISMARCK SEA
8	.55	39728.	29	COLUMBIA-EQUADOR
9	.38	40046.	2	TONGA ISLANDS

* WAVES SHOWN IN FOLLOWING 2 FIGURES

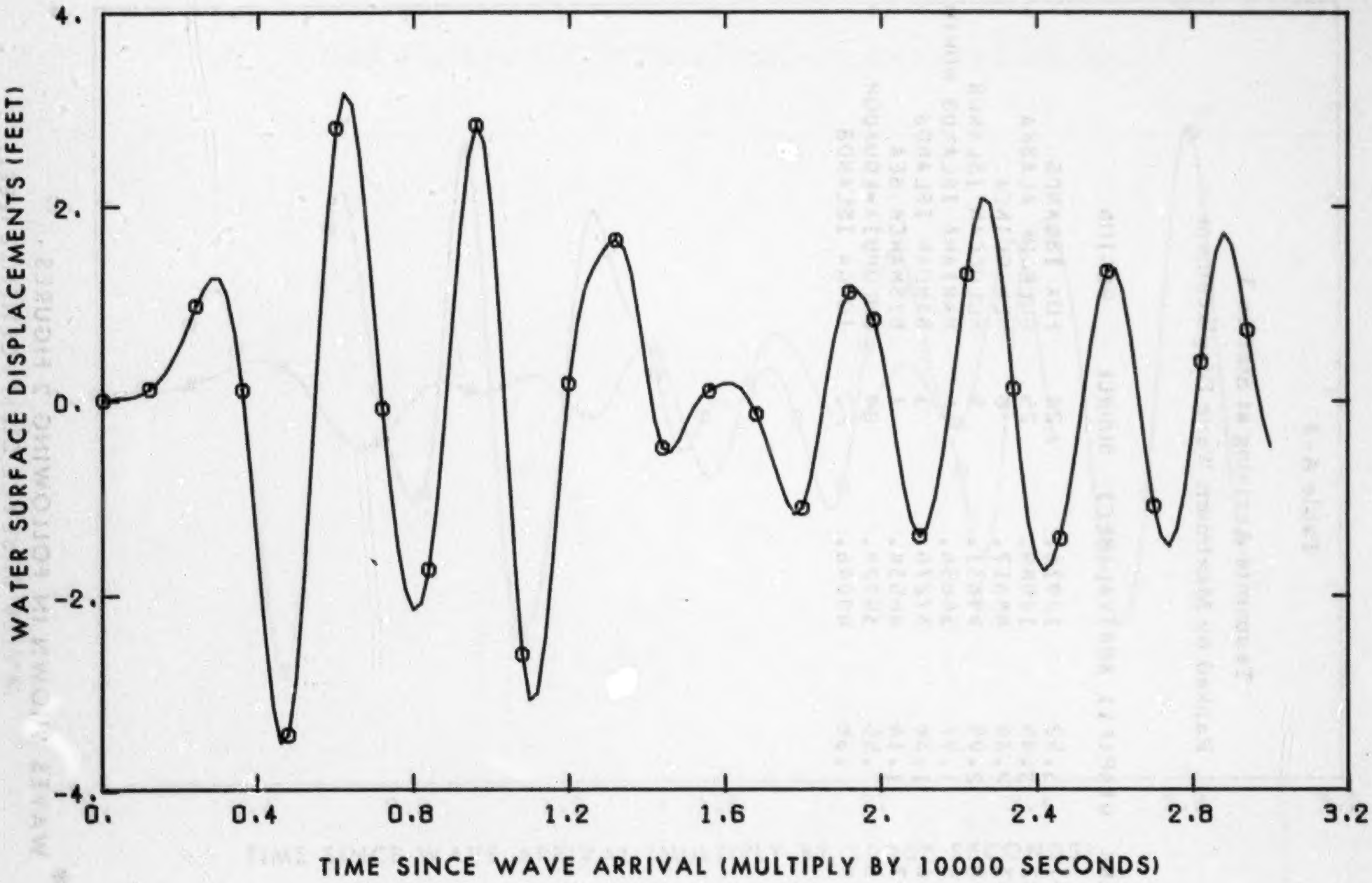

Figure A-5: Largest Tsunami Arriving at Station 3 Offshore of Tillamook Head, OR

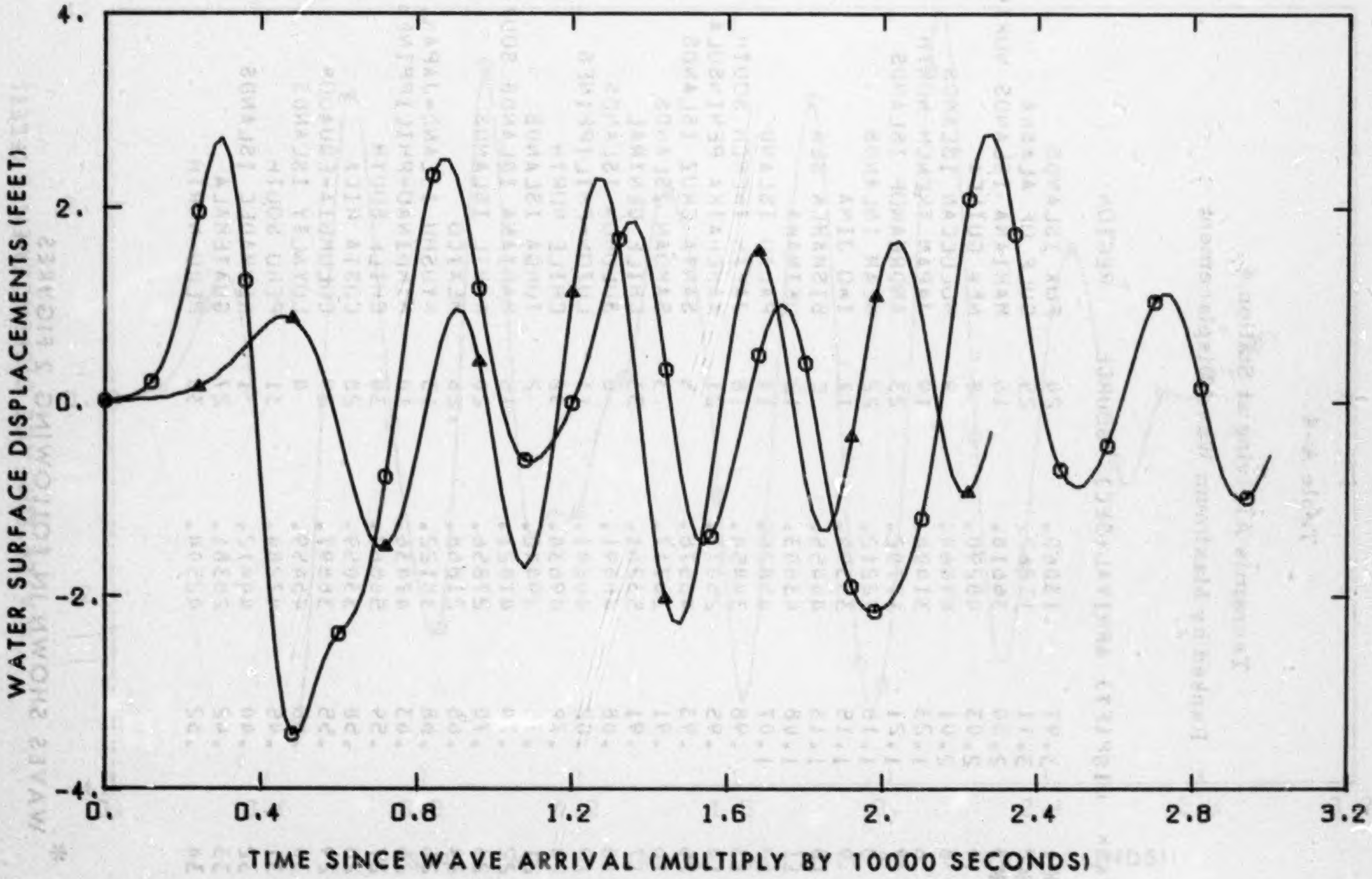

Figure A-6: Second and Third Largest Tsunamis Arriving at Station 3

Table A-4

Tsunamis Arriving at Station 4
Ranked by Maximum Wave Displacement

RANK	DISP(FT)	ARRIVAL(SEC)	SOURCE	REGION
*1	3.97	13060.	24	FOX ISLANDS
*2	3.11	11262.	25	GULF OF ALASKA
*3	2.34	36618.	16	MARIANA ISLANDS NORTH
4	2.03	48290.	8	NEW GUINEA
5	2.01	49864.	9	MOLUCCAN ISLANDS
6	1.23	31404.	19	JAPAN TRENCH NORTH
7	1.21	17702.	23	ANDREANOF ISLANDS
8	1.18	22212.	22	NEAR ISLANDS
9	1.15	35399.	17	IWO JIMA
10	1.13	46455.	7	BISMARCK SEA
11	1.08	43603.	12	OKINAWA
12	1.07	45826.	14	PALAU ISLAND
13	.98	34454.	18	JAPAN TRENCH SOUTH
14	.95	25071.	21	KAMCHATKA PENINSULA
15	.93	43578.	5	SANTA CRUZ ISLANDS
16	.91	36717.	3	SAMOAN ISLANDS
17	.91	53261.	33	CHILE CENTRAL
18	.88	46491.	6	SOLOMON ISLANDS
19	.82	46241.	11	LUZON-PHILIPPINES
20	.79	49634.	32	CHILE NORTH
21	.75	39442.	2	TONGA ISLANDS
22	.74	41821.	15	MARIANA ISLANDS SOUTH
23	.70	27856.	20	KURIL ISLANDS
24	.68	21868.	26	MEXICO
25	.68	38122.	13	KYUSHU ISLAND-JAPAN
26	.63	47436.	10	MINDINAO-PHILIPPINES
27	.59	56867.	34	CHILE SOUTH
28	.58	33059.	28	COSTA RICA
29	.55	38897.	29	COLUMBIA-EQUADOR
30	.55	46459.	4	LOYALTY ISLANDS
31	.45	47284.	31	PERU SOUTH
32	.44	44412.	1	KERMADEC ISLANDS
33	.42	28381.	27	GUATEMALA
34	.32	42504.	30	PERU NORTH

* WAVES SHOWN IN FOLLOWING 2 FIGURES

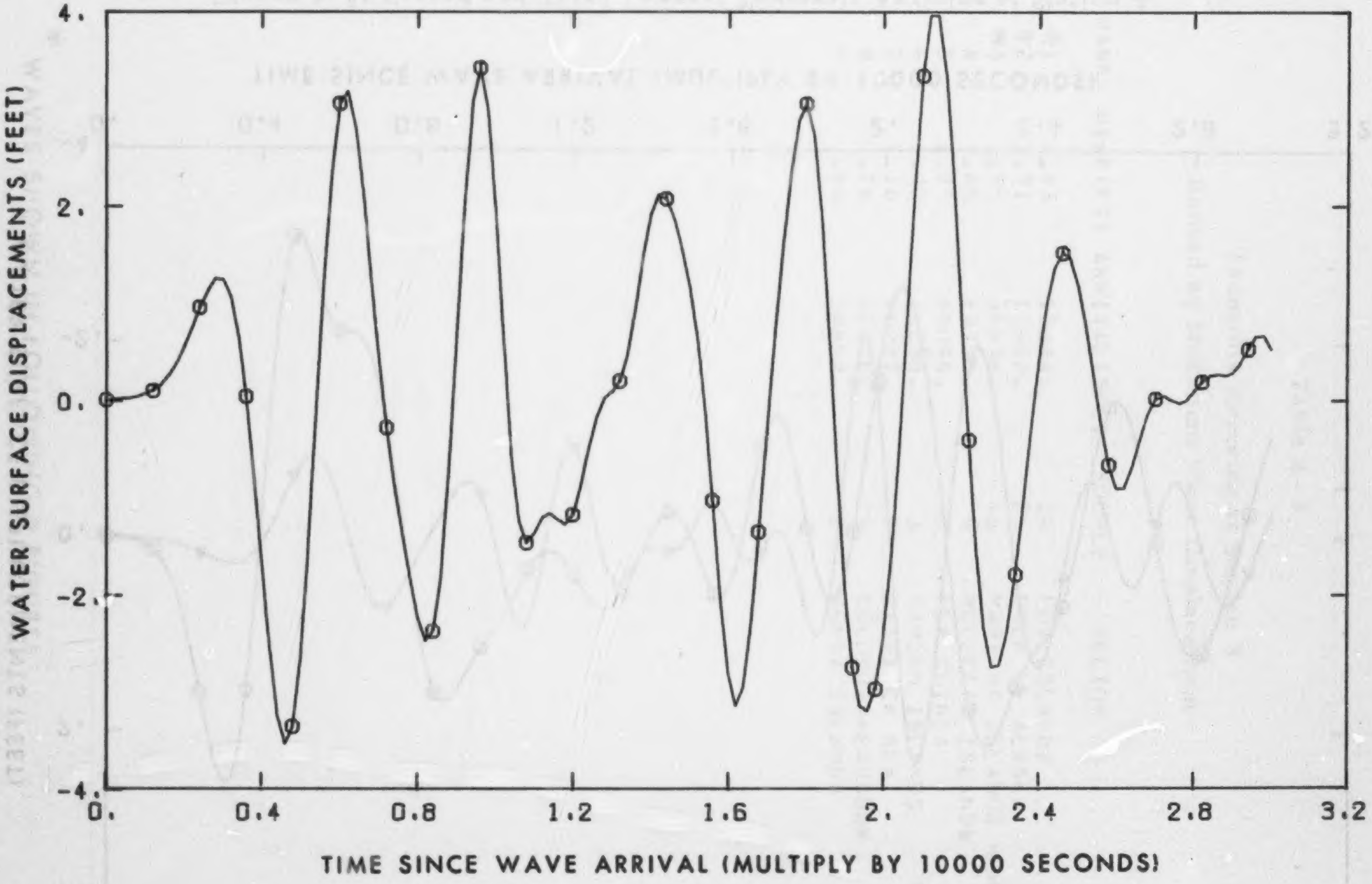

Figure A-7: Largest Tsunami Arriving at Station 4 Offshore of Cascade Head, OR

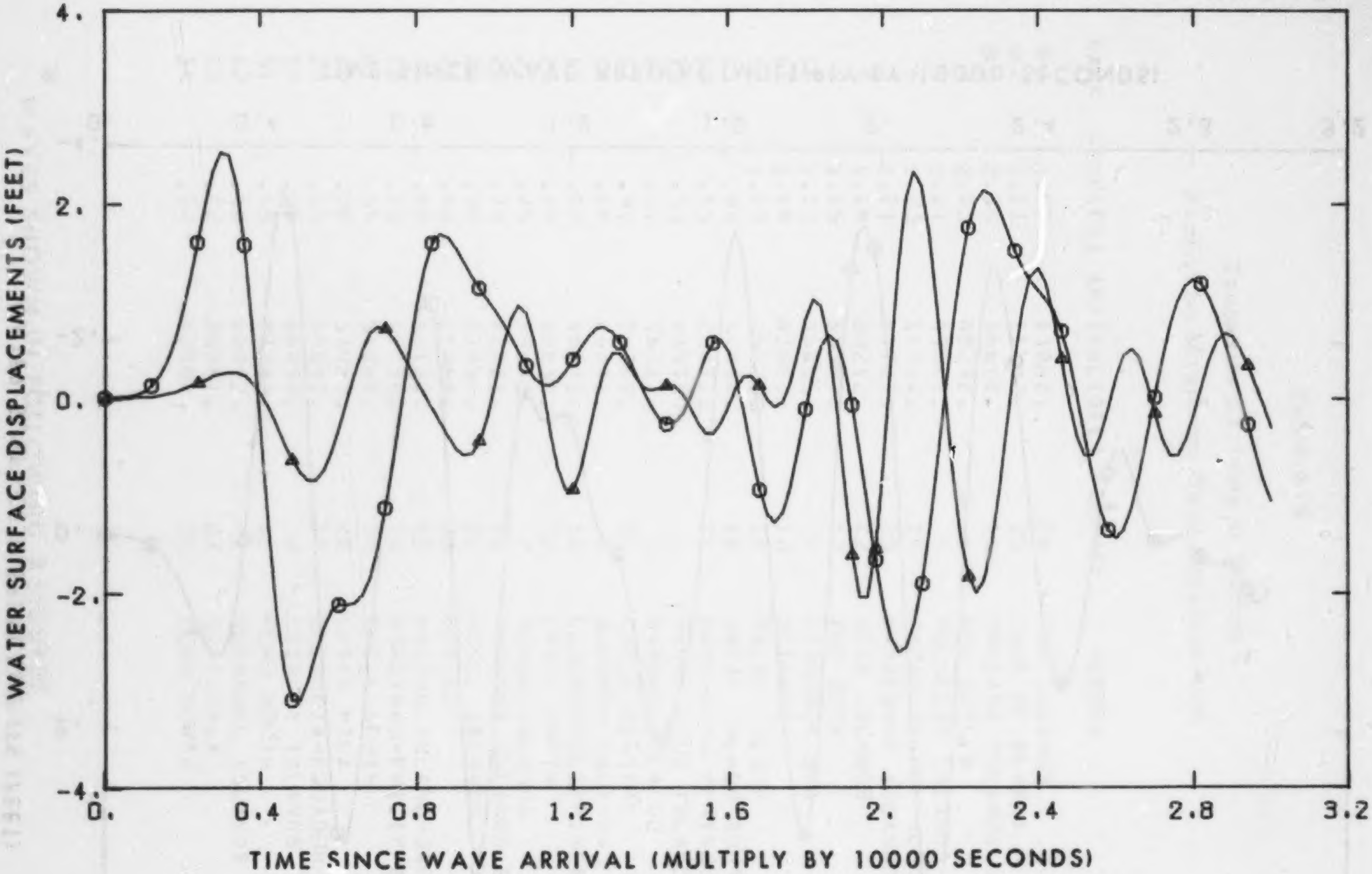

Figure A-8: Second and Third Largest Tsunamis Arriving at Station 4

Table A-5

Tsunamis Arriving at Station 5
Ranked by Maximum Wave Displacement

RANK	DISP(FT)	ARRIVAL(SEC)	SOURCE	REGION
*1	4.43	13244.	24	FOX ISLANDS
*2	3.91	11602.	25	GULF OF ALASKA
*3	1.95	36636.	16	MARIANA ISLANDS NORTH
4	1.85	49718.	9	MOLUCCAN ISLANDS
5	1.79	48090.	8	NEW GUINEA
6	1.42	36238.	3	SAMOAN ISLANDS
7	1.16	46207.	7	BISMARCK SEA
8	.76	38048.	29	COLUMBIA-EQUADOR
9	.66	38664.	2	TONGA ISLANDS

* WAVES SHOWN IN FOLLOWING 2 FIGURES

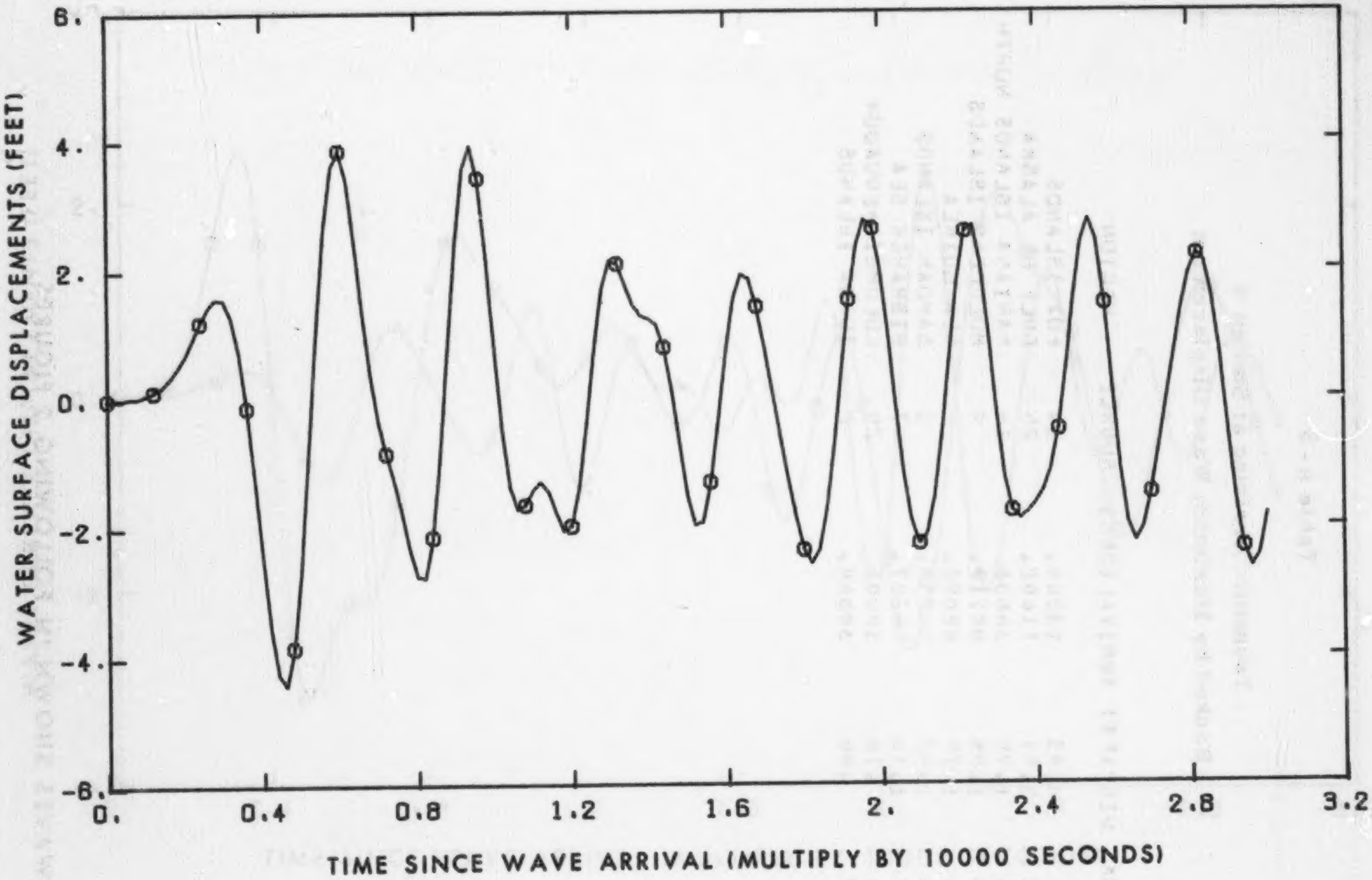

Figure A-9: Largest Tsunami Arriving at Station 5 Offshore of Hecata Head, OR

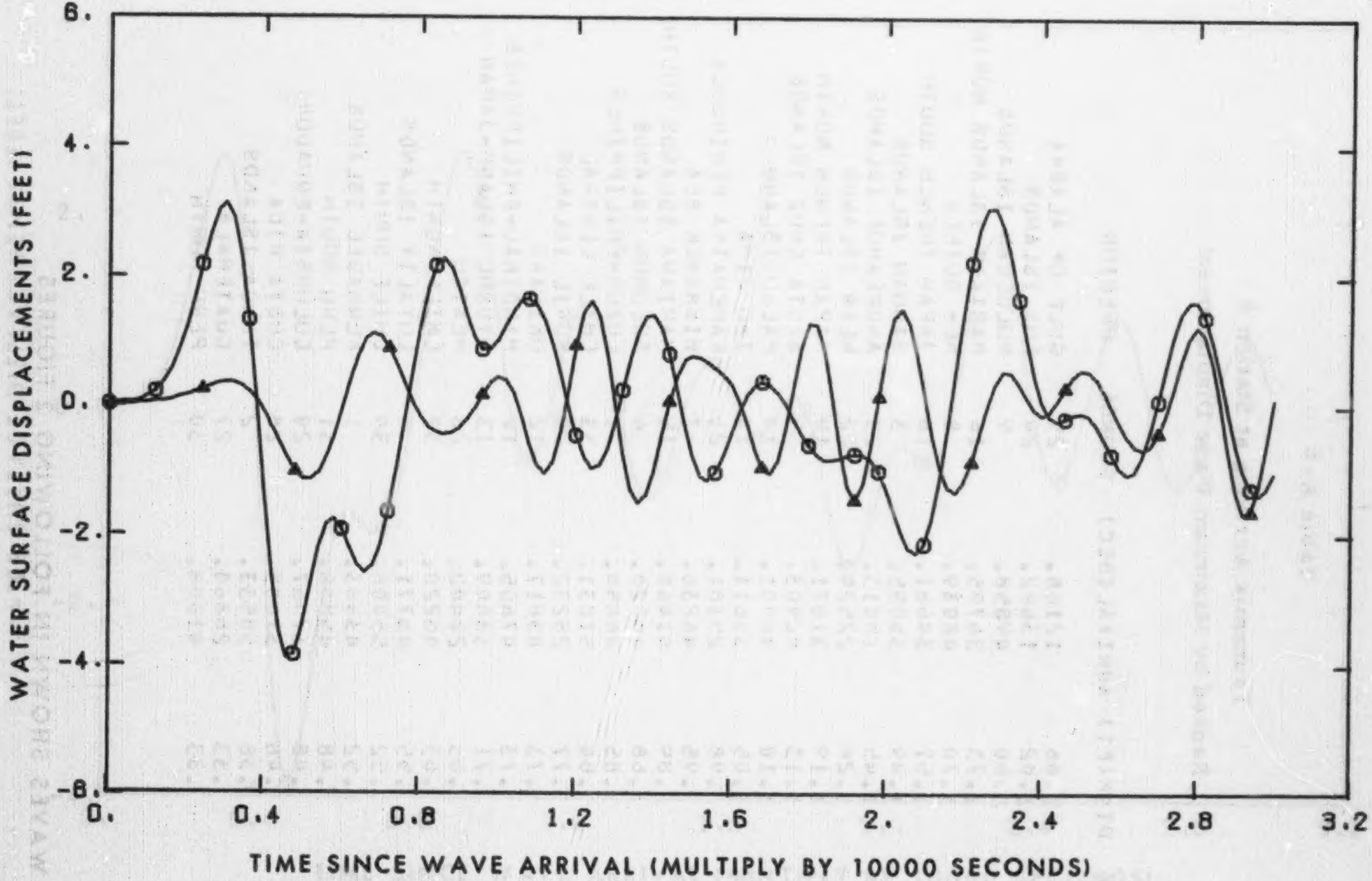

Figure A-10:Second and Third Largest Tsunamis Arriving at Station 5

Table A- 6

Tsunamis Arriving at Station 6
Ranked by Maximum Wave Displacement

RANK	DISP(FT)	ARRIVAL(SEC)	SOURCE	REGION
*1	3.86	12108.	25	GULF OF ALASKA
*2	3.82	13602.	24	FOX ISLANDS
*3	2.60	49858.	9	MOLUCCAN ISLANDS
4	1.73	36795.	16	MARIANA ISLANDS NORTH
5	1.70	48039.	8	NEW GUINEA
6	1.57	34661.	18	JAPAN TRENCH SOUTH
7	1.49	35855.	3	SAMOAN ISLANDS
8	1.45	18013.	23	ANDREANOF ISLANDS
9	1.26	22529.	22	NEAR ISLANDS
10	1.19	31671.	19	JAPAN TRENCH NORTH
11	1.13	42903.	5	SANTA CRUZ ISLANDS
12	1.10	46001.	14	PALAU ISLAND
13	1.05	35611.	17	IWO JIMA
14	.98	25381.	21	KAMCHATKA PENINSULA
15	.95	46236.	7	BISMARCK SEA
16	.89	41460.	15	MARIANA ISLANDS SOUTH
17	.88	46020.	6	SOLOMON ISLANDS
18	.85	46454.	11	LUZON-PHILIPPINES
19	.84	51831.	33	CHILE CENTRAL
20	.77	28232.	20	KURIL ISLANDS
21	.73	43817.	12	OKINAWA
22	.73	47605.	10	MINDINAO-PHILIPPINES
23	.71	38409.	13	KYUSHU ISLAND-JAPAN
24	.65	20442.	26	MEXICO
25	.63	48220.	32	CHILE NORTH
26	.55	45771.	4	LOYALTY ISLANDS
27	.52	55408.	34	CHILE SOUTH
28	.52	43443.	1	KERMADEC ISLANDS
29	.48	45846.	31	PERU SOUTH
30	.48	37467.	29	COLUMBIA-EQUADOR
31	.46	31605.	28	COSTA RICA
32	.38	38533.	2	TONGA ISLANDS
33	.33	26860.	27	GUATEMALA
34	.33	41008.	30	PERU NORTH

* WAVES SHOWN IN FOLLOWING 2 FIGURES

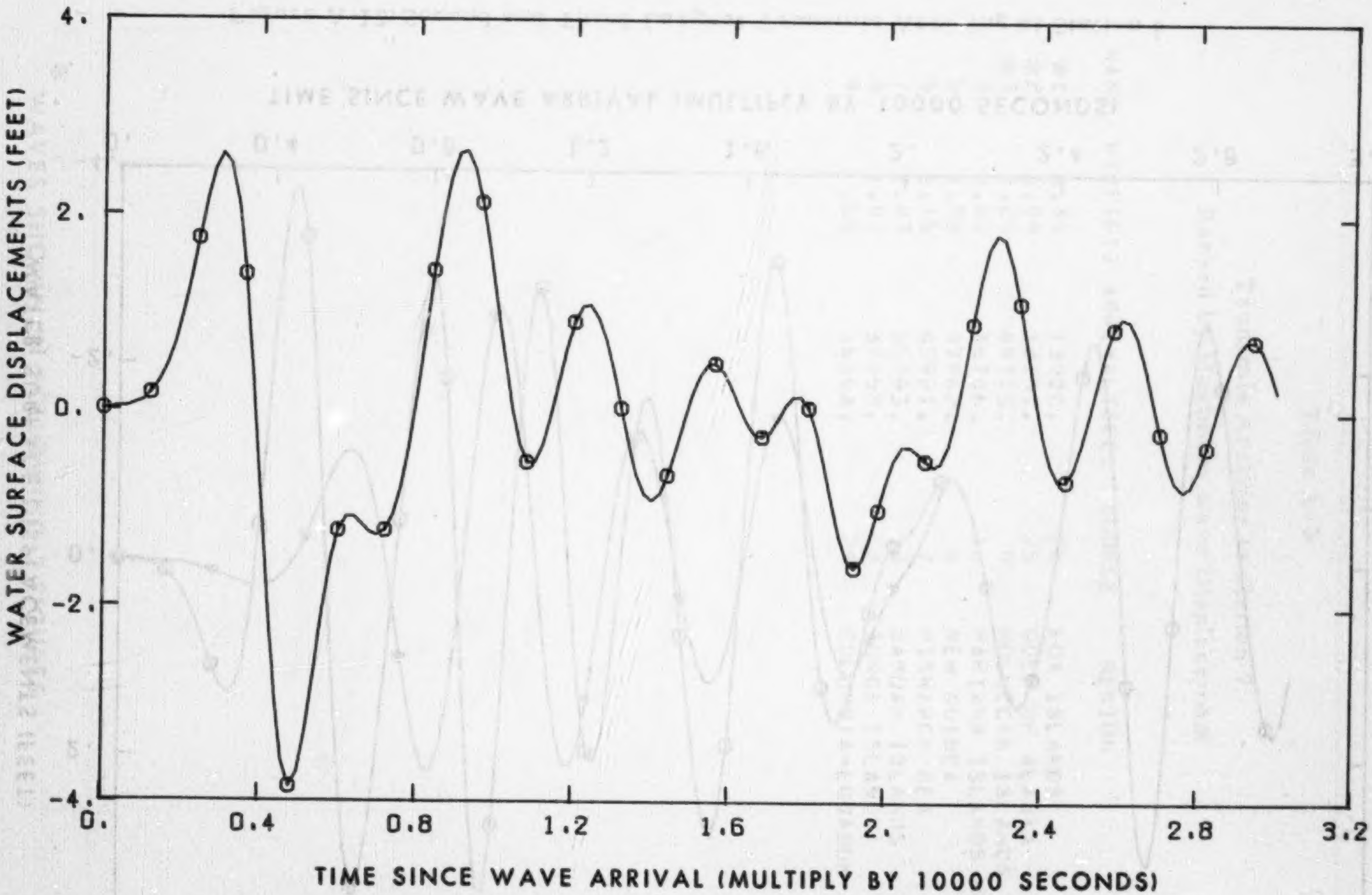

Figure A-11: Largest Tsunami Arriving at Station 6 Offshore of Cape Blanco, OR

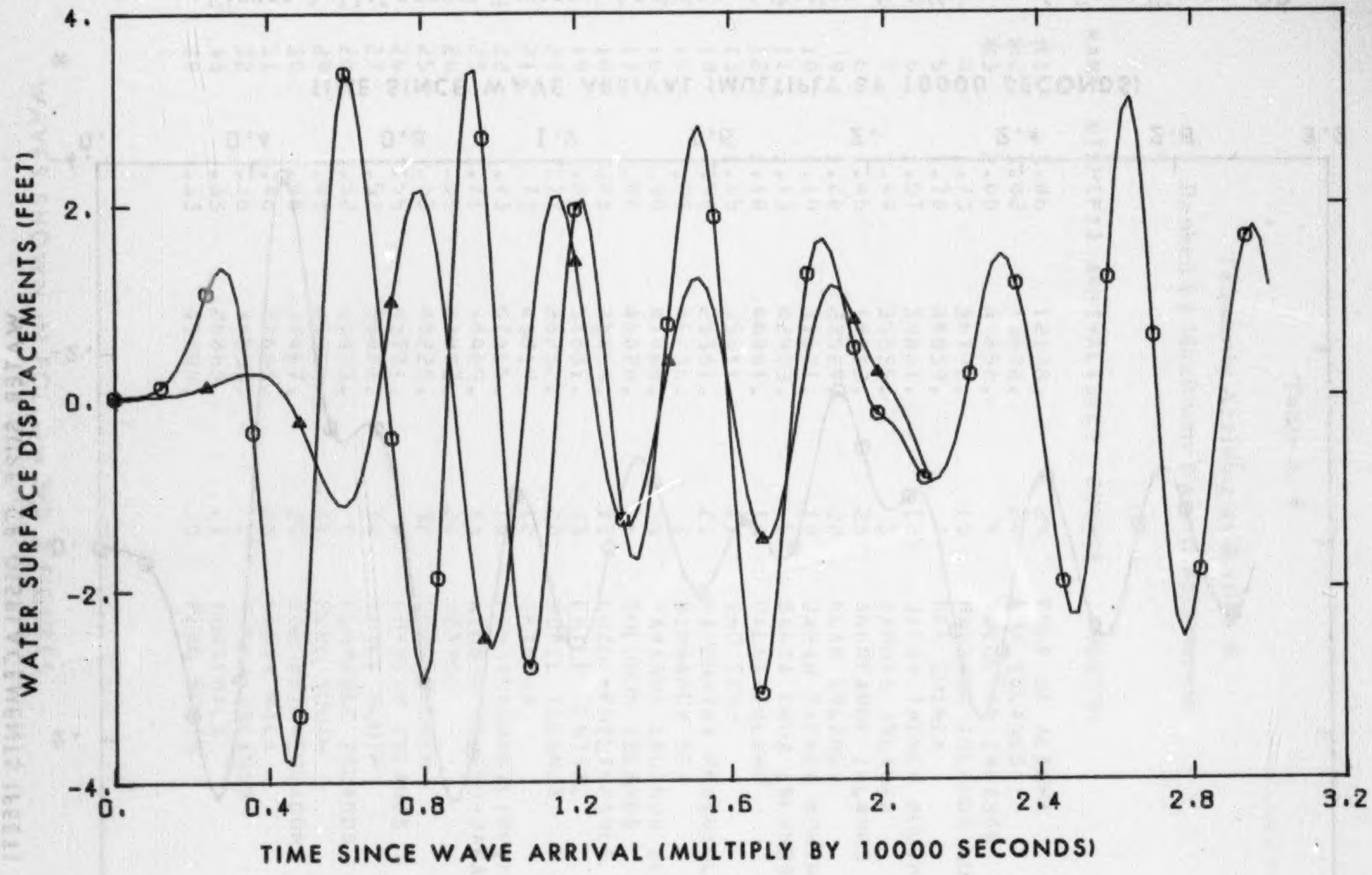

Figure A-12: Second and Third Largest Tsunamis Arriving at Station 6

Table A-7

Tsunamis Arriving at Station 7
Ranked by Maximum Wave Displacement

RANK	DISP(FT)	ARRIVAL(SEC)	SOURCE	REGION
*1	4.39	13900.	24	FOX ISLANDS
*2	3.89	12357.	25	GULF OF ALASKA
*3	3.25	49773.	9	MOLUCCAN ISLANDS
4	2.61	36706.	16	MARIANA ISLANDS NORTH
5	1.75	47862.	8	NEW GUINEA
6	1.15	45921.	7	BISMARCK SEA
7	1.07	35263.	3	SAMOAN ISLANDS
8	1.03	37858.	2	TONGA ISLANDS
9	.58	36464.	29	COLUMBIA-EQUADOR

* WAVES SHOWN IN FOLLOWING 2 FIGURES

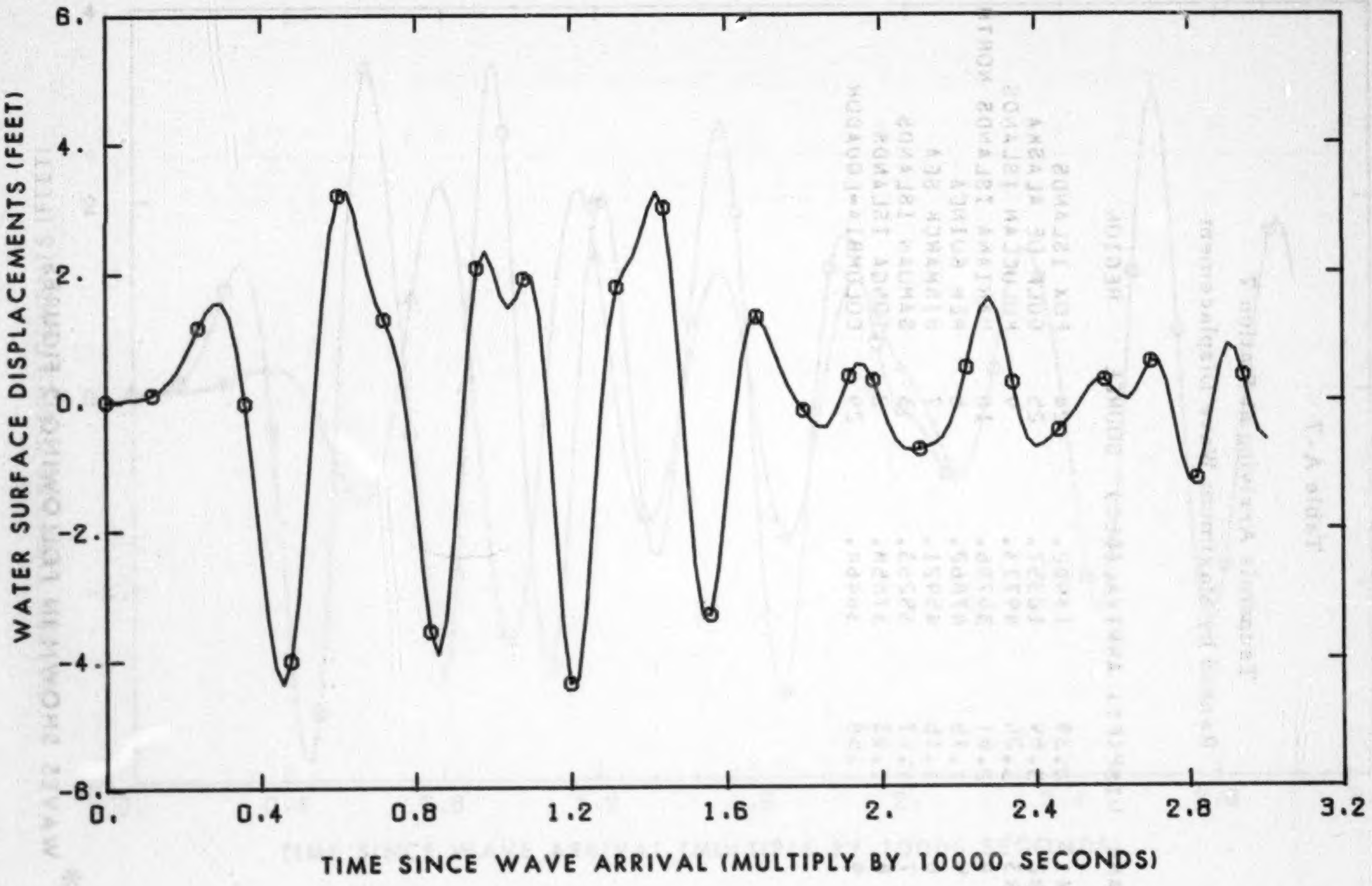

Figure A-13: Largest Tsunami Arriving at Station 7 Offshore of Crescent City, CA

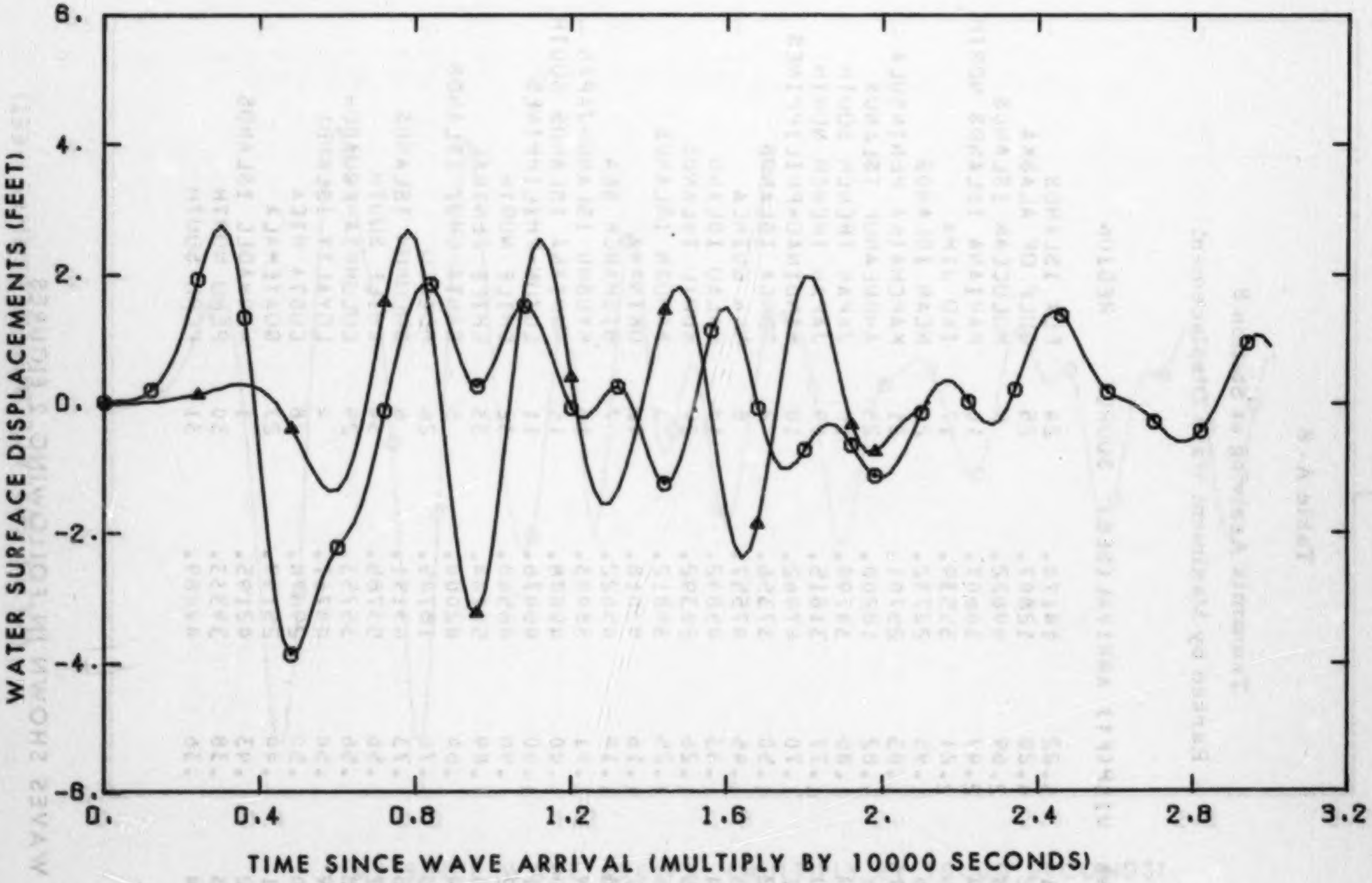

Figure A-14: Second and Third Largest Tsunamis Arriving at Station 7

Table A- 8

Tsunamis Arriving at Station 8
Ranked by Maximum Wave Displacement

RANK	DISP(FT)	ARRIVAL(SEC)	SOURCE	REGION
*1	5.22	14174.	24	FOX ISLANDS
*2	4.20	12807.	25	GULF OF ALASKA
*3	2.69	49622.	9	MOLUCCAN ISLANDS
4	2.47	36607.	16	MARIANA ISLANDS NORTH
5	2.21	35539.	17	IWO JIMA
6	1.95	22732.	22	NEAR ISLANDS
7	1.83	25701.	21	KAMCHATKA PENINSULA
8	1.82	18200.	23	ANDREANOF ISLANDS
9	1.80	34790.	18	JAPAN TRENCH SOUTH
10	1.77	31815.	19	JAPAN TRENCH NORTH
11	1.70	47462.	10	MINDINAO-PHILIPPINES
12	1.50	37356.	2	TONGA ISLANDS
13	1.45	47557.	8	NEW GUINEA
14	1.33	45842.	14	PALAU ISLAND
15	1.26	28392.	20	KURIL ISLANDS
16	1.25	34812.	3	SAMOAN ISLANDS
17	1.16	43818.	12	OKINAWA
18	1.14	45622.	7	BISMARCK SEA
19	1.01	38403.	13	KYUSHU ISLAND-JAPAN
20	1.00	40808.	15	MARIANA ISLANDS SOUTH
21	1.00	46476.	11	LUZON-PHILIPPINES
22	.90	46540.	32	CHILE NORTH
23	.89	50104.	33	CHILE CENTRAL
24	.84	42004.	5	SANTA CRUZ ISLANDS
25	.76	18745.	26	MEXICO
26	.73	45191.	6	SOLOMON ISLANDS
27	.56	53785.	34	CHILE SOUTH
28	.56	35753.	29	COLUMBIA-EQUADOR
29	.54	44767.	4	LOYALTY ISLANDS
30	.50	29874.	28	COSTA RICA
31	.44	25159.	27	GUATEMALA
32	.43	42195.	1	KERMADEC ISLANDS
33	.38	39333.	30	PERU NORTH
34	.36	44089.	31	PERU SOUTH

* WAVES SHOWN IN FOLLOWING 2 FIGURES

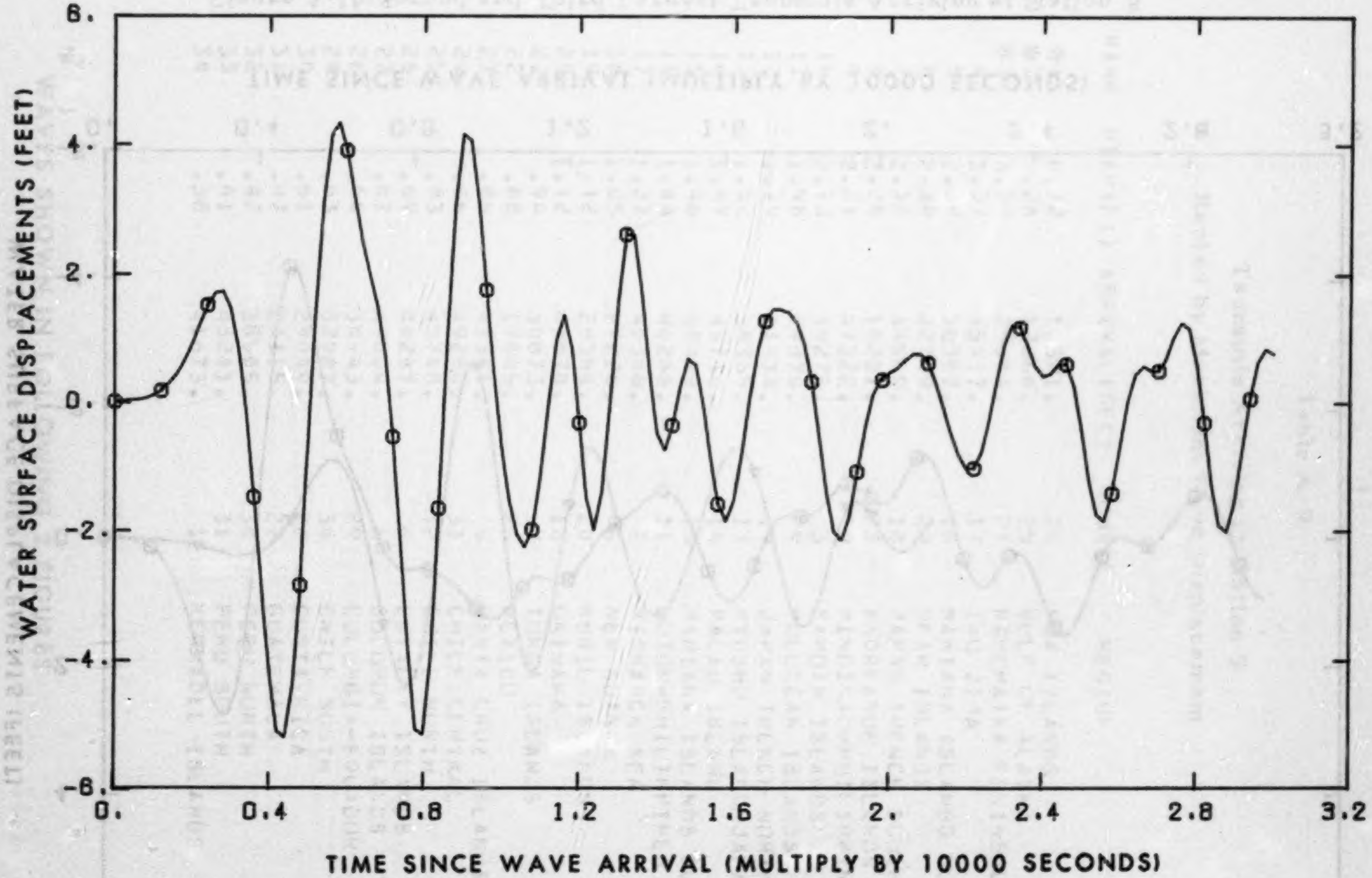

Figure A-15: Largest Tsunami Arriving at Station 8 Offshore of Eureka, CA

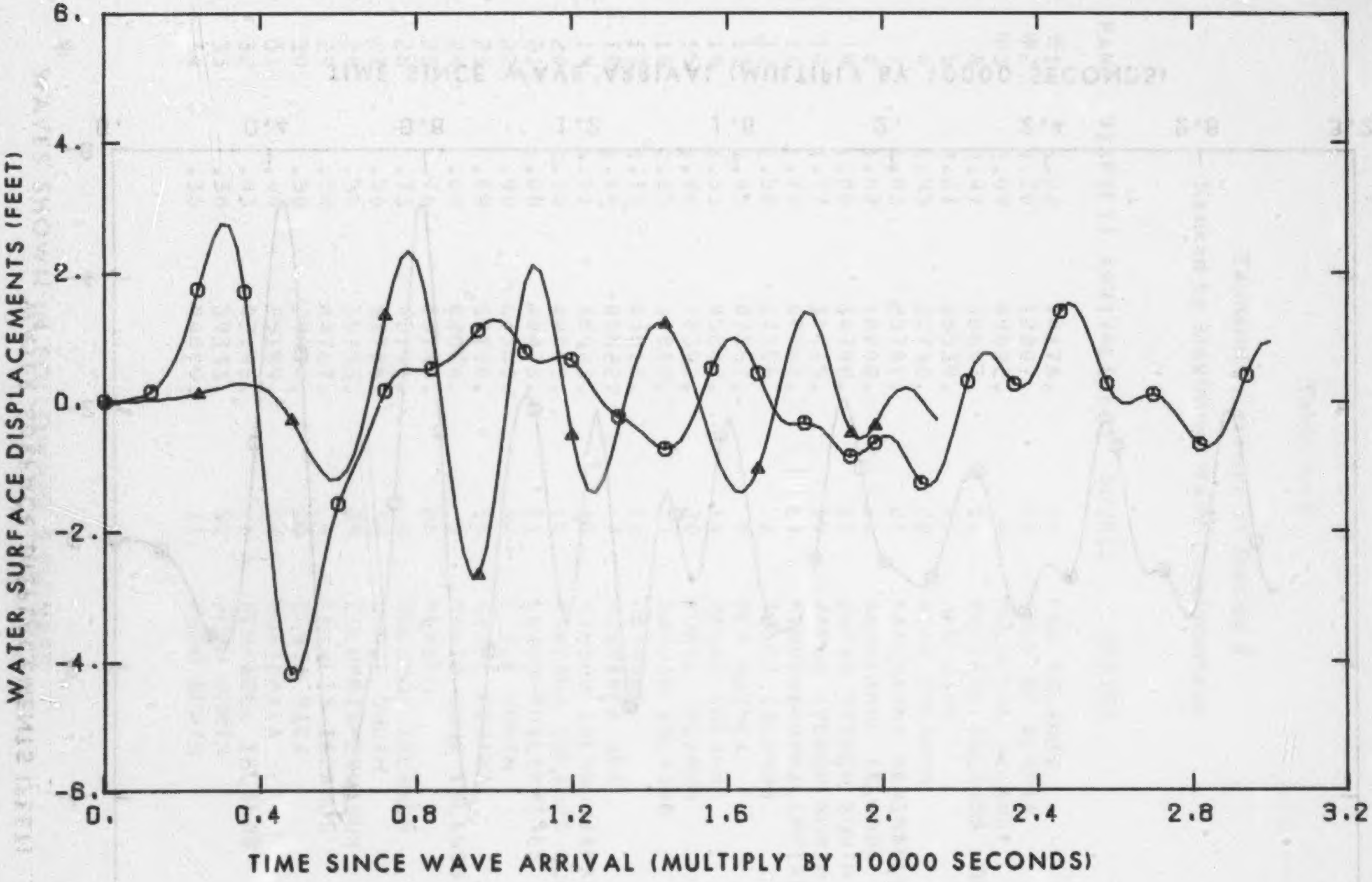

Figure A-16: Second and Third Largest Tsunamis Arriving at Station 8

Table A-9

Tsunamis Arriving at Station 9
Ranked by Maximum Wave Displacement

RANK	DISP(FT)	ARRIVAL(SEC)	SOURCE	REGION
*1	6.72	14321.	24	FOX ISLANDS
*2	4.26	12864.	25	GULF OF ALASKA
*3	3.54	25614.	21	KAMCHATKA PENINSULA
4	3.37	35417.	17	IWO JIMA
5	2.38	36387.	16	MARIANA ISLANDS NORTH
6	2.34	22749.	22	NEAR ISLANDS
7	2.32	34669.	18	JAPAN TRENCH SOUTH
8	2.28	18201.	23	ANDREANOF ISLANDS
9	2.21	47322.	10	MINDINAO-PHILIPPINES
10	2.13	34275.	3	SAMOAN ISLANDS
11	1.98	49370.	9	MOLUCCAN ISLANDS
12	1.79	31874.	19	JAPAN TRENCH NORTH
13	1.52	38365.	13	KYUSHU ISLAND-JAPAN
14	1.47	45730.	14	PALAU ISLAND
15	1.46	40489.	15	MARIANA ISLANDS SOUTH
16	1.44	46286.	11	LUZON-PHILIPPINES
17	1.27	45346.	7	BISMARCK SEA
18	1.25	47226.	8	NEW GUINEA
19	1.12	28364.	20	KURIL ISLANDS
20	1.12	43674.	12	OKINAWA
21	.94	36873.	2	TONGA ISLANDS
22	.88	17945.	26	MEXICO
23	.86	41561.	5	SANTA CRUZ ISLANDS
24	.86	49280.	33	CHILE CENTRAL
25	.83	45748.	32	CHILE NORTH
26	.69	44287.	4	LOYALTY ISLANDS
27	.67	44804.	6	SOLOMON ISLANDS
28	.64	34943.	29	COLUMBIA-EQUADOR
29	.63	52987.	34	CHILE SOUTH
30	.61	29049.	28	COSTA RICA
31	.47	24315.	27	GUATEMALA
32	.42	38505.	30	PERU NORTH
33	.41	43241.	31	PERU SOUTH
34	.38	41673.	1	KERMADEC ISLANDS

* WAVES SHOWN IN FOLLOWING 2 FIGURES

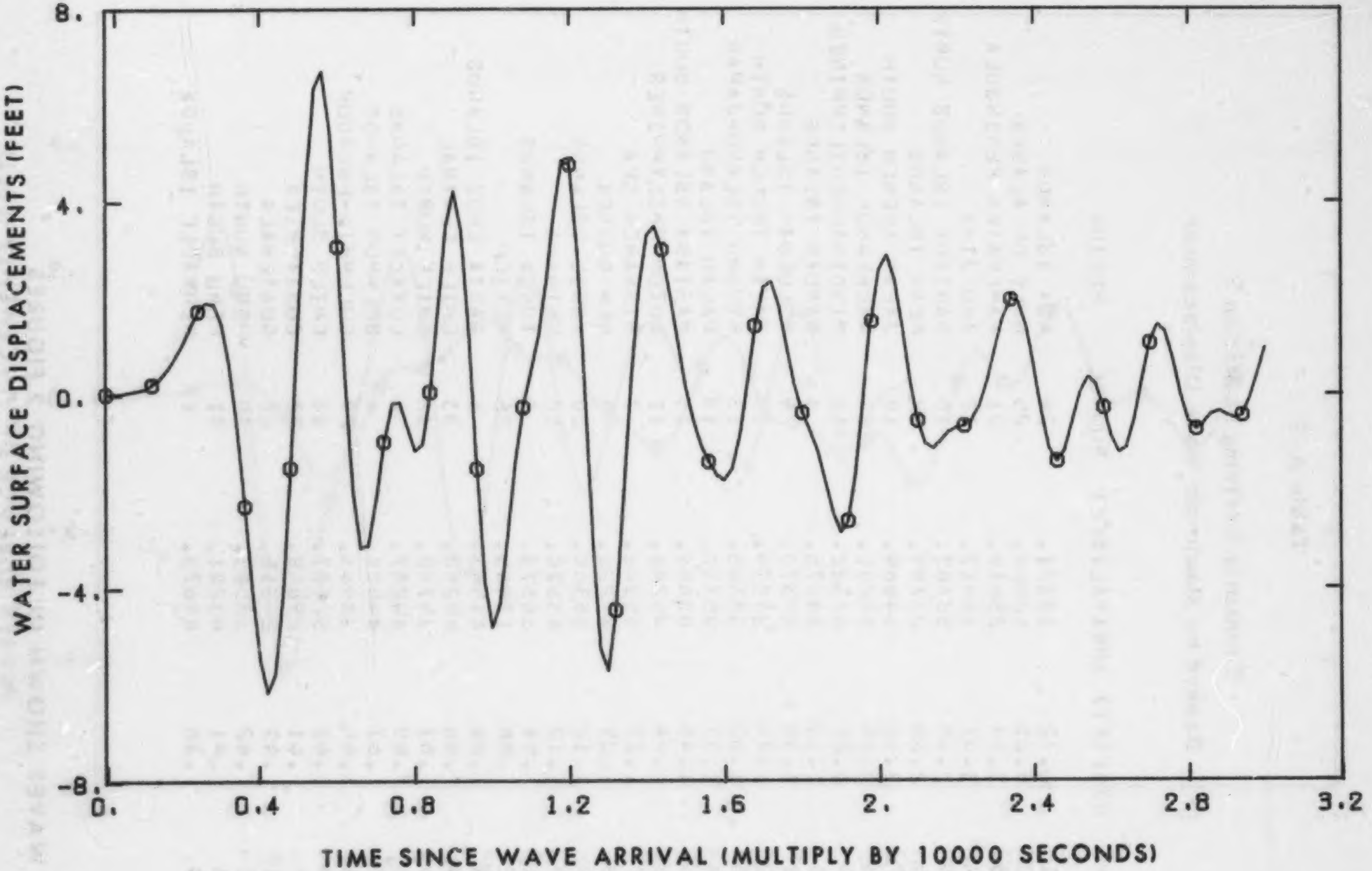

Figure A-17: Largest Tsunami Arriving at Station 9 Offshore of Cape Mendocino

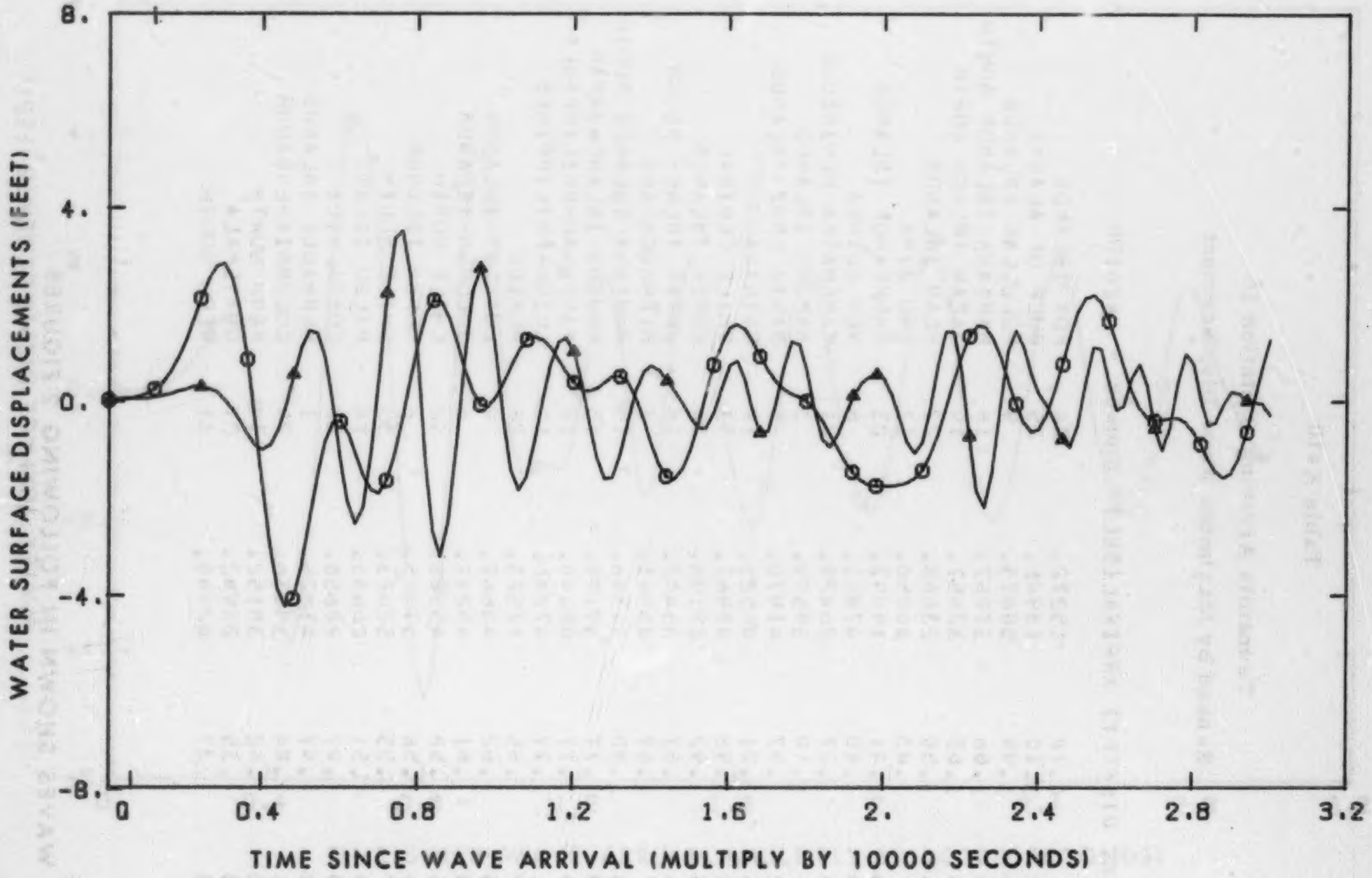

Figure A-18:Second and Third Largest Tsunamis Arriving at Station 9

Table A-10

Tsunamis Arriving at Station 10
Ranked by Maximum Wave Displacement

RANK	DISP(FT)	ARRIVAL(SEC)	SOURCE	REGION
*1	4.78	15272.	24	FOX ISLANDS
*2	3.10	13948.	25	GULF OF ALASKA
*3	1.99	50073.	9	MOLUCCAN ISLANDS
4	1.66	37067.	16	MARIANA ISLANDS NORTH
5	1.63	32657.	19	JAPAN TRENCH NORTH
6	1.50	23668.	22	NEAR ISLANDS
7	1.43	36050.	17	IWO JIMA
8	1.41	19093.	23	ANDREANOF ISLANDS
9	1.40	47841.	8	NEW GUINEA
10	1.27	26429.	21	KAMCHATKA PENINSULA
11	1.19	34599.	3	SAMOAN ISLANDS
12	1.07	41970.	5	SANTA CRUZ ISLANDS
13	1.01	44525.	12	OKINAWA
14	.98	48967.	33	CHILE CENTRAL
15	.92	29196.	20	KURIL ISLANDS
16	.87	35402.	18	JAPAN TRENCH SOUTH
17	.87	45961.	7	BISMARCK SEA
18	.80	41346.	15	MARIANA ISLANDS SOUTH
19	.77	39199.	13	KYUSHU ISLAND-JAPAN
20	.77	48040.	10	MINDINAO-PHILIPPINES
21	.77	47046.	11	LUZON-PHILIPPINES
22	.65	17523.	26	MEXICO
23	.62	44667.	4	LOYALTY ISLANDS
24	.61	45267.	6	SOLOMON ISLANDS
25	.58	45366.	32	CHILE NORTH
26	.56	37055.	2	TONGA ISLANDS
27	.53	52623.	34	CHILE SOUTH
28	.51	46630.	14	PALAU ISLAND
29	.47	28658.	28	COSTA RICA
30	.47	41825.	1	KERMADEC ISLANDS
31	.44	34536.	29	COLUMBIA-ECUADOR
32	.42	38152.	30	PERU NORTH
33	.35	23942.	27	GUATEMALA
34	.27	42940.	31	PERU SOUTH

*WAVES SHOWN IN FOLLOWING 2 FIGURES

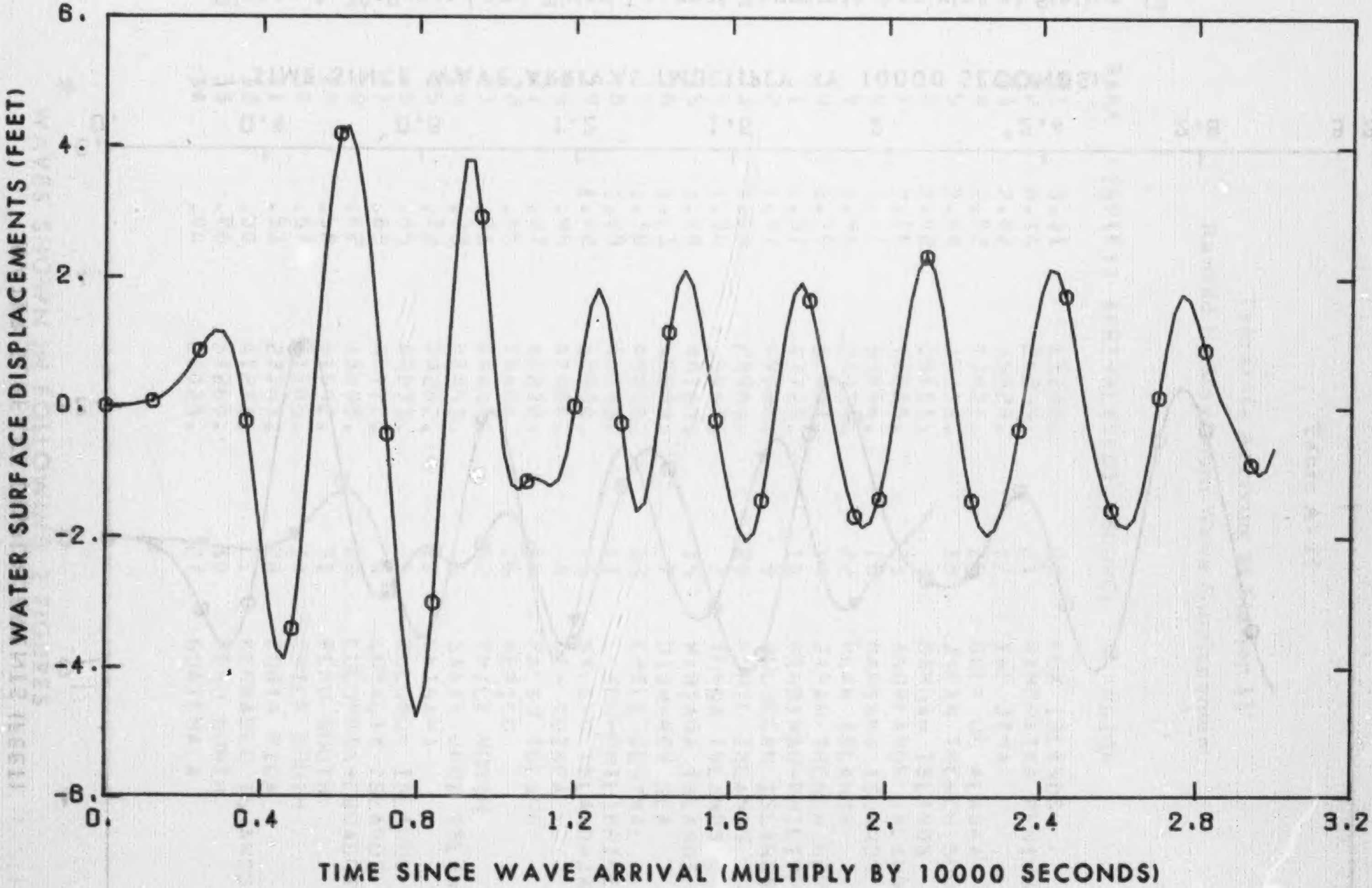

Figure A-19: Largest Tsunami Arriving at Station 10 Offshore of Point Arena, CA

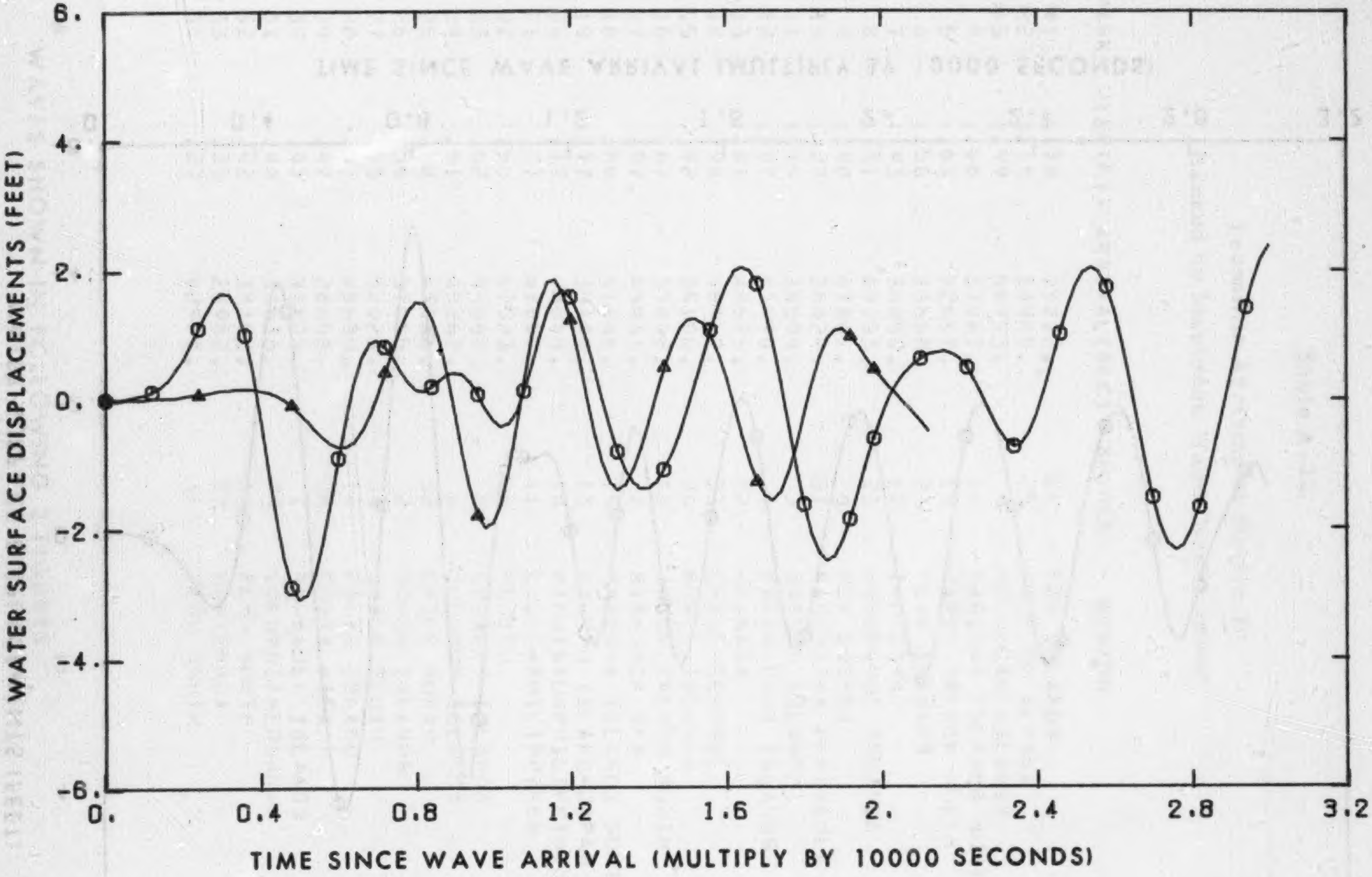

Figure A-20:Second and Third Largest Tsunamis Arriving at Station 10

Table A-11

Tsunamis Arriving at Station 11
Ranked by Maximum Wave Displacement

RANK	DISP(FT)	ARRIVAL(SEC)	SOURCE	REGION
*1	5.31	15246.	24	FOX ISLANDS
*2	4.10	26289.	21	KAMCHATKA PENINSULA
*3	2.82	35829.	17	IWO JIMA
4	2.82	13821.	25	GULF OF ALASKA
5	2.44	35234.	18	JAPAN TRENCH SOUTH
6	2.42	34111.	3	SAMOAN ISLANDS
7	2.18	18888.	23	ANDREANOF ISLANDS
8	2.01	36696.	16	MARIANA ISLANDS NORTH
9	1.96	23474.	22	NEAR ISLANDS
10	1.79	32437.	19	JAPAN TRENCH NORTH
11	1.57	47766.	10	MINDINAU-PHILIPPINES
12	1.47	49668.	9	MOLUCCAN ISLANDS
13	1.38	28984.	20	KURIL ISLANDS
14	1.36	36463.	2	TONGA ISLANDS
15	1.18	40789.	15	MARIANA ISLANDS SOUTH
16	1.13	45594.	7	BISMARCK SEA
17	1.10	48008.	33	CHILE CENTRAL
18	1.09	46793.	11	LUZON-PHILIPPINES
19	1.02	38904.	13	KYUSHU ISLAND-JAPAN
20	.95	47489.	8	NEW GUINEA
21	.87	46272.	14	PALAU ISLAND
22	.85	16606.	26	MEXICO
23	.83	44448.	32	CHILE NORTH
24	.83	41453.	5	SANTA CRUZ ISLANDS
25	.72	44262.	12	OKINAWA
26	.65	44873.	6	SOLOMON ISLANDS
27	.65	44172.	4	LOYALTY ISLANDS
28	.62	33608.	29	COLUMBIA-EQUADOR
29	.58	41992.	31	PERU SOUTH
30	.57	51745.	34	CHILE SOUTH
31	.53	27767.	28	COSTA RICA
32	.50	41273.	1	KERMADEC ISLANDS
33	.46	37260.	30	PERU NORTH
34	.44	23028.	27	GUATEMALA

* WAVES SHOWN IN FOLLOWING 2 FIGURES

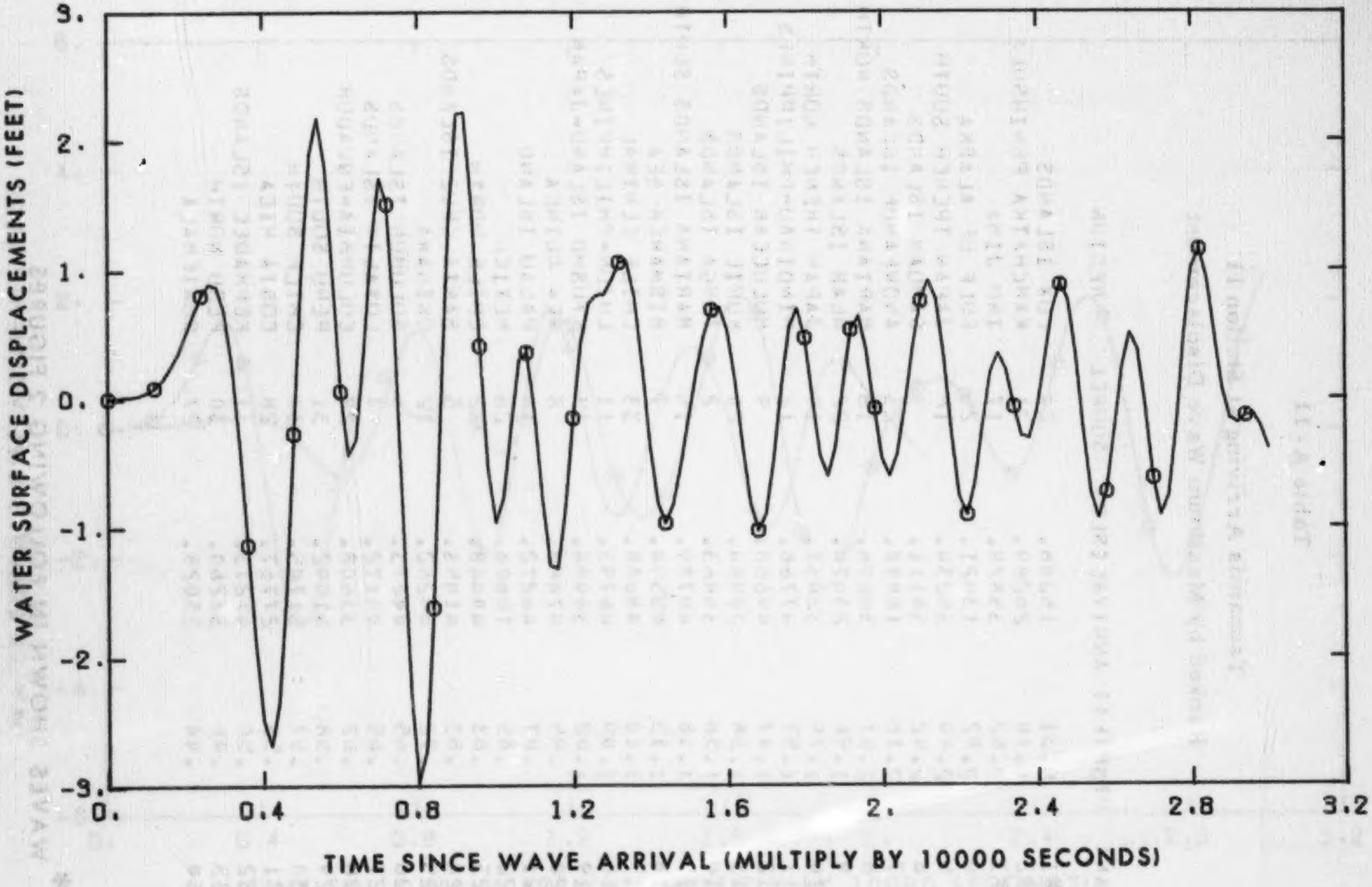

Figure A-21: Largest Tsunami Arriving at Station 11 Offshore of Point Reyes, CA

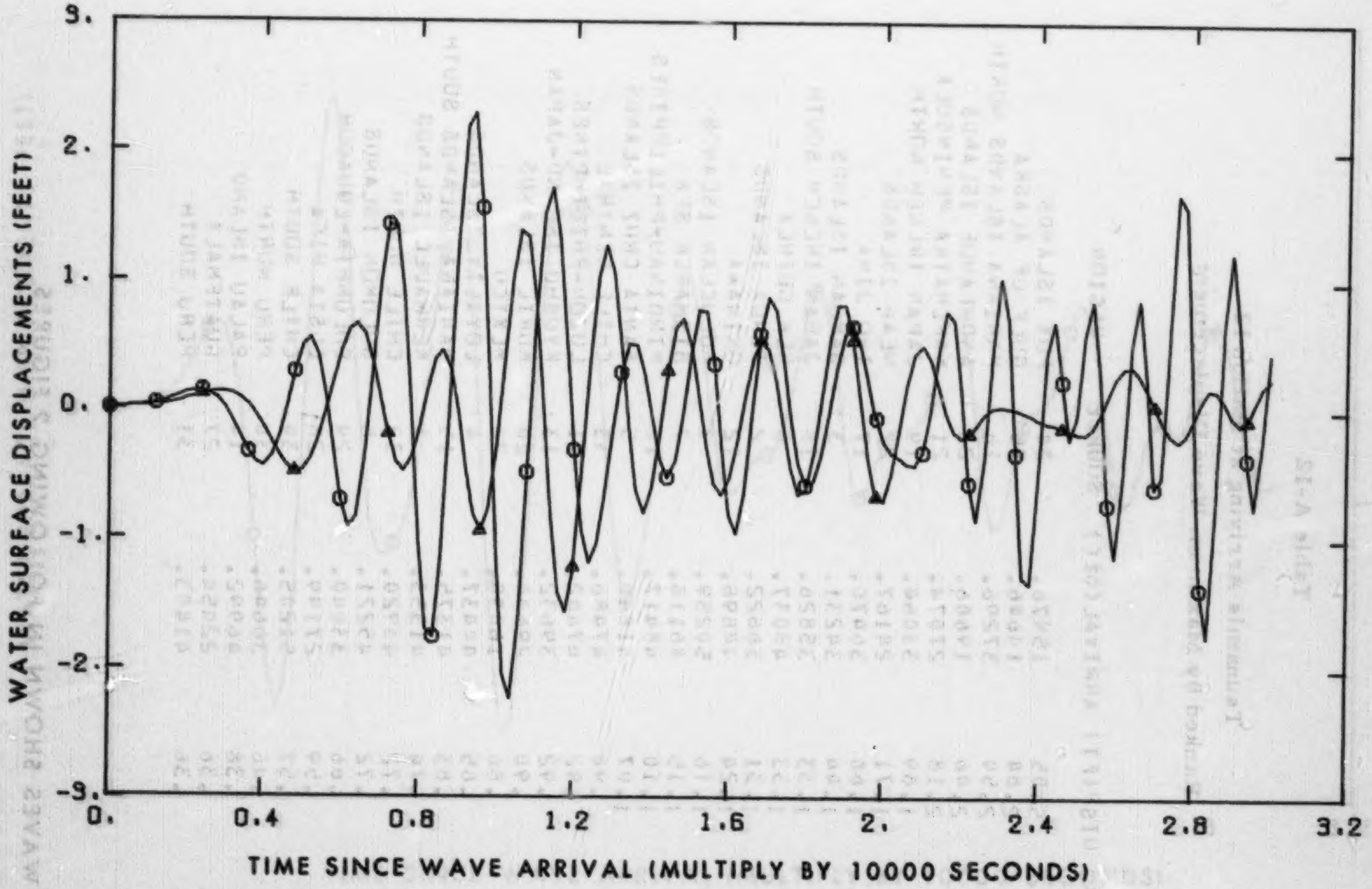

Figure A-22: Second and Third Largest Tsunamis Arriving at Station 11

Table A-12

Tsunamis Arriving at Station 12
Ranked by Maximum Wave Displacement

RANK	DISP(FT)	ARRIVAL(SEC)	SOURCE	REGION
*1	5.05	15976.	24	FOX ISLANDS
*2	2.84	14646.	25	GULF OF ALASKA
*3	2.59	37296.	16	MARIANA ISLANDS NORTH
4	2.46	19606.	23	ANDREANOF ISLANDS
5	2.18	27074.	21	KAMCHATKA PENINSULA
6	1.89	33064.	19	JAPAN TRENCH NORTH
7	1.71	24167.	22	NEAR ISLANDS
8	1.60	36470.	17	IWO JIMA
9	1.44	34231.	3	SAMOAN ISLANDS
10	1.33	35826.	18	JAPAN TRENCH SOUTH
11	1.33	48037.	8	NEW GUINEA
12	1.31	36622.	2	TONGA ISLANDS
13	1.24	44898.	12	OKINAWA
14	1.16	50259.	9	MOLUCCAN ISLANDS
15	1.15	46118.	7	BISMARCK SEA
16	1.10	48417.	10	MINDINAO-PHILIPPINES
17	1.07	41860.	5	SANTA CRUZ ISLANDS
18	.94	47486.	33	CHILE CENTRAL
19	.92	47402.	11	LUZON-PHILIPPINES
20	.92	39632.	13	KYUSHU ISLAND-JAPAN
21	.90	29644.	20	KURIL ISLANDS
22	.86	16038.	26	MEXICO
23	.85	44437.	4	LOYALTY ISLANDS
24	.83	41375.	15	MARIANA ISLANDS SOUTH
25	.74	41353.	1	KERMADEC ISLANDS
26	.72	43920.	32	CHILE NORTH
27	.72	45221.	6	SOLOMON ISLANDS
28	.66	33040.	29	COLUMBIA-EQUADOR
29	.59	27199.	28	COSTA RICA
30	.57	51205.	34	CHILE SOUTH
31	.46	36646.	30	PERU NORTH
32	.38	46992.	14	PALAU ISLAND
33	.36	22454.	27	GUATEMALA
34	.36	41403.	31	PERU SOUTH

* WAVES SHOWN IN FOLLOWING 2 FIGURES

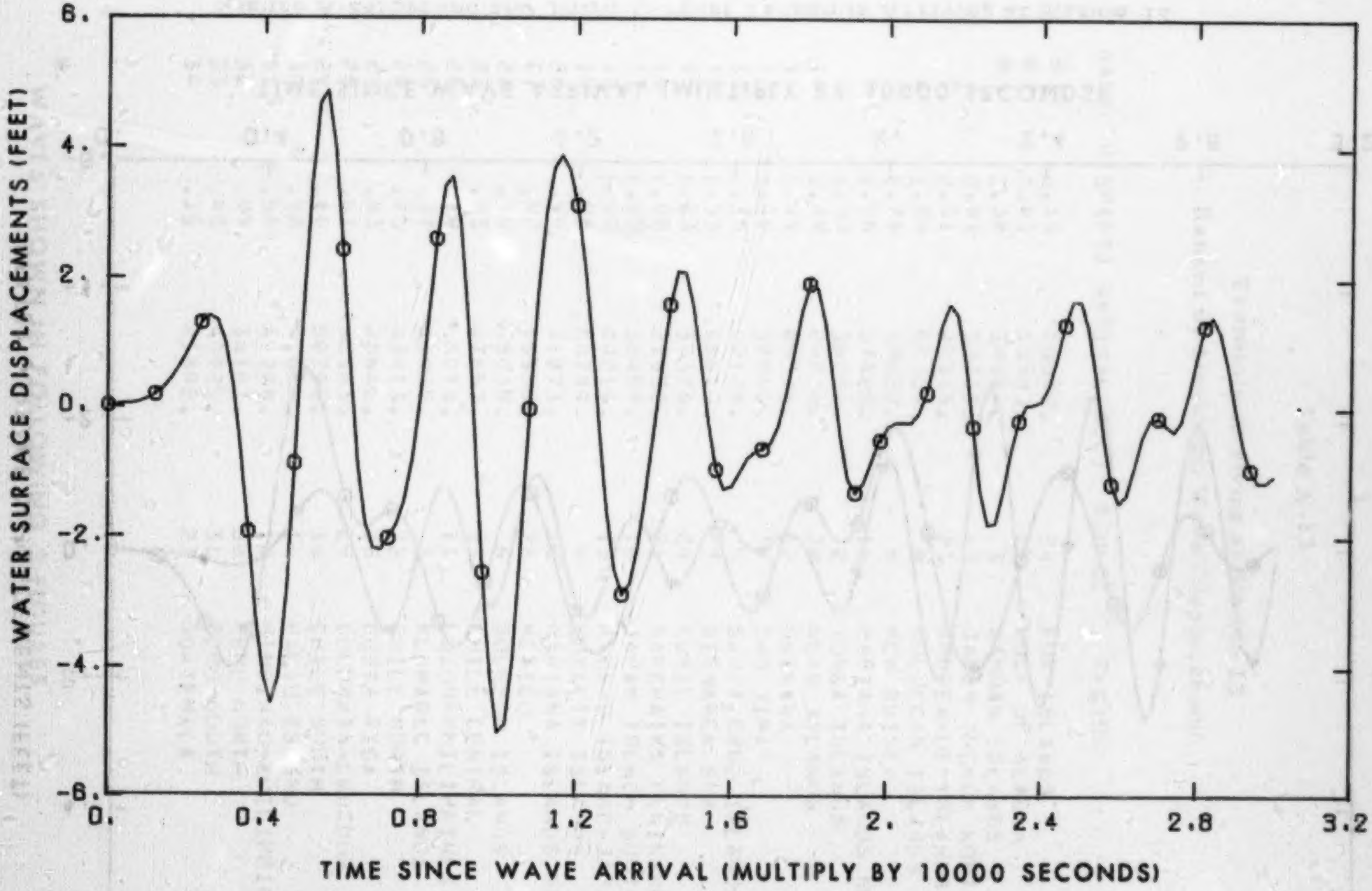

Figure A-23: Largest Tsunami Arriving at Station 12 Offshore of Monterey Bay, CA

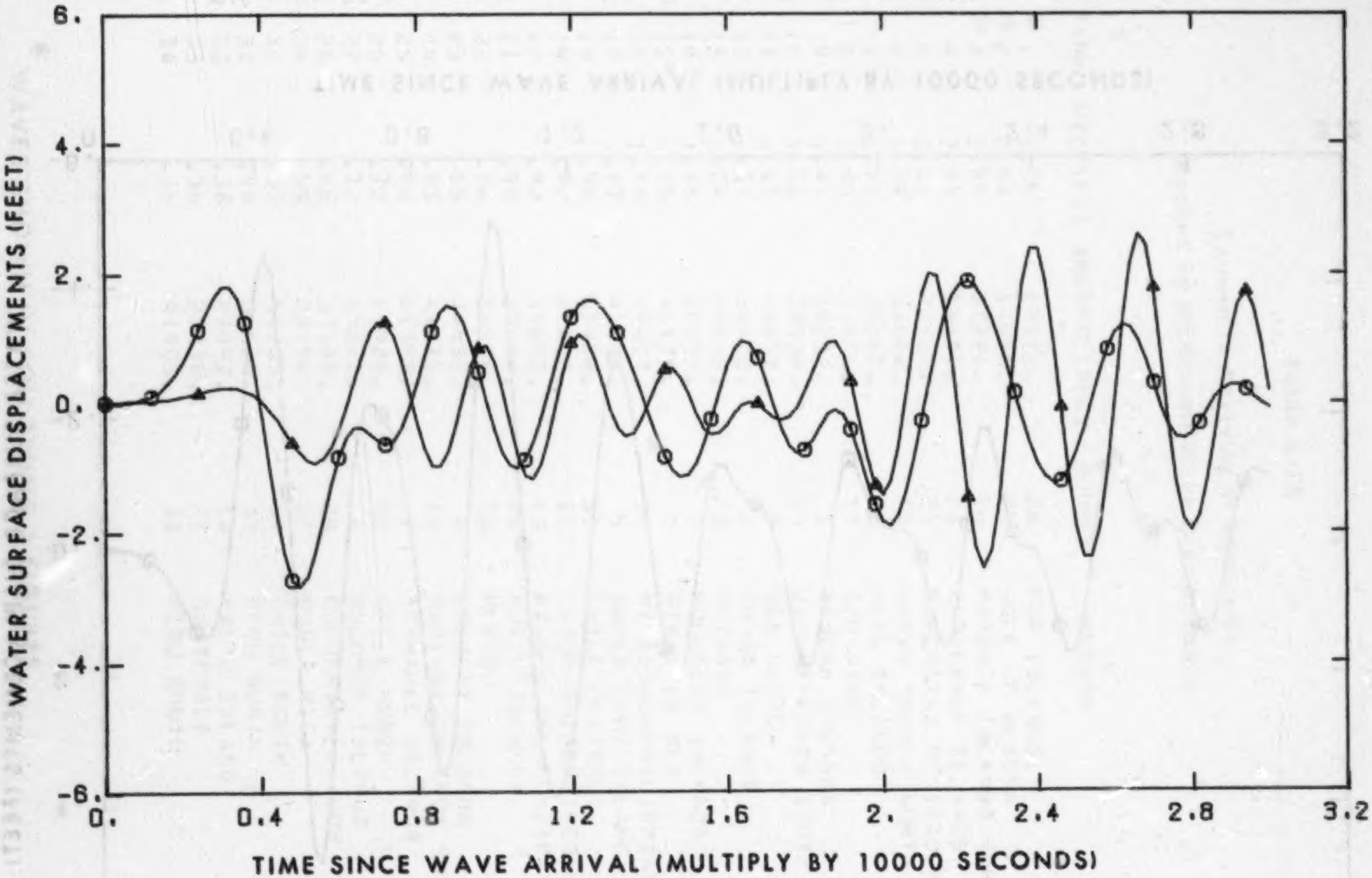

Figure A-24:Second and Third Largest Tsunamis Arriving at Station 12

Table A-13

Tsunamis Arriving at Station 13
Ranked by Maximum Wave Displacement

RANK	DISP(FT)	ARRIVAL(SEC)	SOURCE	REGION
*1	6.10	16642.	24	FOX ISLANDS
*2	3.61	15583.	25	GULF OF ALASKA
*3	2.38	34464.	3	SAMOAN ISLANDS
4	2.01	33735.	19	JAPAN TRENCH NORTH
5	2.01	20315.	23	ANDREANOF ISLANDS
6	1.79	50809.	9	MOLUCCAN ISLANDS
7	1.76	48622.	8	NEW GUINEA
8	1.56	37860.	16	MARIANA ISLANDS NORTH
9	1.52	36856.	2	TONGA ISLANDS
10	1.49	24814.	22	NEAR ISLANDS
11	1.49	45525.	12	OKINAWA
12	1.46	37060.	17	IWO JIMA
13	1.39	42128.	5	SANTA CRUZ ISLANDS
14	1.33	46610.	7	BISMARCK SEA
15	1.23	30326.	20	KURIL ISLANDS
16	1.08	27652.	21	KAMCHATKA PENINSULA
17	1.05	36459.	18	JAPAN TRENCH SOUTH
18	1.00	40210.	13	KYUSHU ISLAND-JAPAN
19	.98	44749.	4	LOYALTY ISLANDS
20	.95	41873.	15	MARIANA ISLANDS SOUTH
21	.92	15560.	26	MEXICO
22	.90	45609.	6	SOLOMON ISLANDS
23	.83	47057.	33	CHILE CENTRAL
24	.79	48014.	11	LUZON-PHILIPPINES
25	.77	41437.	1	KERMADEC ISLANDS
26	.75	43413.	32	CHILE NORTH
27	.63	26646.	28	COSTA RICA
28	.61	32563.	29	COLUMBIA-EQUADOR
29	.60	50798.	34	CHILE SOUTH
30	.58	47604.	14	PALAU ISLAND
31	.56	49008.	10	MINDINAU-PHILIPPINES
32	.49	36183.	30	PERU NORTH
33	.40	40925.	31	PERU SOUTH
34	.35	21892.	27	GUATEMALA

* WAVES SHOWN IN FOLLOWING 2 FIGURES

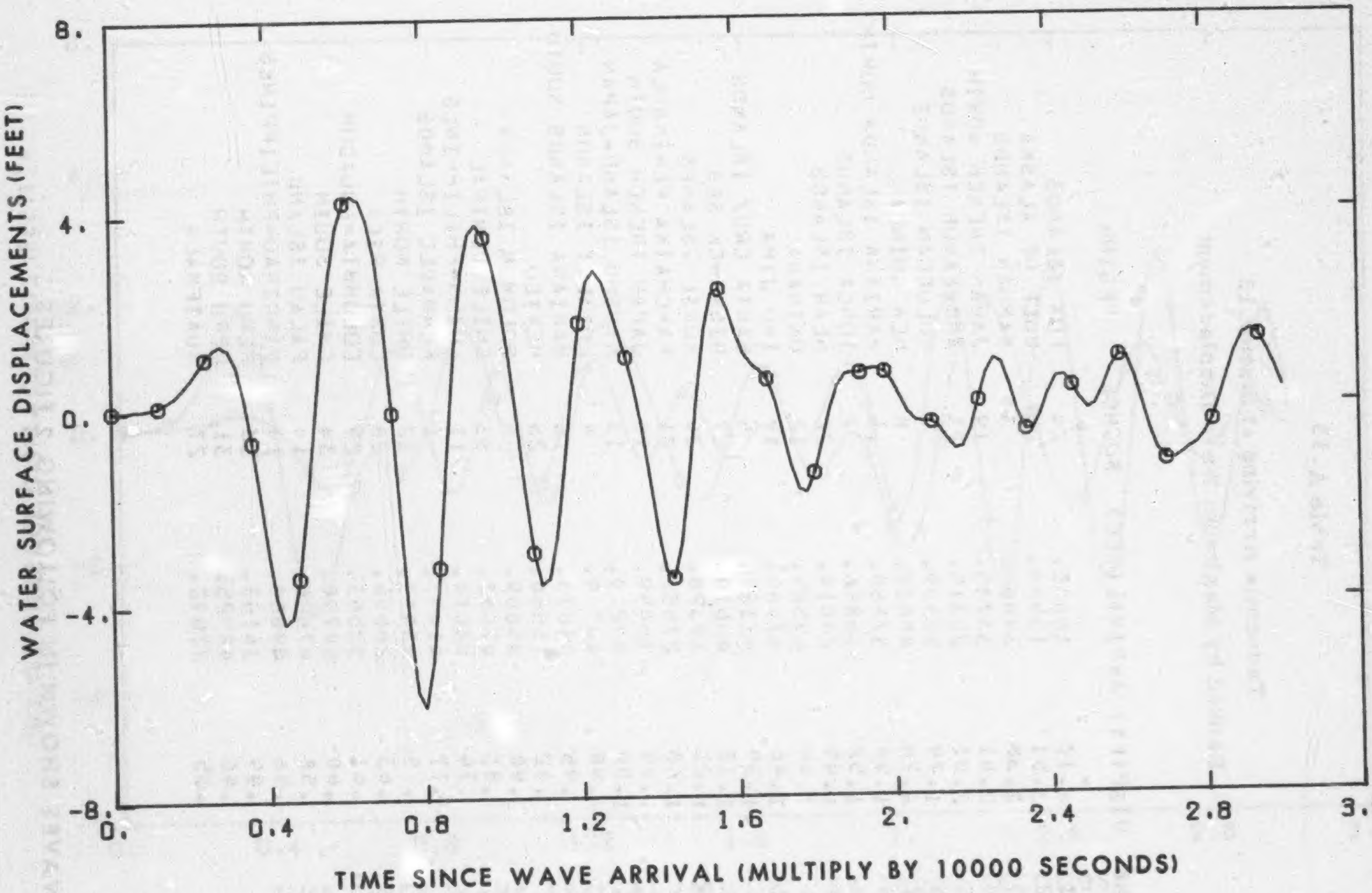

Figure A-25: Largest Tsunami Arriving at Station 13 Offshore of Point Sur, CA

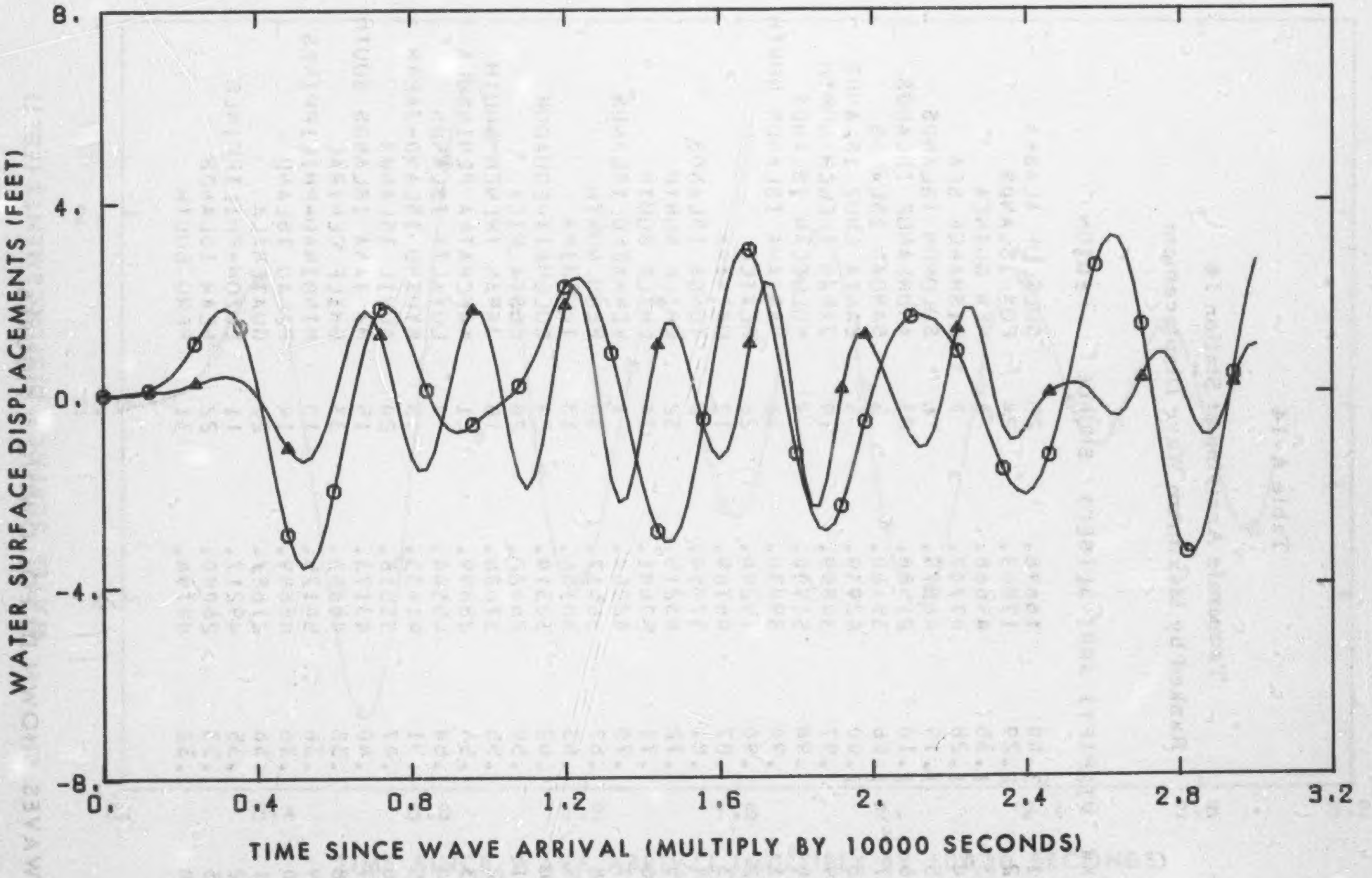

Figure A-26: Second and Third Largest Tsunamis Arriving at Station 13

Table A-14

Tsunamis Arriving at Station 14
Ranked by Maximum Wave Displacement

RANK	DISP(FT)	ARRIVAL(SEC)	SOURCE	REGION
*1	3.40	16698.	25	GULF OF ALASKA
*2	2.29	17863.	24	FOX ISLANDS
*3	1.35	49668.	8	NEW GUINEA
4	1.28	47707.	7	BISMARCK SEA
5	1.19	46579.	6	SOLOMON ISLANDS
6	1.10	21588.	23	ANDREANOF ISLANDS
7	1.06	35160.	3	SAMOAN ISLANDS
8	1.00	42939.	5	SANTA CRUZ ISLANDS
9	.97	34899.	19	JAPAN TRENCH NORTH
10	.94	51990.	9	MOLUCCAN ISLANDS
11	.90	39030.	16	MARIANA ISLANDS NORTH
12	.90	15294.	26	MEXICO
13	.87	46769.	12	OKINAWA
14	.81	37454.	2	TONGA ISLANDS
15	.72	43215.	32	CHILE NORTH
16	.71	50641.	34	CHILE SOUTH
17	.70	42064.	1	KERMADEC ISLANDS
18	.67	36017.	30	PERU NORTH
19	.63	38156.	17	IWO JIMA
20	.62	32314.	29	COLUMBIA-EQUADOR
21	.59	26422.	28	COSTA RICA
22	.55	37606.	18	JAPAN TRENCH SOUTH
23	.54	28899.	21	KAMCHATKA PENINSULA
24	.54	45544.	4	LOYALTY ISLANDS
25	.51	41433.	13	KYUSHU ISLAND-JAPAN
26	.47	31516.	20	KURIL ISLANDS
27	.40	43173.	15	MARIANA ISLANDS SOUTH
28	.38	46883.	33	CHILE CENTRAL
29	.36	50175.	10	MINDINAO-PHILIPPINES
30	.36	48889.	14	PALAU ISLAND
31	.36	21687.	27	GUATEMALA
32	.35	49217.	11	LUZON-PHILIPPINES
33	.33	26080.	22	NEAR ISLANDS
34	.32	40794.	31	PERU SOUTH

* WAVES SHOWN IN FOLLOWING 2 FIGURES

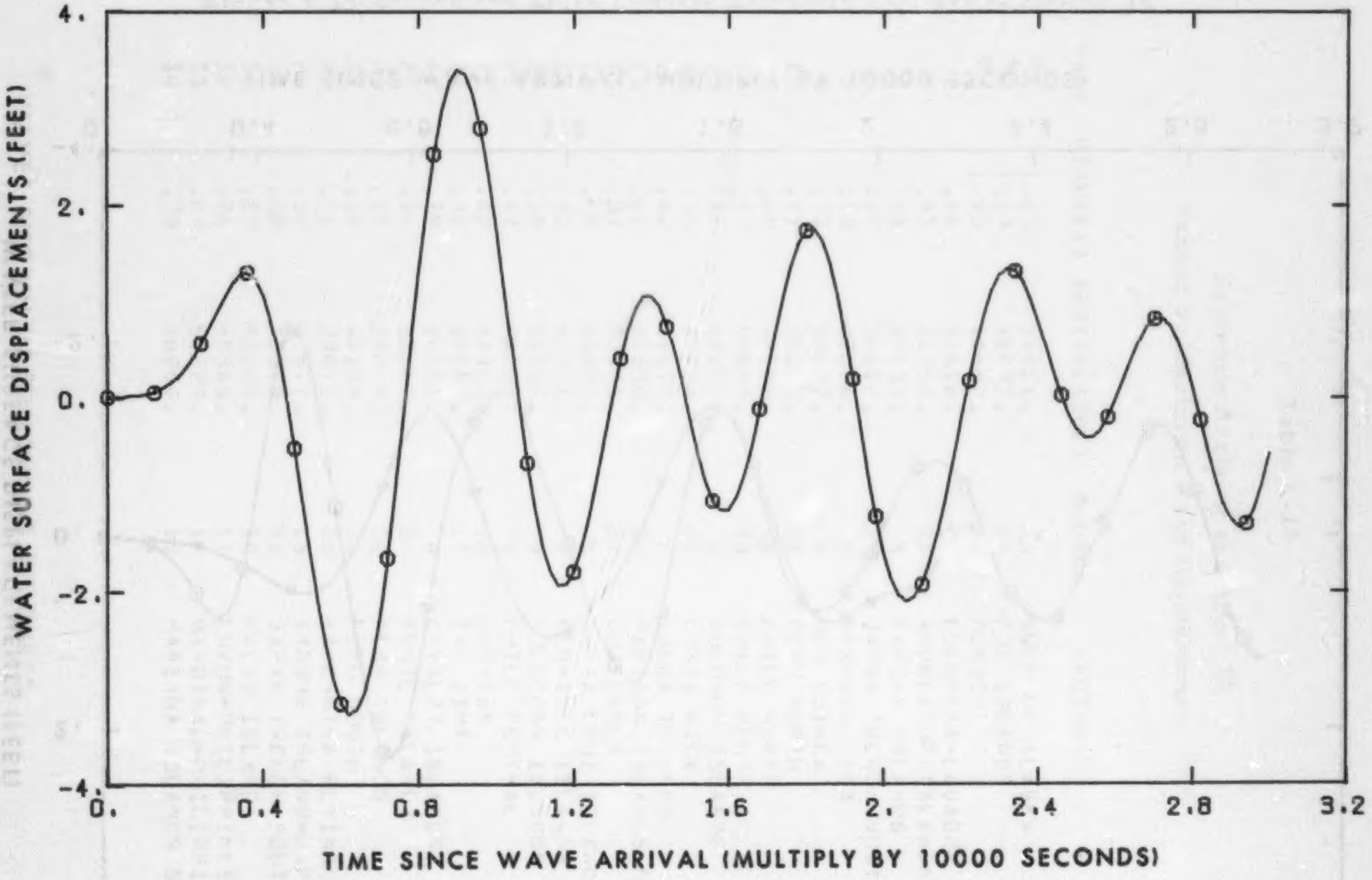

Figure A-27: Largest Tsunami Arriving at Station 14 Offshore of Point Buchon, CA

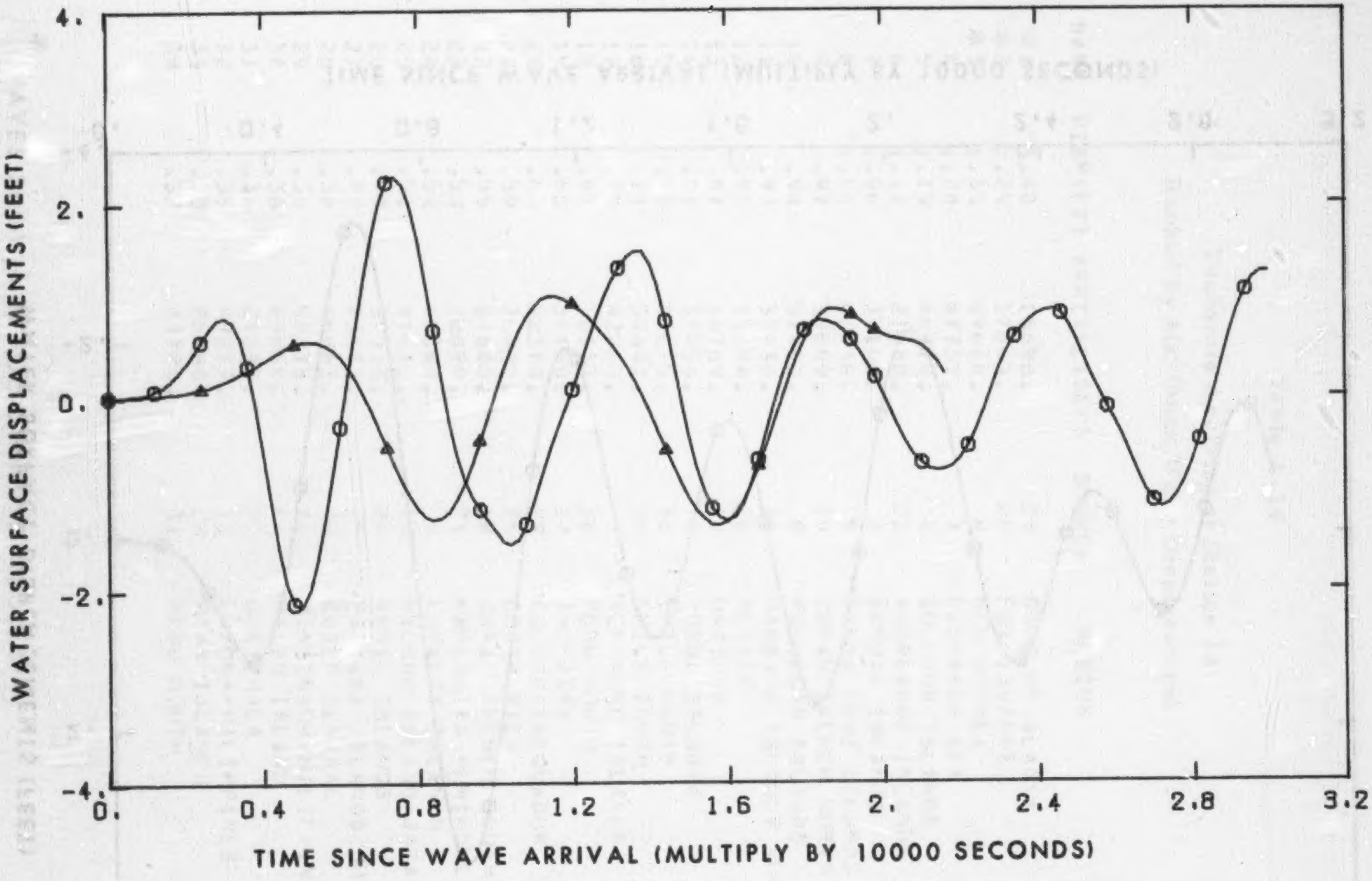

Figure A-28: Second and Third Largest Tsunamis Arriving at Station 14

Table A-15

Tsunamis Arriving at Station 15
Ranked by Maximum Wave Displacement

RANK	DISP(FT)	ARRIVAL(SEC)	SOURCE	REGION
*1	1.63	17711.	25	GULF OF ALASKA
*2	1.39	18807.	24	FOX ISLANDS
*3	1.03	14582.	26	MEXICO
4	.96	31618.	29	COLUMBIA-EQUADOR
5	.93	22750.	23	ANDREANOF ISLANDS
6	.92	35536.	3	SAMOAN ISLANDS
7	.82	36012.	19	JAPAN TRENCH NORTH
8	.74	48624.	7	BISMARCK SEA
9	.73	50627.	8	NEW GUINEA
10	.71	35317.	30	PERU NORTH
11	.69	42582.	32	CHILE NORTH
12	.67	50054.	34	CHILE SOUTH
13	.66	47270.	6	SOLOMON ISLANDS
14	.65	25716.	28	COSTA RICA
15	.62	37678.	2	TONGA ISLANDS
16	.61	40038.	16	MARIANA ISLANDS NORTH
17	.57	20991.	27	GUATEMALA
18	.54	43483.	5	SANTA CRUZ ISLANDS
19	.50	42231.	1	KERMADEC ISLANDS
20	.50	53034.	9	MOLUCCAN ISLANDS
21	.47	46262.	33	CHILE CENTRAL
22	.42	47913.	12	OKINAWA
23	.40	39202.	17	IWO JIMA
24	.39	46061.	4	LOYALTY ISLANDS
25	.36	32660.	20	KURIL ISLANDS
26	.35	27264.	22	NEAR ISLANDS
27	.34	40134.	31	PERU SOUTH
28	.31	29876.	21	KAMCHATKA PENINSULA
29	.30	42611.	13	KYUSHU ISLAND-JAPAN
30	.28	38678.	18	JAPAN TRENCH SOUTH
31	.27	50248.	14	PALAU ISLAND
32	.26	50363.	11	LUZON-PHILIPPINES
33	.24	51229.	10	MINDINAO-PHILIPPINES
34	.20	46004.	15	MARIANA ISLANDS SOUTH

* WAVES SHOWN IN FOLLOWING 2 FIGURES

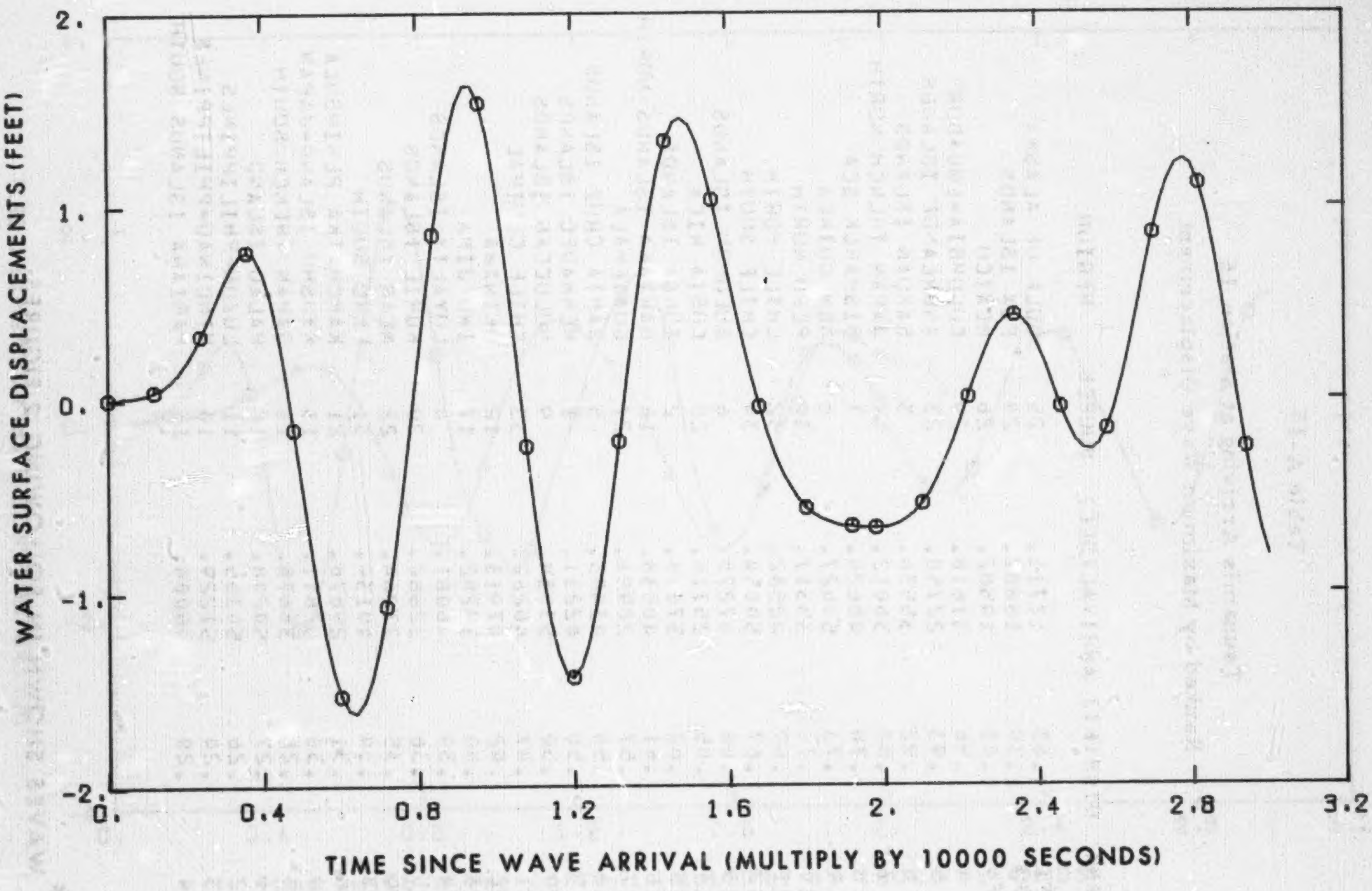

Figure A-29: Largest Tsunami Arriving at Station 15 Offshore of Santa Rosa Island, CA

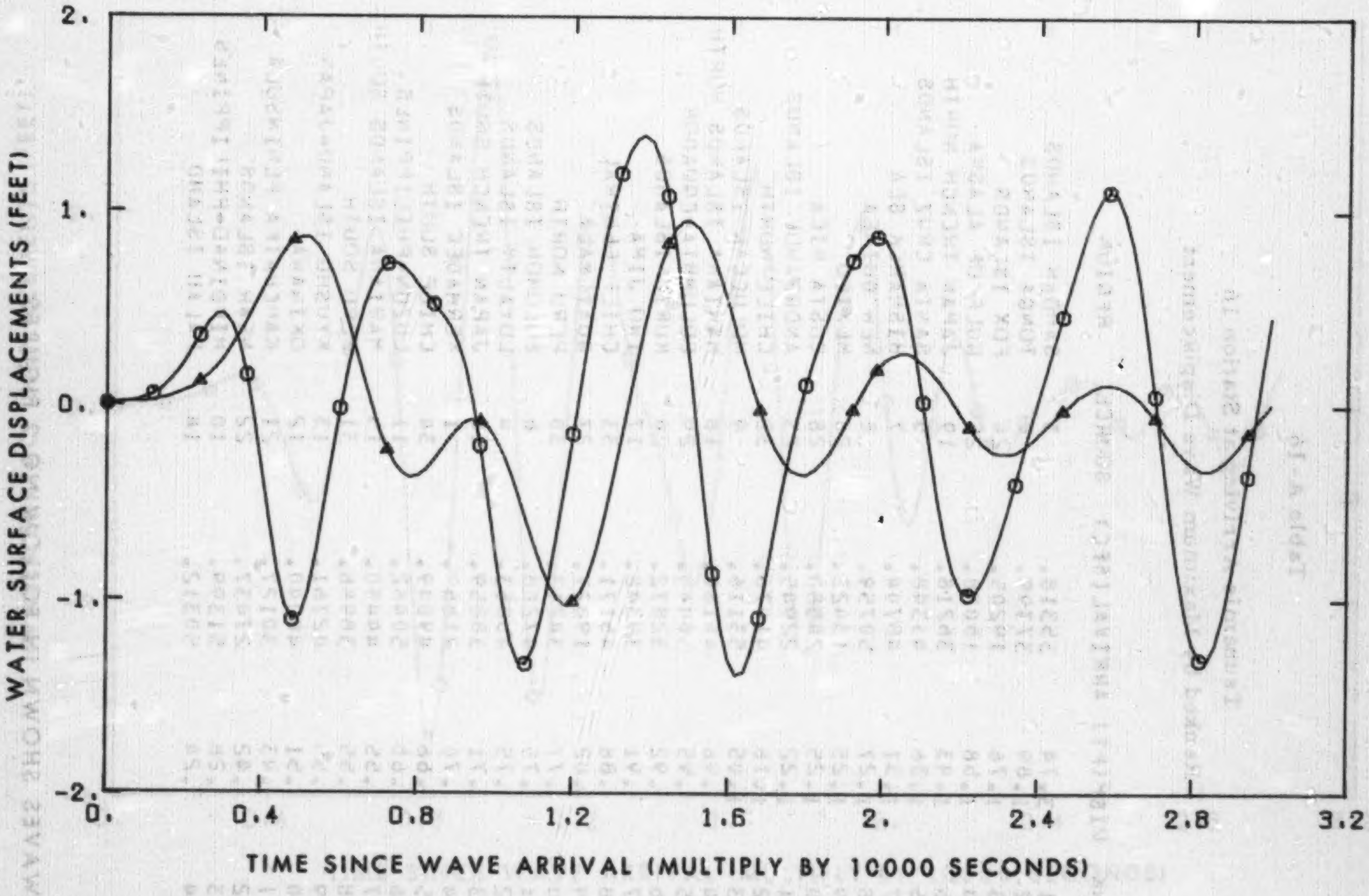

Figure A-30: Second and Third Largest Tsunamis Arriving at Station 15

Table A-16

Tsunamis Arriving at Station 16
Ranked by Maximum Wave Displacement

RANK	DISP(FT)	ARRIVAL(SEC)	SOURCE	REGION
*1	3.74	35318.	3	SAMOAN ISLANDS
*2	1.89	37399.	2	TONGA ISLANDS
*3	1.76	19205.	24	FOX ISLANDS
4	1.58	18028.	25	GULF OF ALASKA
5	1.43	36218.	19	JAPAN TRENCH NORTH
6	1.36	43348.	5	SANTA CRUZ ISLANDS
7	1.31	48704.	7	BISMARCK SEA
8	1.27	50759.	8	NEW GUINEA
9	1.25	13423.	26	MEXICO
10	1.25	24588.	28	COSTA RICA
11	1.22	22945.	23	ANDREANOF ISLANDS
12	1.16	41476.	32	CHILE NORTH
13	1.05	53116.	9	MOLUCCAN ISLANDS
14	.96	40160.	16	MARIANA ISLANDS NORTH
15	.95	30445.	29	COLUMBIA-EQUADOR
16	.92	32872.	20	KURIL ISLANDS
17	.91	39348.	17	IWO JIMA
18	.88	45171.	33	CHILF CENTRAL
19	.82	19827.	27	GUATEMALA
20	.77	34213.	30	PERU NORTH
21	.75	47208.	6	SOLOMON ISLANDS
22	.75	45853.	4	LOYALTY ISLANDS
23	.71	38859.	18	JAPAN TRENCH SOUTH
24	.70	41869.	1	KERMADEC ISLANDS
25	.66	49049.	34	CHILE SOUTH
26	.60	50482.	11	LUZON-PHILIPPINES
27	.55	44480.	15	MARIANA ISLANDS SOUTH
28	.55	38986.	31	PERU SOUTH
29	.55	42761.	13	KYUSHU ISLAND-JAPAN
30	.51	48040.	12	OKINAWA
31	.43	30127.	21	KAMCHATKA PENINSULA
32	.42	27437.	22	NEAR ISLANDS
33	.28	51399.	10	MINDINAO-PHILIPPINES
34	.24	50312.	14	PALAU ISLAND

* WAVES SHOWN IN FOLLOWING 2 FIGURES

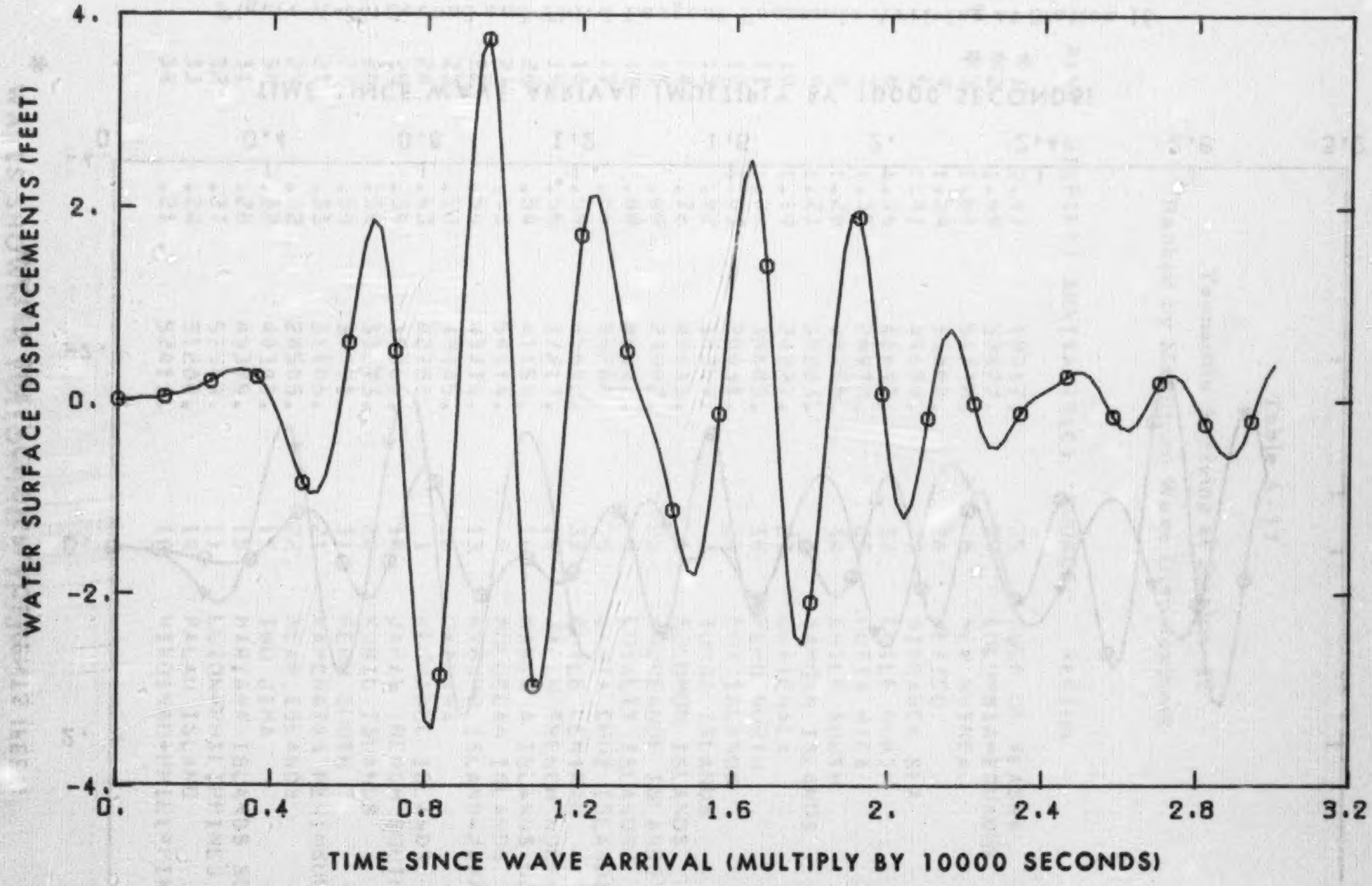

Figure A-31: Largest Tsunami Arriving at Station 16 Offshore of Santa Catalina Island, CA

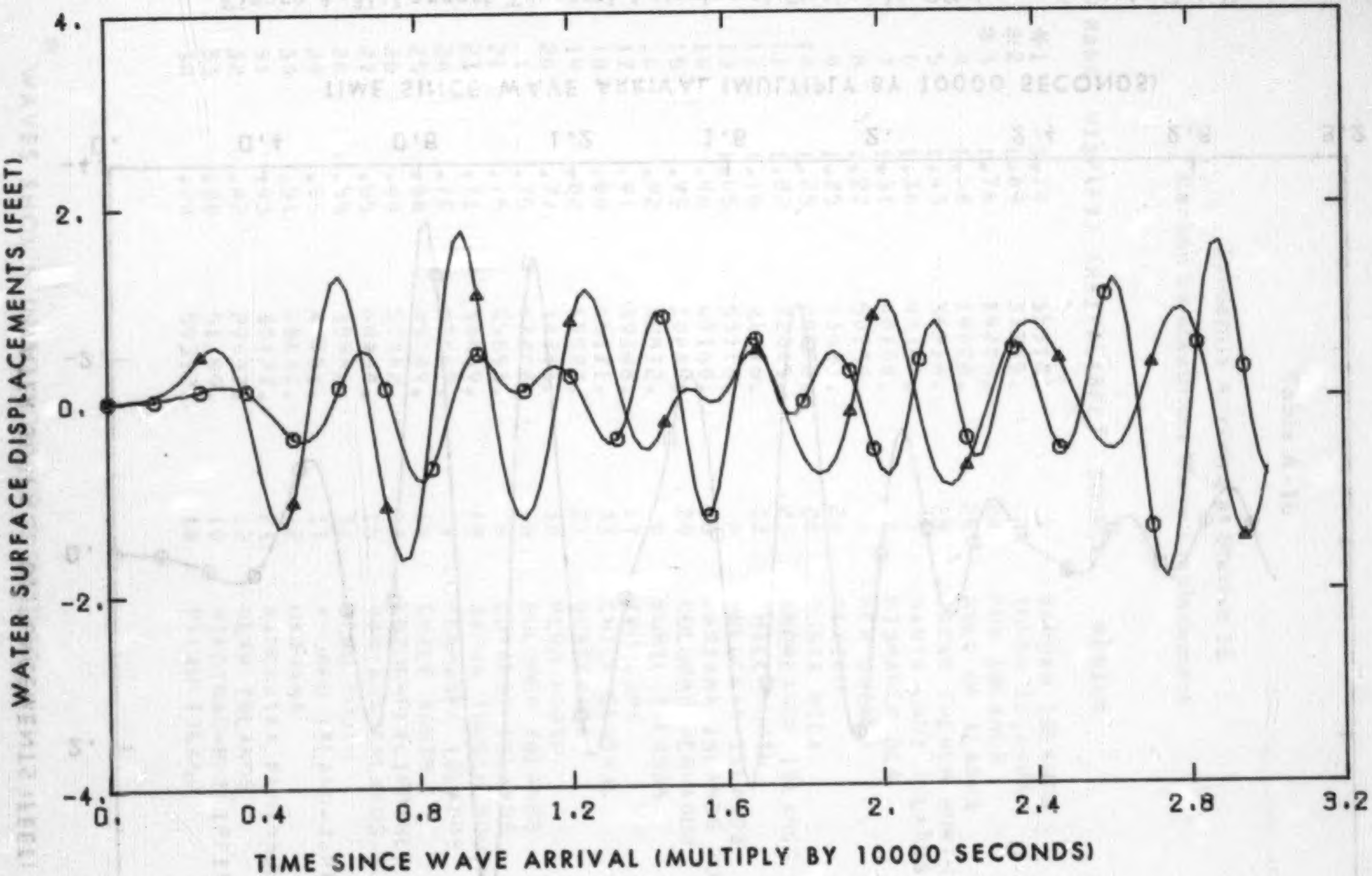

Figure A-32: Second and Third Largest Tsunamis Arriving at Station 16

Table A-17

Tsunamis Arriving at Station 17
Ranked by Maximum Wave Displacement

RANK	DISP(FT)	ARRIVAL(SEC)	SOURCE	REGION
*1	2.07	19017.	25	GULF OF ALASKA
*2	1.69	30877.	29	COLUMBIA-EQUADOR
*3	1.64	51738.	8	NEW GUINEA
4	1.54	13880.	26	MEXICO
5	1.41	49679.	7	BISMARCK SEA
6	1.36	41897.	32	CHILE NORTH
7	1.35	24974.	28	COSTA RICA
8	1.26	49458.	34	CHILE SOUTH
9	1.21	36283.	3	SAMOAN ISLANDS
10	1.19	20227.	27	GUATEMALA
11	1.06	34643.	30	PERU NORTH
12	1.03	20051.	24	FOX ISLANDS
13	.92	38249.	2	TONGA ISLANDS
14	.76	48133.	6	SOLOMON ISLANDS
15	.69	23992.	23	ANDREANOF ISLANDS
16	.68	46841.	4	LOYALTY ISLANDS
17	.66	44260.	5	SANTA CRUZ ISLANDS
18	.59	45642.	33	CHILE CENTRAL
19	.55	37217.	19	JAPAN TRENCH NORTH
20	.54	41154.	16	MARIANA ISLANDS NORTH
21	.53	54114.	9	MOLUCCAN ISLANDS
22	.50	43774.	13	KYUSHU ISLAND-JAPAN
23	.50	49045.	12	OKINAWA
24	.43	42788.	1	KERMADEC ISLANDS
25	.39	39860.	18	JAPAN TRENCH SOUTH
26	.38	33873.	20	KURIL ISLANDS
27	.34	39401.	31	PERU SOUTH
28	.33	31106.	21	KAMCHATKA PENINSULA
29	.32	28505.	22	NEAR ISLANDS
30	.32	40348.	17	IWO JIMA
31	.28	45379.	15	MARIANA ISLANDS SOUTH
32	.27	51504.	11	LUZON-PHILIPPINES
33	.24	51280.	14	PALAU ISLAND
34	.21	52411.	10	MINDINAO-PHILIPPINES

* WAVES SHOWN IN FOLLOWING 2 FIGURES

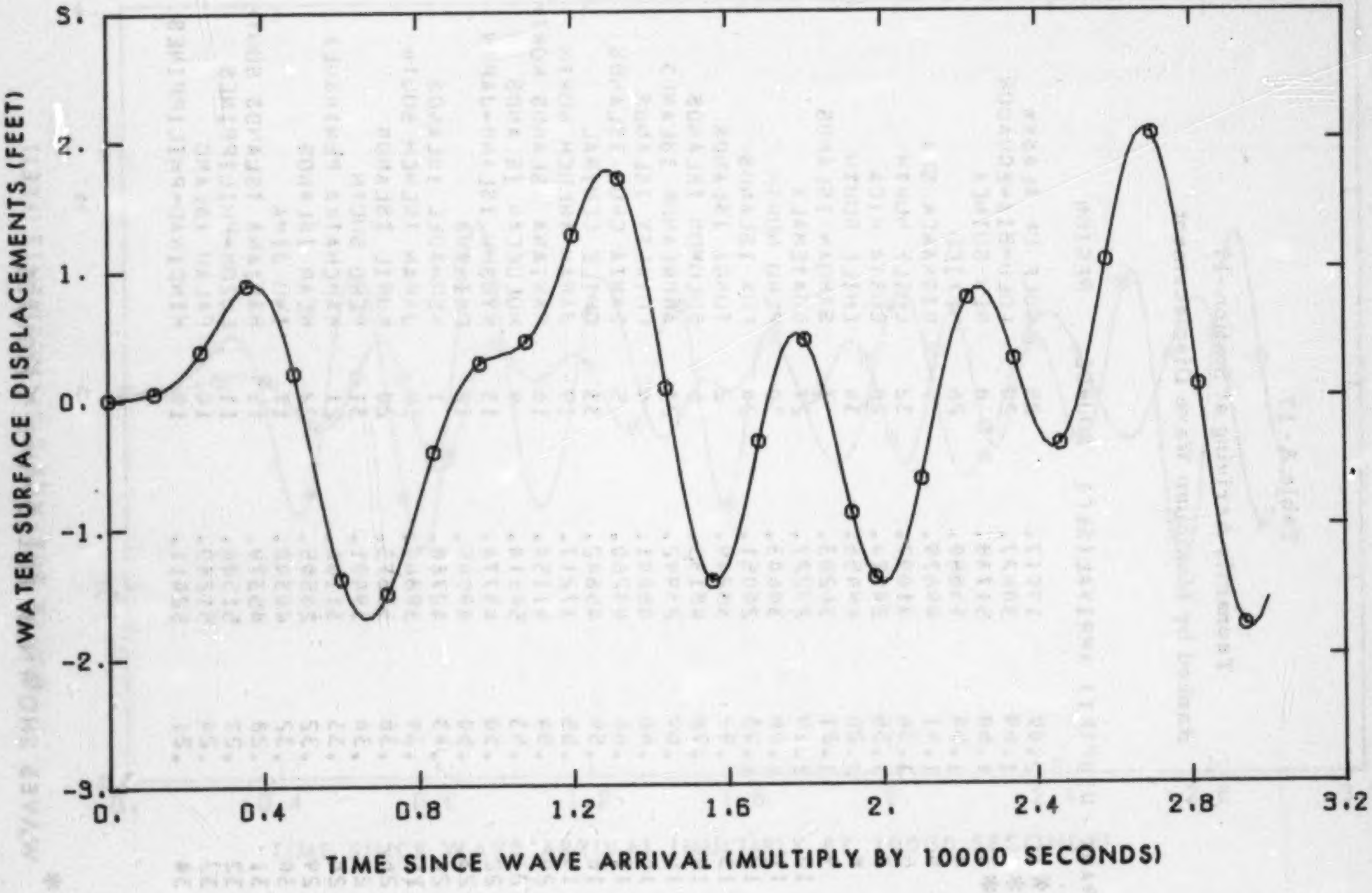

Figure A-33: Largest Tsunami Arriving at Station 17 Offshore of San Onofre, CA

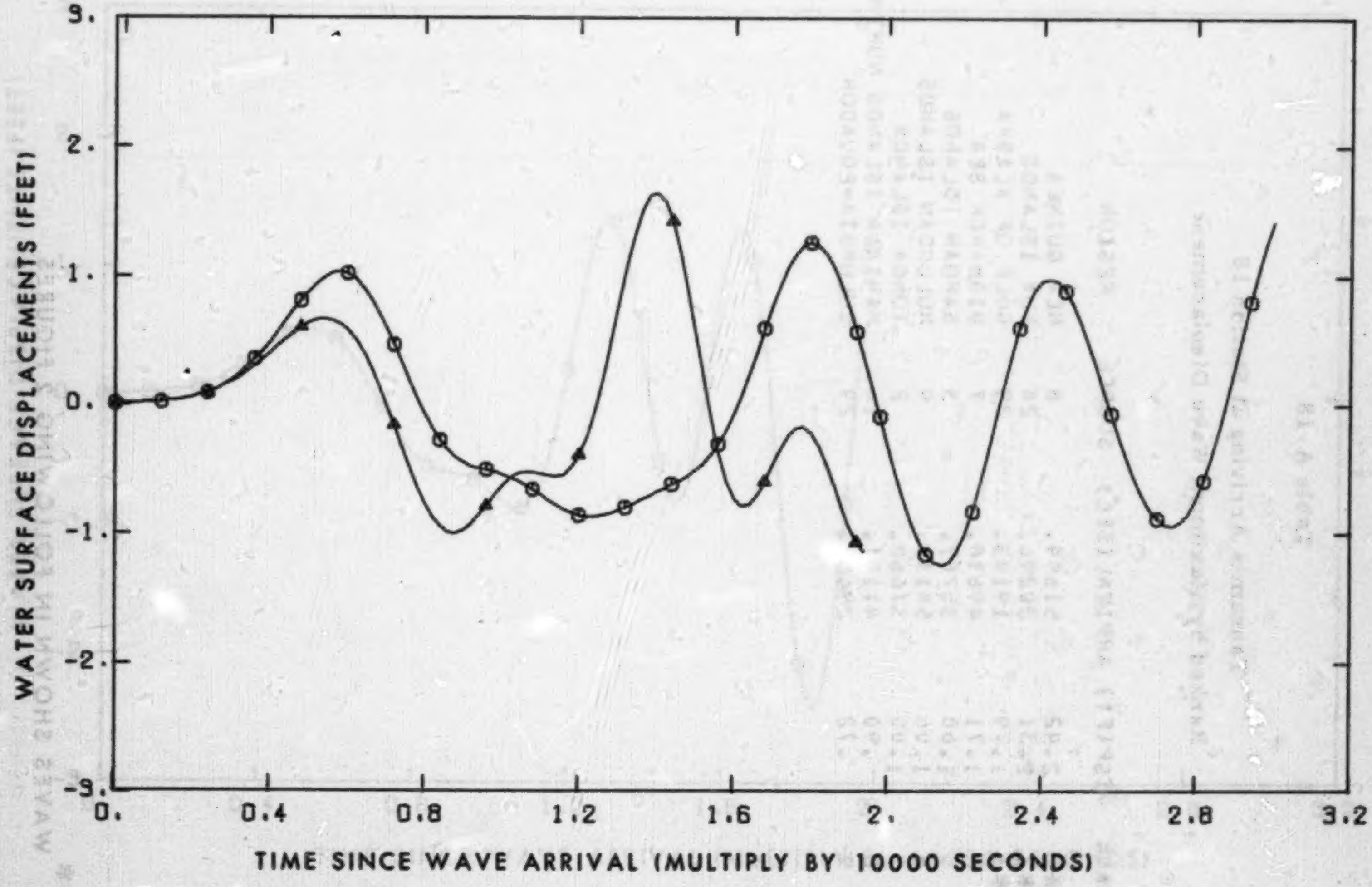

Figure A-34: Second and Third Largest Tsunamis Arriving at Station 17

Table A-18

Tsunamis Arriving at Station 18

Ranked by Maximum Wave Displacement

RANK	DISP(FT)	ARRIVAL(SEC)	SOURCE	REGION
*1	2.42	51699.	8	NEW GUINEA
*2	2.31	20296.	24	FOX ISLANDS
*3	1.79	19143.	25	GULF OF ALASKA
4	1.71	49638.	7	BISMARCK SEA
5	1.60	35707.	3	SAMOAN ISLANDS
6	1.06	54134.	9	MOLUCCAN ISLANDS
7	1.00	37668.	2	TONGA ISLANDS
8	.90	41191.	16	MARIANA ISLANDS NORTH
9	.72	29652.	29	COLUMBIA-EQUADOR

* WAVES SHOWN IN FOLLOWING 2 FIGURES

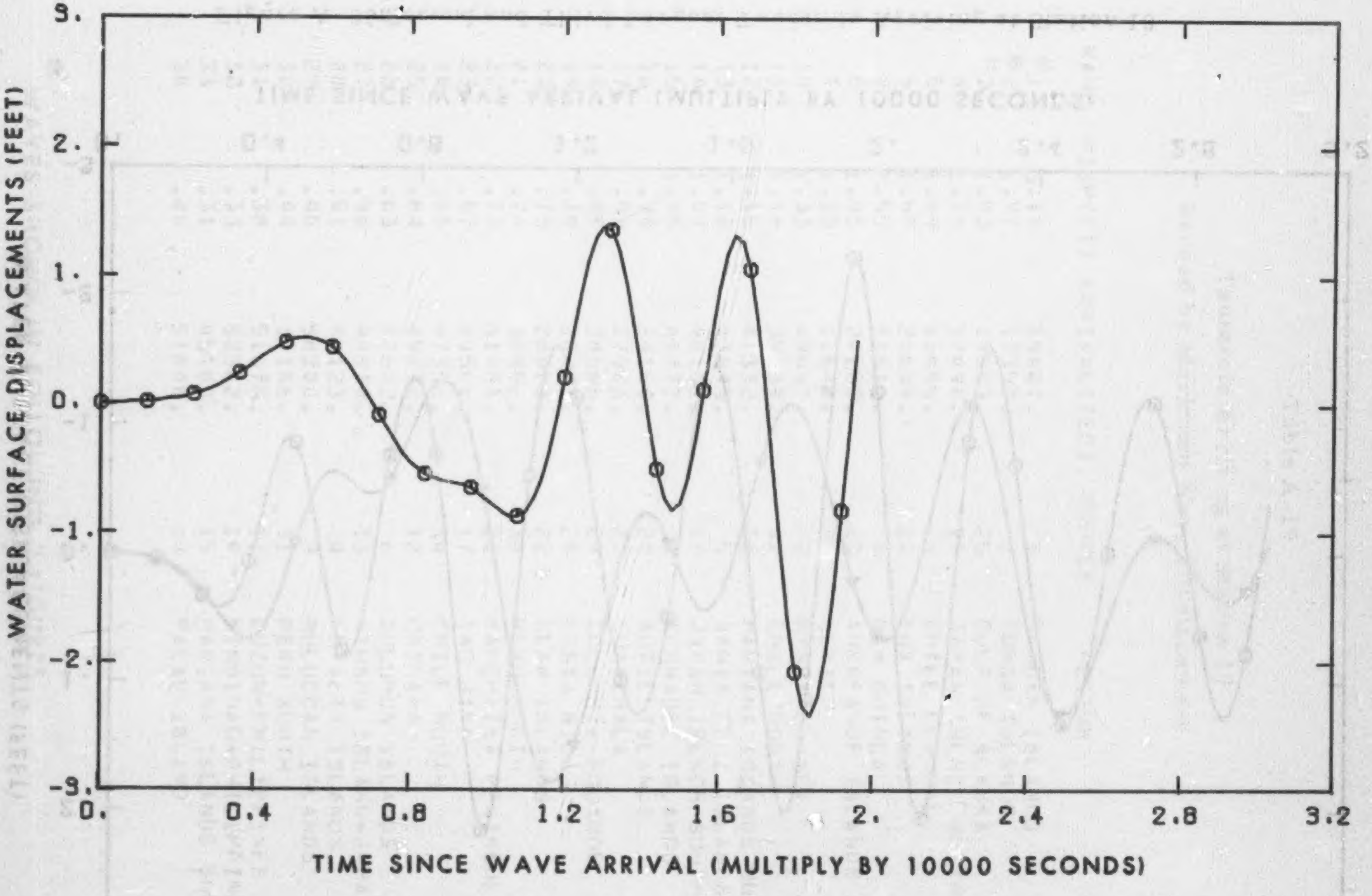

Figure A-35:Largest Tsunami Arriving at Station 18 Offshore of Punta San Miguel, B. C. , Mexico

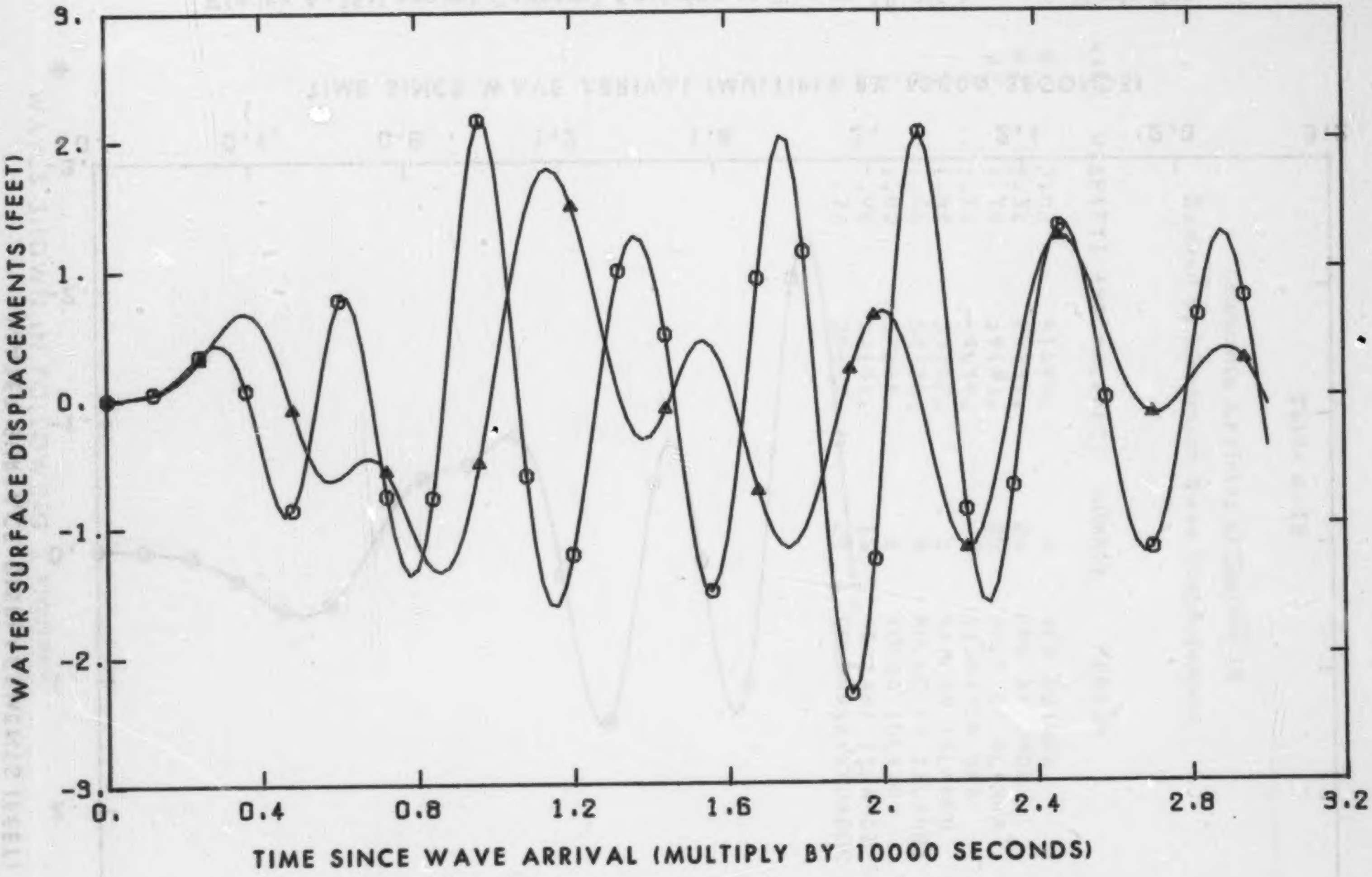

Figure A-36:Second and Third Largest Tsunamis Arriving at Station 18

Table A-19

Tsunamis Arriving at Station 19
Ranked by Maximum Wave Displacement

RANK	DISP(FT)	ARRIVAL(SEC)	SOURCE	REGION
*1	3.18	35447.	3	SAMOAN ISLANDS
*2	1.97	37351.	2	TONGA ISLANDS
*3	1.83	19513.	25	GULF OF ALASKA
4	1.76	37498.	19	JAPAN TRENCH NORTH
5	1.69	43455.	33	CHILE CENTRAL
6	1.69	20649.	24	FOX ISLANDS
7	1.55	51811.	8	NEW GUINEA
8	1.45	24283.	23	ANDREANOF ISLANDS
9	1.35	11648.	26	MEXICO
10	1.33	49657.	7	BISMARCK SEA
11	1.16	39809.	32	CHILE NORTH
12	1.15	41332.	16	MARIANA ISLANDS NORTH
13	1.12	43645.	5	SANTA CRUZ ISLANDS
14	1.07	40165.	18	JAPAN TRENCH SOUTH
15	1.05	41777.	1	KERMADEC ISLANDS
16	.90	34160.	20	KURIL ISLANDS
17	.90	17966.	27	GUATEMALA
18	.88	28666.	29	COLUMBIA-EQUADOR
19	.79	22771.	28	COSTA RICA
20	.75	28828.	22	NEAR ISLANDS
21	.74	32452.	30	PERU NORTH
22	.73	31481.	21	KAMCHATKA PENINSULA
23	.67	40581.	17	IWO JIMA
24	.65	47356.	34	CHILE SOUTH
25	.64	49232.	12	OKINAWA
26	.63	47642.	6	SOLOMON ISLANDS
27	.58	44030.	13	KYUSHU ISLAND-JAPAN
28	.51	46123.	4	LOYALTY ISLANDS
29	.48	54200.	9	MOLUCCAN ISLANDS
30	.44	37186.	31	PERU SOUTH
31	.38	51674.	11	LUZON-PHILIPPINES
32	.33	52562.	10	MINDINAO-PHILIPPINES
33	.31	45180.	15	MARIANA ISLANDS SOUTH
34	.20	51400.	14	PALAU ISLAND

* WAVES SHOWN IN FOLLOWING 2 FIGURES

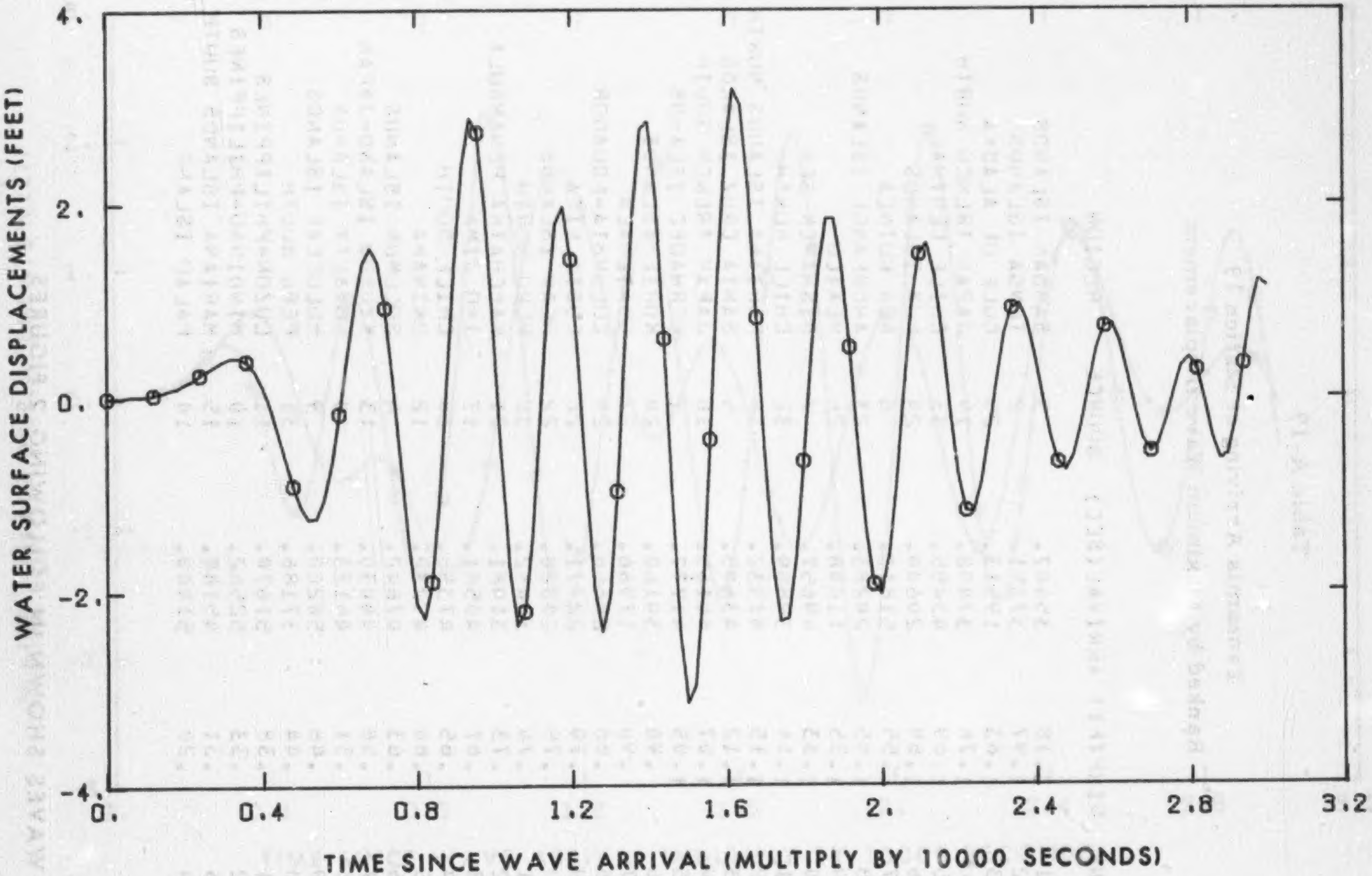

Figure A-37:Largest Tsunami Arriving at Station 19 Offshore of Punta Colnett, B. C., Mexico

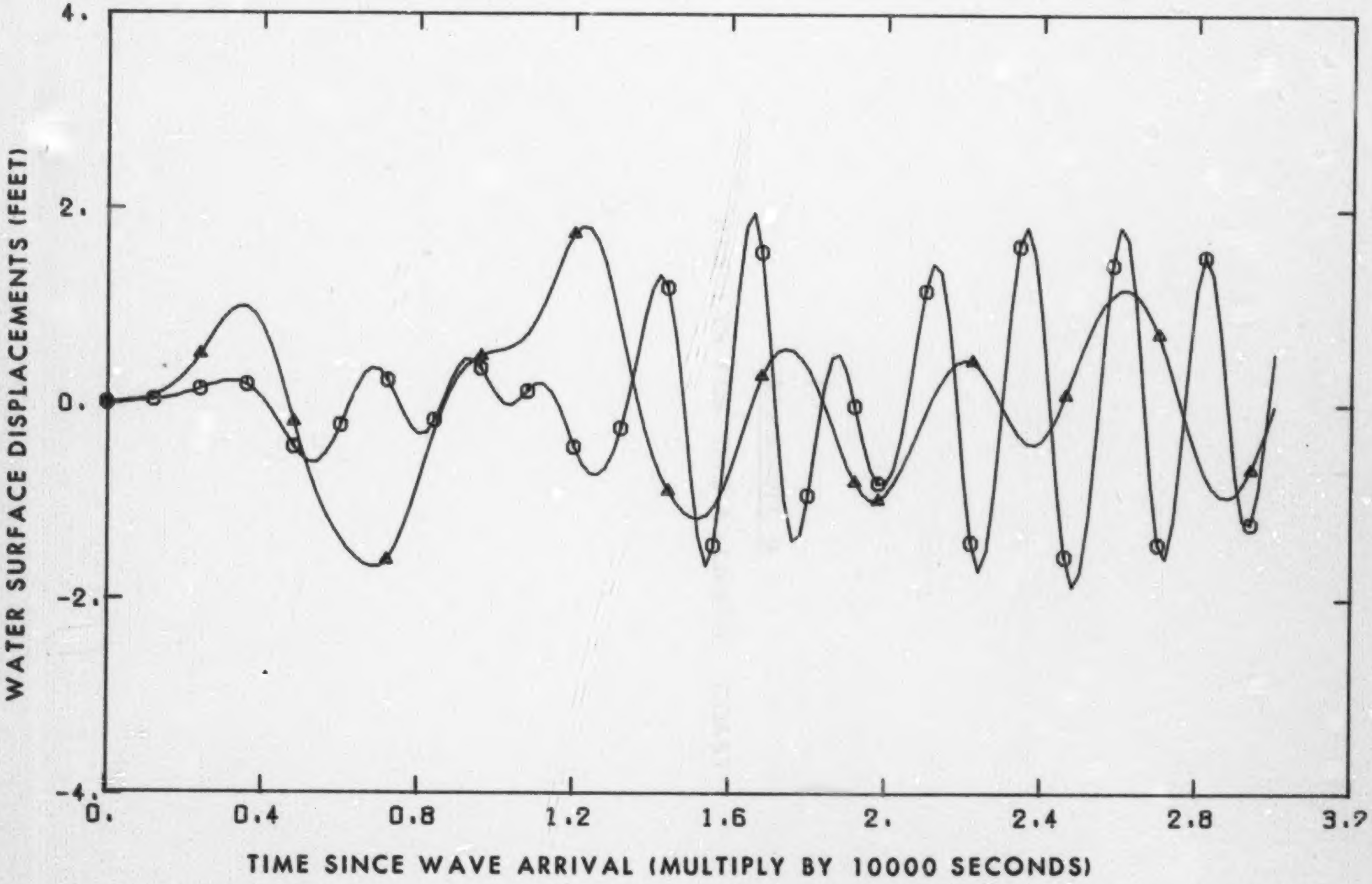

Figure A-38:Second and Third Largest Tsunamis Arriving at Station 19

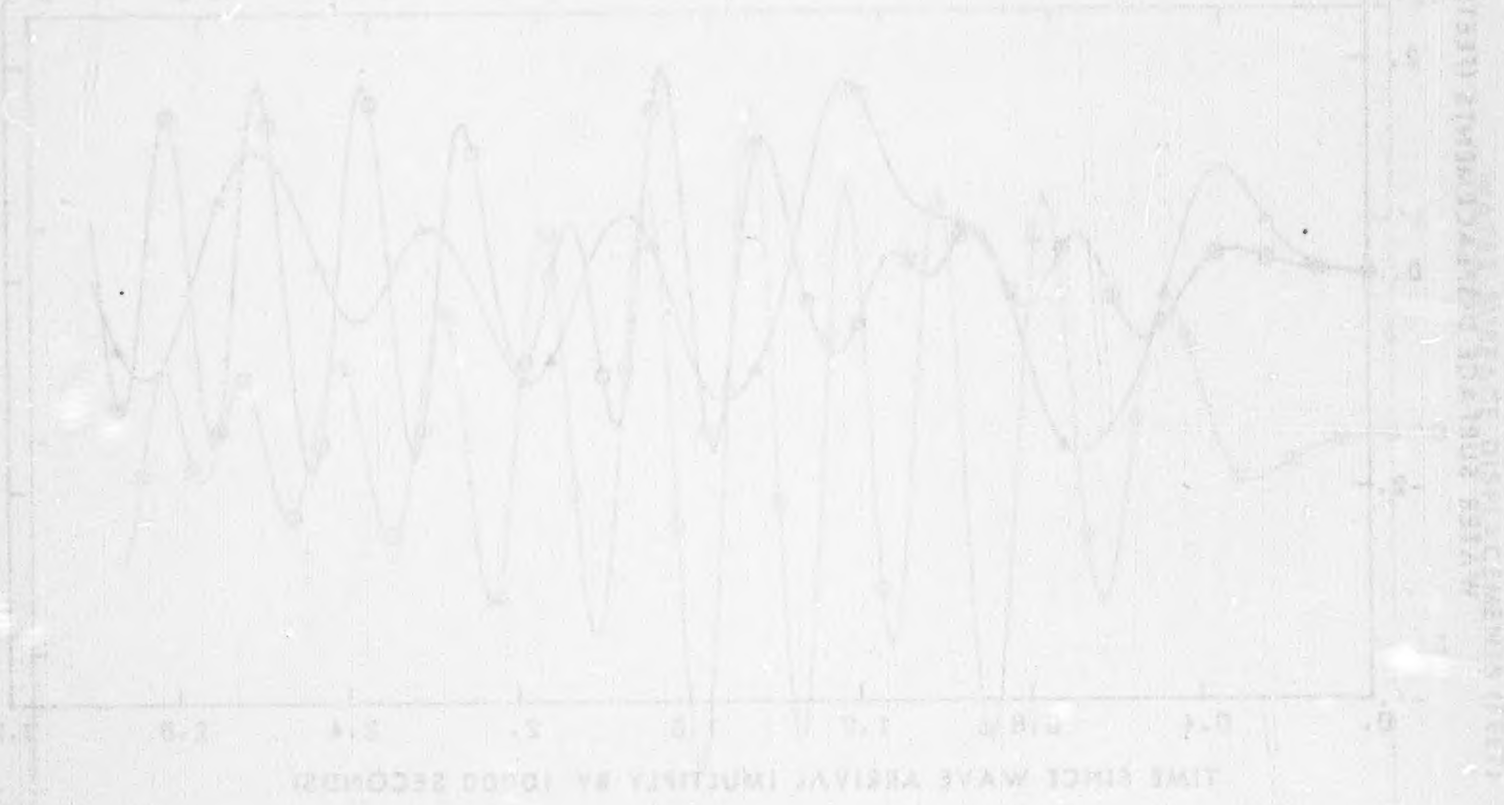

Figure A-18. Second and Third Largest Tsunamis Arriving at Station 15

APPENDIX B

RESULTS FOR THE ATLANTIC COAST

Table B-1

Tsunamis Arriving at Station 1

Ranked by Maximum Wave Displacement

RANK	DISP(FT)	ARRIVAL(SEC)	SOURCE	REGION
*1	1.20	13416.	2	HAITI
2	.45	15693.	3	LEEWARD ISLANDS
3	.13	27388.	4	PORTUGAL
4	.06	33113.	1	CUBA
5	.03	61156.	5	SOUTH SANDWICH ISLANDS

* Wave Shown in Following Figure

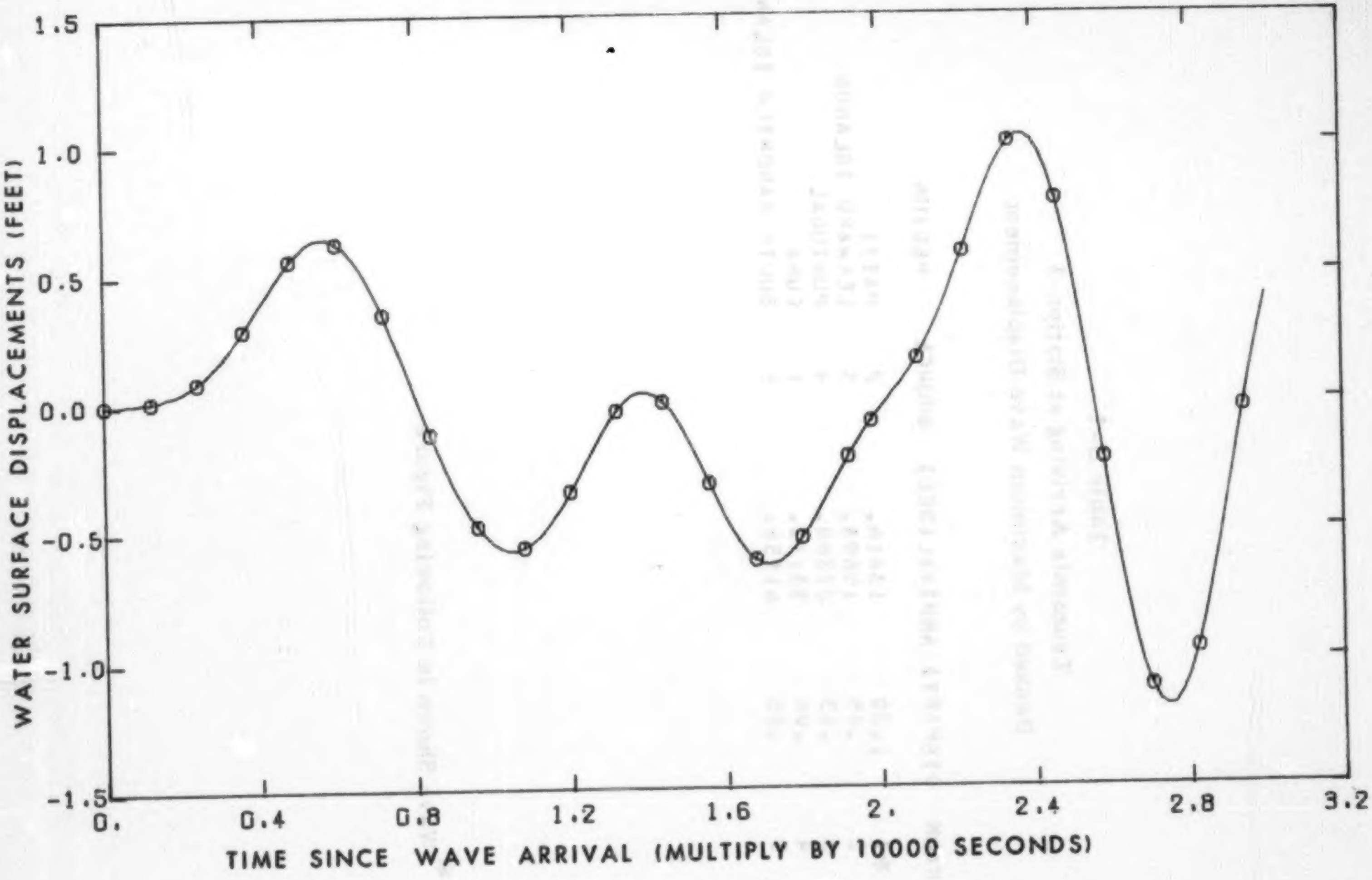

Figure B-1: Largest Tsunami arriving at Station 1 Offshore of Mouth of Bay of Fundy

Table B-2
Tsunamis Arriving at Station 2
Ranked by Maximum Wave Displacement

RANK	DISP(FT)	ARRIVAL(SEC)	SOURCE	REGION
* 1	1.24	14014.	2	HAITI
2	.66	16546.	3	LEEWARD ISLANDS
3	.09	28445.	4	PORTUGAL
4	.06	31428.	1	CUBA
5	.04	62076.	5	SOUTH SANDWICH ISLANDS

* Wave Shown in Following Figure

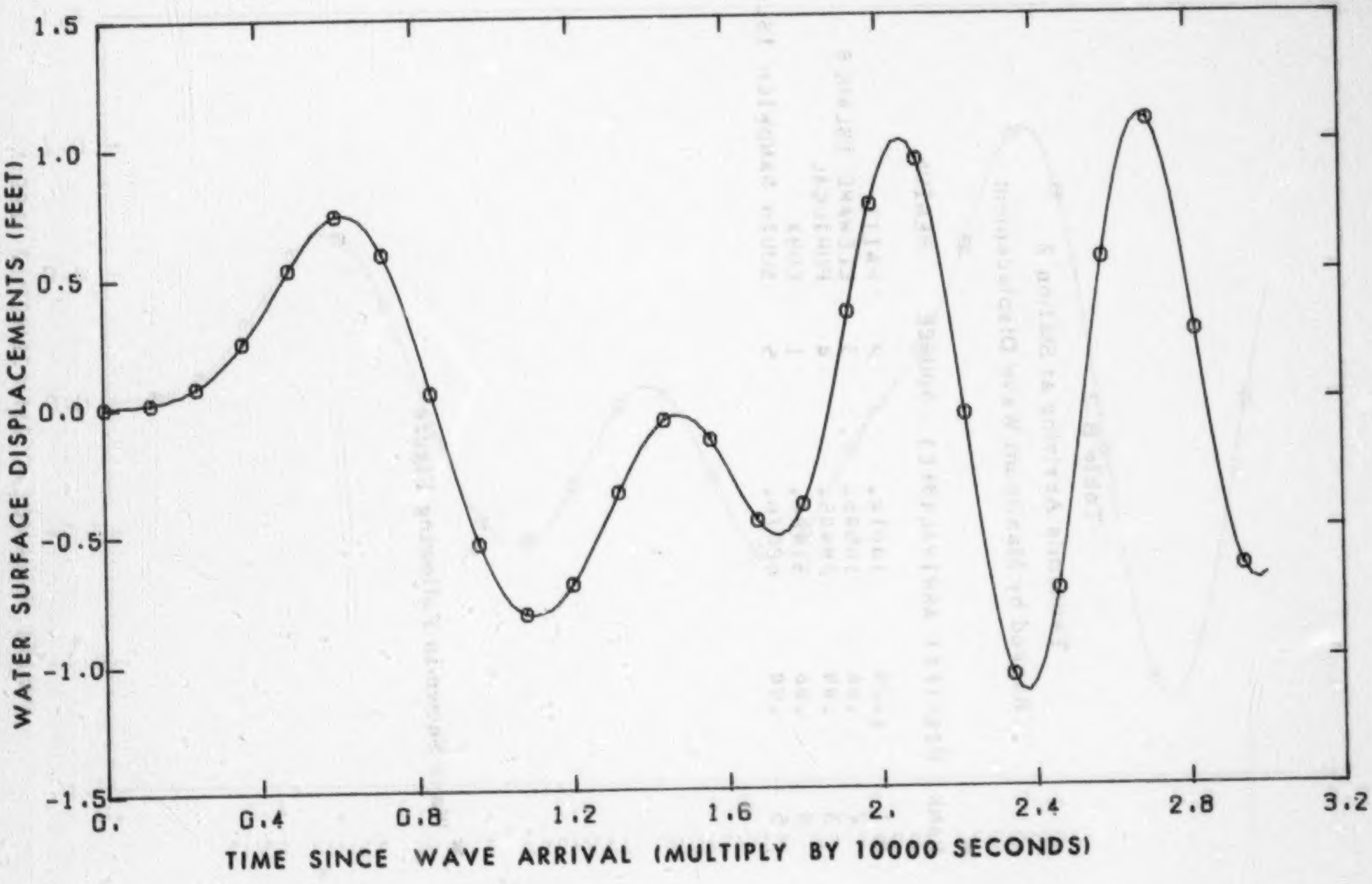

Figure B-2: Largest Tsunami arriving at Station 2 Offshore of Mt. Desert Rock, Maine

Table B-3
Tsunamis Arriving at Station 3
Ranked by Maximum Wave Displacement

RANK	DISP(FT)	ARRIVAL(SEC)	SOURCE	REGION
* 1	1.59	14577.	2	HAITI
2	.60	17344.	3	LEEWARD ISLANDS
3	.20	29607.	4	PORTUGAL
4	.12	27832.	1	CUBA
5	.06	62999.	5	SOUTH SANDWICH ISLANDS

* Wave Shown in Following Figure

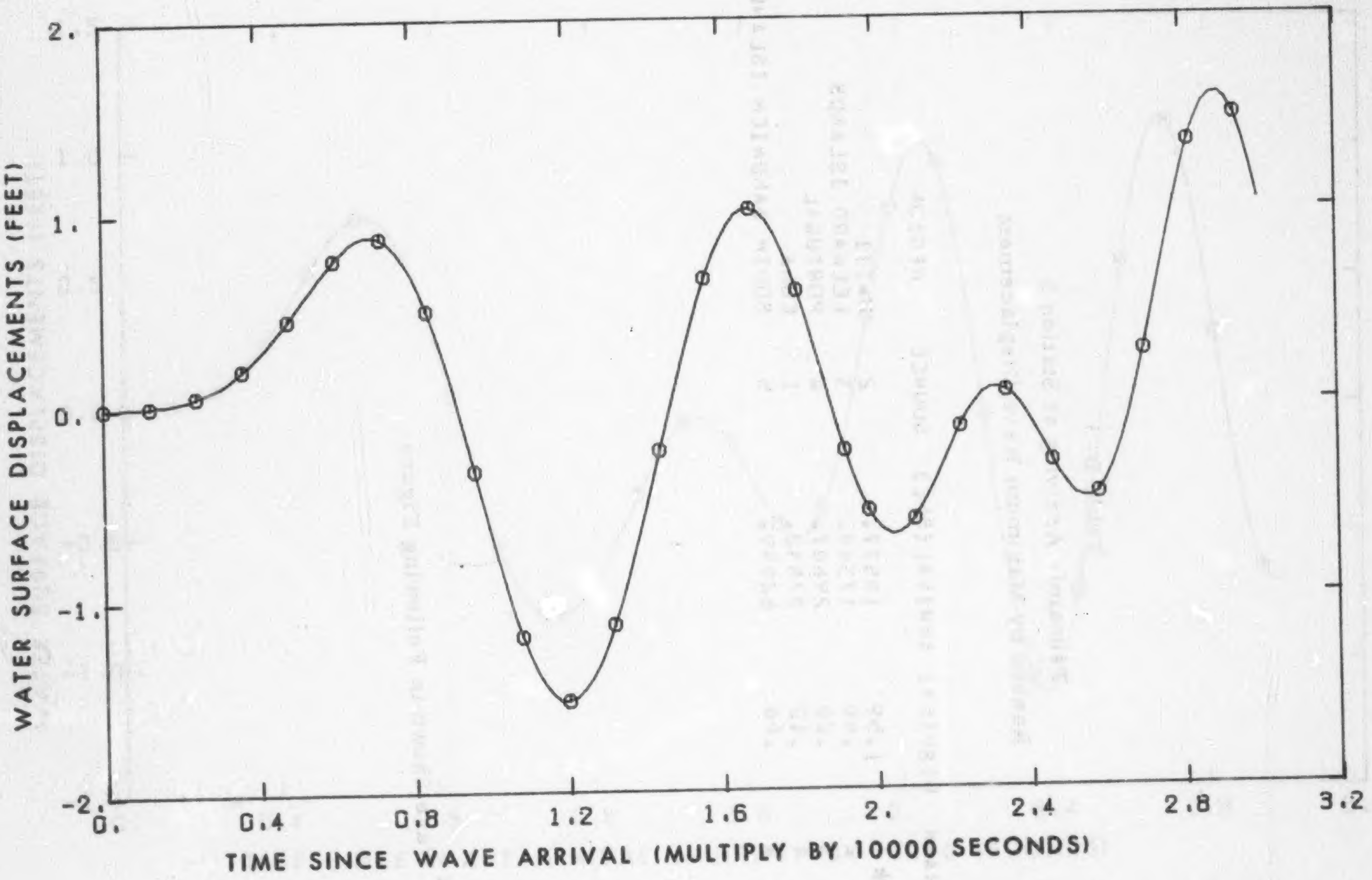

Figure B-3: Largest Tsunami arriving at Station 3 Offshore of Owls Head, Maine

Table B-4

Tsunamis Arriving at Station 4

Ranked by Maximum Wave Displacement

RANK	DISP(FT)	ARRIVAL(SEC)	SOURCE	REGION
*1	1.12	14358.	2	HAITI
2	.53	17251.	3	LEEWARD ISLANDS
3	.14	29847.	4	PORTUGAL
4	.07	29967.	1	CUBA
5	.04	63325.	5	SOUTH SANDWICH ISLANDS

* Wave Shown in Following Figure

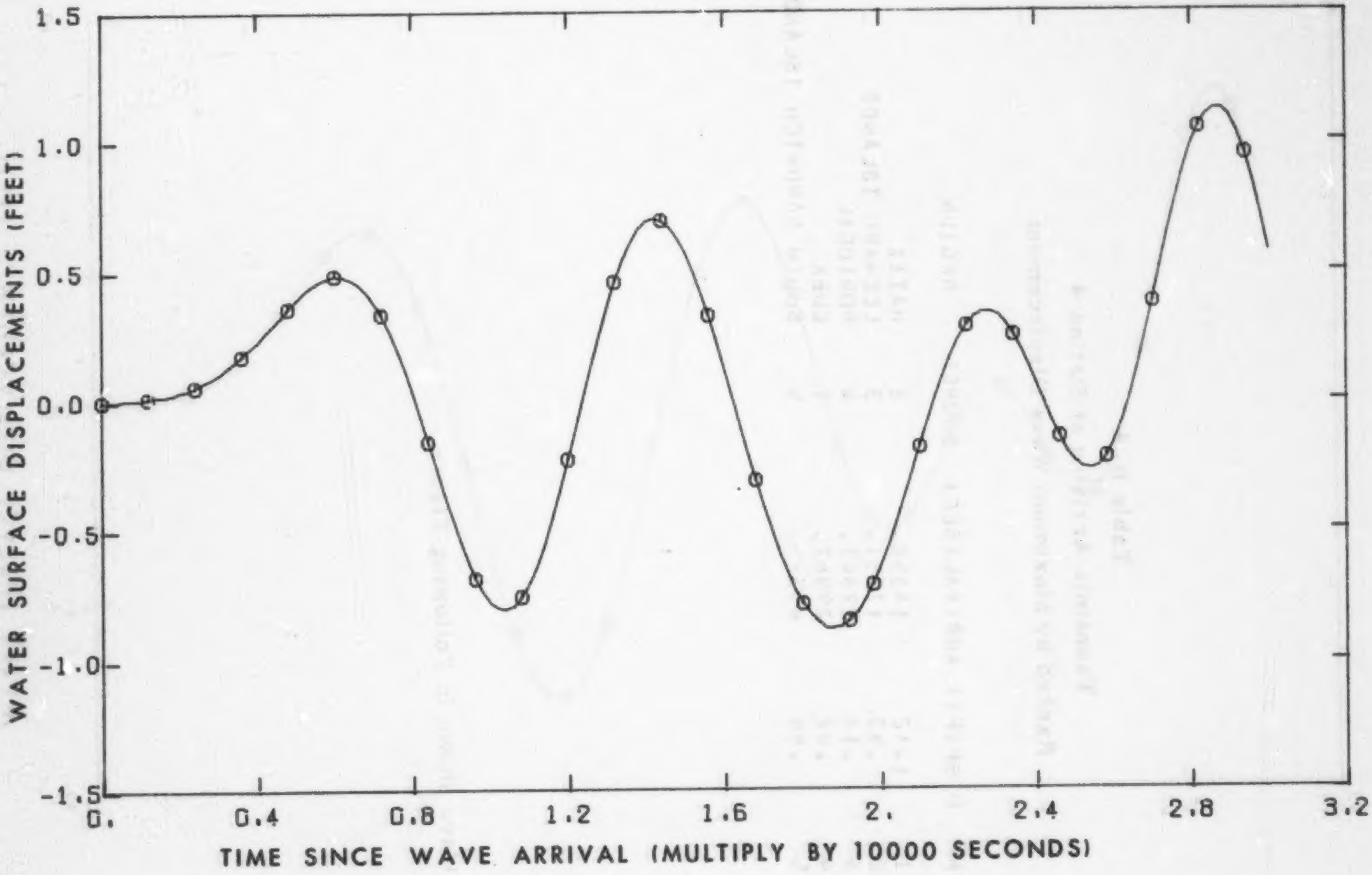

Figure B-4: Largest Tsunami arriving at Station 4 Offshore of Walkers Point, Maine

Table B-5
Tsunamis Arriving at Station 5
Ranked by Maximum Wave Displacement

RANK	DISP(FT)	ARRIVAL(SEC)	SOURCE	REGION
*1	1.36	11071.	2	HAITI
2	.63	13569.	3	LEEWARD ISLANDS
3	.25	26415.	4	PORTUGAL
4	.10	21053.	1	CUBA
5	.09	59217.	5	SOUTH SANDWICH ISLANDS

* Wave Shown in Following Figure

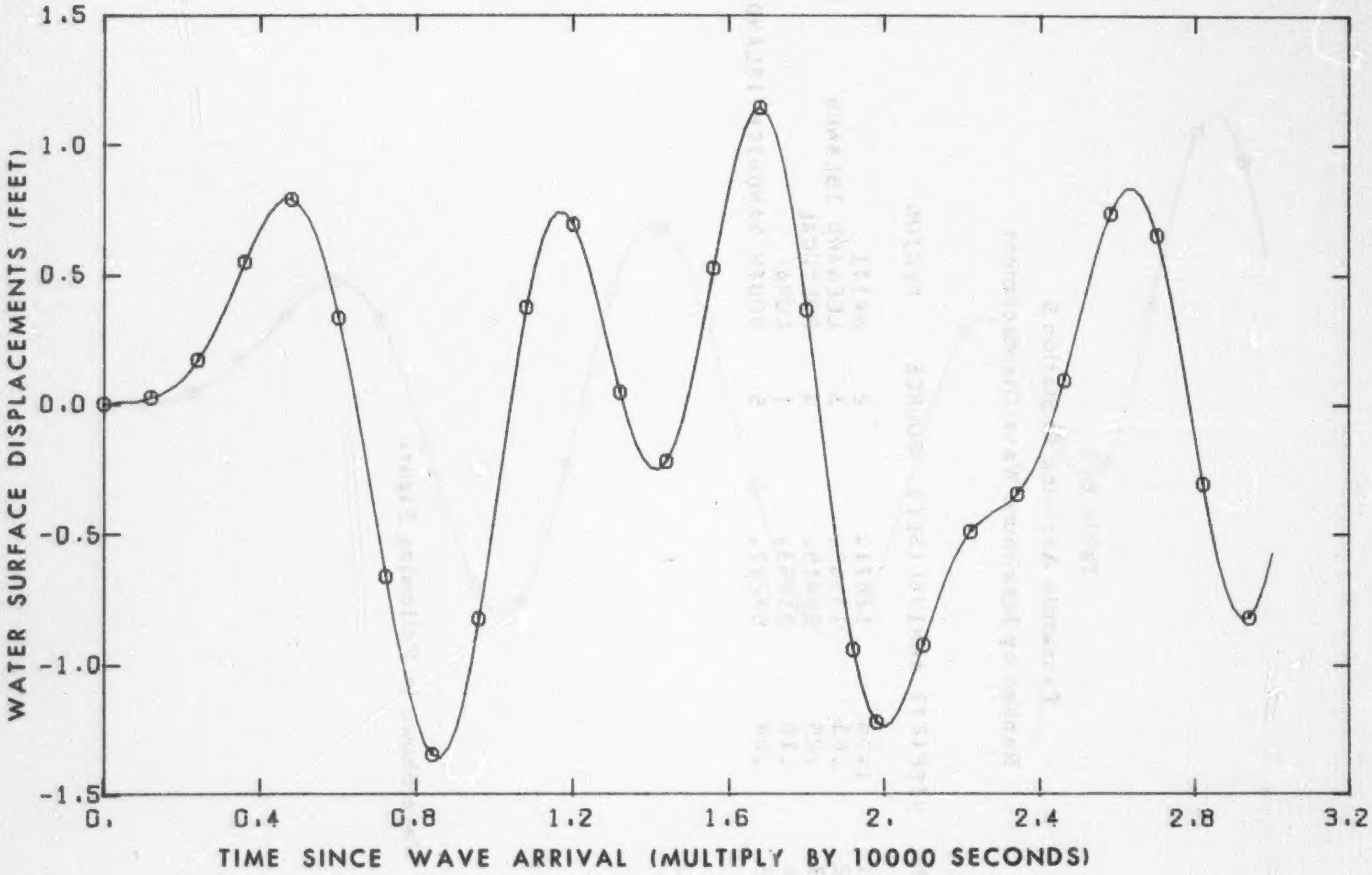

Figure B-5: Largest Tsunami arriving at Station 5 Offshore of Cape Code, Mass.

Table B-6

Tsunamis Arriving at Station 6

Ranked by Maximum Wave Displacement

RANK	DISP(FT)	ARRIVAL(SEC)	SOURCE	REGION
*1	3.08	10020.	2	HAITI
2	1.27	12572.	3	LEEWARD ISLANDS
3	.24	26013.	4	PORTUGAL
4	.15	16006.	1	CUBA
5	.07	58217.	5	SOUTH SANDWICH ISLANDS

* Wave Shown in Following Figure

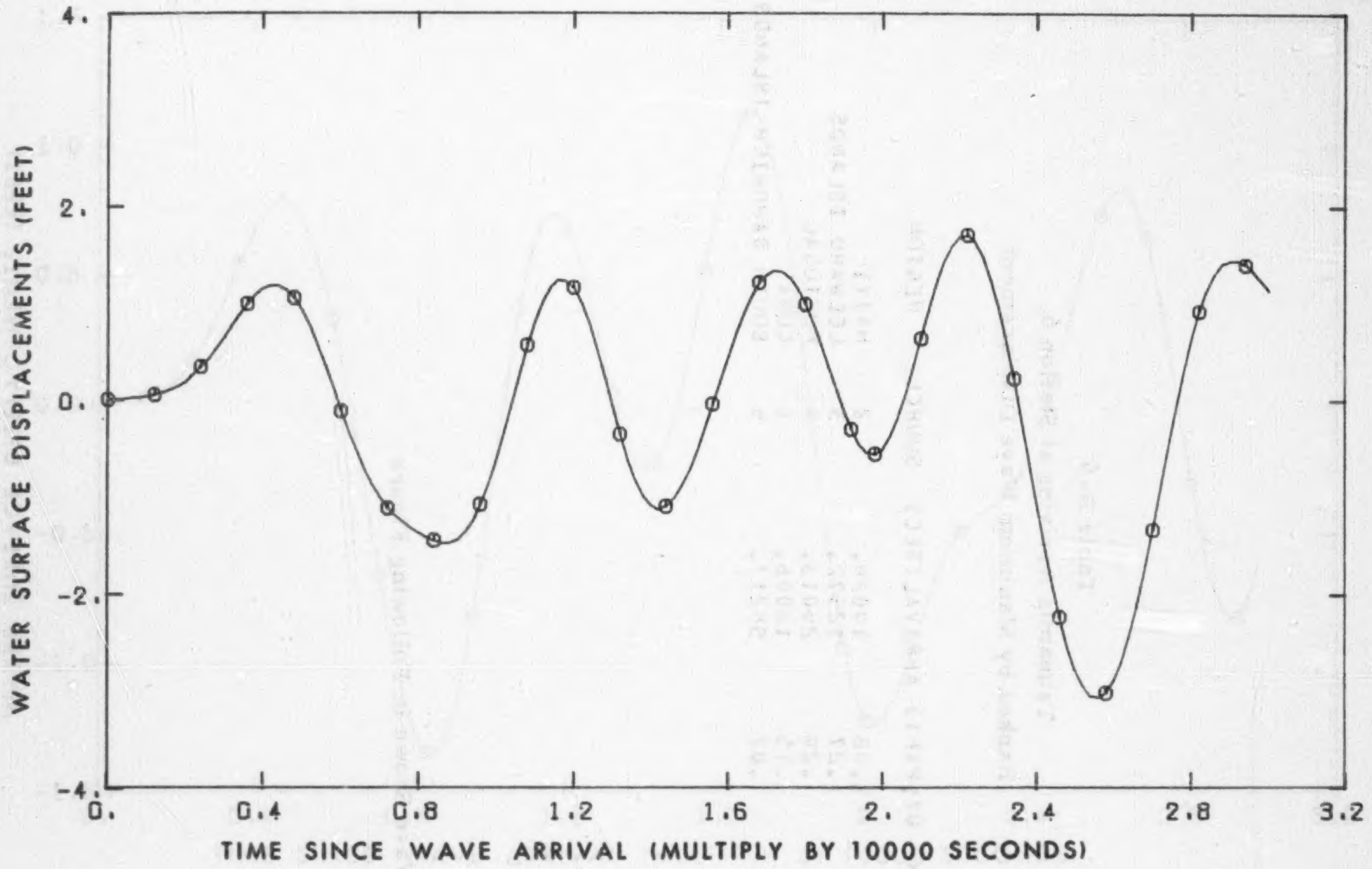

Figure B-6: Largest Tsunami arriving at Station 6 Offshore of Nantucket Island, Mass.

Table B-7

Tsunamis Arriving at Station 7

Ranked by Maximum Wave Displacement

RANK	DISP(FT)	ARRIVAL(SEC)	SOURCE	REGION
*1	1.75	10036.	2	HAITI
2	1.42	12851.	3	LEEWARD ISLANDS
3	.34	26695.	4	PORTUGAL
4	.11	16005.	1	CUBA
5	.04	58609.	5	SOUTH SANDWICH ISLANDS

* Wave Shown in Following Figure

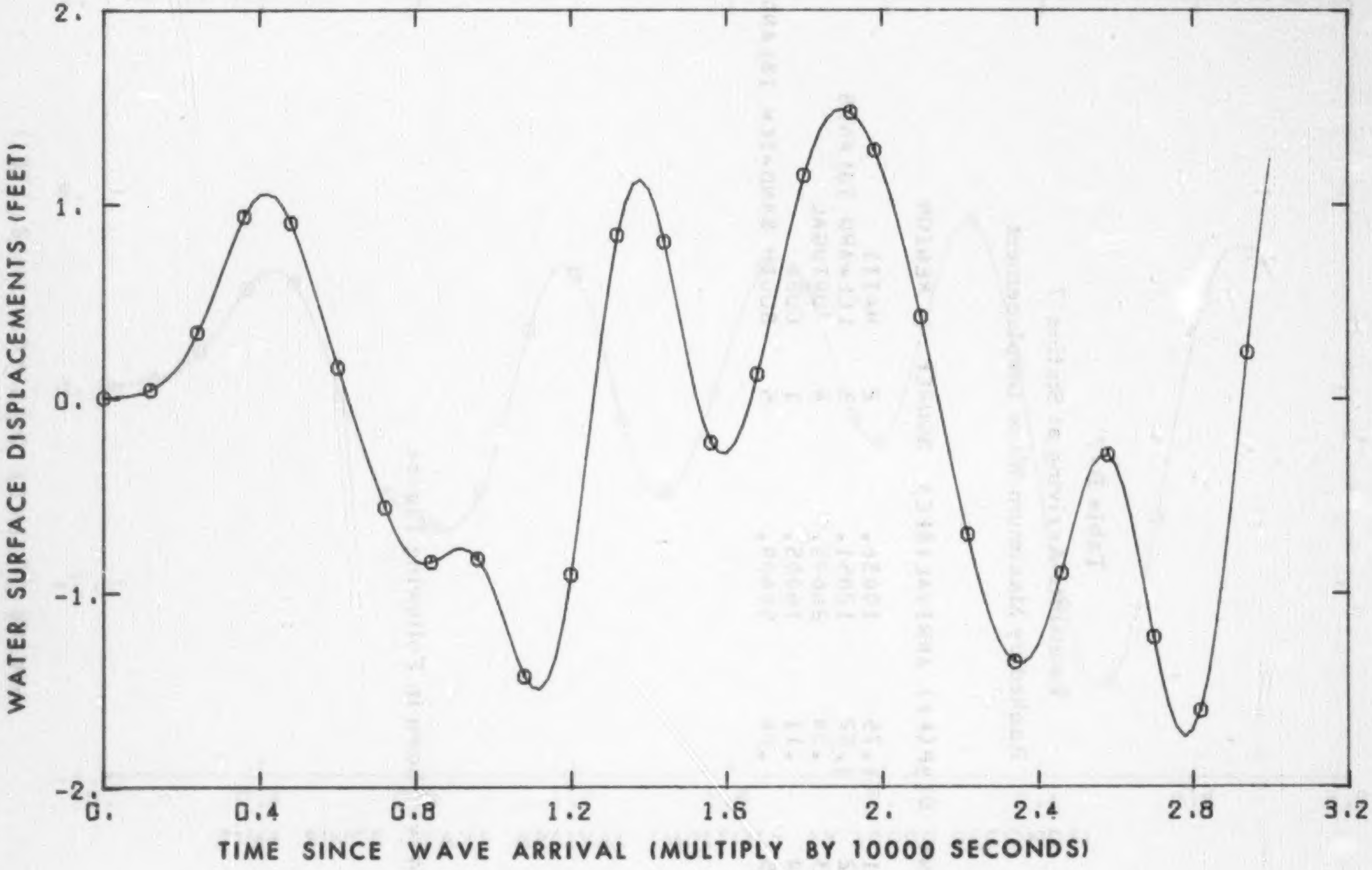

Figure B-7: Largest Tsunami arriving at Station 7 Offshore of Newport, R.I.

Table B-8

Tsunamis Arriving at Station 8

Ranked by Maximum Wave Displacement

RANK	DISP(FT)	ARRIVAL(SEC)	SOURCE	REGION
*1	2.01	10411.	2	HAITI
2	.75	13404.	3	LEEWARD ISLANDS
3	.18	27486.	4	PORTUGAL
4	.15	16428.	1	CUBA
5	.05	59219.	5	SOUTH SANDWICH ISLANDS

* Wave Shown in Following Figure

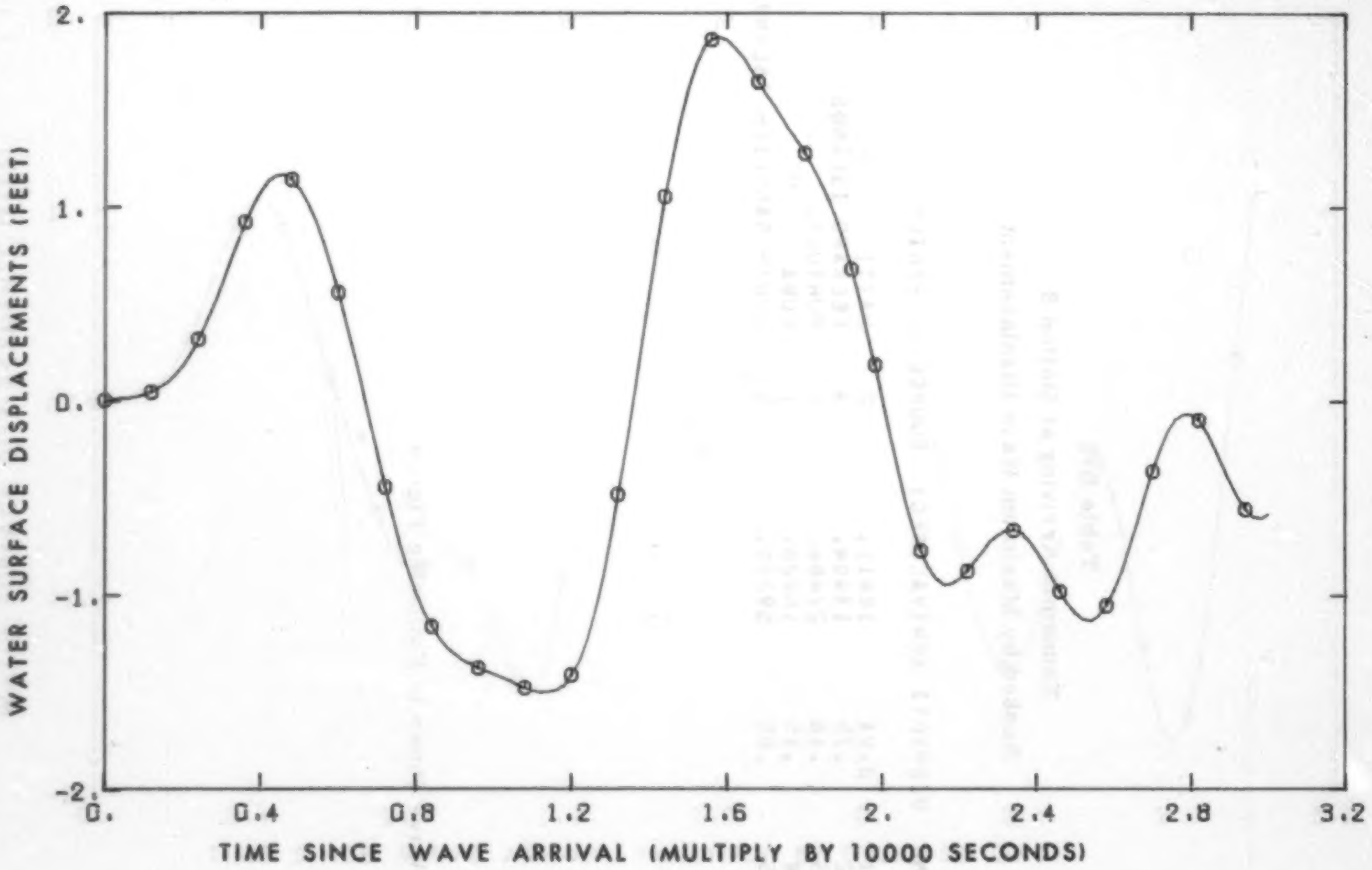

Figure B-8: Largest Tsunami arriving at Station 8 Offshore of Montauk Point, N.Y.

Table B- 9

Tsunamis Arriving at Station 9

Ranked by Maximum Wave Displacement

```
RANK  DISP(FT)  ARRIVAL(SEC)  SOURCE     REGION

*1     2.44        9855.         2      HAITI
 2     1.24       12789.         3      LEEWARD ISLANDS
 3      .54       27001.         4      PORTUGAL
 4      .19       15122.         1      CUBA
 5      .09       58521.         5      SOUTH SANDWICH ISLANDS
```

* Wave Shown in Following Figure

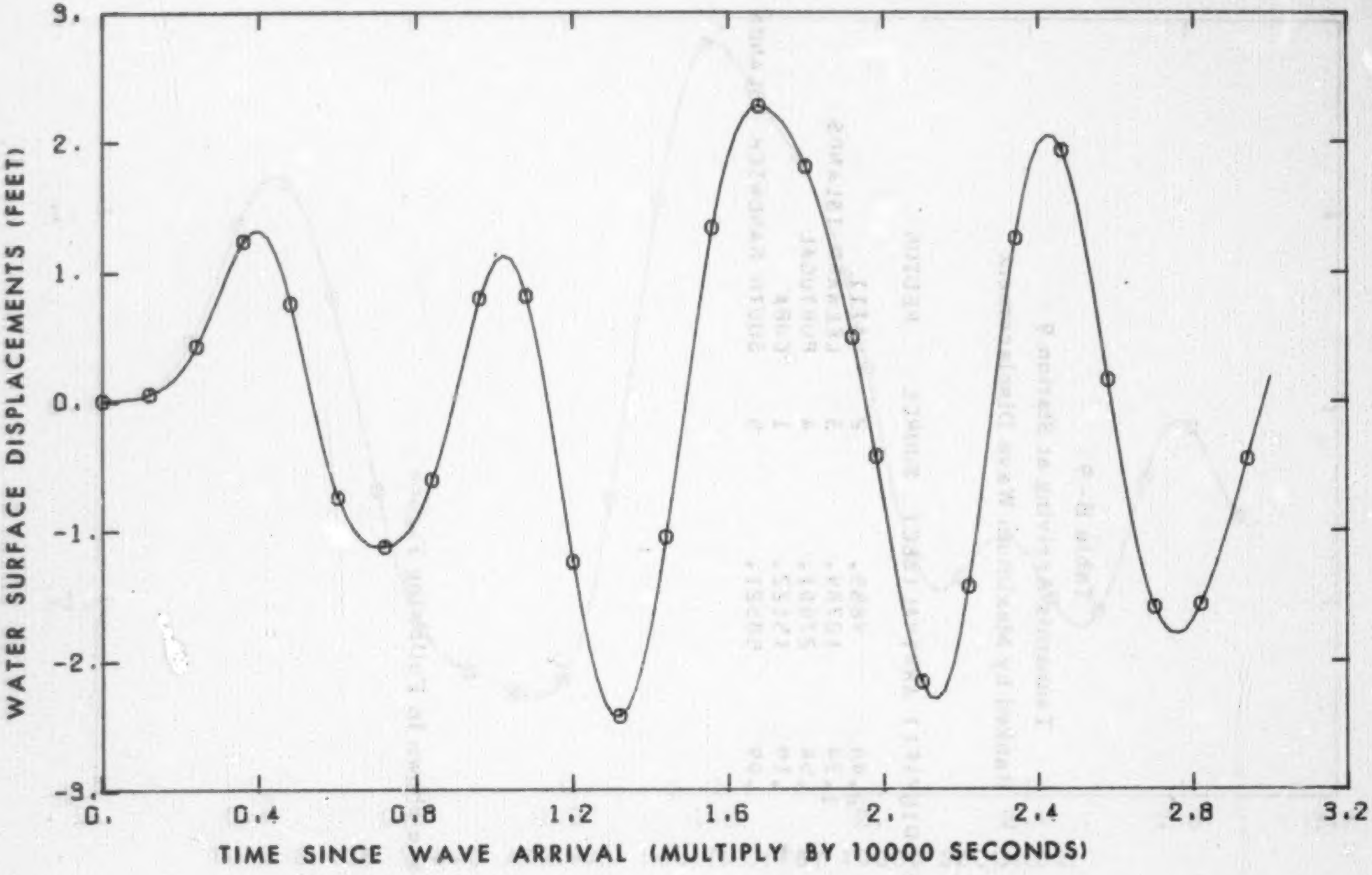

Figure B-9: Largest Tsunami arriving at Station 9 Offshore of New York, N.Y.

Table B-10

Tsunamis Arriving at Station 10

Ranked by Maximum Wave Displacement

RANK	DISP(FT)	ARRIVAL(SEC)	SOURCE	REGION
*1	2.75	10920.	2	HAITI
2	.81	14033.	3	LEEWARD ISLANDS
3	.26	28416.	4	PORTUGAL
4	.15	16577.	1	CUBA
5	.07	59803.	5	SOUTH SANDWICH ISLANDS

* Wave Shown in Following Figure

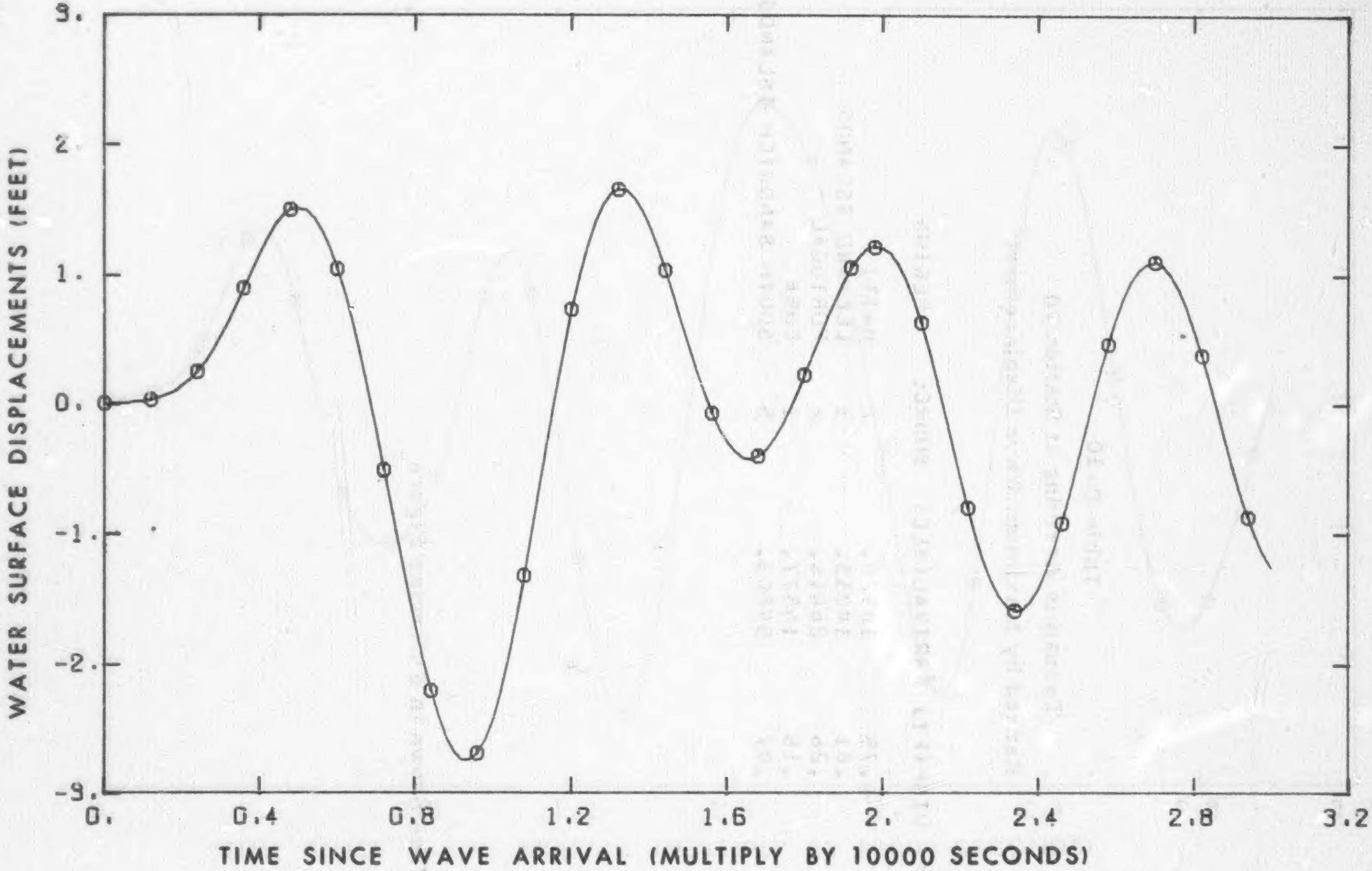

Figure B-10: Largest Tsunami arriving at Station 10 Offshore of Point Pleasant, N.J.

Table B-11

Tsunamis Arriving at Station 11

Ranked by Maximum Wave Displacement

RANK	DISP(FT)	ARRIVAL(SEC)	SOURCE	REGION
* 1	1.47	9511.	2	HAITI
2	.77	12639.	3	LEEWARD ISLANDS
3	.17	27001.	4	PORTUGAL
4	.14	14411.	1	CUBA
5	.06	58243.	5	SOUTH SANDWICH ISLANDS

* Wave Shown in Following Figure

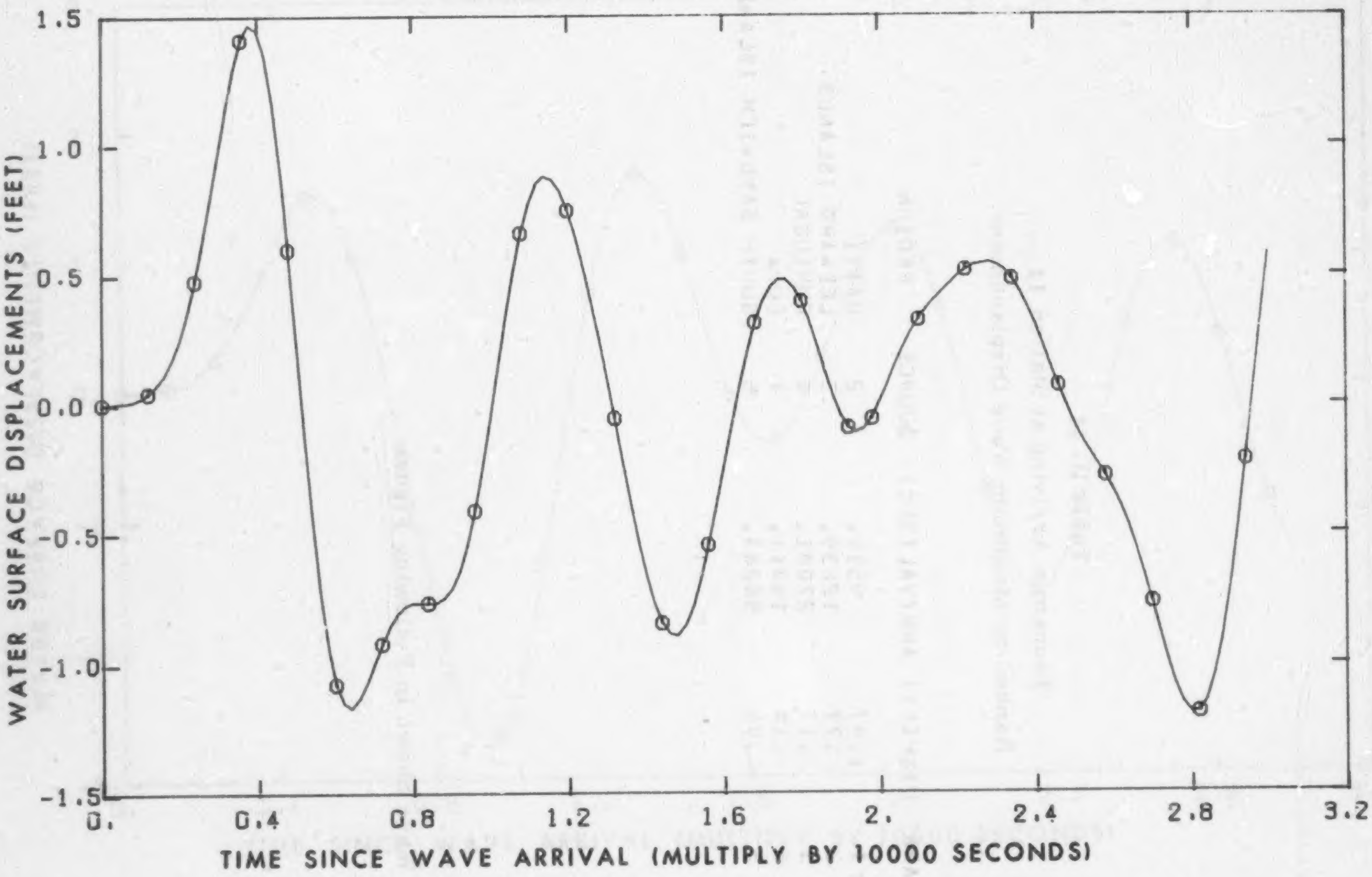

Figure B-11: Largest Tsunami arriving at Station 11 Offshore of Atlantic City, N.J.

Table B- 12

Tsunamis Arriving at Station 12

Ranked by Maximum Wave Displacement

RANK	DISP(FT)	ARRIVAL(SEC)	SOURCE	REGION
*1	2.77	9370.	2	HAITI
2	.92	12890.	3	LEEWARD ISLANDS
3	.31	27431.	4	PORTUGAL
4	.24	14097.	1	CUBA
5	.09	58248.	5	SOUTH SANDWICH ISLANDS

* Wave Shown in Following Figure

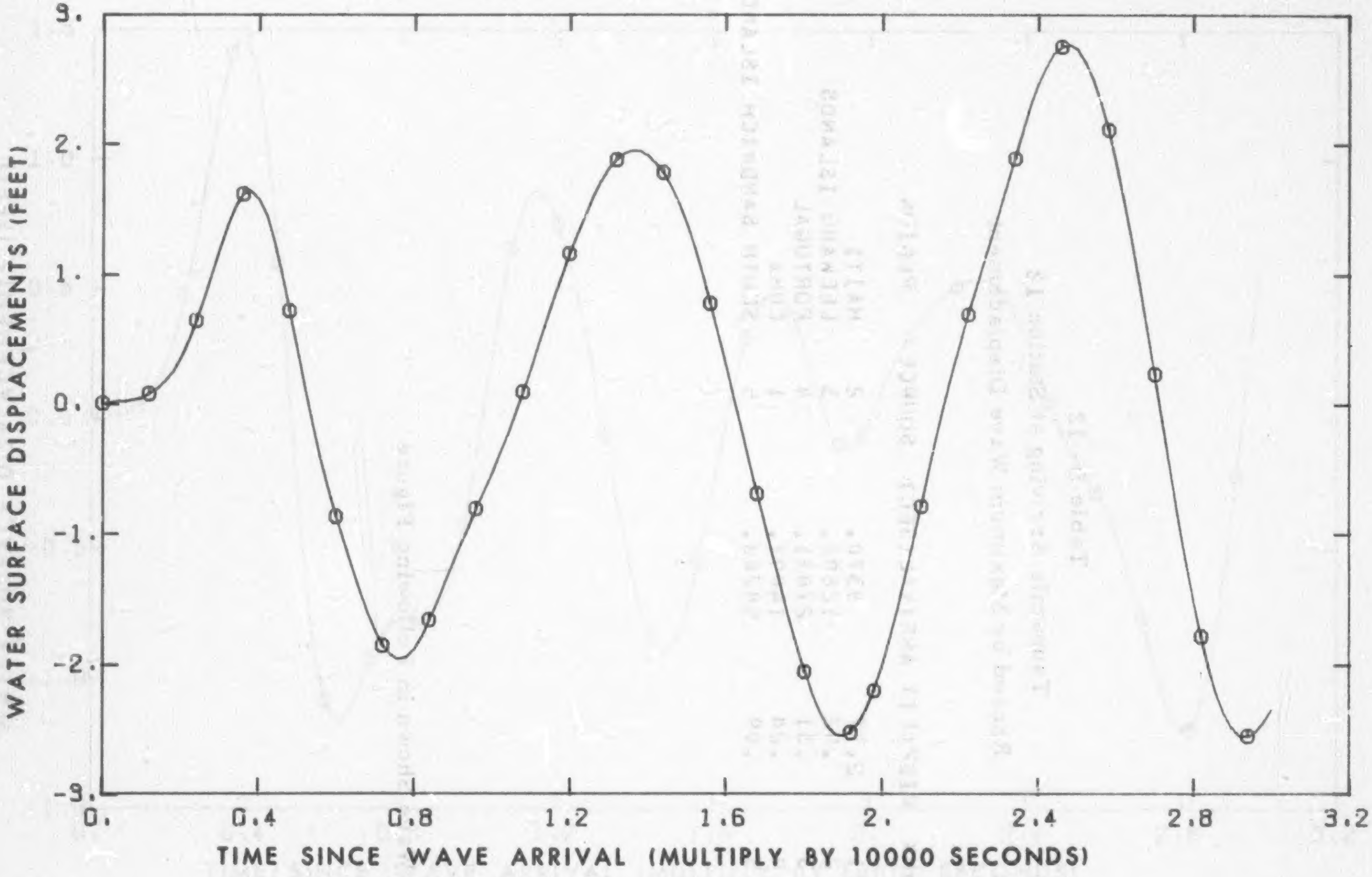

Figure B-12: Largest Tsunami arriving at Station 12 Offshore of Assateague Island, M.D.

Table B-13
Tsunamis Arriving at Station 13
Ranked by Maximum Wave Displacement

```
RANK  DISP(FT) ARRIVAL(SEC)  SOURCE    REGION

*1     3.06       8241.        2     HAITI
 2     1.48      13526.        3     LEEWARD ISLANDS
 3     1.16      26404.        4     PORTUGAL
 4      .38      12200.        1     CUBA
 5      .23      56876.        5     SOUTH SANDWICH ISLANDS
```

* Wave Shown in Following Figure

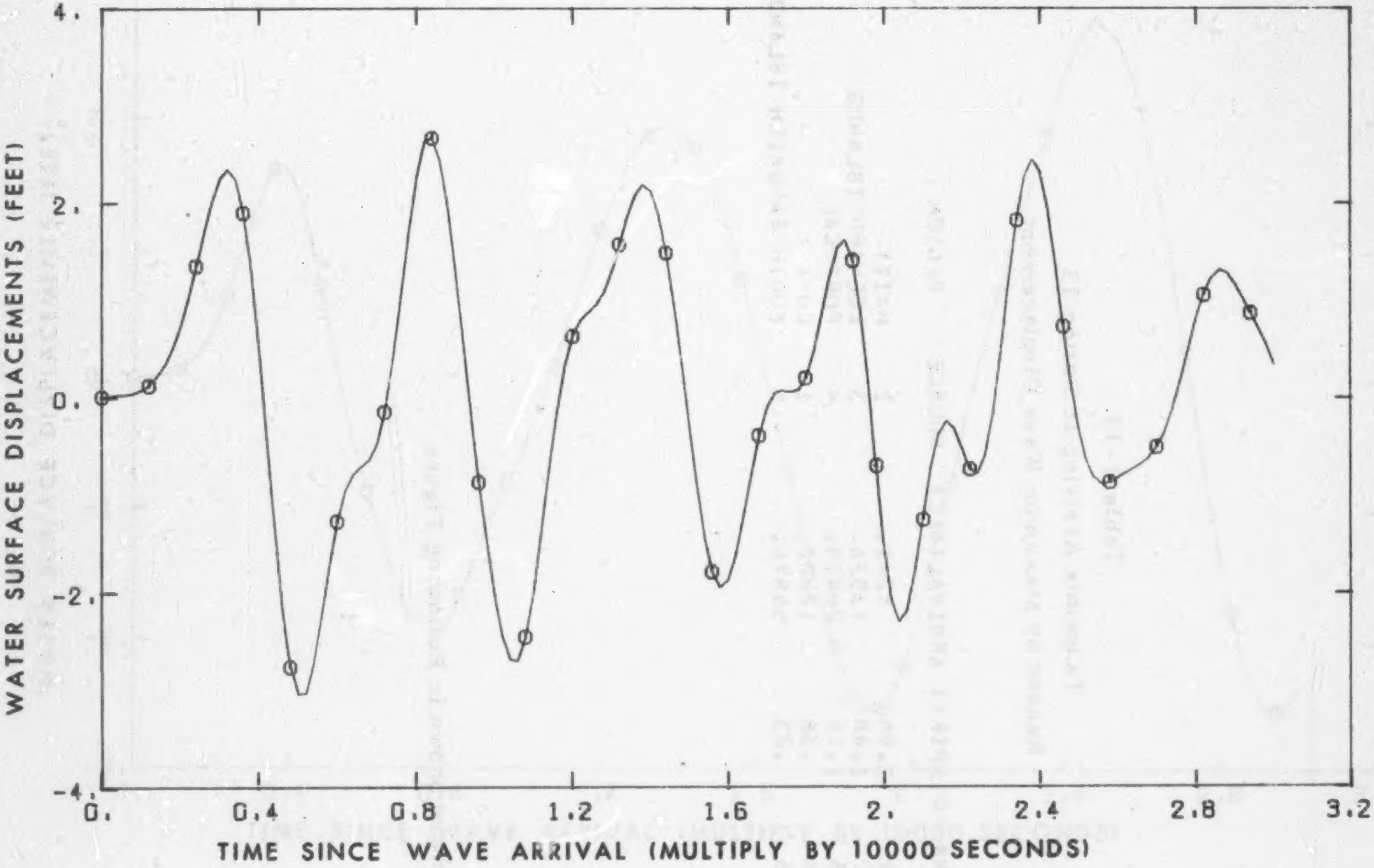

Figure B-13: Largest Tsunami arriving at Station 13 Offshore of Newport News, VA

Table B-14

Tsunamis Arriving at Station 14

Ranked by Maximum Wave Displacement

RANK	DISP(FT)	ARRIVAL(SEC)	SOURCE	REGION
*1	4.47	7633.	2	HAITI
2	2.75	10110.	3	LEEWARD ISLANDS
3	1.00	26251.	4	PORTUGAL
4	.33	11061.	1	CUBA
5	.21	56315.	5	SOUTH SANDWICH ISLANDS

* Wave Shown in Following Figure

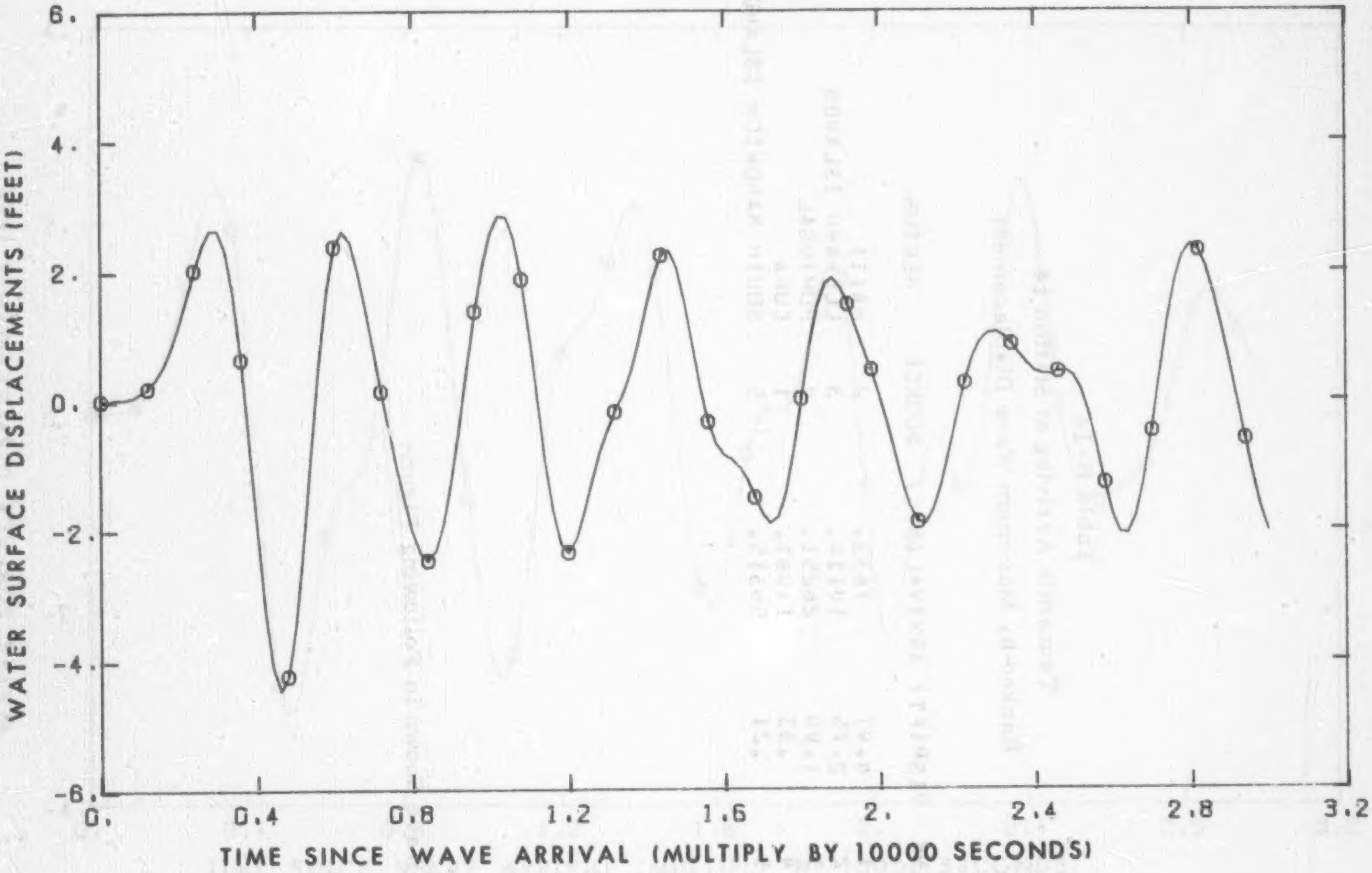

Figure B-14: Largest Tsunami arriving at Station 14 Offshore of Albemarle Sound, N.C.

Table B-15

Tsunamis Arriving at Station 15

Ranked by Maximum Wave Displacement

RANK	DISP(FT)	ARRIVAL(SEC)	SOURCE	REGION
*1	3.88	7673.	2	HAITI
2	1.79	10172.	3	LEEWARD ISLANDS
3	.77	26929.	4	PORTUGAL
4	.41	11017.	1	CUBA
5	.20	56505.	5	SOUTH SANDWICH ISLANDS

* Wave Shown in Following Figure

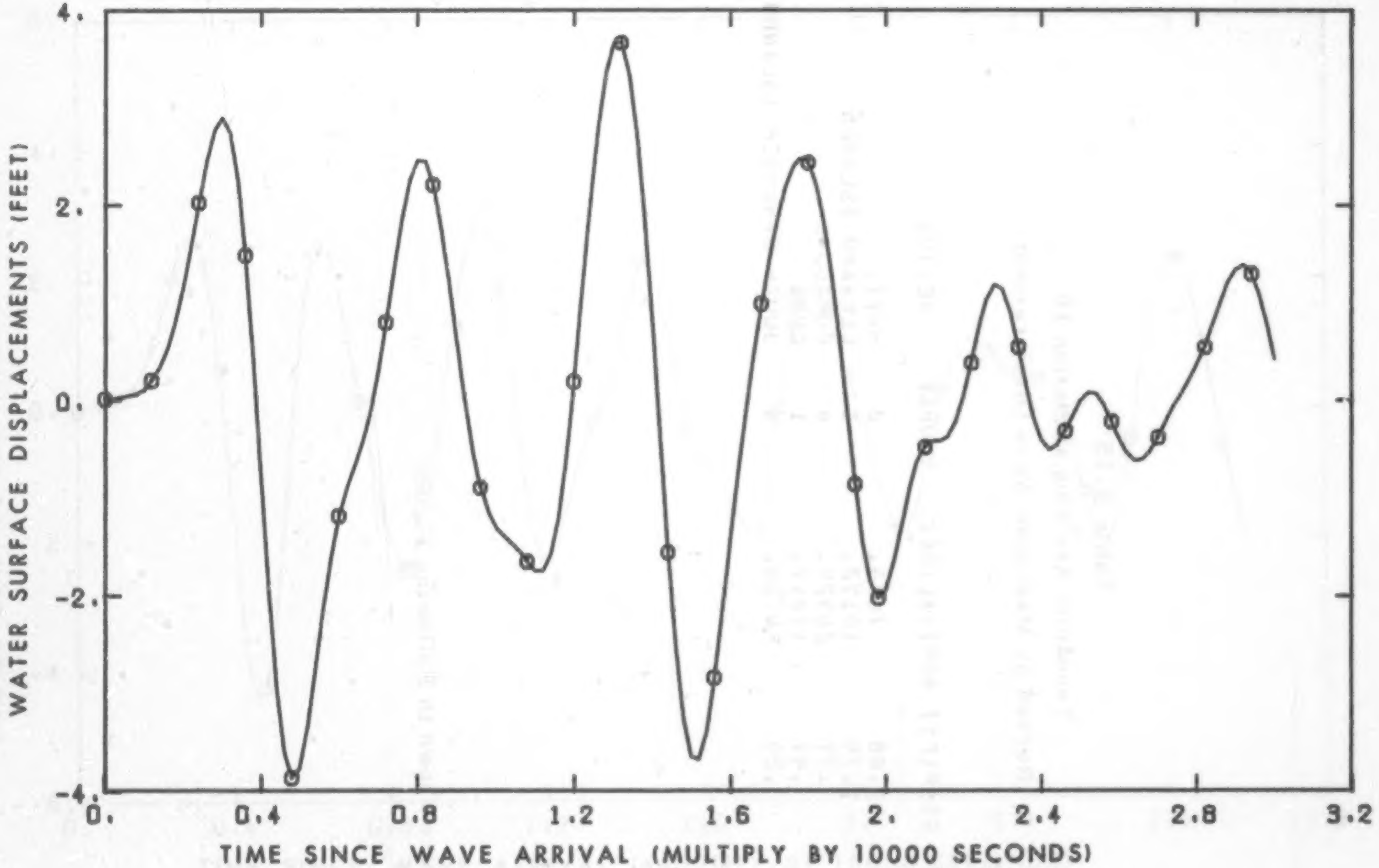

Figure B-15: Largest Tsunami arriving at Station 15 Offshore of Pamlico Sound, N.C.

Table B-16

Tsunamis Arriving at Station 16

Ranked by Maximum Wave Displacement

RANK	DISP(FT)	ARRIVAL(SEC)	SOURCE	REGION
* 1	3.42	7882.	2	HAITI
2	1.68	11041.	3	LEEWARD ISLANDS
3	.61	27872.	4	PORTUGAL
4	.17	11275.	1	CUBA
5	.09	57112.	5	SOUTH SANDWICH ISLANDS

* Wave Shown in Following Figure

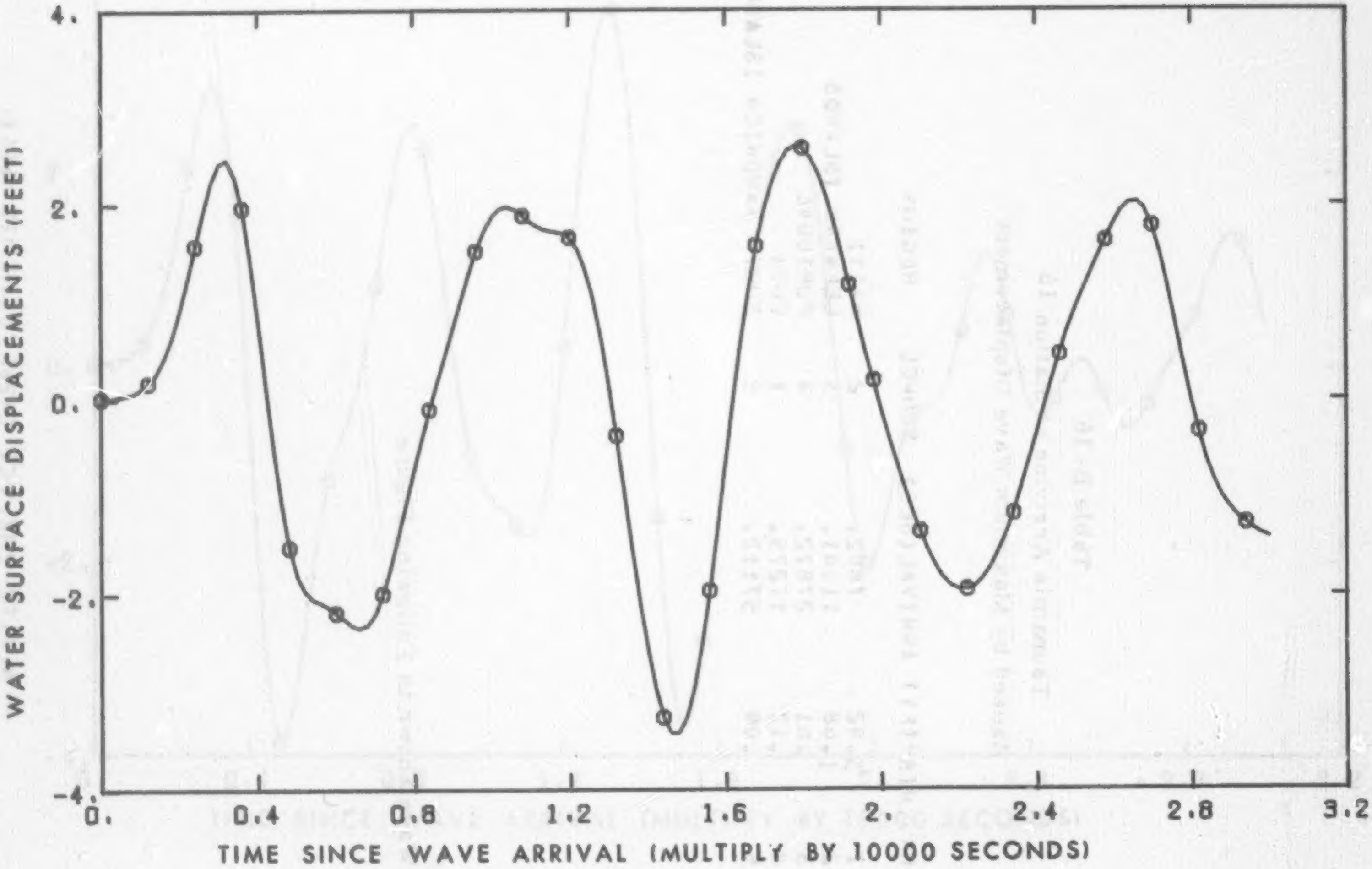

Figure B-16: Largest Tsunami arriving at Station 16 Offshore of Onslow Bay, N.C.

Table B-17

Tsunamis Arriving at Station 17

Ranked by Maximum Wave Displacement

RANK	DISP(FT)	ARRIVAL(SEC)	SOURCE	REGION
*1	2.25	8009.	2	HAITI
2	1.00	11300.	3	LEEWARD ISLANDS
3	.52	28998.	4	PORTUGAL
4	.25	11418.	1	CUBA
5	.06	57938.	5	SOUTH SANDWICH ISLANDS

* Wave Shown in Following Figure

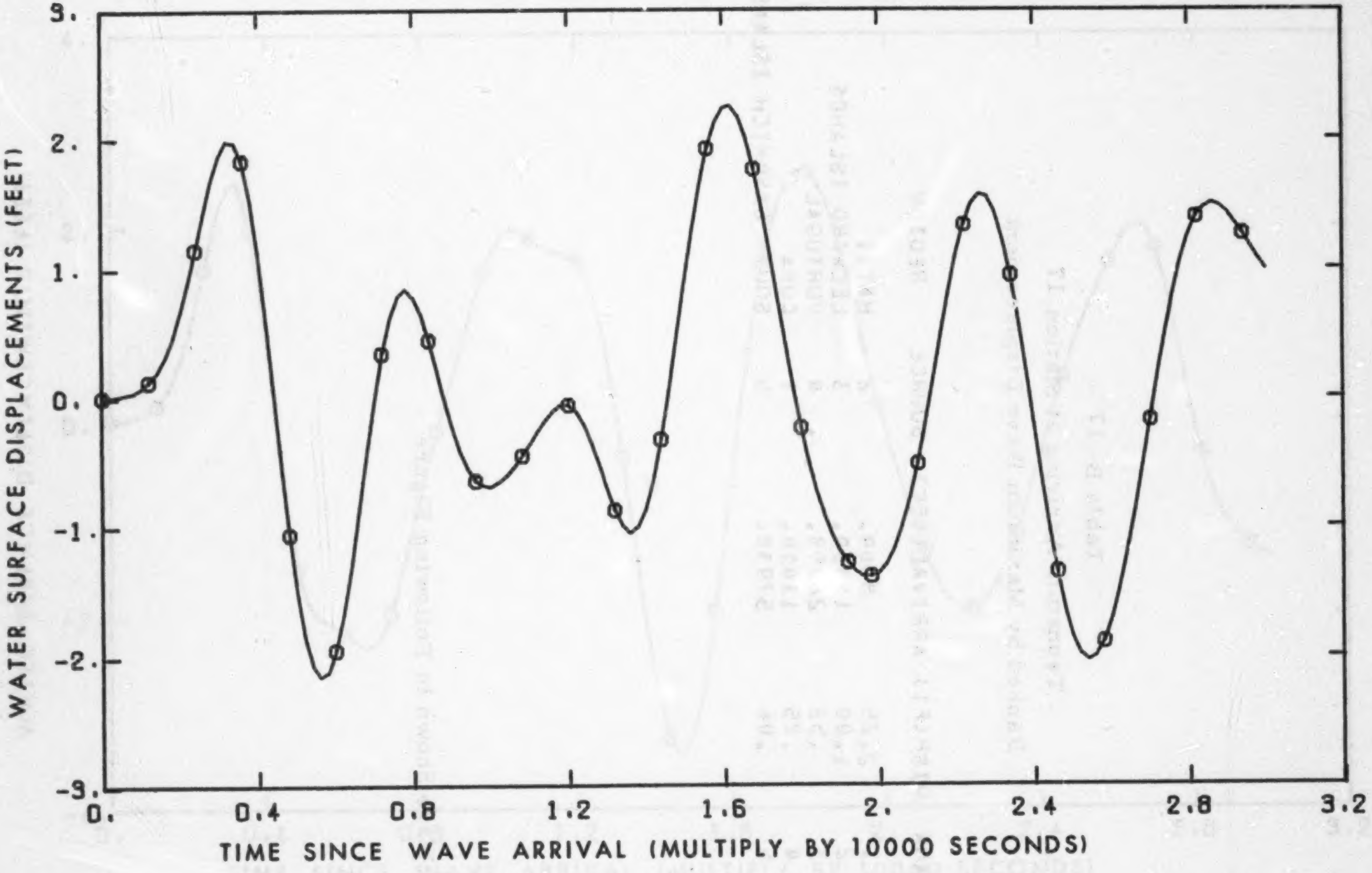

Figure B-17: Largest Tsunami arriving at Station 17 Offshore of Myrtle Beach, S.C.

Table B- 18

Tsunamis Arriving at Station 18

Ranked by Maximum Wave Displacement

RANK	DISP(FT)	ARRIVAL(SEC)	SOURCE	REGION
*1	2.19	9082.	2	HAITI
2	1.06	12470.	3	LEEWARD ISLANDS
3	.34	30550.	4	PORTUGAL
4	.20	12968.	1	CUBA
5	.05	59343.	5	SOUTH SANDWICH ISLANDS

* Wave Shown in Following Figure

READEX FICHE

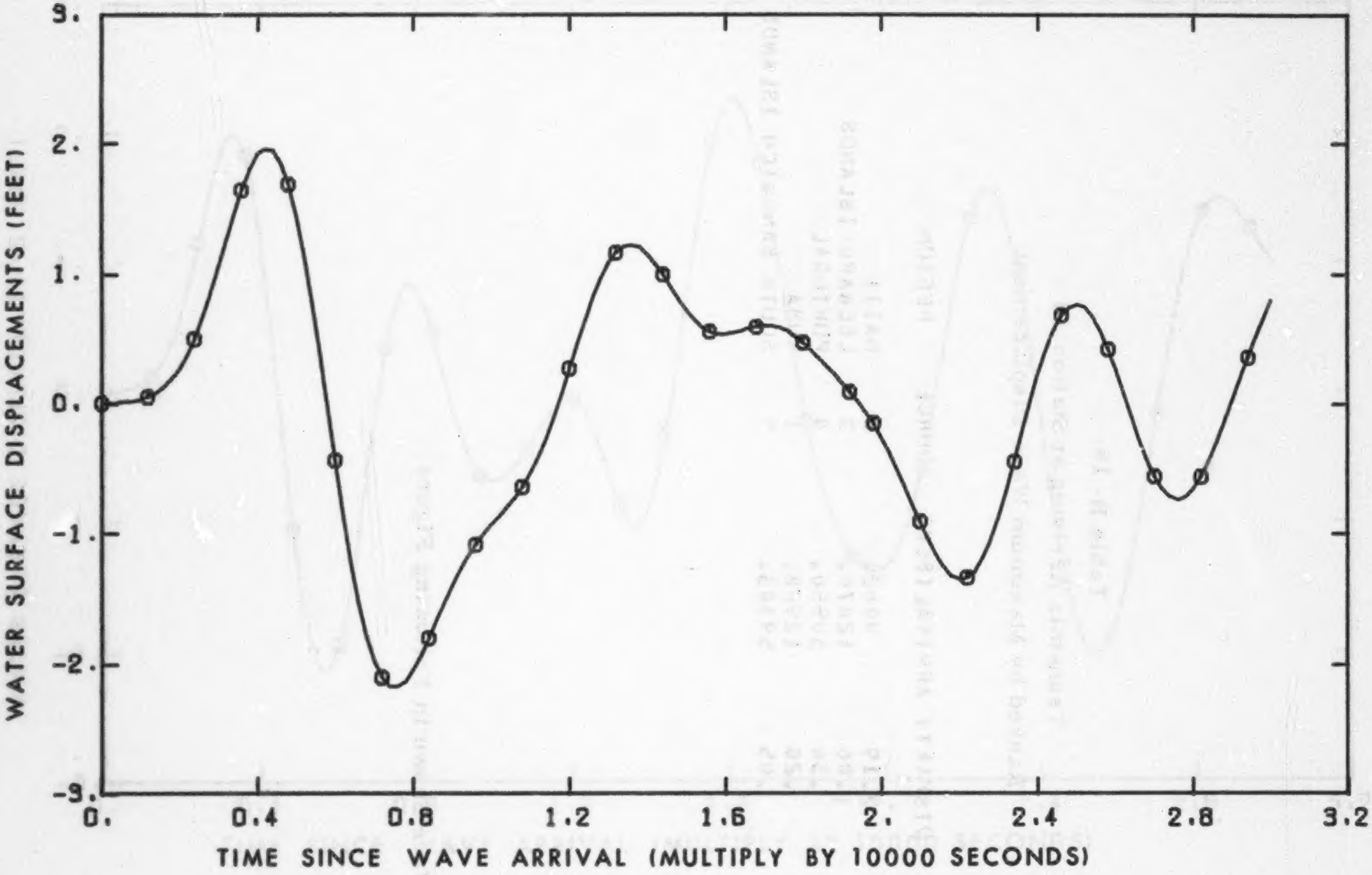

Figure B-18: Largest Tsunami arriving at Station 18 Offshore of Cape Romain, S.C.

Table B-19

Tsunamis Arriving at Station 19

Ranked by Maximum Wave Displacement

RANK	DISP(FT)	ARRIVAL(SEC)	SOURCE	REGION
*1	1.65	9277.	2	HAITI
2	.77	12613.	3	LEEWARD ISLANDS
3	.43	31099.	4	PORTUGAL
4	.19	13027.	1	CUBA
5	.04	59808.	5	SOUTH SANDWICH ISLANDS

* Wave Shown in Following Figure

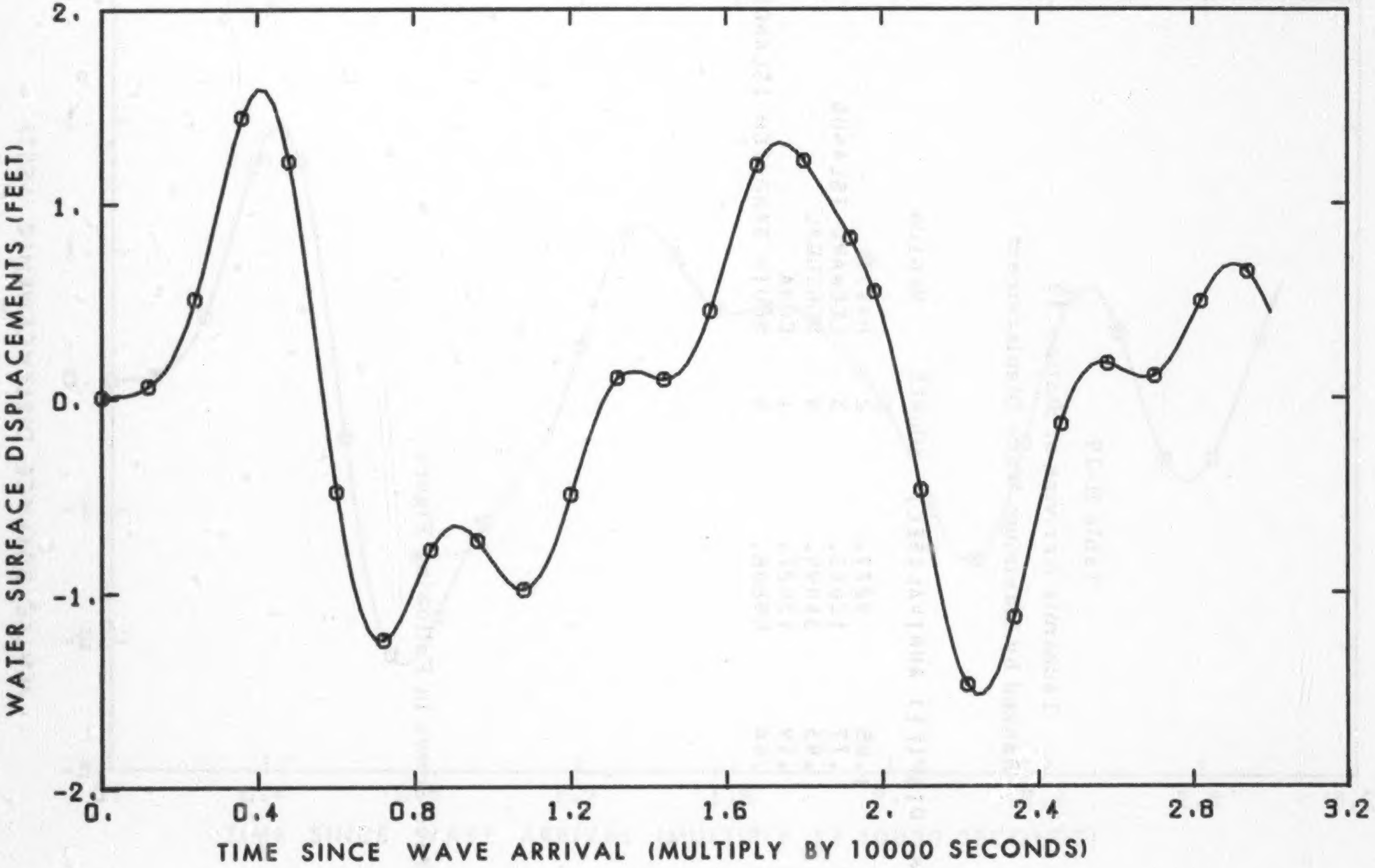

Figure B-19: Largest Tsunami arriving at Station 19 Offshore of Parris Island, S.C.

Table B- 20

Tsunamis Arriving at Station 20

Ranked by Maximum Wave Displacement

RANK	DISP(FT)	ARRIVAL(SEC)	SOURCE	REGION
*1	1.59	9862.	2	HAITI
2	.60	15206.	3	LEEWARD ISLANDS
3	.22	32558.	4	PORTUGAL
4	.11	14405.	1	CUBA
5	.02	61339.	5	SOUTH SANDWICH ISLANDS

* Wave Shown in Following Figure

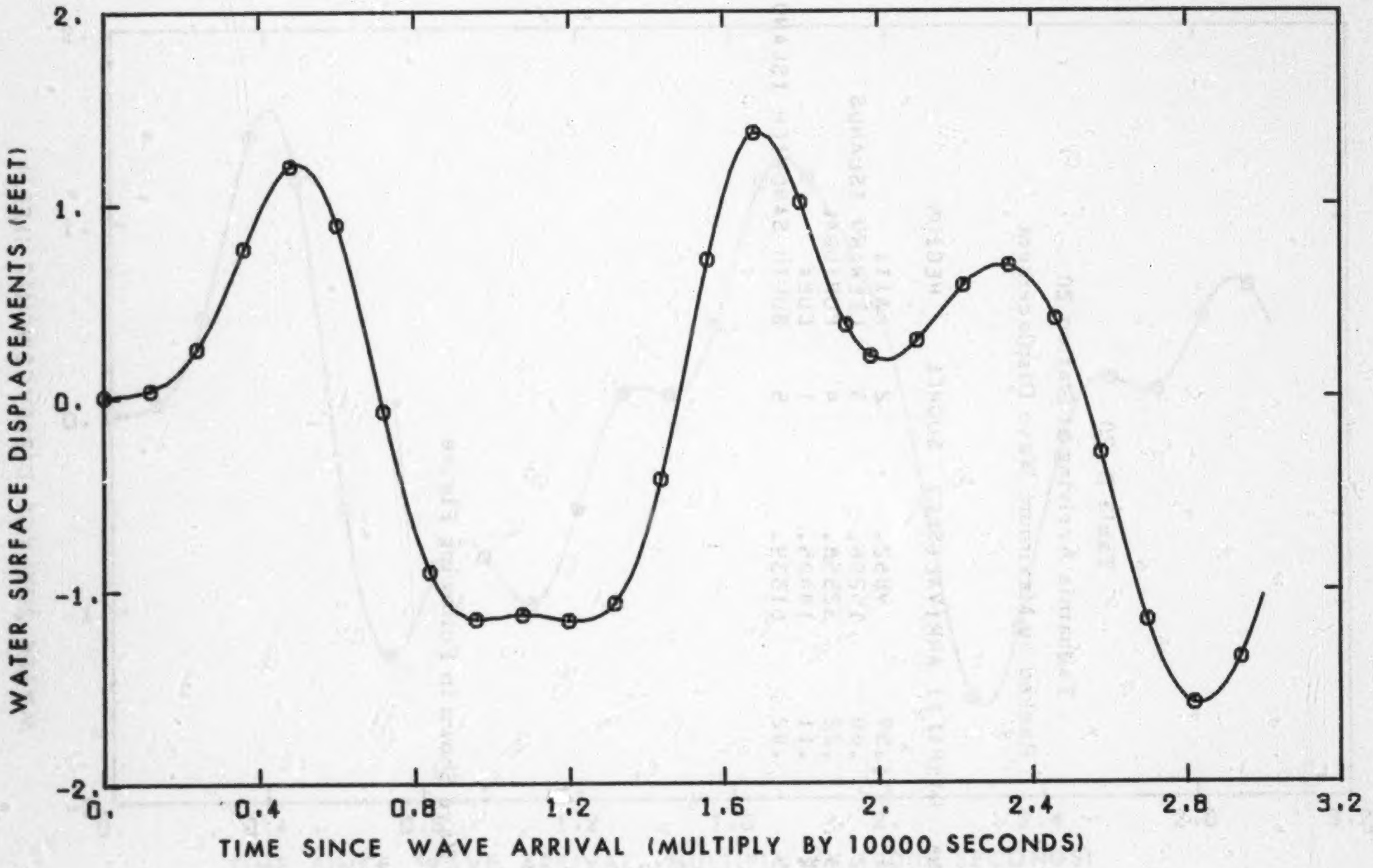

Figure B-20: Largest Tsunami arriving at Station 20 Offshore of St. Andrew Sound, GA

Table B- 21

Tsunamis Arriving at Station 21

Ranked by Maximum Wave Displacement

RANK	DISP(FT)	ARRIVAL(SEC)	SOURCE	REGION
*1	1.94	9381.	2	HAITI
2	.86	12981.	3	LEEWARD ISLANDS
3	.34	32216.	4	PORTUGAL
4	.13	13358.	1	CUBA
5	.04	60731.	5	SOUTH SANDWICH ISLANDS

* Wave Shown in Following Figure

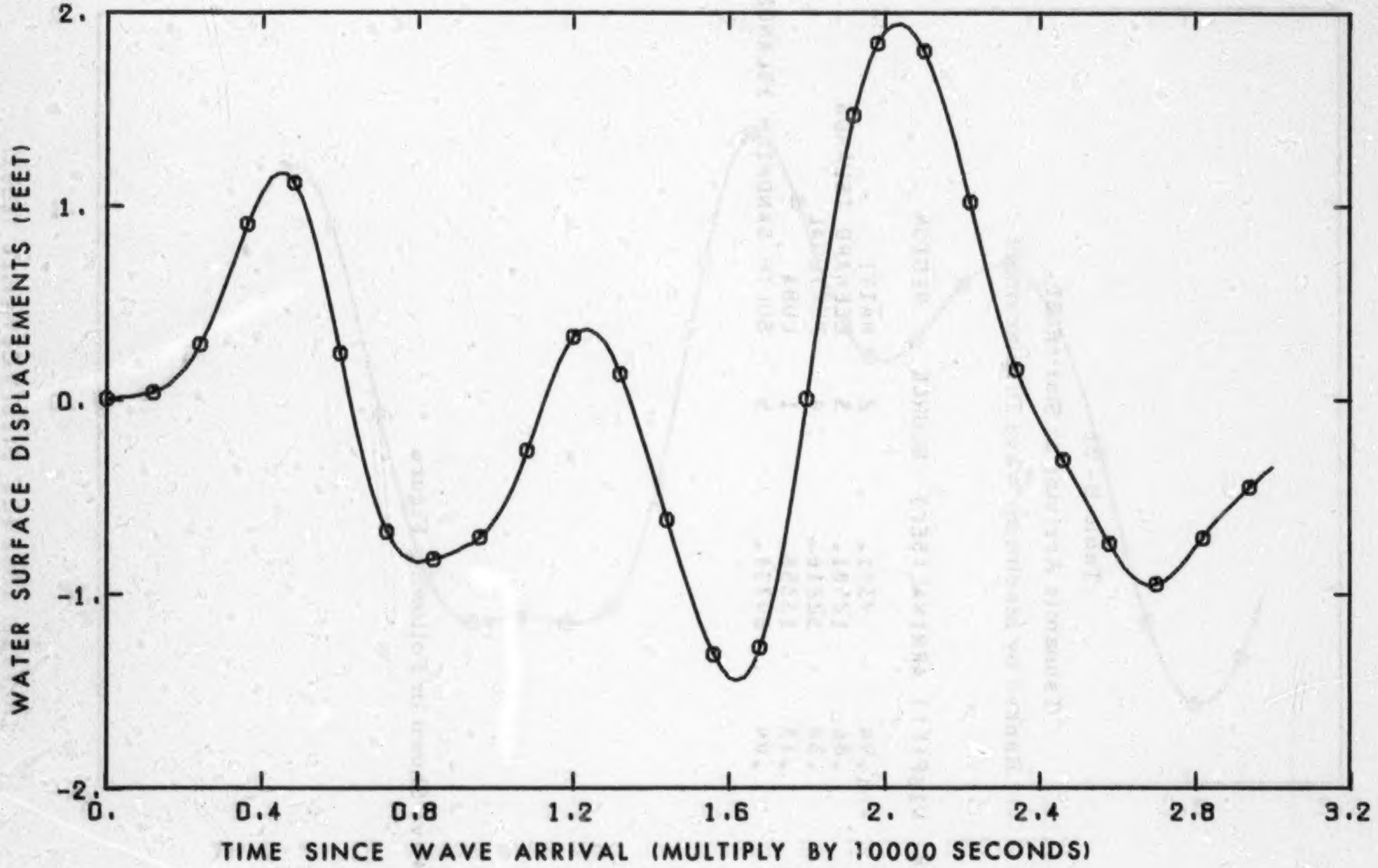

Figure B-21: Largest Tsunami arriving at Station 21 Offshore of St. Augustine, Fla.

Table B-22

Tsunamis Arriving at Station 22

Ranked by Maximum Wave Displacement

RANK	DISP(FT)	ARRIVAL(SEC)	SOURCE	REGION
*1	2.48	7888.	2	HAITI
2	.98	11028.	3	LEEWARD ISLANDS
3	.53	30895.	4	PORTUGAL
4	.20	11002.	1	CUBA
5	.08	58816.	5	SOUTH SANDWICH ISLANDS

* Wave Shown in Following Figure

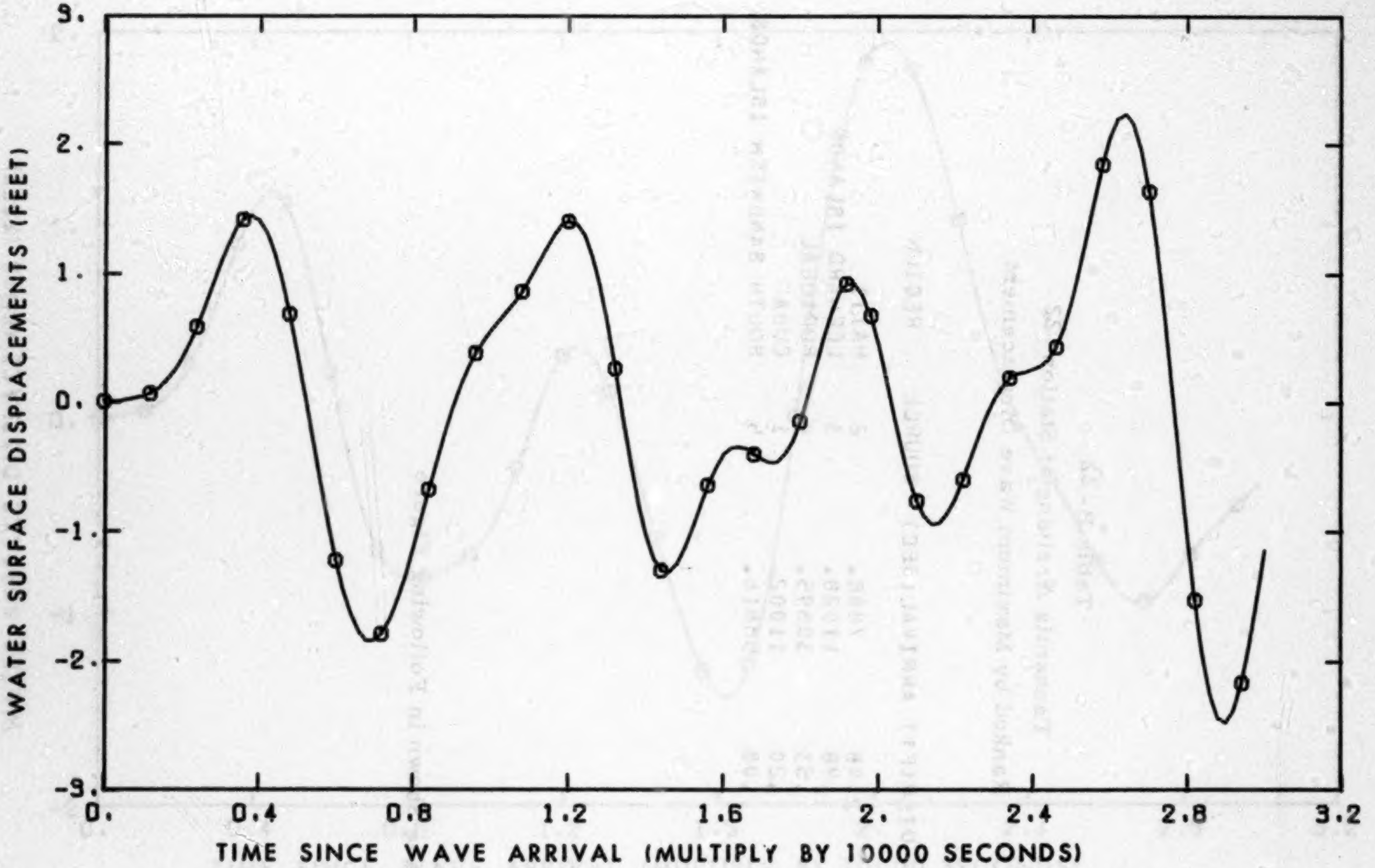

Figure B-22: Largest Tsunami arriving at Station 22 Offshore of Merritt Island, Fla.

Table B-23

Tsunamis Arriving at Station 23

Ranked by Maximum Wave Displacement

RANK	DISP(FT)	ARRIVAL(SEC)	SOURCE	REGION
* 1	1.88	7537.	2	HAITI
2	.94	10764.	3	LEEWARD ISLANDS
3	.44	31059.	4	PORTUGAL
4	.13	10750.	1	CUBA
5	.03	58919.	5	SOUTH SANDWICH ISLANDS

* Wave Shown in Following Figure

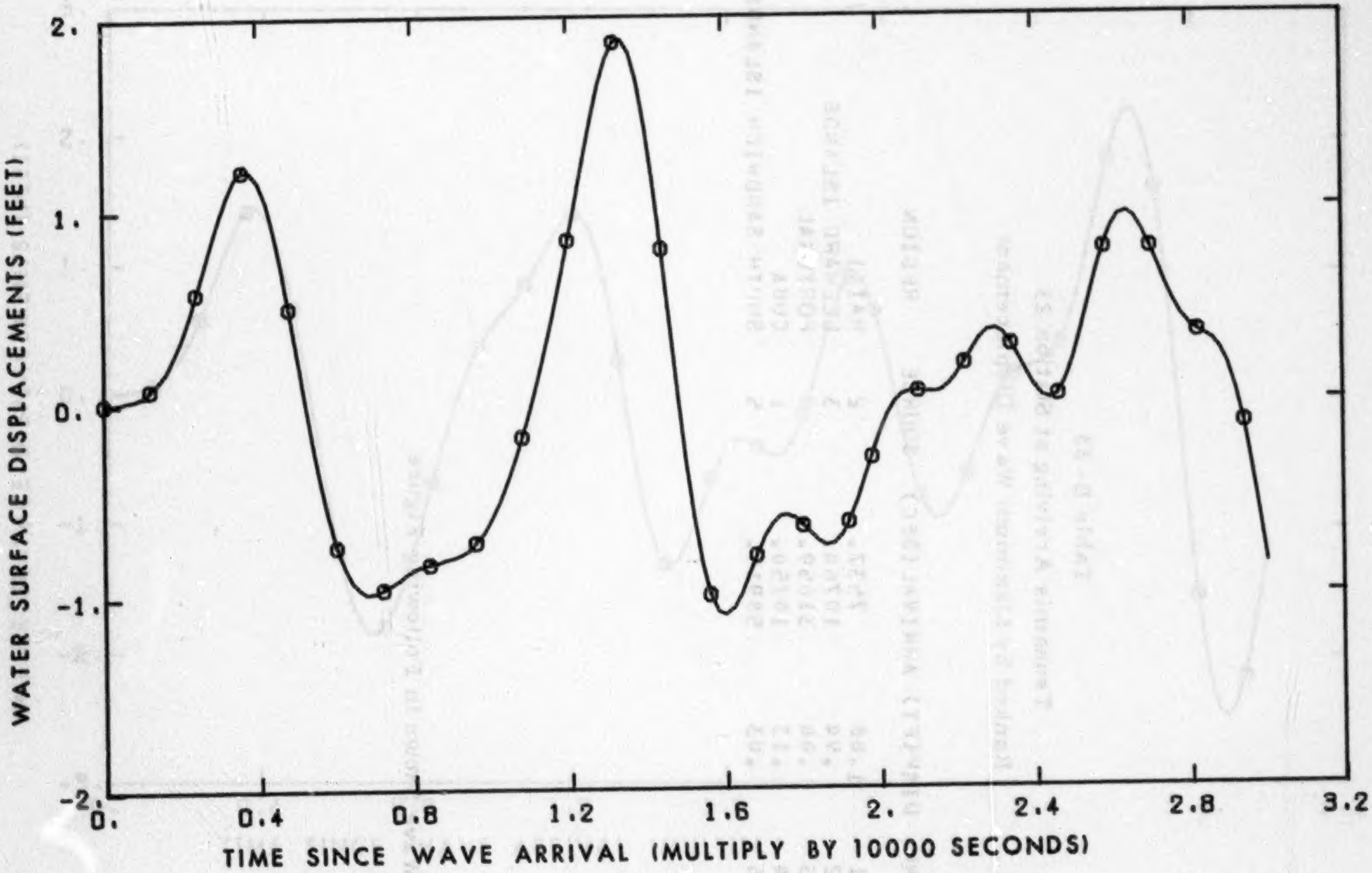

Figure B-23: Largest Tsunami arriving at Station 23 Offshore of Vero Beach, Fla.

Table B-24

Tsunamis Arriving at Station 24

Ranked by Maximum Wave Displacement

RANK	DISP(FT)	ARRIVAL(SEC)	SOURCE	REGION
*1	2.12	8136.	2	HAITI
2	.90	11801.	3	LEEWARD ISLANDS
3	.29	32249.	4	PORTUGAL
4	.20	13887.	1	CUBA
5	.03	60054.	5	SOUTH SANDWICH ISLANDS

* Wave Shown in Following Figure

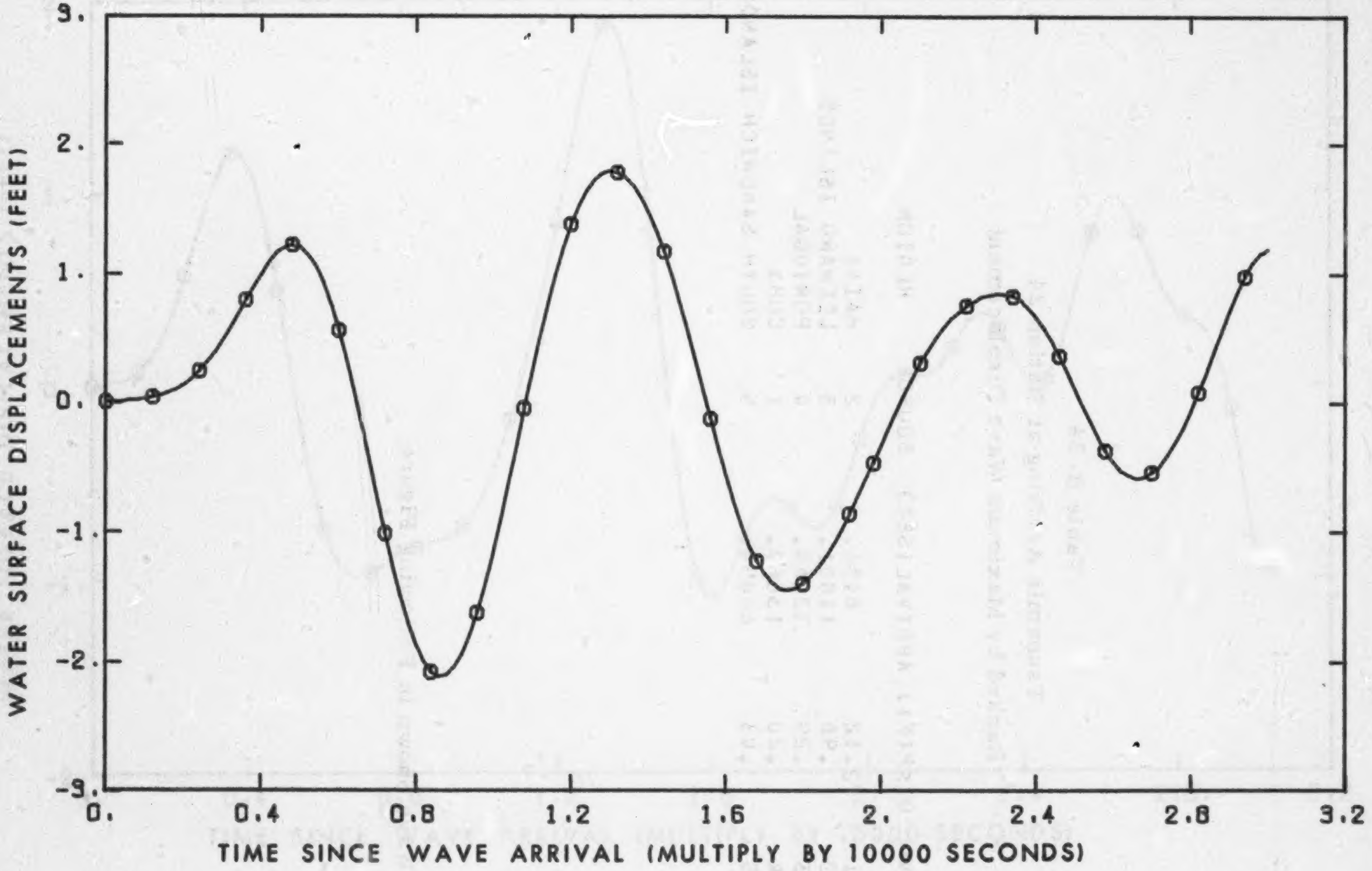

Figure B-24: Largest Tsunami arriving at Station 24 Offshore of Jupiter, Fla.

Table B-25

Tsunamis Arriving at Station 25

Ranked by Maximum Wave Displacement

RANK	DISP(FT)	ARRIVAL(SEC)	SOURCE	REGION
* 1	2.56	7626.	2	HAITI
2	.75	11426.	3	LEEWARD ISLANDS
3	.41	32368.	4	PORTUGAL
4	.31	9743.	1	CUBA
5	.02	76294.	5	SOUTH SANDWICH ISLANDS

* Wave Shown in Following Figure

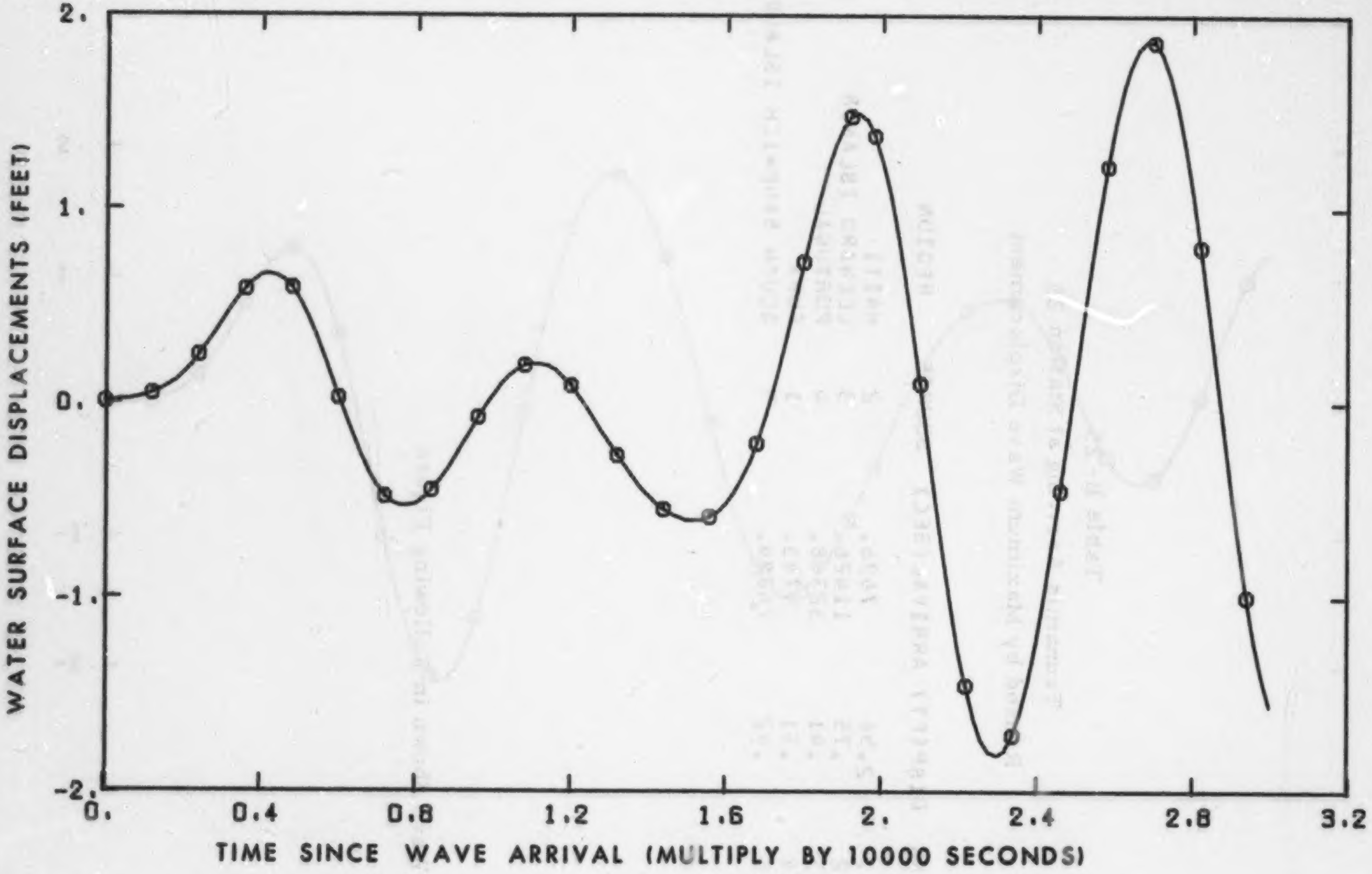

Figure B-25: Largest Tsunami arriving at Station 25 Offshore of Hollywood, Fla.

Table B- 26

Tsunamis Arriving at Station 26

Ranked by Maximum Wave Displacement

RANK	DISP(FT)	ARRIVAL(SEC)	SOURCE	REGION
* 1	1.18	8420.	2	HAITI
2	.75	12546.	3	LEEWARD ISLANDS
3	.56	8012.	1	CUBA
4	.35	33301.	4	PORTUGAL
5	.02	75616.	5	SOUTH SANDWICH ISLANDS

* Wave Shown in Following Figure

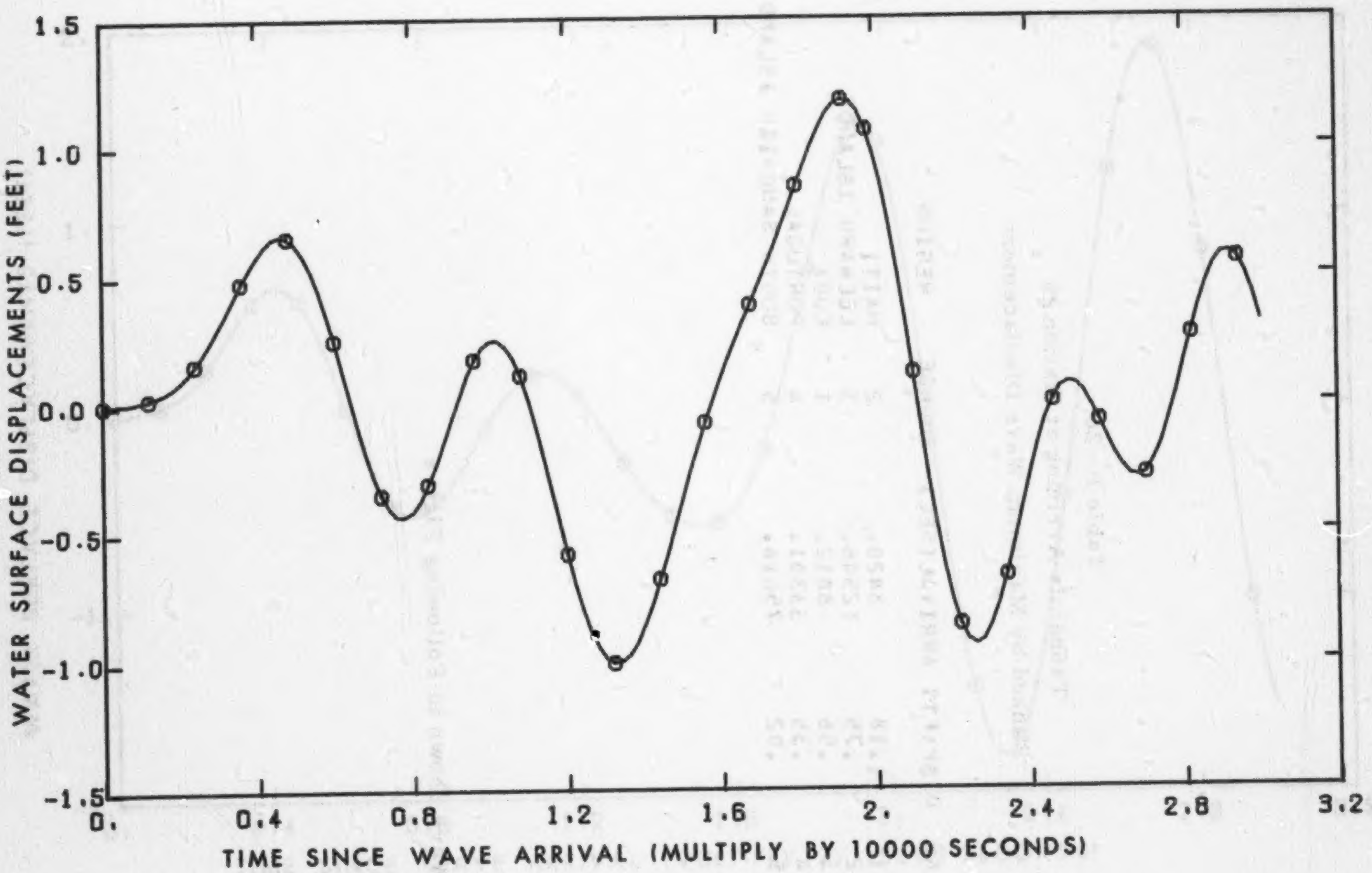

Figure B-26: Largest Tsunami arriving at Station 26 Offshore of Key Largo, Fla.

Table B- 27

Tsunamis Arriving at Station 27

Ranked by Maximum Wave Displacement

RANK	DISP(FT)	ARRIVAL(SEC)	SOURCE	REGION
* 1	.99	9808.	2	HAITI
2	.66	17637.	3	LEEWARD ISLANDS
3	.63	7052.	1	CUBA
4	.31	34945.	4	PORTUGAL
5	.01	75545.	5	SOUTH SANDWICH ISLANDS

* Wave Shown in Following Figure

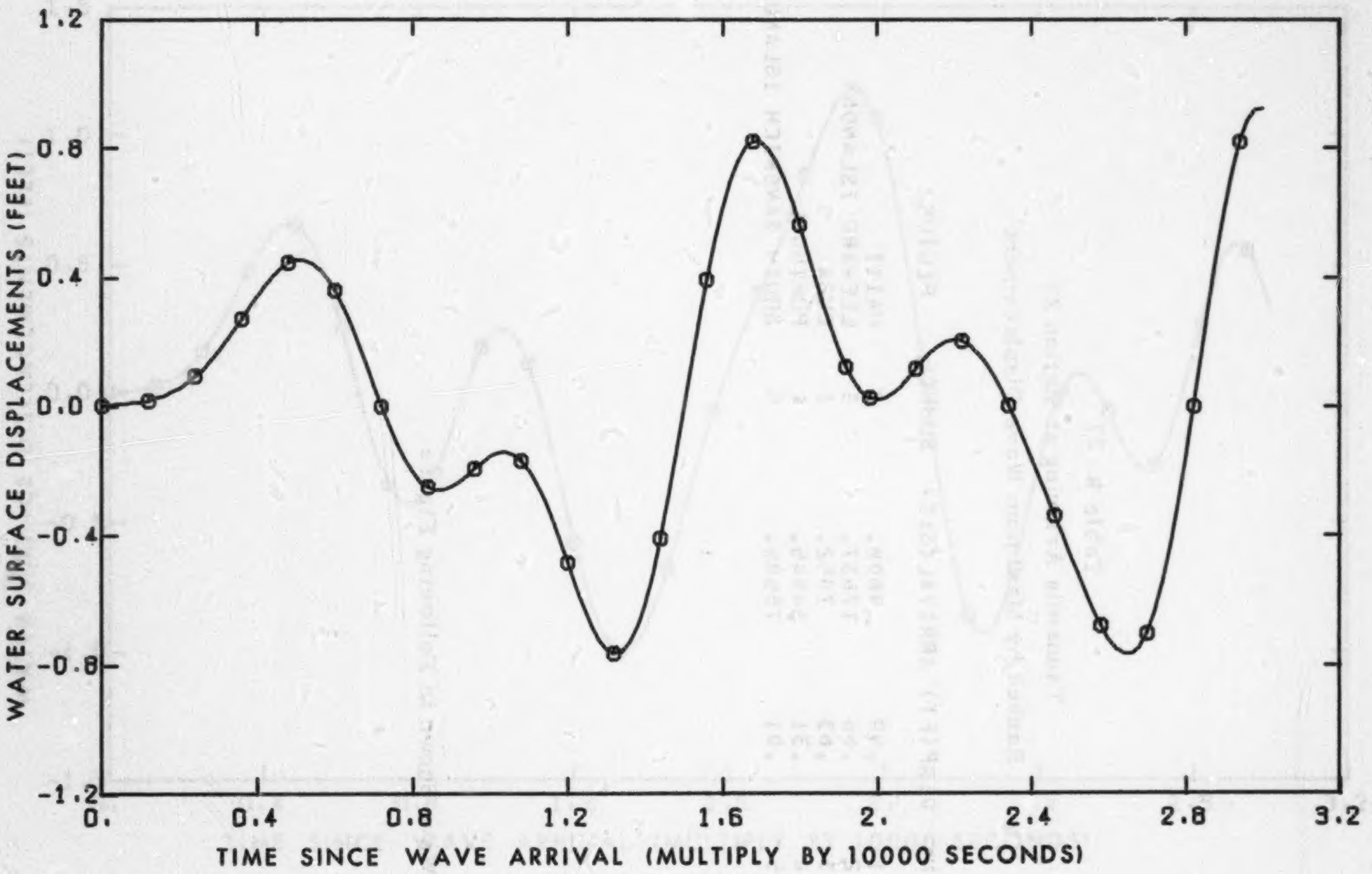

Figure B-27: Largest Tsunami arriving at Station 27 Offshore of Cape Sable, Fla.

APPENDIX C

LISTING OF PROGRAM SEAWAVE

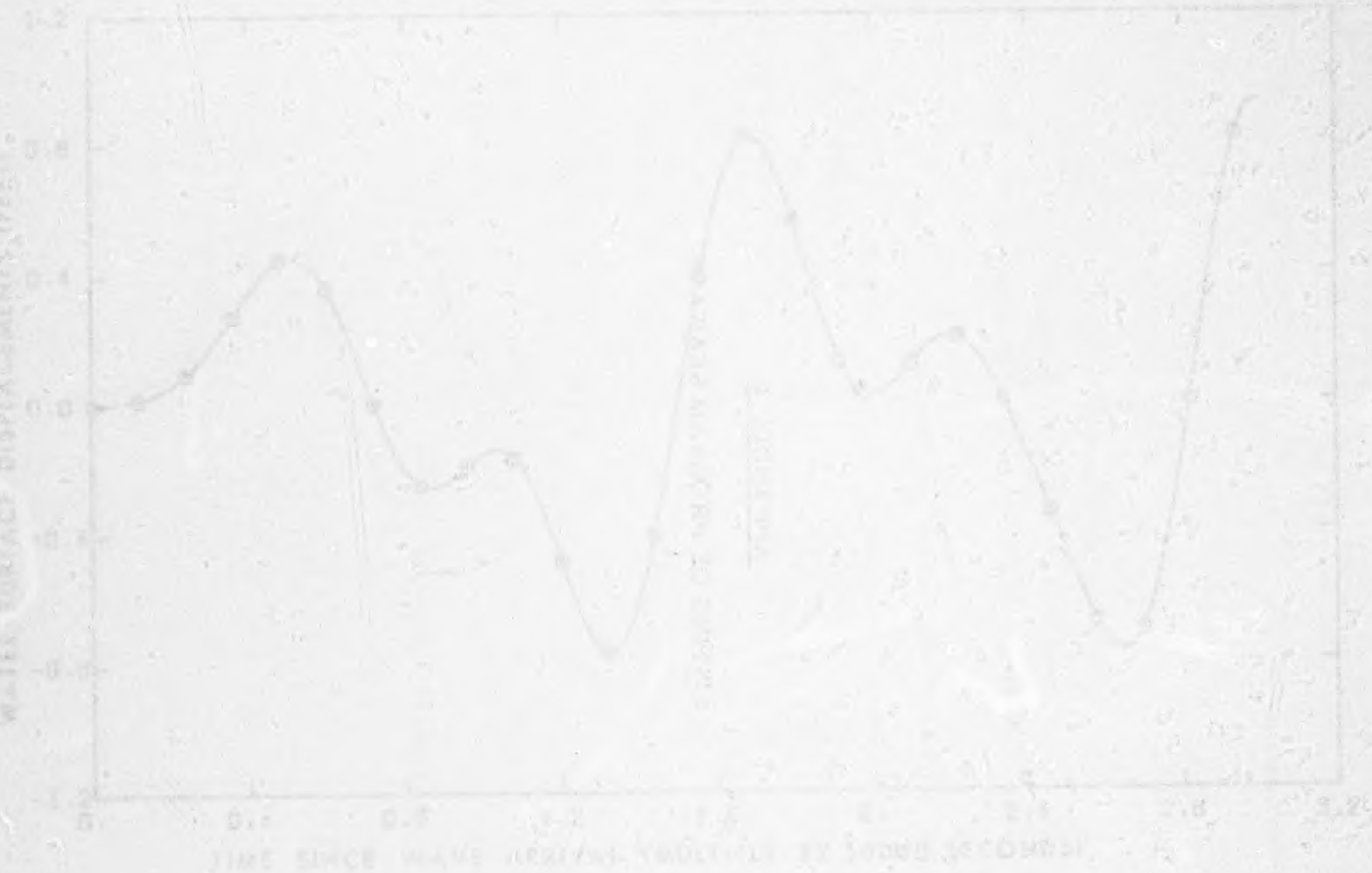

Figure B-37: Largest Tsunami Waves at Station 67 Offshore of Cape Sable, Fla.

```
      PROGRAM SEAWAVE(INPUT,OUTPUT,TAPE5=INPUT,TAPE6=OUTPUT,TAPE2,TAPE9)
C     ....PROGRAM TO COMPUTE PROPAGATION OF LONG WATER WAVES THROUGH
C         ARBITRARY GEOMETRIES....
C     ---VERSION FOR TWIN CITIES CYBER 70 (7600)---
C     ---THIS VERSION HAS BEEN OPTIMIZED TO DECREASE EXECUTION TIME, AND
C        IS ONLY APPLICABLE TO SPHERICAL COORDINATES---
C-----------------------------------------------------------------------
C     VERSION TC-486     30 JUNE 1976
C-----------------------------------------------------------------------
      COMMON/A1/ DT,TMAX, TCHT,DTN,T,N1,N2,N3,N4,M1,M2,M3,M4,K1,K2,K3,K4
     1, THEIN,THETCHG,THETS,DTHET1,DTHET2,PHIW,PHIE,DPHI,ITIME,NCOUNT
     2, IGMC,IXOUT,BND,PI,RAD,TADD,RE,TAUP,VELP,XZERO,YZERO,CINIT,CINPUT
     3, XSTR,YSTR,NPTS,NPTINC,NPRINT(32),NTRANS,TRANS(20),G
     4, NCNT,NGRID,IPLOT,ICOORD,IOUT1,IOUT2,NCOR1,NCOR2,SDT,ISKP,IP,JP
     5, MAXCMP,MINCMP,NAXCMP,NINCMP,CONV,DC1,DC2,DEPMIN,ITAB
      COMMON     SN(131),SNPHALF(131),SNMHALF(131),F(131),MCOMP(300)
     1, MFIRST( 8,300),MLAST( 8,300),NCOMP(131),NFIRST( 7,131)
     2, NLAST( 7,131), NPOT(61),MPOT(61)
      COMMON/A4/PTAB(451,62)
      LEVEL 2, PTAB
      COMMON/A5/ TVAL(001),VAL(001),PERT,AMPL,TINIT,IBNDRY
     1, XIP,YIP,WANGLE,DEXT,DELT
      COMMON/AB/REL,HOUR,NDIV,NH,NVD,NLAB,INCH
      COMMON/TAPES/ NTAPE,NTSU,NCTR,INCTR
      COMMON /L1/  SE(21010)
      COMMON /L3/   U(21010)
      COMMON /L5/   V(21010)
      COMMON /L7/   D(21010)
      LEVEL 2, U,V
      LEVEL 2, PSEUDO
      INTEGER PSEUDO
      DIMENSION PSEUDO(1)
      EQUIVALENCE(PSEUDO(1),U(1))
      LOGICAL IPNT
      DATA G,DEPMIN/32.2,1.0/
      REWIND 9
      READ(5,5) NCASES,NTAPE
      DO 999 NCASE=1,NCASES
      WRITE(6,2) NCASE
    2 FORMAT(1H1//10X,*BEGIN CASE NO. *,I2)
      CALL SECOND(T1)
      READ(5,5) NTSU,NCTR
      READ(5,5) NMAX,MMAX
    5 FORMAT(2I5)
      CALL INITIAL(NMAX,MMAX,D,SE,U,V,PSEUDO)
      INCTR=TMAX/(DT*(NCTR-1))
C
C     ....BEGIN COMPUTATION BY BRANCHING TO END OF TIME LOOP AND SETTING
C          ARRAYS AND SAVING SPECIAL POINTS AT TIME T = 0....
      SAVFLG=1.0
      GO TO 160
C
C     ....START OF TIME-STEP COMPUTATION LOOP....
  100 T=ITIME*DT + TADD
C
C     ....COMPUTE LATEST WAVE ELEVATION AND VELOCITIES....
C     ....IN SPHERICAL COORDINATES....
      CALL EQUATS(NMAX,MMAX,SE,U,V,D)
C     ....CHECK TO SAVE WAVE ELEVATIONS AT SPECIAL POINTS....
```

```
      SAVFLG=0.
      IF(NPTS .EQ. 0) GO TO 160
      NCOUNT=NCOUNT+1
      IF((NCOUNT-(NCOUNT/NPTINC)*NPTINC) .NE. 0) GO TO 160
      SAVFLG=1.0
      NCNT=NCNT+1
C
C     ....SHIFT WAVE AND VELOCITY INFORMATION AFTER COMPUTATION, THEN
C         SAVE SPECIAL POINT INFO IF SAVFLG=1.0...
  160 IF(SAVFLG .EQ. 1.0) CALL SPECP(NMAX,MMAX,SE)
C
C     ....CHECK FOR PRINTOUT OF SURFACE ELEVATION ARRAY....
      IPNT=ITIME.EQ.IABS(NPRINT(IP))
      IF(IPNT)IP=IP+1
      IF(.NOT.IPNT) GO TO 210
      TP=T
      CALL PRINTA(SE ,NMAX,MMAX,1,NMAX,TP)
C
C     ....INCREMENT TIME INDEX AND CHECK FOR END OF RUN....
  210 ITIME=ITIME+1
      IF(T  .LT. TMAX) GO TO 100
C
C     ....HERE AFTER COMPLETION OF TIME STEPPING CALCULATIONS, SET
C         CONSTANTS FOR END OF RUN PRINTING....
      NPN1=1 $ NPN=0 $ EXI=0.0 $ TADD=0.
      NPTS1=NPTS+1
C
C     ....HERE TO BEGIN PRINTING SPECIAL POINT TIME HISTORIES....
  220 WRITE(6,25)TMAX
   25 FORMAT(/* FINAL TIME REACHED, *,F7.1,* SECONDS*//)
      IF(ITAB .NE. 1) GO TO 300
      IF(NPTS .EQ. 0) GO TO 300
      IF(NPTS .LE. 10) GO TO 250
      EXI=1.0
  250 NPN=NPN+10
      IF(NPN-NPTS) 270,260,260
  260 NPN=NPTS
      EXI=0.0
  270 WRITE(6,35)(NPOT(I),MPOT(I),I=NPN1,NPN)
   35 FORMAT(5X,*T *,10(5X,I3,*,*,I3))
      DO 280 I=1,NCNT
      WRITE(6,45) PTAB(I,NPTS1),(PTAB(I,J),J=NPN1,NPN)
   45 FORMAT(F10.3,10G12.4)
  280 CONTINUE
      IF(EXI .EQ. 0.0) GO TO 300
      NPN1=NPN+1
      GO TO 220
C
C     ....HERE AFTER PRINTING OUT TIME HISTORIES, COMPUTE PROGRAM TIME..
  300 CALL SECOND(T2)
      T3=T2-T1
      WRITE(6,55)T3
   55 FORMAT(///5X,*PROGRAM TIME =*,F8.3,* CPU SECONDS*)
C
C
C     ....SAVE PTAB ARRAY ON TAPE, IF REQUESTED....
      IF(NTAPE .LT. 1) GO TO 350
      WRITE(9)      NCNT,NPTS1
      WRITE(9)     ((PTAB(I,J),I=1,NCNT),J=1,NPTS1)
  350 CONTINUE
```

```
C     ....CHECK IF SPECIAL POINT TIME HISTORIES ARE TO BE PLOTTED.
C          IF SO, READ PLOT INFORMATION....
      IF(IPLOT .EQ. 0) GO TO 998
      READ(5,75)NDIV,NH,NLAB,NVD,REL,HOUR
   75 FORMAT(4I5,2F5.0)
      WRITE(6,95)NDIV,NH,NLAB,NVD,REL,HOUR
   95 FORMAT(//5X,*PLOT INFORMATION - NDIV,NH,NLAB,NVD,REL,HOUR*,/19X,
     1 4I6,2F7.3)
C
C     ....PLOT TIME HISTORIES ON PRINTER....
      CALL PRTPLT
  998 CONTINUE
      IF(NTAPE .GT. 0) ENDFILE 9
  999 CONTINUE
      CALL EXIT
      END
      SUBROUTINE INITIAL(NDM,MDM,D,SE,U,V,ICODE)
C     ....SUBPROGRAM TO READ IN DATA, SET INITIAL CONDITIONS, AND SET
C         UP COMPUTATIONAL TABLES....
C
      LEVEL 2, U,V,ICODE
      DIMENSION D(NDM,MDM),SE(NDM,MDM),U(NDM,MDM),V(NDM,MDM)
     1, ICODE(NDM,MDM),CODE(300),NBD(32),MBD(32)
      COMMON/A1/ DT,TMAX, TCHT,DTN,T,N1,N2,N3,N4,M1,M2,M3,M4,K1,K2,K3,K4
     1, THETN,THETCHG,THETS,DTHET1,DTHET2,PHIW,PHIE,DPHI,ITIME,NCOUNT
     2, IGMC,IXOUT,BND,PI,RAD,TADD,RE,TAUP,VELP,XZERO,YZERO,CINIT,CINPUT
     3, XSTR,YSTR,NPTS,NPTINC,NPRINT(32),NTRANS,TRANS(20),G
     4, NCNT,NGRID,IPLOT,ICOORD,IOUT1,IOUT2,NCOR1,NCOR2,SDT,ISKP,IP,JP
     5, MAXCMP,MINCMP,NAXCMP,NINCMP,CONV,DC1,DC2,DEPMIN,ITAB
      COMMON    SN(131),SNPHALF(131),SNMHALF(131),F(131),MCOMP(300)
     1, MFIRST( 8,300),MLAST( 8,300),NCOMP(131),NFIRST( 7,131)
     2, NLAST( 7,131), NPOT(61),MPOT(61)
      COMMON/A4/PTAB(451,62)
      LEVEL 2, PTAB
      COMMON/A5/ TVAL(001),VAL(001),PERI,AMPL,TINIT,TBNDRY
     1, XIP,YIP,WANGLE,DEXT,DELT
      COMMON/A8/REL,HOUR,NDIV,NH,NVD,NLAB,INCH
      COMMON /L10/GD(50,50)
      LEVEL 2, GD
      DIMENSION ID(8)
      COMMON/TAPES/ NTAPE,NTSU,NCTR,INCTR
C
C     ....SET INITIAL VALUES....
      ITIME=0 $ NCOUNT=0 $ IP=1 $  BND=1.0E-06 $ JP=1
      PI=3.1415927 $ RAD=PI/180. $ TADD=0.0 $ RE=2.1E+07
      ISKP=1 $ NCNT=1
      T=0
C
C     ....READ RUN IDENTIFICATION AND RUN DATA AND PRINT ID....
      READ(5,15)ID
      READ(5,25) ITYPE,NGRID,IPLOT,ICOORD,IGMC,IXOUT,ITAB
      WRITE(6,35)ID
   35 FORMAT(/1X,8A10/)
      WRITE(6,36) NTSU,NCTR
   36 FORMAT(10X,18HTSUNAMI INDEX NO. ,I3,30H, NUMBER OF CONTOURS REQUES
     1TED ,I5)
C
C     ....READ RUN DATA....
      IF(ICOORD .EQ. 1) READ(5,45) ANGLT,CINIT,CINPUT,XSTR,YSTR,RE
      IF(IGMC .GT. 0) READ(5,45)TAUP,VELP,XZERO,YZERO
      IF(ITYPE .LE. 0) GO TO 711
C
C     ....INPUT GRID PARAMETERS AND DEPTH GRID IN ITYPE IS GREATER THAN
C         ZERO....
      READ(5,25)N1,N2,N3,N4,M1,M2,M3,M4,K1,K2,K3,K4
      READ(5,25) NCOR1,NCOR2,IOUT1,IOUT2,INCH
      READ(5,45) THETN,THETCHG,THETS,DTHET1,DTHET2,PHIW,PHIE,DPHI
      READ(5,45) CONV,DC1,DC2,DEPMIN
C     ....READ INITIAL INDICES FOR SUBSET GRID....
      READ(5,25) NINCMP,NAXCMP,MINCMP,MAXCMP
C
C     ....PRINT INPUT DATA....
      WRITE(6,505) N1,N2,N3,N4,M1,M2,M3,M4,K1,K2,K3,K4,NCOR1,NCOR2,
     1 IOUT1,IOUT2,ITYPE,ITAB
  505 FORMAT(///5X,*INPUT DATA.........*///5X,*N1    N2    N3    N4    M1    M
     12    M3    M4    K1    K2    K3    K4 NCOR1 NCOR2 IOUT1 IOUT2 ITYPE ITAB
```

```
    2 *//2X,12I5,I4,5I6)
      WRITE(6,515) ICOORD,IGMC,NGRID,IPLOT
  515 FORMAT(////5X,*ICOORD IGMC NGRID IPLOT*//3X,4I6)
      IF(ICOORD .EQ.2) GC TO 10
      WRITE(6,525)THETN,THETCHG,THETS,DTHET1,DTHET2,PHIW,PHIE,DPHI
  525 FORMAT(///3X,*GRID COORDINATES...(FT)...*/8F14.8)
      GO TO 20
   10 WRITE(6,535)THETN,THETCHG,THETS,DTHET1,DTHET2,PHIW,PHIE,DPHI
  535 FORMAT(///3X,*GRID COORDINATES...(DEGREES).....*//5X,*  THETN = *,
     1F14.8/5X,*THETCHG = *,F14.8/5X,*  THETS = *,F14.8/5X,* DTHET1 = *,
     2F14.8/5X,* DTHET2 = *,F14.8/5X,*   PHIW = *,F14.8/5X,*   PHIE = *,
     3F14.8/5X,*   DPHI = *,F14.8)
   20 WRITE(6,545) CONV,DC1,DC2,DEPMIN,BND
  545 FORMAT(///5X,*CONVERSION FACTOR(TO FEET) = *,F9.4//5X,*CORRECTION
     1VARIABLES(FEET) --  DC1 = *,F8.1,7X,*DC2 = *,F8.1,7X,*DEPMIN = *,
     2 F8.1//5X,*COMPUTATIONS CARRIED OUT TO VALUES GREATER THAN *,G14.8
     3)
      WRITE(6,405) NINCMP,NAXCMP,MINCMP,MAXCMP
  405 FORMAT(///5X,*COMPUTATIONAL SUBSET INDICES INITIALIZED TO.....*/
     1 5X,* NINCMP,NAXCMP,MINCMP,MAXCMP*/3X,5(4X,I3))
      IF(IXOUT .EQ. 0) GC TO 70
      GO TO (40,50),ICOORD
   40 WRITE(6,465)
  465 FORMAT(///5X,*NON-LINEAR TERMS INCLUDED IN RECTANGULAR COORDINATES
     1*)
      GO TO 70
   50 WRITE(6,475)
  475 FORMAT(///5X,*CORIOLIS TERMS INCLUDED IN SPHERICAL COORDINATES*)
   70 CONTINUE
C
C     ....READ DEPTH GRID..
      GO TO(100,200,300,400,500),ITYPE
C
C     ....CARD TO TAPE (LUN2)....
  400 REWIND 2
      WRITE (2) N3,N4
      DO 410 M=1,N3
      READ(5,55)(CODE(N),N=1,N4)
      WRITE(2)(CODE(N),N=1,N4)
  410 CONTINUE
      ENDFILE 2
      REWIND 2
C
C     ...TAPE INPUT  --  SELECT INPUT GRID (LUN2)....
  100 REWIND 2
      READ(2) MDIM,NDIM
      DO 120 M=1,MDIM
      READ(2)(CODE(N),N=1,NDIM)
      IF(M .LT. K1) GO TO 120
      IF(M .GT. K2) GO TO 600
      MM=M-K1+1
      DO 110 N=K3,K4
      NN=N-K3+1
      DDD=CONV*CODE(N)
      IF(DDD .EQ. 0.) GO TO 110
      DDD=AMAX1(DDD,DEPMIN)
  110 D(NN,MM)=DDD
  120 CONTINUE
      GO TO 550
```

```
C       ....MERGE OF CARD INPUT AND PACIFIC OCEAN DEPTH TAPE ON LUN2....
  200 MM=N3-100
      MM1=MM+1
      READ(2)((D(N,M),M=MM1,N3),N=1,N4)
      DO 210 N=1,N4
      DO 210 M=MM1,N3
  210 D(N,M)=-D(N,M)/.3048
      DO 220 N=1,N4
      READ(5,215)(D(N,M),M=1,MM)
      DO 220 M=1,MM
  220 D(N,M)=CONV*D(N,M)
      GO TO 550
C
C       ....CARD INPUT....
  300 DO 310 M=1,N3
      READ(5,55)(D(N,M),N=1,N4)
      DO 310 N=1,N4
      D(N,M)=CONV*D(N,M)
      IF(D(N,M).EQ.0.) GO TO 310
      IF(D(N,M).LT.DEPMIN) D(N,M)=DEPMIN
  310 CONTINUE
      GO TO 550
C
C       ....HERE FOR SPECIAL CODE FOR NON-STANDARD INPUT....
  500 CONTINUE
C
C       ...HERE SET UP GROUND MOTION SPECIFIED BY COORDINATES OF CENTER,
C       AXES, ORIENTATION,SHAPE AND AMPLITUDE...
  550 IF(IGMC .EQ. -2) CALL WARP
C       ....INPUT GROUND DISTURBANCE IN FEET....
  600 IF(IGMC .LT. 0) GO TO 611
      NN=M2-M1+1
      MM=M4-M3+1
      DO 610 M=1,MM
      READ(5,55)(GD(N,M),N=1,NN)
  610 CONTINUE
C
C       ....INPUT CORRECTIONS TO INPUT GRID....
  611 IF(NCOR1 .EQ. 0) GO TO 630
      READ(5,25) (NBD(I),I=1,NCOR1)
      READ(5,25) (MBD(I),I=1,NCOR1)
      DO 620 I=1,NCOR1
      NN=NBD(I)
      MM=MBD(I)
  620 D(NN,MM)=DC1
  630 IF(NCOR2 .EQ. 0) GO TO 650
      READ(5,25) (NBD(I),I=1,NCOR2)
      READ(5,25) (MBD(I),I=1,NCOR2)
      DO 640 I=1,NCOR2
      NN=NBD(I)
      MM=MBD(I)
  640 D(NN,MM)=DC2
C
C       ....OPTIONAL INCLUSION OF BOTTOM MOVEMENT IN DEPTH GRID....
  650 IF(IGMC .EQ. 0 .OR. IGMC .EQ. -2) 651,670
  651 NN=M2-M1+1
      MM=M4-M3+1
      DO 660 N=1,NN
      DO 660 M=1,MM
      NZ=N+M1-1
      MZ=M+M3-1
      IF(D(NZ,MZ) .LE. 0.) GO TO 660
      D(NZ,MZ)=D(NZ,MZ)-GD(N,M)
      IF(D(NZ,MZ) .LT. 0.0) D(NZ,MZ)=0.0
  660 CONTINUE
C
C     ....SET DEPTH=0 AT POINTS WHERE UPLIFT EXCEEDS WATER DEPTH....
  670 IF(IGMC .LT. 1) GO TO 681
      NN=M2-M1 +1
      MM=M4 - M3 +1
      DO 680 N=1,NN
      DO 680 M=1,MM
      NZ=N+M1-1
      MZ=M+M3-1
      IF(D(NZ,MZ) .LT. GD(N ,M ))D(NZ,MZ)=0.0
  680 CONTINUE
  681 CONTINUE
C
C     ....OPTIONAL PRINTOUT OF DEPTH GRID....
      IF(IOUT1 .EQ. 0) GO TO 701
      K6=N4/20
      IN1=1
      IN2=20
      IF(N4 .LT. 20) IN2=N4
      WRITE(6,555)
  555 FORMAT(/////* START PRINTOUT OF DEPTH GRID*)
      DO 690 IK=1,K6
      WRITE (6,565) (K,K=IN1,IN2)
  565 FORMAT(1H1,20I6/)
      DO 689 M=1,N3
      WRITE(6,575)(D(N,M),N=IN1,IN2)
  689 CONTINUE
  575 FORMAT(1X,20F6.0)
C
      IN1=IN2+1
  690 IN2=IN2+20
      IF(N4 .LT. 20) GO TO 701
      IF((N4-20*K6) .EQ. 0) GO TO 701
      IN2=N4
      WRITE (6,565)(K,K=IN1,IN2)
      WRITE(6,585)
  585 FORMAT(1H )
      DO 700 M=1,N3
      WRITE (6,575) (D(N,M),N=IN1,IN2)
  700 CONTINUE
  701 CONTINUE
C
C     ....SET UP CODED GRID....
      DO 710 M=1,N3
      DO 710 N=1,N4
      ICODE(N,M)=0
      IF(D(N,M) .GE. 5.0) ICODE(N,M)=1
  710 CONTINUE
  711 CONTINUE
C
C     ....OPTIONAL PRINTOUT OF CODED ARRAY AND GROUND MOTION....
      IF(IOUT2 .EQ. 0) GO TO 761
      K6=N4/60
      IN1=1
      IN2=60
      WRITE(6,705)
  705 FORMAT(/////* START PRINTOUT OF CODED ARRAY*)
      IF (K6 .EQ. 0) GO TO 730
      DO 720 IK=1,K6
      WRITE (6,715)IN1,IN2
  715 FORMAT(1H1,5X,*RANGE OF N --*,I3,* TO *,I3)
      WRITE (6,725)((ICODE(N,M),N=IN1,IN2),M=1,N3)
  725 FORMAT(1X,60I2)
      IN1=IN2+1
  720 IN2=IN2+60
  730 IF((N4-60*K6) .EQ. 0) GO TO 750
      IN2=N4
      WRITE(6,715) IN1,IN2
      DO 740 M=1,N3
      WRITE(6,725)(ICODE(N,M),N=IN1,IN2)
  740 CONTINUE
C
C     ....OPTIONAL PRINTOUT OF GROUND MOTION....
  750 IF(IGMC .EQ. -1) GO TO 761
      NN=M2-M1+1
      MM=M4-M3+1
      WRITE(6,735)
  735 FORMAT(1H1,* START PRINTOUT OF GROUND MOTION*///)
      DO 760 M=1,MM
      WRITE(6,745) (GD(N,M),N=1,NN)
  745 FORMAT(1X,43F3.0)
  760 CONTINUE
  761 CONTINUE
      CALL WHATDT(D,NDM,MDM)
      IF(NGRID .EQ. 1) CALL EXIT
C
C     ....SET UP ARRAYS GOVERNING COMPUTATION....
      CALL TABLE(ICODE,NDM,MDM)
C
C     ....COMPLETE READING OF INPUT DATA....
      READ(5,45) DT,TMAX, TCHT,DTN
      READ(5,25) NPTS,NPTINC,IBNDRY
      READ(5,25) NPRINT
      IF(NPTS .EQ. 0) GO TO 770
      READ(5,25)(NPOI(I),I=1,NPTS)
      READ(5,25)(MPOT(I),I=1,NPTS)
  770 CONTINUE
      IF(IBNDRY    .EQ. 0) GO TO 810
C
C     ....HERE TO READ INPUT FOR A TIME DEPENDENT BOUNDARY CONDITION....
      READ(5,65) NVAL,IREFL,TINIT,DELT,AMPL,PERI,XIP,YIP,WANGLE,DEXT
      IF(IBNDRY    .EQ.-1) GO TO 790
      READ(5,55)(VAL(I),I=1,NVAL)
      TVAL(1)=TINIT
      DO 780 I=2,NVAL
  780 TVAL(I)=(I-1)*DELT+TINIT
      GO TO 810
C
C     ...HERE TO SET UP BUILT-IN SINUSOIDAL FUNCTION FOR TIME DEPENDENT
C        BOUNDARY CONDITION....
  790 TVAL(1)=TINIT
      VAL(1)=0.0
      DO 800 I=2,NVAL
      TVAL(I)=TVAL(I-1)+DELT
  800 VAL(I)=AMPL*SIN(2.*PI*TVAL(I)/PERI)
  810 CONTINUE
C
C        ....READ TRANSIENT UPLIFT DATA IF REQUIRED....
         IF (IGMC .NE. 3  ) GO TO 811
         READ(5,25) NTRANS
         READ(5,55) (TRANS(I),I=1,NTRANS)
  811 CONTINUE
C
C
C        ....SAVE INPUT PARAMETERS ON TAPE9 IF REQUESTED....
         IF(NTAPE .EQ. 0) GO TO 768
         WRITE(9)      NTSU
         WRITE(9)      ID
         WRITE(9)      NDM,MDM,NPTS,NPTINC,DT,TMAX,NTAPE
         WRITE(9)         THETN,THETCHG,THETS,DTHET1,DTHET2,PHIW,PHIE,DPHI
         WRITE(9)     (NPOT(I),I=1,NPTS)
         WRITE(9)     (MPOT(I),I=1,NPTS)
         IF(NTAPE .LT. 2) GO TO 768
C        ....SAVE CONTOUR INFO FOR INITIAL CONDITION....
         WRITE(9)      NCTR
         WRITE(9)      T
         WRITE(9)     ((SE(N,M),N=1,NDM),M=1,MDM)
  768 CONTINUE
C
C        ....PRINT OUT REST OF INPUT DATA....
         WRITE(6,35)ID
         IF(ICOORD .EQ.1) WRITE(6,805) ANGLT,CINIT,CINPUT,XSTR,YSTR
  805 FORMAT(///5X,*ANGLT,CINIT,CINPUT,XSTR,YSTR*//5X,6G13.5)
         IF(IGMC .GT. 0) WRITE(6,815) TAUP,VELP,XZERO,YZERO
  815 FORMAT(///5X,*TAUP,VELP,XZERO,YZERO*//5X,4G13.5)
         IF(IGMC .EQ.3) WRITE(6,825) NTRANS,(TRANS(I),I=1,NTRANS)
  825 FORMAT(///5X,*TRANSIENT UPLIFT*/*5X,ANTRANS = *,I5,5X,*,  TRANS(I)
     1 . . . .*/5X,/6F5.2)
         WRITE(6,835) DT,TMAX, TCHT,DTN
  835 FORMAT(///5X,*DT,TMAX, TCHT,DTN*//5X,4G13.5)
         WRITE(6,845) NPTS,NPTINC,IBNDRY
  845 FORMAT(///5X,*NPTS,NPTINC,IBNDRY*//5X,16I5)
         WRITE(6,855) NPRINT
  855 FORMAT(///5X,*NPRINT ARRAY*,//5X,16I5/5X,16I5)
         IF(NPTS .LE. 0) GO TO 820
         WRITE(6,865)(NPOT(I),I=1,NPTS)
  865 FORMAT(///5X,*NPOT ARRAY*/(5X,24I5))
         WRITE(6,875)(MPOT(I),I=1,NPTS)
  875 FORMAT(//5X,*MPOT ARRAY*/(5X,24I5))
  820 CONTINUE
         IF(IBNDRY     .EQ. 0) GO TO 830
         WRITE(6,885) NVAL,IREFL,TINIT,DELT,AMPL,PERI
  885 FORMAT(///5X,*WAVE ELEVATION TIME HISTORY GIVEN AT ONE BOUNDARY*/,
     1 5X,*NVAL,IREFL,TINIT,DELT,AMPL,PERI*//5X,2I6,5X,4G13.5)
         IF(DEXT .NE. 0.) WRITE(6,895) XIP,YIP,WANGLE,DEXT
  895 FORMAT(/5X,* XIP,YIP,WANGLE,DEXT*/5X,4G13.5)
         WANGLE = WANGLE*RAD
         XIP = XIP*RAD
         YIP = YIP*RAD
  830 CONTINUE
C
C        ....GENERATE CONSTANTS....
         GO TO (840,850),ICOORD
C
C            IN RECTANGULAR COORDINATES
```

```
  840 CONTINUE
      GO TO 881
C
C         IN SPHERICAL COORDINATES
  850 DTHET1=DTHET1*RAD
      DTHET2=DTHET2*RAD
      DPHI=DPHI*RAD
      THETCHG=THETCHG*RAD
      THETN=THETN*RAD
      PHIW=PHIW*RAD
      THETS = THETS*RAD
      PHIE = PHIE*RAD
C
C     ....SET UP SPATIAL STEPS AND CORIOLIS PARAMETERS....
      DTH=DTHET1
      SUM=THETN
      II=1
      DO 880 I=1,MDM
      IF(I-N2) 870,860,870
  860 II=I
      SUM=SUM + (I-1)*DTH
      DTH=DTHET2
  870 ARG=(I-II)*DTH + SUM
      SN(I)= SIN(ARG)
      SNPHALF(I)=SIN(ARG+.5*DTH)
      SNMHALF(I)=SIN(ARG-.5*DTH)
  880 F(I)=2.*7.29E-05*COS(ARG)
  881 CONTINUE
C
C     ....INITIALIZE ARRAYS....
      DO 883 M=1,MDM
      DO 883 N=1,NDM
      SE(N,M) =0.
      U(N,M)  =0.
  883 V(N,M)  =0.
C
C     ....SET INITIAL WATER SURFACE ELEVATION....
      IF(IGMC .EQ. 0 .OR. IGMC .EQ. -2) 884,990
  884 NN=M2-M1+1
      MM=M4-M3+1
      DO 886 M=1,MM
      MZ=M+M3-1
      DO 886 N=1,NN
      NZ=N+M1-1
      IF(D(NZ,MZ) .LE. 0.) GO TO 886
      SE(NZ,MZ) = SE(NZ,MZ) + GD(N,M)
  886 CONTINUE
C     TRIM SUBSET BOUNDS
  900 SMAX=0.
      NT=NINCMP+1
      DO 910 M=MINCMP,MAXCMP
  910 SMAX=AMAX1(SMAX,ABS(SE(NT,M)))
      IF(SMAX .GT. BND) GO TO 920
      NINCMP=NINCMP+1
      GO TO 900
  920 SMAX=0.
      NT=NAXCMP-1
      DO 930 M=MINCMP,MAXCMP
  930 SMAX=AMAX1(SMAX,ABS(SE(NT,M)))
      IF(SMAX .GT. BND) GO TO 940
      NAXCMP=NAXCMP-1
      GO TO 920
  940 SMAX=0.
      MT=MINCMP+1
      DO 950 N=NINCMP,NAXCMP
  950 SMAX=AMAX1(SMAX,ABS(SE(N,MT)))
      IF(SMAX .GT. BND) GO TO 960
      MINCMP=MINCMP+1
      GO TO 940
  960 SMAX=0.
      MT=MAXCMP-1
      DO 970 N=NINCMP,NAXCMP
  970 SMAX=AMAX1(SMAX,ABS(SE(N,MT)))
      IF(SMAX .GT. BND) GO TO 980
      MAXCMP=MAXCMP-1
      GO TO 960
  980 WRITE(6,985) NINCMP,NAXCMP,MINCMP,MAXCMP
  985 FORMAT(///10X,*SUBSET GRID IS TRIMMED TO NEW SIZE....NINCMP   NAXC
     1MP   MINCMP   MAXCMP*/48X,4(I5,4X))
C     CALCULATE AND PRINT GROUND MOTION SUMMARY
      TAREA=0.
      TVOL=0.
      PE=0.
      RHOGEE=1.025*62.4
      DO 988 M=MINCMP,MAXCMP
      TH1=THETN+(FLOAT(M)-1.5)*DTHET1
      TH2=TH1+DTHET1
      P1=COS(TH1)-COS(TH2)
      DO 988 N=NINCMP,NAXCMP
      DP=SE(N,M)
      IF(ABS(DP) .LT. 1.E-10) GO TO 988
      PH1=PHIW+(FLOAT(N)-1.5)*DPHI
      PH2=PH1+DPHI
      DP=SE(N,M)
      RI=RE-DP
      A=RI*RI*P1*(PH2-PH1)
      P2=RI*DP*(RI+DP)+.333333*DP**3
      VOL=P2*P1*(PH2-PH1)
      TAREA=TAREA+A
      TVOL=TVOL+ABS(VOL)
      PE=PE + 0.5*RHOGEE*A*DP**2
  988 CONTINUE
      AKM2=TAREA*9.295E-08
      PEERGS=PE*1.357E+07
      WRITE(6,989) TAREA,TVOL,PE,AKM2,PEERGS
  989 FORMAT(///10X,16HGROUND MOTION.../12X,19HTOTAL AREA(SQFT) = ,G12.4
     1 / 12X,41HTOTAL VOLUME OF WATER DISPLACED (CUFT) = ,G12.4
     2  / 12X,38HESTIMATED POTENTIAL ENERGY (LB.FT.) = ,G12.4
     3  ///12X,21HTOTAL AREA(SQ.KM.) = ,G12.4
     4  /12X,25HPOTENTIAL ENERGY(ERGS) = ,G12.4)
  990 CONTINUE
C
C     ...SET UP TIME VARIATION IN GROUND MOTION IF REQUIRED -- IF NOT,
C        RETURN....
      IF(IGMC .LE. 0) RETURN
      RETURN
C
C        READ FORMATS
   15 FORMAT(8A10)
   25 FORMAT(16I5)
   45 FORMAT(8E10.0)
   55 FORMAT(16F5.0)
   65 FORMAT(2I5,4F5.0,4E10.0)
  215 FORMAT(20F4.0)
      END
```

```
      SUBROUTINE WHATDT(D,NDM,MDM)
C     ROUTINE TO DETERMINE MAXIMUM POSSIBLE TIME STEP,DT
      LEVEL 2, D
      COMMON/A1/ DT,TMAX, TCHT,DTN,T,N1,N2,N3,N4,M1,M2,M3,M4,K1,K2,K3,K4
     1, THETN,THETCHG,THETS,DTHET1,DTHET2,PHIW,PHIE,DPHI,ITIME,NCOUNT
     2, IGMC,IXOUT,BND,PI,RAD,TADD,RE,TAUP,VELP,XZERO,YZERO,CINIT,CINPUT
     3, XSTR,YSTR,NPTS,NPTINC,NPRINT(32),NTRANS,TRANS(20),G
     4, NCNT,NGRID,IPLOT,ICOORD,IOUT1,IOUT2,NCOR1,NCOR2,SDT,ISKP,IP,JP
     5, MAXCMP,MINCMP,NAXCMP,NINCMP,CONV,DC1,DC2,DEPMIN,ITAB
      DIMENSION D(NDM,MDM)
      DTM=999.
      DTHET=DTHET1
      JM=1
      DO 500 M=1,N3
      THET=(M-1)*DTHET1+THETN
      IF(M .LE. N2) GO TO 100
      THET=THETCHG+(M-N2)*DTHET2
      DTHET=DTHET2
  100 CONTINUE
      A=DTHET*RAD
      B=DPHI*RAD*SIN(THET*RAD)
      COUR=(RE*A*B)/SQRT(A**2+B**2)
      NN=1
      DMAX=D(1,M)
      DO 200 N=1,N4
      DD=D(N,M)
      MSK=SHIFT(DMAX-DD,-60)
      DMAX=(DD.AND.MSK).OR.(DMAX.AND..NOT.MSK)
  200 NN=(N.AND.MSK).OR.(NN.AND..NOT.MSK)
      IF(DMAX .LE. .001) GO TO 500
      DTX=COUR/SQRT(G*DMAX)
      MSK=SHIFT(DTX-DTM,-60)
      DTM=(DTX.AND.MSK).OR.(DTM.AND..NOT.MSK)
      JN=(NN.AND.MSK).OR.(JN.AND..NOT.MSK)
      JM=(M.AND.MSK).OR.(JM.AND..NOT.MSK)
  500 CONTINUE
      WRITE(6,505) DTM,JN,JM,D(JN,JM)
  505 FORMAT(//10X,32HMAXIMUM PERMISSIBLE TIME STEP = ,F10.4,8H SECONDS,
     1 32H , AT CONSTRAINING POINT...N = ,I3,7H    M = ,I3,3X,4HD = ,
     2  G14.3)
      RETURN
      END
      SUBROUTINE WARP
C     ...ROUTINE TO SET UP GROUND MOTION SPECIFIED BY COORDINATES OF
C     CENTER,AXES, ORIENTATION, SHAPE AND AMPLITUDE
      COMMON/A1/ DT,IMAX, TCHT,DTN,T,N1,N2,N3,N4,M1,M2,M3,M4,K1,K2,K3,K4
     1, THETN,THETCHG,THETS,DTHET1,DTHET2,PHIW,PHIE,DPHI,ITIME,NCOUNT
     2, IGMC,IXOUT,BND,PI,RAD,TADD,RE,TAUP,VELP,XZERO,YZERO,CINIT,CINPUT
     3, XSTR,YSTR,NPTS,NPTINC,NPRINT(32),NTRANS,TRANS(20),G
     4, NCNT,NGRID,IPLOT,ICOORD,IOUT1,IOUT2,NCOR1,NCOR2,SDT,ISKP,IP,JP
     5, MAXCMP,MINCMP,NAXCMP,NINCMP,CONV,DC1,DC2,DEPMIN,ITAB
      LEVEL 2, GD
      COMMON /L10/GD(50,50)
      READ(5,15) CLAT,CLONG,HEAD,AXMAJ,AXMIN,MTYPE,PEAK
   15 FORMAT(5E10.0,I10,E10.0)
      WRITE(6,25) CLAT,CLONG,HEAD,AXMAJ,AXMIN,MTYPE,PEAK
   25 FORMAT(//10X,*ANALYTICALLY SPECIFIED GROUND MOTION IS DESCRIBED BY
     1 FOLLOWING VARIABLES...*/14X, 4HCLAT,9X,5HCLONG,9X,4HHEAD,8X
     2, 5HAXMAJ,7X,5HAXMIN,5X,5HMTYPE,3X,4HPEAK/10X,5G13.5,I5,G13.5)
      DEG=180./3.14159
      HEAD=HEAD*RAD
C     CONVERT MAJOR AND MINOR AXES TO SEMI-MAJOR AND SEMI-MINOR RESPECTIVELY
      AXMAJ=AXMAJ/2.
      AXMIN=AXMIN/2.
      DLONG=(AXMAJ*ABS(COS(HEAD))+AXMIN*ABS(SIN(HEAD)))*6080./
     1     (RE*SIN(CLAT*RAD))
      DLAT=(AXMAJ*ABS(SIN(HEAD))+AXMIN*ABS(COS(HEAD)))*6080./RE
      XLAT=CLAT-DLAT*DEG
      SLAT=CLAT+DLAT*DEG
      WLONG=CLONG-DLONG*DEG
      ELONG=CLONG+DLONG*DEG
      M1=(WLONG-PHIW)/DPHI
      M2=(ELONG-PHIW)/DPHI  + 2.5
      M3=(XLAT-THETN)/DTHET1
      M4=(SLAT-THETN)/DTHET1 + 2.5
      M1=MAX0(1,M1)
      M2=MIN0(N4,M2)
      M3=MAX0(1,M3)
      M4=MIN0(N3,M4)
      NINCMP=M1-1
      NAXCMP=M2+1
      MINCMP=M3-1
      MAXCMP=M4+1
      NINCMP=MAX0(1,NINCMP)
      NAXCMP=MIN0(N4,NAXCMP)
      MINCMP=MAX0(1,MINCMP)
      MAXCMP=MIN0(N3,MAXCMP)
      WRITE(6,45) M1,M2,M3,M4
   45 FORMAT(/11X,*COMPUTED BOUNDS OF GROUND MOTION GRID...M1   M2   M3
     1  M4*/48X,4I5/)
      NN=M2-M1+1
      MM=M4-M3+1
      IF(NN .LE. 50. .AND.MM .LE. 50) GO TO 58
      WRITE(6,55)
   55 FORMAT(///10X,*A COMPUTED DIMENSION EXCEEDS AVAILABLE SPACE IN ARR
     1AY GD...CALL EXIT*)
      CALL EXIT
   58 CONTINUE
      DO 60 M=1,MM
      DO 60 N=1,NN
   60 GD(N,M)=0.
      C1=PEAK*9.0/(AXMIN*6080.)
      C2=9.0/(AXMIN*6080.)
      C3=2.2/(AXMAJ*6080.)
      CLAT=CLAT*RAD
      CLONG=CLONG*RAD
      DO 100 M=1,MM
      DO 100 N=1,NN
C     DETERMINE COORDINATE XP AND YP IN X-PRIME,Y-PRIME SYSTEM
C     OMEGA IS INCLUDED ANGLE BETWEEN XP-YP ORIGIN AND GRID POINT
      PLT=(THETN+(M3+M-2)*DTHET1)*RAD
      PLG=(PHIW+(M1+N-2)*DPHI )*RAD
      SNCLAT=SIN(CLAT)
      SNPLT=SIN(PLT)
      CSCLAT=COS(CLAT)
      CSPLT=COS(PLT)
      OMEGA=0.
      GAMMA=0.
      OMEGA=ACOS(SNCLAT*SNPLT*COS(CLONG-PLG)+CSCLAT*CSPLT)
      IF(ABS(OMEGA) .LT. .0000001) GO TO 80
C     GAMMA IS BEARING (W/R TO TRUE NORTH) OF POINT FROM XPYP SYSTEM
      SNOMGA=SIN(OMEGA)
      SNGMA=(SNPLT*SIN(PLG-CLONG))/SNOMGA
      CSGMA=(SNCLAT*CSPLT-CSCLAT*SNPLT*COS(CLONG-PLG))/SNOMGA
      IF(SNGMA .EQ. 0. .AND. CSGMA .EQ. 0.) GO TO 80
      GAMMA=ATAN2(SNGMA,CSGMA)
   80 GAMMAR=GAMMA-HEAD
      DIST=RE*OMEGA
      XP=DIST*COS(GAMMAR)
      ARG=-DIST*ABS(COS(GAMMAR))*C2-(C3*DIST*SIN(GAMMAR))**2 + 1
      EXP1=0.
      IF(ARG .GT. -10.) EXP1=EXP(ARG)
      GD(N,M)=C1*DIST*COS(GAMMAR)*EXP1
      IF(MTYPE)92,100,96
   92 IF(XP .GT. 0.) GD(N,M)=0.
      GO TO 100
   96 IF(XP .LT. 0.) GD(N,M)=0.
  100 CONTINUE
      WRITE(6,999)
  999 FORMAT(* WARP COMPLETED*)
      RETURN
      END
      SUBROUTINE TABLE(ICODE,NDM,MDM)
C     ...CALLED FROM SUBROUTINE INITIAL--COMPUTES ARRAYS GOVERNING
C        CALCULATIONS....
C
      COMMON/A1/ DT,TMAX, TCHT,DTN,T,N1,N2,N3,N4,M1,M2,M3,M4,K1,K2,K3,K4
     1, THETN,THETCHG,THETS,DTHET1,DTHET2,PHIW,PHIE,DPHI,ITIME,NCOUNT
     2, IGMC,IXOUT,BND,PI,RAD,TADD,RE,TAUP,VELP,XZERO,YZERO,CINIT,CINPUT
     3, XSTR,YSTR,NPTS,NPTINC,NPRINT(30),NTRANS,TRANS(20),G
     4, NCNT,NGRID,IPLOT,ICOORD,IOUT1,IOUT2,NCOR1,NCOR2,SDT,ISKP,IP,JP
     5, MAXCMP,MINCMP,NAXCMP,NINCMP,CONV,DC1,DC2,DERMIN,ITAB
      COMMON     SN(131),SNPHALF(131),SNMHALF(131),F(131),MCOMP(300)
     1, MFIRST( 9,300),MLAST( 8,300),NCOMP(131),NFIRST( 7,131)
     2, NLAST( 7,131), NPOT(61),MPOT(61)
      LEVEL 2, ICODE
      DIMENSION ICODE(NDM,MDM)
      INTEGER ROUTE
C
C     ....CHECK ARRAY DIMENSIONS...
      IF(N3 .LE. 131) GO TO 400
      WRITE(6,395)
  395 FORMAT(* MCOMP DIMENSION EXCEEDED...131...CALL EXIT*)
      CALL EXIT
  400 CONTINUE
      IF(N4 .LE. 300) GO TO 420
      WRITE(6,415)
  415 FORMAT(* NCOMP DIMENSION EXCEEDED...300...CALL EXIT*)
      CALL EXIT
  420 CONTINUE
C
C     ....FOR COMPUTATIONS ALONG MERIDIANS....
      DO 70 K=1,N4
      L=0
      MCOMP(K)=0
C
C     ....FOR EACH MERIDIAN....
      DO 70 J=1,N3
C     ....SET ROUTE....
C                      ROUTE=1 --LAST POINT ON OPEN BOUNDARY
C                      ROUTE=2 --BEGIN COMPUTAIONAL LINE
C                      ROUTE=3 --END COMPUTATIONAL LINE
C                      ROUTE=4 --SINGLE POINT COMPUTATIONAL LINE
      IF(ICODE(K,J) .EQ. 0) GO TO 70
C
      IF(J .NE. 1) GO TO 2
      IF(ICODE(K,J+1) .EQ. 0) GO TO 300
      ROUTE=2
      GO TO 20
C
    2 IF(J .NE. N3) GO TO 4
      IF(ICODE(K,J-1) .EQ. 0) GO TO 300
      ROUTE=1
      GO TO 20
C
    4 IF(ICODE(K,J+1) .EQ. 1) GO TO 6
      ROUTE=4
      IF(ICODE(K,J-1) .EQ. 1) ROUTE=3
      GO TO 20
C
    6 IF(ICODE(K,J-1) .EQ. 1) GO TO 70
      ROUTE=2
```

```
   20 CONTINUE
C
      GO TO(60,30,40,50),ROUTE
C
C     ...HERE TO BEGIN A COMPUTATIONAL LINE....
   30 MCOMP(K)=MCOMP(K)+1
      L=MCOMP(K)
C     CHECK ARRAY DIMENSION
      IF(L .GT. 10) GO TO 900
      MFIRST(L,K)=J
      GO TO 70
C
C     ...HERE TO END A COMPUTATIONAL LINE....
   40 MLAST(L,K)=J
      GO TO 70
C
C     ...HERE FOR A COMPUTATIONAL LINE CONSISTING OF A SINGLE POINT...
   50 MCOMP(K)=MCOMP(K)+1
      L=MCOMP(K)
C     CHECK ARRAY DIMENSION
      IF(L .GT. 10) GO TO 900
      MFIRST(L,K)=J
      MLAST(L,K) =J
      GO TO 70
C
C     ...HERE FOR LAST POINT ON OPEN BOUNDARY....
   60 IF(J .EQ. N3   ) MLAST(L,K)=N3
C
C     ...END OF COMPUTATIONS ON MERIDIANS....
C
   70 CONTINUE
C
C     ....FOR COMPUTATIONS ALONG PARALLELS....
      DO 170 J=1,N3
      L=0
      NCOMP(J)=0
C
C     ...FOR EACH PARALLEL....
      DO 170 K=1,N4
C     ....SET ROUTE....
      IF(ICODE(K,J) .EQ. 0) GO TO 170
      IF(K .NE. 1) GO TO 102
      IF(ICODE(K+1,J) .EQ. 0) GO TO 300
      ROUTE=2
      GO TO 120
C
  102 IF(K .NE. N4) GO TO 104
      IF(ICODE(K-1,J) .EQ. 0) GO TO 300
      ROUTE=1
      GO TO 120
C
  104 IF(ICODE(K+1,J) .EQ. 1) GO TO 106
      ROUTE=4
      IF(ICODE(K-1,J) .EQ. 1) ROUTE=3
      GO TO 120
C
  106 IF(ICODE(K-1,J) .EQ. 1) GO TO 170
      ROUTE = 2
  120 CONTINUE
C
      GO TO(160,130,140,150),ROUTE
C
C     ...HERE TO BEGIN A COMPUTATIONAL LINE....
  130 NCOMP(J)=NCOMP(J)+1
      L=NCOMP(J)
C     CHECK ARRAY DIMENSION
      IF(L .GT. 10) GO TO 900
      NFIRST(L,J)=K
      GO TO 170
C
C     ...HERE TO END A COMPUTATIONAL LINE....
  140 NLAST(L,J)=K
      GO TO 170
C
C     ...HERE FOR A COMPUTATIONAL LINE CONSISTING OF A SINGLE POINT...
  150 NCOMP(J)=NCOMP(J)+1
      L=NCOMP(J)
C     CHECK ARRAY DIMENSION
      IF(L .GT. 10) GO TO 900
      NFIRST(L,J)=K
      NLAST(L,J)=K
      GO TO 170
C
C     ...HERE FOR LAST POINT ON OPEN BOUNDARY....
  160 IF(K .EQ. N4   ) NLAST(L,J)=N4
C
C     ...END OF COMPUTATIONS ON PARALLELS....
  170 CONTINUE
      IF(IOUT2 .EQ. 0) RETURN
C
C     ...HERE FOR OPTIONAL PRINTOUT OF COMPUTATIONAL ARRAYS....
      WRITE(6,15)
   15 FORMAT(1H1,5X,*COMPUTATIONAL ARRAYS FOLLOW . . . . . . . . . .*///
     1 5X,*  COMPUTATIONS ALONG MERIDIANS *//7X,*N   NCOMP   NFIRST   NL
     2AST*//)
      DO 200 I=1,NDM
      L=MCOMP(I)
      WRITE(6,25)I,L
   25 FORMAT(6X,I3,3X,I3)
      IF(L .EQ. 0) GO TO 190
      WRITE(6,35)(MFIRST(K,I),MLAST(K,I),K=1,L)
   35 FORMAT(20X,I3,5X,I3)
      GO TO 200
  190 WRITE(6,55)
   55 FORMAT(/)
  200 CONTINUE
      WRITE(6,45)
   45 FORMAT(1H1,5X,*COMPUTATIONS ALONG PARALLELS*//5X,*M   NCOMP   NFIR
     1ST   NLAST*//)
      DO 220 I=1,MDM
      L=NCOMP(I)
      WRITE(6,25)I,L
      IF(L .EQ. 0) GO TO 210
      WRITE(6,35)(NFIRST(K,I),NLAST(K,I),K=1,L)
      GO TO 220
  210 WRITE(6,55)
  220 CONTINUE
      RETURN
  300 CONTINUE
C       ....HERE FOR ILLEGAL GEOMETRY
        WRITE(6,305) K,J
  305 FORMAT(* ILLEGAL GRID BOUNDARY GEOMETRY....K= *,I5,*  J= *,I5/
     1  * CALL EXIT*)
        CALL EXIT
  900 CONTINUE
        WRITE(6,905)
  905 FORMAT(* ARRAY DIMENSION EXCEEDED...TOO MANY COMP. LINES ON ONE ME
     1RIDIAN OR PARALLEL. CALL EXIT*)
        CALL EXIT
        END
```

```
        SUBROUTINE SPECP(ND,MD,SE)
C       ....SUBPROGRAM TO SAVE WAVE ELEVATIONS AT SPECIAL POINTS....
        DIMENSION SE(ND,MD)
        COMMON/A1/ DT,IMAX, TCHT,DTV,T,N1,N2,N3,N4,M1,M2,M3,M4,K1,K2,K3,K4
     1, THETN,THETCHG,THETS,DTHET1,DTHET2,PHIW,PHIE,DPHI,ITIME,NCOUNT
     2, IGMC,IXCUT,BND,PI,RAD,TADD,RE,TAUP,VELP,XZERO,YZERO,CINIT,CINPUT
     3, XSTR,YSTR,NPTS,NPTINC,NPRINT(32),NTRANS,TRANS(20),G
     4, NCNT,NGRID,IPLOT,ICOORD,IOUT1,IOUT2,NCOR1,NCOR2,SDT,ISKP,IP,JP
     5, MAXCMP,MINCMP,NAXCMP,NINCMP,CONV,DC1,DC2,DEPMIN,ITAB
        COMMON    SN(131),SNPHALF(131),SNMHALF(131),F(131),MCOMP(300)
     1, MFIRST( 8,300),MLAST( 8,300),NCOMP(131),NFIRST( 7,131)
     2, NLAST( 7,131), NPOT(61),MPOT(61)
        LEVEL 2, PTAB
        COMMON/A4/PTAB(451,62)
        DO 4 I=1,NPTS
        K=NPOT(I)
        L=MPOT(I)
    4 PTAB(NCNT,I)=SE(K,L)
        PTAB(NCNT,NPTS+1)=T
        RETURN
        END
```

```
      SUBROUTINE EQUATS(NDM,MDM,SE,U,V,D)
C     ---VERSION 2----
C     ----THIS DECK IS FOR CDC CYBER 76----
C     ....PROGRAM TO SOLVE THE LONG WAVE EQUATIONS IN SPHERICAL
C         COORDINATES FOR A TSUNAMI PROPAGATING OVER AN OCEAN....
      LEVEL 2, U,V
      DIMENSION D(NDM,MDM),SE(NDM,MDM),U(NDM,MDM),V(NDM,MDM)
      COMMON/A1/ DT,TMAX, TCHT,DTN,T,N1,N2,N3,N4,M1,M2,M3,M4,K1,K2,K3,K4
     1, THEIN,THETCHG,THETS,DTHET1,DTHET2,PHIW,PHIE,DPHI,ITIME,NCOUNT
     2, IGMC,IXOUT,BND,PI,RAD,TADD,RE,TAUP,VELP,XZERO,YZERO,CINIT,CINPUT
     3, XSTR,YSTR,NPTS,NPTINC,NPRINT(32),NTRANS,TRANS(20),G
     4, NCNT,NGRID,IPLOT,ICOORD,IOUT1,IOUT2,NCOR1,NCOR2,SDT,ISKP,IP,JP
     5, MAXCMP,MINCMP,NAXCMP,NINCMP,CONV,DC1,DC2,DEPMIN,ITAB
      COMMON    SN(131),SNPHALF(131),SNMHALF(131),F(131),MCOMP(300)
     1, MFIRST( 8,300),MLAST( 8,300),NCOMP(131),NFIRST( 7,131)
     2, NLAST( 7,131), NPOT(61),MPOT(61)
      COMMON/A5/ TVAL(001),VAL(001),PERI,AMPL,TINIT,IBNDRY
     1, XIP,YIP,WANGLE,DEXT,DELT
      COMMON/TAPES/ NTAPE,NTSU,NCTR,INCTR
      DIMENSION SESAV(300)
      DATA LEAP/0/
      XODT=IXOUT*DT
      IF(LEAP .GE. 1) GO TO 90
C
C     ....INITIALIZE CONSTANTS....
      C2=DT/(2.*RE*DPHI)
      C3=2.*G*C2
      C4=DT/(2.*RE*DTHET1)
      C5=2.*G*C4
      C5A=C5*DTHET1/DTHET2
      C6 = 2.*C4
      C16=DT/(RE*DTHET2)
      C7 = 2.*C2
      ETACHK=0.
      ONEMBN=1.-BND
      ONEPBN=1.+BND
      LEAP=1
C
C     ....CALL ROUTINE WHICH REGULATES SIZE OF COMPUTATIONAL SUBSET....
   90 CALL SHRINK(SE,NDM,MDM)
C
C     ....COMPUTE U-VELOCITIES MERIDIAN BY MERIDIAN....
      DO 200 K=1,N4
      IF(MCOMP(K) .EQ. 0 .OR. K .LT. NINCMP .OR. K .GT. NAXCMP)GO TO 200
      NCALC=MCOMP(K)
      DO 190 I=1,NCALC
      MA=MFIRST(I,K)
      MB=MLAST(I,K)
      IF(MINCMP .GT. MB .OR. MAXCMP .LT. MA) GO TO 190
      MA=MAX0(MA+1,MINCMP)
      MB=MIN0(MB,MAXCMP)
      DO 140 J=MA,MB
      C5P=C5
      IF(J .GT. N2)C5P=C5A
  140 U(K,J) = U(K,J) -C5P*(SE(K,J)-SE(K,J-1)) + XODT*F(J)*V(K,J)
  190 CONTINUE
  200 CONTINUE
C
C     ....COMPUTE V-VELOCITIES PARALLEL BY PARALLEL....
      DO 400 J=1,N3
      IF(NCOMP(J) .EQ. 0 .OR. J .LT. MINCMP .OR. J .GT. MAXCMP)GO TO 400
      NCALC=NCOMP(J)
      SINJ=SN(J)
      XODTF=XODT*F(J)
      C9=C3/SINJ
      DO 390 I=1,NCALC
      NA=NFIRST(I,J)
      NB=NLAST(I,J)
      IF(MINCMP .GT. NB .OR. MAXCMP .LT. NA) GO TO 390
      NA=MAX0(NA+1,MINCMP)
      NB=MIN0(NB,MAXCMP)
      DO 340 K=NA,NB
  340 V(K,J)=V(K,J)-C9*(SE(K,J)-SE(K-1,J))      - XODTF     *U(K,J)
  390 CONTINUE
  400 CONTINUE
C     ...VELOCITY CALCULATIONS COMPLETED...
C
C     ....BEGIN COMPUTATION OF SURFACE ELEVATIONS....
      N3M1=N3-1
      DO 403 K=1,N4
  403 SESAV(K)=SE(K,N3M1)
      DO 600 J=1,N3
      IF(NCOMP(J) .EQ. 0 .OR. J .LT. MINCMP .OR. J .GT. MAXCMP)GO TO 600
      NCALC=NCOMP(J)
      SINJ=SN(J)
      SNJPH=SNPHALF(J)
      SNJMH=SNMHALF(J)
      IF(J .LE. N2) GO TO 410
C     ....SET CONSTANT FOR CHANGE IN DELTA THETA....
      C4=C4*DTHET1/DTHET2
      C5=2.*G*C4
  410 CONTINUE
      DO 590 I=1,NCALC
      NA=NFIRST(I,J)
      NB=NLAST(I,J)
      IF(MINCMP .GT. NB .OR. MAXCMP .LT. NA) GO TO 590
      NA=MAX0(NA,MINCMP)
      NB=MIN0(NB,MAXCMP)
      IF(J .NE. 1) GO TO 440
C     ....HERE FOR NORTHERN PARALLEL....
      DO 430 K=NA,NB
      SEK1=SE(K,1)
  430 SE(K,1) = SEK1     + C6*SQRT(G*D(K,1))*(SE(K,2)-SEK1    )
      GO TO 580
  440 IF(J .NE. N3) GO TO 480
C     ....HERE FOR SOUTHERN PARALLEL....
      C6P=C6
      IF(J .GT. N2) C6P=C16
      DO 460 K=NA,NB
      SEKJ=SE(K,J)
  460 SE(K,J)=SEKJ  +C6P*SQRT(G*D(K,J))*(SESAV(K) -SEKJ   )
      GO TO 580
C
C     ....HERE FOR INTERIOR PARALLELS....
  480 IF(NA .GT. 1) GO TO 485
C     ....HERE FOR WESTERN BOUNDARY....
      SE1J=SE(1,J)
    - SE(1,J) = SE1J     + C7*SQRT(G*D(1,J))*(SE(2,J)-SE1J    )/SINJ
      NA=NA+1
  485 IF(NB .LT. N4) GO TO 490
```

```
C        ....HERE FOR EASTERN BOUNDARY
         K=NB
         SEKJ=SE(K,J)
         SE(K,J) = SEKJ      + C7*SQRT(G*D(K,J))*(SE(K-1,J)-SEKJ     )/SINJ
         NB=NB-1
     490 C14=C4/SINJ
         C12=C2/SINJ
         JP1=J+1
         JM1=J-1
         DO 550 K=NA,NB
         KP1=K+1
         DKJ=D(K,J)
     550 SE(K,J) = SE(K,J) -C14*(U(K,JP1)*(D(K,JP1)+DKJ     )*SNJPH
        1         -U(K,J)*(DKJ     +D(K,JM1))*SNJMH)
        2        -C12*(V(KP1,J)*(D(KP1,J)+DKJ     )
        3         -V(K,J)*(DKJ     +D(K-1,J)))
     580 DO 585 K=NA,NB
         ABSEKJ=ABS(SE(K,J))
         IJK=AMIN1(ABSEKJ+ONEMBN,ONEPBN)
         SE(K,J)=IJK*SE(K,J)
     585 ETACHK=AMAX1(ETACHK,ABSEKJ)
         IF(ETACHK .LT. 200.) GO TO 590
         DO 587 K=NA,NB
         IF(ETACHK-ABS(SE(K,J)) .LT.  .001) GO TO 9000
     587 CONTINUE
     590 CONTINUE
     600 CONTINUE
C        ....END OF SURFACE ELEVATION STEP....
C
C        ....SAVE CONTOUR INFO ON TAPE9, IF REQUESTED
         IF(NTAPE .LT. 2) GO TO 690
         IF(MOD(ITIME,INCTR) .NE. 0) GO TO 690
         WRITE(9,665) T
     665 FORMAT(F10.2)
         WRITE(9,675)((SE(N,M),N=1,NDM),M=1,MDM)
     675 FORMAT(10F10.6)
     690 CONTINUE
C
         RETURN
    9000 WRITE(6,9005) I,K,J,SE(K,J)
    9005 FORMAT(/* INSTABILITY DEVELOPING. . . .*/* AT T = *,F10.2,
       1 *,  SE(*,I3,*,*,I3,*) = *,G12.4/* CALL EXIT*)
         CALL EXIT
         END
```

```
      SUBROUTINE SHRINK(SE,NDM,MDM)
C     SUBROUTINE TO COMPRESS COMPUTATIONAL GRID TO SMALLER SUBSET IN
C     ORDER TO AVOID COMPUTING AT GRID POINTS THAT THE WAVE HAS NOT REACHED
C     AND THUS REDUCE RUNNING TIME.
C       -OPERATES BY SELECTING (ON THE FIRST CALL FROM SEAWAVE) AN INITIAL
C        SUBSET OF THE COMPUTATIONAL GRID COINCIDENT WITH THE GROUND MOTION
C        GRID.
C       -ON SUBSEQUENT CALLS FROM SEAWAVE, MOVE OUT SUBSET GRID BOUNDARIES
C        ACCORDING TO PROPAGATION SPEEDS OF WAVE WITHIN SUBSET.  TEST TO MAKE
C        SURE THAT WAVE AMPLITUDE ON NEW BOUNDARIES IS EVERYWHERE LESS
C        THAN * BND *, IF NOT, MOVE OFFENDING BOUNDARY OUT.  BOUNDS OF
C        SUBSET ARE RETURNED IN VARIABLES MAXCMP, MINCMP,NAXCMP,NINCMP.
      DIMENSION SE(NDM,MDM)
      COMMON/A1/ DT,IMAX, TCHT,DTN,T,N1,N2,N3,N4,M1,M2,M3,M4,K1,K2,K3,K4
     1, THEIN,THEICHG,THETS,DTHET1,DTHET2,PHIW,PHIE,DPHI,ITIME,NCOUNT
     2, IGMC,IXOUT,BND,PI,RAD,TADD,RE,TAUP,VELP,XZERO,YZERO,CINIT,CINPUT
     3, XSTR,YSTR,NPTS,NPTINC,NPRINT(32),NTRANS,TRANS(20),G
     4, NCNT,NGRID,IPLOT,ICOORD,IOUT1,IOUT2,NCOR1,NCOR2,SDT,ISKP,IP,JP
     5, MAXCMP,MINCMP,NAXCMP,NINCMP,CONV,DC1,DC2,DEPMIN,ITAB
C
C     TEST SURFACE ELEVATIONS ON SUBSET BOUNDARIES.  MOVE BOUNDARIES
C     OUT UNTIL SE IS EVERYWHERE LESS THAN BND.
C
C     AT NORTHERN BOUNDARY
  200 IF(MINCMP .LE. N1) GO TO 230
  210 DO 220 N = NINCMP,NAXCMP
      IF(ABS(SE(N,MINCMP)) .GT. BND  ) GO TO 225
  220 CONTINUE
      GO TO 230
  225 MINCMP = MINCMP - 1
      GO TO 210
C
C     AT SOUTHERN BOUNDARY
  230 IF(MAXCMP .GE. N3) GO TO 250
      DO 235 N = NINCMP,NAXCMP
      IF(ABS(SE(N,MAXCMP)) .GT. BND  ) GO TO 240
  235 CONTINUE
      GO TO 250
  240 MAXCMP = MAXCMP +1
      GO TO 230
C
C     AT WESTERN BOUNDARY
  250 IF(NINCMP .LE. N1) GO TO 270
      DO 255 M = MINCMP,MAXCMP
      IF(ABS(SE(NINCMP,M)) .GT. BND  ) GO TO 260
  255 CONTINUE
      GO TO 270
  260 NINCMP = NINCMP - 1
      GO TO 250
C
C     AT EASTERN BOUNDARY
  270 IF(NAXCMP .GE. N4) GO TO 290
      DO 275 M = MINCMP,MAXCMP
      IF(ABS(SE(NAXCMP,M)) .GT. BND  ) GO TO 280
  275 CONTINUE
      GO TO 290
  280 NAXCMP = NAXCMP + 1
      GO TO 270
  290 CONTINUE
C
      RETURN
      END
      SUBROUTINE PRTPLT
C     SUBPROGRAM TO HANDLE PRINTER PLOTTING OF SPECIAL POINT WAVE
C     ELEVATIONS  VERSUS TIME
      COMMON/A1/ DT,TMAX, TCHT,DTN,T,N1,N2,N3,N4,M1,M2,M3,M4,K1,K2,K3,K4
     1, THETN,THETCHG,THETS,DTHET1,DTHET2,PHIW,PHIE,DPHI,ITIME,NCOUNT
     2, IGMC,IXOUT,BND,PI,RAD,TADD,RE,TAJP,VELP,XZERO,YZERO,CINIT,CINPUT
     3, XSTR,YSTR,NPTS,NPIINC,NPRINT(32),NTRANS,TRANS(20),G
     4, NCNT,NGRID,IPLOT,ICOORD,IOUT1,IOUT2,NCOR1,NCOR2,SDT,ISKP,IP,JP
     5, MAXCMP,MINCMP,NAXCMP,NINCMP,CONV,DC1,DC2,DEPMIN,ITAB
      COMMON    SN(131),SNPHALF(131),SNMHALF(131),F(131),MCOMP(300)
     1, MFIRST( 8,300),MLAST( 8,300),NCOMP(131),NFIRST( 7,131)
     2, NLAST( 7,131), NPOT(61),MPOT(61)
      LEVEL 2, PTAB
      COMMON/A4/PTAB(451,62)
      COMMON/A8/REL,HOUR,NDIV,NH,NVD,NLAB,INCH
      DIMENSION NT1(131),NT2(131),MBD(451),NBD(451)
      EQUIVALENCE(NT1(1),SN(1)),(NT2(1),SNPHALF(1)),(MBD(1),MFIRST(1))
     1, (NBD(1),MLAST(1))
      REAL LATPC,LATEC ,LONGPC,LONGEC
      DATA MINUS/1H-/
      DATA IPLUS/1H+/
      DATA IBLANK/1H /
      DATA IASTK/1H*/
      DATA IBAR/1HI/
      DATA IRBLNK/1R /
C     LOOP ON NUMBER OF SPECIAL POINTS
      N1=NPTS+1
      DO 100 NP=1,NPTS
      IF(IPLOT .EQ. -1) GO TO 1000
C     DETERMINE TIME AXIS
      DO 1 I=1,NCNT
      K=I
      IF (ABS(PTAB(I,NP)) .GT. 1.0E-03) GO TO 2
    1 CONTINUE
      GO TO 100
    2 IF (HOUR .GT. 0.0) GO TO 3
      MINN=PTAB(K,N1)/NDIV
      MAXX=PTAB(NCNT,N1)/NDIV
      GO TO 4
    3 MINN=PTAB(K,N1)/3600.
      MAXX=PTAB(NCNT,N1)/3600.
    4 MAXX=MAXX+1
      NDIF=MAXX-MINN
      IDEL=NH/NDIF
      XMIN=MINN*NDIV
C     DETERMINE Y AXIS
      YMAX=0.0
      DO 5 I=K,NCNT
      APTAB=ABS(PTAB(I,NP))
      IF (APTAB .GT. YMAX) YMAX=APTAB
      PTAB(I,NP)=PTAB(I,NP)/REL
    5 CONTINUE
      YMAX=YMAX/REL
      IF (YMAX-1.) 6,7,8
    6 IF (YMAX-.1) 9,10,11
    7 XLAB=1.
      GO TO 12
   10 XLAB=.1
      GO TO 12
    8 LAB=YMAX+.99
```

```
      XLAB=LAB
      GO TO 12
   11 LAB=(YMAX+.099)*10.
      XLAB=LAB*.1
      GO TO 12
    9 LAB=(YMAX+.0099)*100.
      IF ((LAB/2)*2 .NE. LAB) LAB=LAB+1
      XLAB=LAB*.01
   12 DELL=XLAB/NLAB
      IF (((NP/2)*2+1) .NE. NP) GO TO 1000
      WRITE (6,1001)
 1001 FORMAT (1H1)
 1000 CONTINUE
C     CALCULATE LATITUDE AND LONGITUDE
      LATPC=(THETN+DTHET1*(MPOT(NP)-1))/RAD
      LONGPC=(PHIW+DPHI*(NPOT(NP)-1))/RAD
      IF(LATPC .GT. 90.) GO TO 850
      LATEC=90.-LATPC
      ISYM1=1HN
      GO TO 860
  850 CONTINUE
      LATEC=LATPC-90.
      ISYM1=1HS
  860 IF(LONGPC .GT. 180.) GO TO 870
      LONGEC=LONGPC
      ISYM2=1HE
      GO TO 880
  870 CONTINUE
      LONGEC=360.-LONGPC
      ISYM2=1HW
  880 CONTINUE
C     PRINT INFORMATION ABOVE GRAPH
      WRITE(6,821) NPOT(NP), MPOT(NP),LATEC,ISYM1,LONGEC,ISYM2,NP
  821 FORMAT(////5X,3HN =,I4,5X,3HM =,I4,5X,6HLAT = ,F5.1,1X,A1,5X,
     1 7HLONG = ,F5.1,1X ,A1,33X,9HPLOT NO. ,I2/)
      IF(IPLOT .EQ. -1) GO TO 100
      NDIF1=NDIF+1
      DO 15 I=1,100
   15 NT1(I)=IRBLNK
      L=1
      DO 14 I=1,NDIF1
      ILAB=(MINN+I-1)*NDIV
      NT1(L)=ILAB/10000
      NT1(L+1)=ILAB/1000-10*NT1(L)
      NT1(L+2)=ILAB/100-100*NT1(L)-NT1(L+1)*10
      NT1(L+3)=ILAB/10-1000*NT1(L)-100*NT1(L+1)-10*NT1(L+2)
      NT1(L+4)=ILAB-10000*NT1(L)-1000*NT1(L+1)-100*NT1(L+2)-10*NT1(L+3)
      LLL=L+4
      DO 45 LL=L,LLL
   45 NT1(LL)=NT1(LL)+27
   14 L=L+IDEL
      IF (HOUR .LE. 0.0) GO TO 20
      WRITE (6,16) (NT1(I),I=1,100)
   16 FORMAT (7X,3HHR ,100R1)
      GO TO 21
   20 WRITE (6,22) (NT1(I),I=1,100)
   22 FORMAT (6X,4HSEC ,100R1)
 21 DO 17 I=1,NH
 17 NT1(I)=MINUS
    L=1
    DO 18 I=1,NDIF1
    NT1(L)=IPLUS
 18 L=L+IDEL
    DY=DELL/NVD
    WRITE (6,19) XLAB,(NT1(I),I=1,NH)
 19 FORMAT (3X,F6.2,1X,100A1)
    DX=NDIV
    DX=DX/IDEL
    DO 23 I=K,NCNT
    APTAB=PTAB(I,N1)
    IF (HOUR .GT. 0.0) APTAB=APTAB/3600.
    NBD(I)=(APTAB-XMIN)/DX+1.5
 23 MBD(I)=(XLAB-PTAB(1,NP))/DY+1.5
    NL2=2*NLAB
    JS=0
    DO 25 I=1,NL2
    XLA=XLAB-I*DELL
    DO 26 J=1,NVD
173 JJ=J+JS
    DO 27 L=1,NH
 27 NT2(L)=IBLANK
    DO 28 L=K,NCNT
    IF (MBD(L)-JJ) 28,29,28
 29 IT=NBD(L)
    NT2(IT)=IASTK
 28 CONTINUE
    IF (J .EQ. NVD) GO TO 30
    IF (JJ .NE. 1) GO TO 171
    WRITE (6,172) (NT2(L),L=1,NH)
172 FORMAT (1H+,9X,100A1)
    JS=1
    GO TO 173
171 NT2(1)=IBAR
    NT2(NH)=IBAR
    WRITE (6,31) (NT2(L),L=1,NH)
 31 FORMAT (10X,100A1)
 26 CONTINUE
 30 NT2(1)=IPLUS
    IF (((ABS(XLA)-.0001) .GT. 0.0).AND.(NL2.NE.I)) NT2(NH)=IPLUS
    JS=JJ
    WRITE (6,19) XLA,(NT2(L),L=1,NH)
    IF (ABS(XLA)-.0001) 32,32,250
 32 WRITE (6,35) (NT1(L),L=1,NH)
 35 FORMAT (3H+RE,7X,100A1)
250 IF (I .NE. NL2) GO TO 25
    WRITE (6,172) (NT1(L),L=1,NH)
 25 CONTINUE
100 CONTINUE
    RETURN
    END
```

```
      SUBROUTINE PRINTA (S,NDM,MDM,JLO,JHI,TP)
C     SUBPROGRAM TO HANDLE THE PRINTING OF A GRID SNAPSHOT OF WAVE
C     ELEVATIONS AS WELL AS CHECKING TO SAVE ELEVATIONS FOR LATER
C     CONTOURING
      DIMENSION I(10), IARY(120),S(NDM,MDM)
      COMMON/A1/ DT,TMAX, TCHT,DTN,T,N1,N2,N3,N4,M1,M2,M3,M4,K1,K2,K3,K4
     1, THETN,THETCHG,THETS,DTHET1,DTHET2,PHIW,PHIE,DPHI,ITIME,NCOUNT
     2, IGMC,IXOUT,BND,PI,RAD,TADD,RE,TAUP,VELP,XZERO,YZERO,CINIT,CINPUT
     3, XSTR,YSTR,NPTS,NPTINC,NPRINT(32),NTRANS,TRANS(20),G
     4, NCNT,NGRID,IPLOT,ICOORD,IOUT1,IOUT2,NCOR1,NCOR2,SDT,ISKP,IP,JP
     5, MAXCMP,MINCMP,NAXCMP,NINCMP,CONV,DC1,DC2,DEPMIN,ITAB
      COMMON/A8/REL,HOUR,NDIV,NH,NVD,NLAB,INCH
      DATA IDOT /1H./
      DATA IBLK/1H /
      DATA IATK/1H*/
      DATA MIN/1H-/
      DATA IW/1HW/
      DATA (I(LL),LL=1,10)/1H0,1H1,1H2,1H3,1H4,1H5,1H6,1H7,1H8,1H9/
C     CHECK FOR KEY TO SAVE ELEVATIONS FOR LATER CONTOURING
      IF (NPRINT(IP-1) .GE. 0) GO TO 75
      WRITE (9) TP
      WRITE(9)((S(N,M),N=1,NDM),M=1,MDM)
   75 CONTINUE
      WRITE (6,50) TP
   50 FORMAT (1H1,7H TIME =,F11.2,5H SECS, 20X,13HOUTPUT OF ETA/)
C     ---MODIFICATION TO PRINT ONLY SUBSET GRID---
      J=NINCMP
      K=NAXCMP
C     -----------------------------------------------
      I1=J-24
      I2=J-1
      I4=K-J+1
   10 IF (I4-24) 11,11,12
   12 I2=I2+24
      I4=I4-24
      IJ=1
      GO TO 13
   11 I2=K
      IJ=2
   13 I1=I1+24
      I3=I2-I1+1
      DO 18 N=I1,I2
      NN=N-I1+1
   18 IARY(NN)=N
      WRITE (6,17) (IARY(N),N=1,I3)
   17 FORMAT (7H  M   N,I4,23I5)
C     ---MODIFICATION TO PRINT ONLY SUBSET GRID---
      DO 2 M=MINCMP,MAXCMP
C                                                            MDM,1=M 2 OD
C     -----------------------------------------------
      L=1
      DO 3 N=1,120
    3 IARY(N)=IBLK
      DO 1 N=I1,I2
      A=S(N,M)
      IF (INCH .EQ. 1) A=A*12.
      B=ABS(A)
C     DETERMINE SYMBOLS TO PRINT
      IF (B .GE. 99.5) GO TO 26
      IF (B .GE. 9.55) GO TO 21
      IF (B .GE. .995) GO TO 22
      IF (B .GE. .0995) GO TO 23
      IF (B .GE. .00995) GO TO 24
      IF (B .GE. .000995) GO TO 25
      IARY(L+3)=I(1)
      GO TO 16
   26 IARY(L+3)=IW
      GO TO 16
   25 IARY(L+3)=IATK
      GO TO 16
   24 IARY(L+2)=IDOT
      IARY(L+3)=I(1)
      NF=100.*B+.5
      IF(NF .EQ. 10) GO TO 110
      IARY(L+4)=I(NF+1)
      GO TO 4
  110 IARY(L+3) = I(2)
      IARY(L+4) = I(1)
   23 IARY(L+2)=IDOT
      NA=100.*B+.5
      NF=MOD(NA,10)
      NL=(NA-NF)/10
      IARY(L+3)=I(NL+1)
      IARY(L+4)=I(NF+1)
      GO TO 4
   22 IARY(L+3)=IDOT
      NA=10.*B+.5
      NF=MOD(NA,10)
      NL=(NA-NF)/10
      IARY(L+2)=I(NL+1)
      IARY(L+4)=I(NF+1)
      GO TO 4
   21 IARY(L+4)=IDOT
      NA=B+.5
      NF=MOD(NA,10)
      NL=(NA-NF)/10
      IARY(L+2)=I(NL+1)
      IARY(L+4)=I(NF+1)
    4 IF (A .LT. 0.0) IARY(L+1)=MIN
   16 L=L+5
    1 CONTINUE
      WRITE (6,5) M,(IARY(N),N=1,120)
    5 FORMAT (I4,2X,120A1)
    2 CONTINUE
      IF(IJ .EQ. 2) GO TO 20
   30 WRITE (6,31)
   31 FORMAT (1H1)
      GO TO 10
   20 RETURN
      END
```

APPENDIX D

USER'S MANUAL FOR PROGRAM SEAWAVE

This appendix describes the use of the FORTRAN code. The program is composed of the routines listed and described below.

SEAWAVE	This is the management program which sets array dimensions, controls input and output and calls the equation solving routine.
INITIAL	Subroutine which sets the problem and its initial conditions. Called by SEAWAVE.
WHATDT	Subroutine which computes the maximum permissible time step based on the Courant criterion. Called from INITIAL.
WARP	Subroutine which performs a vertical displacement of the sea-floor as an intial condition. The displacement is Gaussian along the major axis and of the form x exp - |x| along the minor axis. Called from INITIAL.
TABLE	Subroutine which prepares the tables which guide the computation. Called by INITIAL.
SHRINK	Subroutine which regulates the size of the computational region so as to reduce running time. Called by EQUATS.
EQUATS	Subroutine which solves the governing equations for one time step.Called by SEAWAVE.

SPECP	Subroutine to save wave elevations at specified points within the computational field. Called from SEAWAVE.
PRTPLT	Subroutine to handle printer plotting of the wave histories saved by SPECP. Called by SEAWAVE.
PRINTA	Subroutine which gives synoptic printout of wave elevations over computational field. Called by SEAWAVE.

The input data for program SEAWAVE is organized into card groups numbered consecutively in the order they are required.

A group may consist of one or more cards. Problem requirements will dictate which groups are to be included in or deleted from the input. At present, the program is set up to run in spherical coordinates only. The coordinate system is defined as follows:

Spherical Coordinates: Longitude is measured positive East from Greenwich and ranges from 0° to 360°. Latitude is measured positive downward from the pole and ranges from 0° to 180°. Since a 0° or a 180° latitude is a singularity in the equations of motion, the computational grid cannot include a pole. The computational grid is as defined in Figure D1.

The space steps $\Delta\theta$ and $\Delta\phi$ must be defined such that there is a minimum of 7 grid points per wavelength of interest. It is best to use 12-15 grid points per wavelength when possible.

The time step DT must observe the Courant condition very strictly. In spherical coordinates, DT must satisfy:

$$DT \leq \frac{R \cdot \Delta\theta \cdot \Delta\phi \cdot \sin\theta}{C\sqrt{(\Delta\theta)^2 + (\Delta\phi \cdot \sin\theta)^2}}$$

where $\Delta\theta$ and $\Delta\phi$ are expressed in radians and C is the wave celerity.

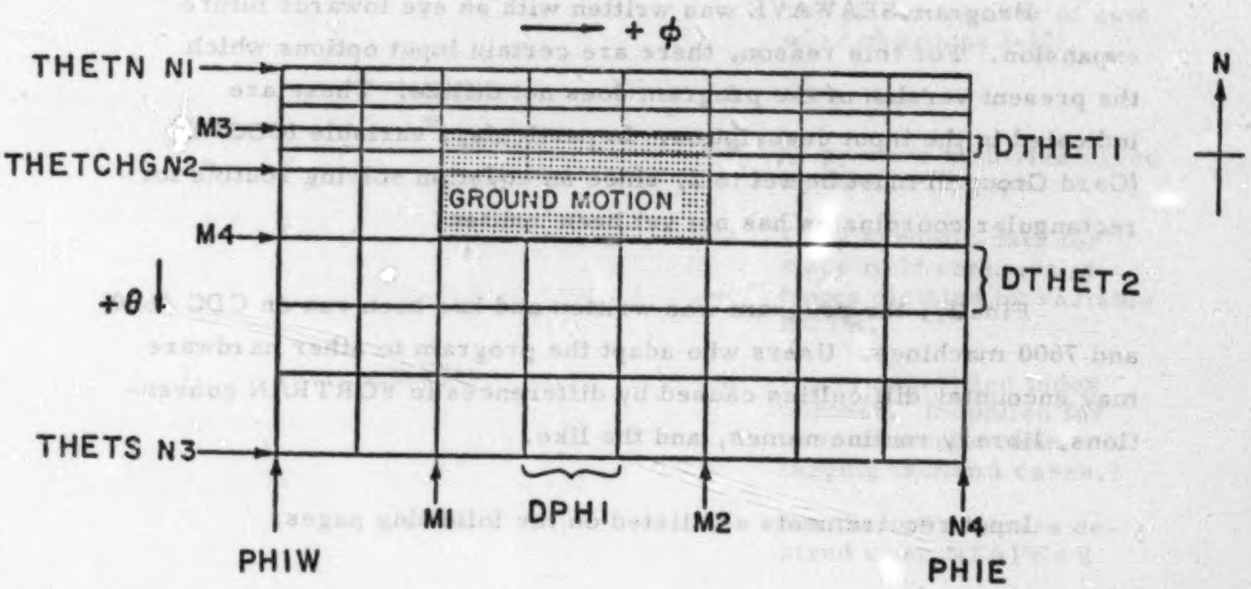
+ φ
THETN N1
M3
THETCHG N2
GROUND MOTION
M4
+θ
THETS N3
M1
DPHI
M2
N4
PHIW
PHIE
DTHET1
DTHET2
N

Figure D1. Computational Grid

The finite difference scheme assumes that the grid point one step inside any open water boundary point will also be in water. Subroutine TABLE will check for satisfaction of this condition. A diagnostic message will be printed identifying the first grid point encountered which does not satisfy this condition and the program will stop.

Program SEAWAVE was written with an eye towards future expansion. For this reason, there are certain input options which the present version of the program does not utilize. These are indicated in the input description. In particular, variable ICOORD (Card Group 3) must be set to 2, since an equation solving routine for rectangular coordinates has not yet been written.

Finally, the program was written and has been run on CDC 6600 and 7600 machines. Users who adapt the program to other hardware may encounter difficulties caused by differences in FORTRAN conventions, library routine names, and the like.

Input requirements are listed on the following pages.

Group No.	No. of Cards FORTRAN VARIABLE	Format	DESCRIPTION
0.	1 card		
	NCASES	= n	Number of cases for this run (i.e., number of sets of card groups 1-19).
	NTAPE	= 0	No action
		= 1	Copy wave histories saved by SPECP to tape.
		= 2	Copy synoptic data for wave field contours at times dictated by variable NCTR.
1.	NTSU	= n	A user specified index number. (Supplied for user convenience in tagging tsunami cases.)
	NCTR		Number of contours desired when NTAPE= 2

Note: In Group 2, the product of NMAX times MMAX should be less than or equal to the dimensions of the arrays in COMMON blocks L1, L3, L5, L7 in SEAWAVE.

Group No.	No. of Cards FORTRAN VARIABLE	Format	DESCRIPTION
2.	1 card	16I5	
	NMAX		Number of computational points along a parallel of latitude. Same as N4.
	MMAX		Number of computational points along a meridian of longitude. Same as N3.
3.	1 card	20A4	
	ID		Alphanumeric identification.
4.	1 card	16I5	
	ITYPE		Indicates the method used to read in depths for computational grid. (See Group 10).

Group No.	No. of Cards	Format	
	FORTRAN VARIABLE	DESCRIPTION	
		= 1	Tape input of depths from LUN2. Can select a subset.
		= 2	Merge of card input and Pacific Ocean Depth Tape on LUN2 (available at Los Alamos Scientific Laboratory).
		= 3	Card input of depths over entire grid.
		= 4	Card input of depths to be written on tape (see ITYPE = 1).
		= 5	Requires special code for non-standard input data.
	NGRID	= 1	Set up and print grids and terminate execution.
		≠ 1	Normal execution.
	IPLOT	= 0	No action.
		= 1	Plot special point time histories with printer plot package. Card group 19 supplies info to plotting routine.
	ICOORD	= 1	Rectangular coordinates are being used for this problem. (Not allowed at present since equation solving routine is not yet available in rectangular coordinates.)
		= 2	Spherical coordinates are being used.
	IGMC		This variable indicates the form of the instantaneous sea floor displacement to be used.
		= 0	Sea floor displacement specified explicitly by user. Values for displacement array GD read from cards (See Card Group 12).
		= -2	Sea floor displacement generated by subroutine WARP based on dimensions supplied by the user.

Group No.	No. of Cards FORTRAN VARIABLE	Format	DESCRIPTION
	IXOUT	= 0	No action.
		= 1	Include Coriolis terms.
	ITAB	= 0	No action.
		= 1	Print wave histories at conclusion of calculation.
5.	1 card	16I5	
	N1 N2 N3 N4		Grid line numbers defining grid boundaries (see Figure 1). N2 indicates point where latitudinal stepsize changes (not allowed in present version). If no change in stepsize, set N2 > N3.
	M1 M2 M3 M4		Grid line numbers defining ground motion region.
	K1 K2 K3 K4		Grid line numbers defining a subset of a grid stored on tape to be used as the depth grid. (ITYPE = 1 or 4) K1 and K2 along meridians. K3 and K4 along parallels.
6.	1 card	16I5	
	NCOR1	= 0	No action.
		= n	Number of grid coordinates where input depth is to be changed to DC1.
	NCOR2	= 0	No action.
		= n	Number of grid coordinates where input depth is to be changed to DC2.

Group No.	No. of Cards FORTRAN VARIABLE	Format DESCRIPTION	
	IOUT1	= 0	No action.
		= 1	Print depth grid.
	IOUT2	= 0	No action.
		= 1	Print coded array, ground motion and computational tables.
	INCH	= 0	Printouts of surface wave in feet.
		= 1	Printouts in inches.

Note: In Card Group 7, variables THETCHG and DTHET2 are for use if the latitudinal step size changes. In the present version of the code, these variables are ignored since no change of step size is allowed.

Group No.	No. of Cards FORTRAN VARIABLE	Format DESCRIPTION	
7.	1 card	8E10.0	
	THETN THETCHG THETS DTHET1 DTHET2 PHIW PHIE DPHI		Grid limits and stepsized in program coordinates. (See Figure 2 for definitions.)
8.	1 card	8E10.0	
	CONV		Conversion factor to charge depth data to feet (usually 6ft/fathom when input depths are in fathoms).
	DC1		Value used to correct input depth grid after conversion (See Card Group 12).

Group No.	No. of Cards FORTRAN VARIABLE	Format	
	DC2		Value used to correct input depth grid after conversion. (See Card Group 13.)
	DEPMIN		Minimum water depth (feet) allowed for depth grid. (Depths greater than 5 feet but less than DEPMIN are increased to DEPMIN.

Note: In Card Group 9, if IGMC = -2, this card should be left blank.

9.	1 card	16I5	
	NINCMP		Grid index defining initial position of Western meridian of computational subset grid. If IGMC = 0, set equal to M1.
	NAXCMP		Grid index defining initial position of Eastern meridian of computational subset grid. If IGMC = 0, set equal to M2.
	MINCMP		Grid index defining initial position of Northern parallel. If IGMC = 0, set equal to M3.
	MAXCMP		Grid index defining initial position of Southern parallel. If IGMC = 0, set equal to M4.

Note: Omit Group 10 if ITYPE = 1.

10.	Several cards	16F5.0	
	D_{ij}		Depths.

Group No.	No. of Cards	Format
	FORTRAN VARIABLE	DESCRIPTION

Note: These depths are prepared in groups, each group taken along a different parallel. Each group begins on a new card. The format of Group 10 depends upon the parameter ITYPE.

ITYPE = 2

Merge of card input and Pacific Ocean Depth Tape on LUN2. The Pacific Depth Tape (available only at Los Alamos Scientific Laboratory) is read meridian by meridian from left to right as described in LONGWAY users manual. The depths on cards are read in the same manner (meridian by meridian, left to right) and are placed to the north of the Pacific depth tape grid.

ITYPE = 3 Card Input of Entire Grid

Depths are read parallel by parallel (west to east) from top to bottom (north to south).

ITYPE = 4 Card Input of Ocean Depths to be Written on Tape (LUN2)

Depths are read in same manner as for ITYPE = 3. The parameters N3 (number of grid points along a meridian) and N4 (number of grid points along a parallel) are written on the tape, one parallel at a time from top to bottom.

ITYPE = 5 Special Input

This indicates user's written special code to generate the input data is inserted following statement 500 in subroutine INITIAL.

ITYPE = 1 Input from Tape

This indicates depth input from a tape generated using ITYPE = 4.

Group No.	No. of Cards FORTRAN VARIABLE	Format DESCRIPTION

Note: Omit Group 11 if IGMC ≠ -2.

Group No.	No. of Cards FORTRAN VARIABLE	Format DESCRIPTION
11.	1 card	5E10.0, I10, E10.0
	CLAT	Latitude (program coordinates) of center of sea-floor displacement.
	CLONG	Longitude (program coordinates) of center of sea-floor displacement.
	HEAD	The bearing with respect to true North of a line directed from its center to the positive peak (degrees positive clockwise).
	AXMAJ	Length of major (Gaussian) axis of displacement region (nautical miles).
	AXMIN	Length of minor (x exp $-\lvert x^2 \rvert$ form) axis of displacement region (nautical miles).
	MTYPE	= 0 Dipolar displacement.
		= -1 Negative monopole.
		= 1 Positive monopole.
	PEAK	Peak displacement (feet).

Note: Omit Group 12 if IGMC ≠ 0.

Group No.	No. of Cards FORTRAN VARIABLE	Format DESCRIPTION
12.	Several cards	16F5.0

Group No.	No. of Cards FORTRAN VARIABLE	Format DESCRIPTION
	GD_{ij}	Ground displacement in feet. These values are prepared in a similar fashion as the ocean depths in Group 10 (ITYPE = 3) except that this input is on a subset of the input grid defined by the quantities M1, M2, M3, M4.

Note: Omit Group 13 if NCOR1 = 0.

Group No.	No. of Cards FORTRAN VARIABLE	Format DESCRIPTION
13.	Several cards	16I5
	NBD_i MBD_i	Coordinate points (NBD, MBD) at which depth will be corrected to DC1 feet. (See Group 8). Prepare the NBD array first. Start a new card for MBD array.

Note: Omit Group 14 if NCOR2 = 0.

Group No.	No. of Cards FORTRAN VARIABLE	Format DESCRIPTION
14.	Several cards	16I5
	NBD_i MBD_i	As in Group 13 except depth is set to DC2 feet.
15.	1 card	8E10.0
	DT	Time step in seconds.
	TMAX	Final time (sec.).
16.	1 card	16I5
	NPTS	Number of special points. (The number of points may be n - 1 or less where n is the second dimension of array PTAB in COMMON/A4/.)

Group No.	No. of Cards FORTRAN VARIABLE	Format DESCRIPTION
	NPTINC	Increment of time steps at which special point information is saved. $\text{NPTINC} \geq \frac{\text{TMAX}}{\text{(First dimension of PTAB)*DT}}$
17.	2 cards	16I5
	NPRINT_i	Array of integral numbers of time steps at which a snapshot of the wave elevations over the computational grid is printed. Limited to 32 values.

Note: Omit Group 18 if NPTS = 0.

Group No.	No. of Cards FORTRAN VARIABLE	Format DESCRIPTION
18.	Several cards	16I5
	NPOT_i	Array of coordinate indices of special points.
	MPOT_i	NPOT AND MPOT are in separate groups, MPOT array begins on a new card.

Note: Omit Group 19 if IPLOT = 0.

Group No.	No. of Cards FORTRAN VARIABLE	Format DESCRIPTION
19.	1 card	4I5, 2F5.0
	NDIV	Integral time interval in seconds or hours (see HOUR) to use in labeling time axis.
	NH	Total number of columns across page to use for time axis (limited to 100).
	NLAB	Number of intervals above or below zero elevation to label an elevation axis. (Normally = 2).

Group No.	No. of Cards FORTRAN VARIABLE	Format DESCRIPTION	
	NVD		Number of divisions to use between labels on elevation axis. (Normally = 5).
	REL		Divide all elevations by REL (used to normalize elevations to a unit source).
	HOUR	= 0.0	Time scale in seconds.
		= 1.0	Time scale in hours.

NRC FORM 335
(7-77)

U.S. NUCLEAR REGULATORY COMMISSION

BIBLIOGRAPHIC DATA SHEET

1. REPORT NUMBER *(Assigned by DDC)*
NUREG/CR-1106

4. TITLE AND SUBTITLE *(Add Volume No., if appropriate)*
Tsunami Atlas for the Coasts of the United States

2. *(Leave blank)*

3. RECIPIENT'S ACCESSION NO.

7. AUTHOR(S)
M. Brandsma, D. Divoky, and L. S. Hwang

5. DATE REPORT COMPLETED

MONTH	YEAR
June	1978

9. PERFORMING ORGANIZATION NAME AND MAILING ADDRESS *(Include Zip Code)*
Tetra Tech, Inc.
630 North Rosemead Boulevard
Pasadena, CA 91107

DATE REPORT ISSUED

MONTH	YEAR
November	1979

6. *(Leave blank)*

8. *(Leave blank)*

12. SPONSORING ORGANIZATION NAME AND MAILING ADDRESS *(Include Zip Code)*
U.S. Nuclear Regulatory Commission
Washington, D.C. 20555

10. PROJECT/TASK/WORK UNIT NO.

11. CONTRACT NO.

13. TYPE OF REPORT
Technical Report

PERIOD COVERED *(Inclusive dates)*

15. SUPPLEMENTARY NOTES

14. *(Leave blank)*

16. ABSTRACT *(200 words or less)*

This report presents the results of a study to determine the distribution of offshore wave heights and time histories for coastal segments of the United States due to distantly generated tsunamis. A large hypothetical earthquake is defined by appeal to history and tectonic theory. This canonical source serves as input to a numerical hydrodynamic model which computes the resulting wave history anywhere within the ocean basin. This procedure is repeated for a number of potential source locations, chosen according to degree and type of seismic activity. In this way, hypothetical coastal histories of great tsunamis emanating from any potential source area are simulated. The results of this study are offshore incident wave systems and do not include the complex, site-dependent, nearshore transformations.

17. KEY WORDS AND DOCUMENT ANALYSIS

17a. DESCRIPTORS

Wave heights, Tsunamis, Earthquake, History Theory, Tectonic Theory, Ocean Basin, Coastal Histories

17b. IDENTIFIERS/OPEN-ENDED TERMS

18. AVAILABILITY STATEMENT
Unlimited

19. SECURITY CLASS *(This report)*
Unclassified

20. SECURITY CLASS *(This page)*

21. NO. OF PAGES

22. PRICE
$

UNITED STATES
NUCLEAR REGULATORY COMMISSION
WASHINGTON, D. C. 20555

OFFICIAL BUSINESS
PENALTY FOR PRIVATE USE, $300

POSTAGE AND FEES PAID
U.S. NUCLEAR REGULATORY
COMMISSION

U.S. MAIL